UNIVERSITAT POLITÈCNICA DE VALÈNCIA

CENTRO DE INVESTIGACIÓN PRÍNCIPE FELIPE

Inflammatory Tumor Microenvironment as target in the design of nanoconjugates for the treatment of advanced breast cancer.

PhD. THESIS
Submitted by

Paula Mª Soriano Teruel

PhD. Supervisors:
Dr. Mar Orzáez Calatayud and Dr. María J. Vicent

Valencia, November 2022

PRINCIPE FELIPE
CENTRO DE INVESTIGACION

UNIVERSITAT POLITÈCNICA DE VALÈNCIA

MARÍA DEL MAR ORZÁEZ CALATAYUD, PhD in Biology at the *Universitat de València*, and MARÍA JESÚS VICENT, PhD in Chemistry at the *Universitat Jaume I*

CERTIFY:

That the work ***"Inflammatory Tumor Microenvironment as Target in the Design of Nanoconjugates for the Treatment of Advanced Breast Cancer"*** has been developed by Paula Mª Soriano Teruel under their supervision in the Centro de Investigación Príncipe Felipe (CIPF), as a Thesis Project in order to obtain the degree of PhD in Biotechnology at the *Universitat Politècnica de València.*

Valencia, May 31th 2022

Dra. Mar Orzáez Calatayud
Directora.

Dra. María Jesús Vicent
Directora

A mis padres

Agradecimientos

Acknowlegements

Si me preguntaran cuál es la parte de esta tesis que más me ha costado escribir, sin duda alguna podría decir que estos agradecimientos. Y es que, ¿cómo decir adiós a esta etapa tan importante de mi vida? ¿Cómo expresar todas las emociones que se despiertan al recordar todo este tiempo?

En primerísimo lugar dar gracias de todo corazón a mis directoras de tesis por haberme dado esta oportunidad. Mar y María Jesús, ¡Infinitas gracias!
A ti Mar, gracias por abrirme las puertas de lo que para mí ha sido un hogar durante estos 4 años: El I-12. Me has visto crecer y me has enseñado infinitas cosas, y no solo a nivel profesional, para mí has sido un apoyo incondicional en muchas situaciones a las que me he enfrentado. Gracias por haberme dado alas y haber confiado en mí.
A ti María Jesús, gracias por haber sido un referente e inspiración. Gracias por inculcarnos el valor del esfuerzo y la constancia para conseguir lo que uno se proponga.

En segundo lugar, dar gracias también a mi Moni. Gracias Mónica Sancho por haber sido mi compañera. Gracias por haberme enseñado todo lo que sé con pipeta en mano. Gracias por haber convivido todo este tiempo con tu impecable orden y mi magnífico desorden. Gracias por tus consejos. Gracias por poner practicidad ante mis caos mentales. Junto con Mar, para mí siempre vais a ser muy importantes os llevo conmigo en mi corazoncito allá donde vaya.

Gracias inmensas también a todas las personas que han formado parte del I-12 todo este tiempo. Gracias Ally por tu felicidad, por tu apoyo incondicional, y por llenar todos los ambientes con esa alegría que tanto te caracteriza. Gracias a mi queridísima amiga Estefi. Aunque quizá en la tesis no hayamos compartido tantos momentos profundos, la vida es sabia y nos ha dado una segunda oportunidad siendo compis en Tyris. Gracias a mi tocaya, mi Pauli. Hemos sido compañeras de carrera y hemos tenido el regalazo de haber compartido también parte de esta experiencia. Gracias por haberme aportado risas, locuras y felicidad a esta aventura.

Gracias a todas las chicas UPV: Ale, Alba, Ara, Gema, Irene, Elena, Blanca etc. ¡Juntas creamos un ambientazo de chicas al poder! ¡Ha sido muy guay compartir esta experiencia con todas y cada una de vosotras! Gracias también a todas las personas que han pasado por el labo y han transmitido cosas tan bonitas: Laura, Danya, Carmen, Pauline, Diego, Iván, María etc. Gracias a mi queridísimo Alberto por tantas horas y conversaciones en el confocal. ¡Creo que eres el mayor confidente de todo el CIPF!

Por otro lado, dar inmensas gracias a mi otra mitad: El I-36. Gracias Ana por tu disponibilidad, por tus consejos, por tantas horas en el animalario. Gracias por haberme enseñado todo lo que sé con los ratoncitos. Gracias a Inma por estar siempre que alguien lo necesite y por transmitir esa alegría que desprendes. Gracias también a mi queridísima Paz. ¡Nuestro sufrimiento por la review tenía que quedar reflejado de manera especial! Gracias a Tony, Snez, Irene, Fernanda, Esther, Zoraida, etc. Gracias a mi súper team de química Alessio y María. Sin vosotros la mitad de esta tesis no habría podido darse. Gracias por no volveros locos con el sufrido MM01. Gracias por pelearos con garras y dientes hasta conseguir que saliera toda la parte química.

Gracias también a todo mi equipo de Tyris, aunque forméis parte de mi siguiente etapa os he conocido con la tesis sin defender, así que os meto dentro del saco.

Por último y no menos importante, dar las gracias a mis padres. Gracias, mamá y papá por haberme inculcado el valor de soñar y luchar por lo que uno quiere. Gracias por ser mi pilar fundamental en todos los aspectos de mi vida. Gracias por todo el esfuerzo y por todo el amor que me habéis dado siempre. Gracias a mi tete, a mi teta, a Lucía y a Jesús.

Gracias a mi Ohana querida por ser las mejores amigas que una pueda tener. Somos una pequeña familia llena de amor. Gracias por todas las tardes de cervezas que han sido mi desconexión todo este tiempo y espero que lo sean toda mi vida. Gracias por ser y estar de forma incondicional. ¡Qué bonito es vernos crecer y superar etapas!

Y con esto, cierro con muchísimo amor y alegría esta etapa de mi vida que me ha enseñado tanto. ¡Gracias a la vida por haberme dado esta oportunidad tan bonita y por hacérmela recordar con tanto cariño!

Abstract

This PhD thesis entitled "**The inflammatory tumor microenvironment as a target in the design of nanoconjugates for the treatment of advanced breast cancer**" focuses on the evaluation of a novel inflammasome inhibitor (MM01) as a chemical tool to study the role of the inflammasasome in models of inflammation and cancer.

The **Chapter I** includes an overview of the immune system, ASC-dependent inflammasomes, and the role of different types of inflammasomes in disease development. It also delves into the role of inflammasomes and ASC protein in breast cancer progression. In addition, basic concepts of nanotechnology, nanomedicine and therapeutic polymers are included. Finally, the advantages of using nanomedicines as therapeutics, the interactions of nanomedicines with biological systems, the nanodrugs described in the literature, as well as their translation possibilities to clinical practice are discussed.

Then, the **Chapter II** presents the general objectives of this doctoral thesis and the specific objectives that are addressed in the different experimental chapters. In addition, the **Chapter III** describes all the materials and methods employed for this doctoral thesis.

In **Chapter IV**, we delineate a novel mechanism of action for MM01, a recently identified modulator of inflammasome activity - the inhibition of ASC oligomerization and the subsequently reduced processing of pro-caspase-1 and inhibited caspase-1 activity. We demonstrate that MM01 disrupts the ASC oligomerization process associated with the activity of various inflammasomes and inhibits downstream IL-1β release and pyroptosis in various cellular models of inflammation. MM01 also reduces neutrophil infiltration and pro-inflammatory cytokine accumulation in an *in vivo* model of peritonitis, used as a proof-of-concept for the therapeutic capabilities of this ASC inhibitor. Given the involvement of ASC function in multiple inflammasome complexes, treatment with MM01 may represent an effective therapeutic approach to treat those diseases where the activation of multiple inflammasomes is involved.

Taking into account the results obtained in Chapter IV, in **Chapter V** we employed our inflammasome inhibitor, MM01, to study the role of the inflammasome in tumor progression in different breast cancer models both *in vitro* and *in vivo*. We demonstrated that different breast cancer cell lines respond differently to MM01 treatment. We developed a functional assay comprising the evaluation of breast cancer cell migration in response to the pro-inflammatory M1 macrophage secretome (inflammatory stimulus) in the presence of MM01. Certain cell lines (such as the EO771 cell line) displayed increased migration in response to the inflammatory stimulus and decreased migration in response to treatment with MM01; however, we also identified cell lines that respond negatively to MM01 treatment (such as the 4T1 cell line). Finally, we demonstrated the efficacy of this functional experiment *in vivo* by demonstrating that MM01 treatment reduced tumor size in the EO771 orthotopic model but increased tumor size and lung metastasis in the 4T1 orthotopic model. These two models, which recapitulate contradictory responses to treatment with our inflammasome inhibitor, may be used in the future to determine biomarkers that predict the response.

In **Chapter VI**, we developed a synthetic strategy to obtain a novel nanomedicine that improved the solubility and tumor-targeting of MM01 in a breast cancer model. We implemented a hybrid conjugation-complexation approach by comprising the conjugation of β-cyclodextrin to a linear poly-L-glutamic acid (PGA) (L-PGA-βCD) to provide with the capability of entrapping MM01 within the cyclodextrin rings in a concentration dependent manner yielding to L-PGA-βCD-MM01 with different physico-chemical characteristics (i.e. drug loading, size). The obtained nanosystem exhibited improved solubility in aqueous solutions compared to the free form of MM01. While we failed to observe a significant improvement in function in vitro compared to free MM01 as expected due to the different pharmacokinetics, our novel nanosystem demonstrated better efficacy in an orthotopic model of breast cancer by resulting in a more significant reduction in tumor size in those mice treated with L-PGA-βCD-MM01 nanomedicine.

Finally, **Chapters VII and VIII** deal with the discussion and general conclusions, respectively.

Resumen

Esta tesis doctoral titulada "El microambiente tumoral inflamatorio como objetivo en el diseño de nanoconjugados para el tratamiento del cáncer de mama avanzado" se centra en la evaluación de un nuevo inhibidor del inflamasoma (MM01) como herramienta química para estudiar el papel del inflamasoma en modelos de inflamación y cáncer.

El capítulo I incluye una descripción general del sistema inmune, los inflamasomas dependientes de ASC y el papel que juegan en el desarrollo de enfermedades. También se profundiza en el papel de los inflamasomas y de la proteína ASC en la progresión del cáncer de mama. Además, se incluyen conceptos básicos de nanotecnología, nanomedicina y polímeros terapéuticos. Finalmente, se abordan las ventajas de utilizar nanomedicinas como terapia, las interacciones de las nanomedicinas con los sistemas biológicos, los nanofármacos descritos en la literatura, así como sus posibilidades de traslación a la práctica clínica.

A continuación, el capítulo II presenta los objetivos generales de esta tesis doctoral y los objetivos específicos que se abordan en los diferentes capítulos experimentales. Además, en el capítulo III se describen todos los materiales y métodos empleados para la realización de esta tesis doctoral.

En el capítulo IV, delineamos un novedoso mecanismo de acción para MM01, un modulador de la actividad del inflamasoma recientemente identificado: la inhibición de la oligomerización del ASC y el subsiguiente procesamiento reducido de la pro-caspasa-1 y la inhibición de la actividad de la caspasa-1. Demostramos que MM01 interrumpe el proceso de oligomerización de ASC asociado a la actividad de varios inflamasomas e inhibe la liberación de IL-1β y la piroptosis en varios modelos celulares de inflamación. MM01 también reduce la infiltración de neutrófilos y la acumulación de citoquinas pro-inflamatorias en un modelo in vivo de peritonitis. Dada la implicación de la función de ASC en múltiples complejos del inflamasoma, el tratamiento con MM01 puede representar un enfoque terapéutico eficaz para tratar aquellas enfermedades en las que está implicada la activación de múltiples inflamasomas.

Teniendo en cuenta los resultados obtenidos en el capítulo IV, en el capítulo V empleamos nuestro inhibidor del inflamasoma, MM01, para estudiar el papel del inflamasoma en la progresión tumoral en diferentes modelos de cáncer de mama tanto in vitro como in vivo. Demostramos que diferentes líneas celulares de cáncer de mama responden de forma diferente al tratamiento con MM01. Desarrollamos un ensayo funcional que comprende la evaluación de la migración de las células de cáncer de mama en respuesta al secretoma pro-inflamatorio de los macrófagos M1 (estímulo inflamatorio) en presencia de MM01. Ciertas líneas celulares (como la línea celular EO771) mostraron un aumento de la migración en respuesta al estímulo inflamatorio y una disminución de la migración en respuesta al tratamiento con MM01; sin embargo, también identificamos líneas celulares que responden negativamente al tratamiento con MM01 (como la línea celular 4T1). Por último, demostramos la eficacia de este experimento funcional in vivo demostrando que el tratamiento con MM01 redujo el tamaño del tumor en el modelo ortotópico EO771 pero aumentó el tamaño del tumor y la metástasis pulmonar en el modelo ortotópico 4T1. Estos dos modelos, que recapitulan respuestas contradictorias al tratamiento con nuestro inhibidor del inflamasoma, podrán utilizarse en el futuro para determinar biomarcadores que predigan la respuesta.

Por último, en el capítulo VI desarrollamos una estrategia sintética para obtener un nuevo nanomedicamento que mejora la solubilidad y la orientación tumoral del MM01 en un modelo de cáncer de mama. Implementamos un enfoque híbrido de conjugación-complejación que comprende la conjugación de β-ciclodextrina con un ácido lineal poli-L-glutámico (PGA) (L-PGA-βCD) para proporcionar la capacidad de atrapar MM01 dentro de los anillos de ciclodextrina de una manera dependiente de la concentración dando lugar al nanofármaco L-PGA-βCD-MM01 con diferentes características físico-químicas (es decir, carga de fármaco, tamaño). El nanosistema obtenido mostró una mejor solubilidad en soluciones acuosas en comparación con la forma libre de MM01. Si bien no pudimos observar una mejora significativa de la función in vitro en comparación con el MM01 libre, nuestro nanosistema demostró una mejor eficacia en un modelo ortotópico de cáncer de mama al producir una mayor

reducción del tamaño del tumor en aquellos ratones tratados con la nanomedicina L-PGA-CD-MM01.

Finalmente, en los capítulos VII y VIII se aborda la discusión y conclusiones generales respectivamente.

Resum

Aquesta tesi doctoral titulada "El microambient tumoral inflamatori com a objectiu en el disseny de nanoconjugats per al tractament del càncer de mama avançat" se centra en l'avaluació d'un nou inhibidor de l'inflamasoma (MM01) com a eina química per a estudiar el paper de l'inflamasoma en models d'inflamació i càncer.

El capítol I inclou una descripció general del sistema immune, els inflamasomes dependents de ASC i el paper que juguen en el desenvolupament de malalties. També s'aprofundeix en el paper dels inflamasomes i de la proteïna ASC en la progressió del càncer de mama. A més, s'inclouen conceptes bàsics de nanotecnologia, nanomedicina i polímers terapèutics. Finalment, s'aborden els avantatges d'utilitzar nanomedicines com a teràpia, les interaccions de les nanomedicines amb els sistemes biològics, els nanofàrmacs descrits en la literatura, així com les seues possibilitats de translació a la pràctica clínica.

A continuació, el capítol II presenta els objectius generals d'aquesta tesi doctoral i els objectius específics que s'aborden en els diferents capítols experimentals. A més, en el capítol III es descriuen tots els materials i mètodes emprats per a la realització d'aquesta tesi doctoral.

En el capítol IV, delineem un nou mecanisme d'acció per a MM01, un modulador de l'activitat de l'inflamasoma recentment identificat: la inhibició de l'oligomerización de ASC i el subsegüent processament reduït de la pro-caspasa-1 i la inhibició de l'activitat de la caspasa-1. Vam demostrar que MM01 interromp el procés de oligomerización de ASC associat a l'activitat de diversos inflamasomes i inhibeix l'alliberament de IL-1β i la piroptosis en diversos models cel·lulars d'inflamació. MM01 també redueix la infiltració de neutròfils i l'acumulació de citocines pro-inflamatòries en un model in vivo de peritonitis. Donada la implicació de la funció de ASC en múltiples complexos del inflamasoma, el tractament amb MM01 pot representar un enfocament terapèutic eficaç per a tractar aquelles malalties en les quals està implicada l'activació de múltiples inflamasomes.

Tenint en compte els resultats obtinguts en el capítol IV, en el capítol V emprem el nostre inhibidor de l'inflamasoma, MM01, per a estudiar el paper de

l'inflamasoma en la progressió tumoral en diferents models de càncer de mama tant in vitro com in vivo. Vam demostrar que diferents línies cel·lulars de càncer de mama responen de forma diferent del tractament amb MM01. Desenvolupem un assaig funcional que comprén l'avaluació de la migració de les cèl·lules de càncer de mama en resposta al secretoma pro-inflamatori dels macròfags M1 (estímul inflamatori) en presència de MM01. Unes certes línies cel·lulars (com la línia cel·lular EO771) van mostrar un augment de la migració en resposta a l'estímul inflamatori i una disminució de la migració en resposta al tractament amb MM01; no obstant això, també identifiquem línies cel·lulars que responen negativament al tractament amb MM01 (com la línia cel·lular 4T1). Finalment, vam demostrar l'eficàcia d'aquest experiment funcional in vivo demostrant que el tractament amb MM01 va reduir la grandària del tumor en el model ortotòpic EO771 però va augmentar la grandària del tumor i la metàstasi pulmonar en el model ortotòpic 4T1. Aquests dos models, que recapitulen respostes contradictòries al tractament amb el nostre inhibidor de l'inflamasoma, podran utilitzar-se en el futur per a determinar biomarcadors que prediguen la resposta.

Finalment, en el capítol VI desenvolupem una estratègia sintètica per a obtindre un nou nanofàrmac que millora la solubilitat i l'orientació tumoral del MM01 en un model de càncer de mama. Implementem un enfocament híbrid de conjugació-complexació que comprén la conjugació de β-ciclodextrina amb un àcid lineal *poli-L-glutàmic (PGA) (L-PGA- βCD) per a proporcionar la capacitat d'atrapar MM01 dins dels anells de *ciclodextrina d'una manera dependent de la concentració donant lloc al nanofàrmaco L-PGA- βCD -MM01 amb diferents característiques fisicoquímiques (és a dir, càrrega de fàrmac, grandària). El nanosistema obtingut va mostrar una millor solubilitat en solucions aquoses en comparació amb la forma lliure de MM01. Si bé no vam poder observar una millora significativa de la funció in vitro en comparació amb el MM01 lliure, nostre nanosistema va demostrar una millor eficàcia en un model ortotòpic de càncer de mama en produir una major reducció de la grandària del tumor en aquells ratolins tractats amb la nanomedicina L-PGA- βCD-MM01.

Finalment, en els capítols VII i VIII s'aborda la discussió i conclusions generals respectivament.

Abbreviations and Acronyms

A

AAA: Abdominal Aortic Aneurysms

AD: Alzheimer's disease

AIM2: Absent in melanoma 2

ALR: Absent in melanoma 2 type receptors

ALS: Amyotrophic Lateral Sclerosis

Apaf-1: Apoptotic protease-activating factor-1

APC: Antigen-presenting cells

APP: Amyloid precursor protein

ASC: Apoptosis-associated speck-like protein

ATCC: American Type Culture Collection

C

C1: Caspase-1

CARD: Caspase recruitment and activation domain

CCD: Central composite design

CLRs: C-type lectin receptors

CXCL10: CXC motif chemokine ligand 10

D

DAMPs: Damaged-associated molecular patterns

DAPI: 4′,6-diamidino-2-phenylindole

DIEA: N,N-diIsopropylethylamine

DLS: Dynamic Light Scattering

DMF: N,N-dimethylformamide

DMSO: Dimethyl sulfoxide

DMTMM BF4: 4-(4,6-dimethoxy-1,3,5-triazin-2-yl)-4-methyl-morpholinium tetrafluoroborate salt

DNA: Deoxyribonucleic Acid

DSS: Disuccinimidyl suberate

E

ECM: Extracellular Matrix

EDC: 1-ethyl-3-(3-dimethyl aminopropyl)-1-carbodiimide hydrochloride

EIF4G2: Eukaryotic translation initiation factor 4 gamma 2

EM: Electron microscopy

EPR: Enhanced permeability and retention

ER: Estrogen receptor

F

FBS: Fetal bovine serum

FDA: Food and Drug Administration

FIIND: Function-to find domain

FMF: Familial Mediterranean fever

G

G418: Geneticin

GA: Genetic algorithms

GFP: Green fluorescent protein

GO.MF: GO.Molecular Function

GSDMD: Gasdermin

H

HCC: Hepatocellular carcinoma

HER2: Human epidermal growth factor receptor 2

HMPA: N-(2-hydroxypropyl)methacrylamide

I

IBD: Inflammatory Bowel Disease

Icam1: Intercellular Adhesion Molecule 1

Ifi47: Interferon-gamma inducible protein 47

IL: Interleukin

IPTG: Isopropyl-β-D-1-thiogalactopyranoside

IRF: Interferon regulatory factors

Irgm1: Immunity-related GTPase family M protein 1

K

KO: Knock-out

L

LDH: Lactate Dehydrogenase

LPS: Lipopolysaccharide

LRR: C-terminal leucine-rich repeat

LUC2: Luciferase2

M

MDP: Muramyldipeptide

MHC: Major histocompatibility complex

MS: Multiple Sclerosis

MSU: Monosodium Urate Crystals

MTS: Tetrazolium

Mw: Molecular weight

A

$NaDCO_3$: Deuterated sodium hydrogen carbonate

Nfkb2: Nuclear factor-kappaB

NHS: N-hydroxysuccinimide

Nig: Nigericine

NLRs: Nucleotide-binding and oligomerization domain (NOD)-like receptors

NMR: Nuclear Magnetic Resonance

NOD: Nucleotide-binding and oligomerization domain

NPC: Niemann Pick type C disease

NT: Non-Treated

O

OD: Optical density

ORA: Over-representation Analysis

P

PABPC1: Poly(A) Binding Protein Cytoplasmic 1

PAMPs: Pathogen-associated molecular patterns

PBS: Dulbecco's phosphate-buffered saline

PC1: Pro-caspase-1

PD-1: Programmed cell death-1

PEG: Polyethylene glycol

Pf4: Platelet factor 4

PFA: Paraformaldehyde

PFU: Particles forming units

PGA: Polyglutamic acid

PMA: Phorbol 12-myristate 13-acetate

PMSF: Phenylmethylsulfonyl fluoride

PR: Progesterone receptor

PRPF8: Pre-mRNA Processing Factor 8

PRR: Pattern recognition receptors

PSEN1: Presenilin 1

PTS: Polypeptide Therapeutics Solutions

PTX: Paclitaxel

PYD: Pyrin domain

R

RA: Rheumatoid Arthritis

RBM39: RNA-binding motif protein 39

RhoB: Ras Homolog Family Member B

RIG1: Retinoic acid-inducible gene-I

RLRs: Retinoic acid-inducible gene-I (RIG1)-like receptors (RLRs)

RLU: Relative luminescence units

RNASEH2A: Ribonuclease H2 Subunit A

RSM: Response surface methodology

RT: Room Temperature

S

SARS-CoV-2: Severe acute respiratory syndrome coronavirus-2

SDS: Sodium Dodecyl Sulfate

Serpine1: Serine protease inhibitor clade E member 1

Sn: Supernatant

T

TAMs: Tumor-Associated Macrophages

TLRs: Toll-like receptors

TME: Tumor Microenvironment

TNBC: Triple Negative Breast cancer

TNF: Tumor necrosis factor

W

WGA: Wheat Germ Agglutinin

Others

βCD: βCyclodextrin

General Index

Ch.I

General Introduction

I.1 Immune System

The immune system is the body´s primary defense mechanism and comprises a complex network of cells, proteins, tissues, and organs that defend the organism against infections, illness, and disease [1, 2]. It is divided into two subsystems - the innate and the adaptive response [3] (summarized in **Figure 1**).

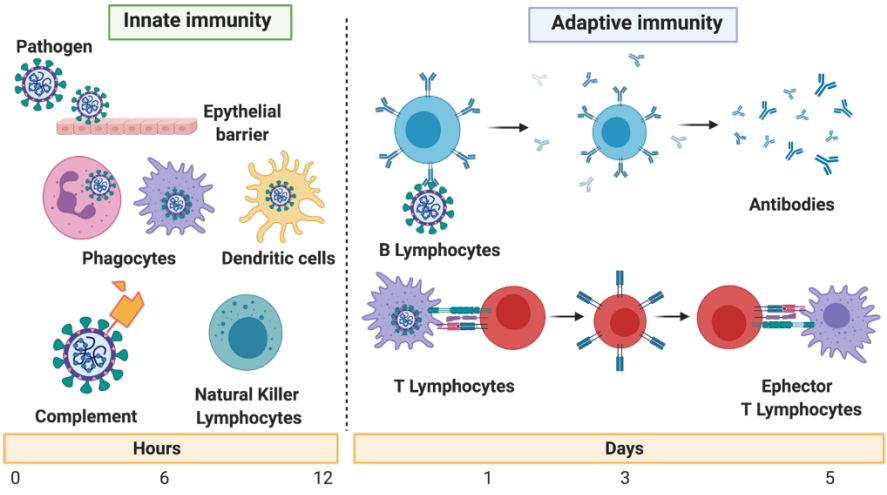

Figure 1. Principal Components of the Innate and Adaptive Responses. The innate response provides an initial defense against infection. It is composed by epithelial barriers, phagocytes, dendritic cells, the complement system, and natural killer cells. Adaptive immune response develops after innate responses through the function T and B lymphocytes and antibodies. Some cells of the innate system, such as dendritic cells and macrophages, are essential for the activation of lymphocytes of the adaptive system.

The innate system represents the first line of defense against infections and does not retain a memory of previous responses. It is characterized by its rapidity and unspecific nature compared to adaptive responses, with the inflammatory response the primary mechanism involved [4]. Components of the innate immune system [1, 5, 6] include:

- **Physical, mechanical, and chemical barriers:** A continuous epithelial layer protects the most frequent entry sites for pathogens, such as the skin and the

digestive/respiratory tracts, by providing a physical and chemical barrier against infection.

- **Phagocytic cells:** These specialized cells "engulf" and destroy pathogenic microorganisms and harmful particles. Phagocytic cells include monocytes, macrophages, neutrophils, and dendritic cells. Macrophages and dendritic cells respond to pathogens by producing pro-inflammatory cytokines that initiate the inflammatory response and stimulate adaptive immune cells. Furthermore, dendritic cells and macrophages also function as antigen-presenting cells (APCs) with the capacity to activate adaptive responses.
- **Non-phagocytic immune cells:** Cells such as mast cells, basophils, and eosinophils regulate inflammatory responses by releasing chemical mediators (e.g., vasoactive amines or proteolytic enzymes) that eliminate pathogens and participate in allergic processes.
- **Natural Killer Cells:** These specialized lymphocytes recognize and destroy infected cells. When activated by infected cells, natural killer cells release the contents at the point of contact with the infected cell. Secreted proteins then enter the infected cell and activate enzymes that induce apoptotic cell death. [7].
- **Complement system:** Comprising more than twenty plasma proteins, the complement system sequentially opsonizes or surface-coats pathogens to facilitate the elimination of pathogens and the recruitment of inflammatory cells to the source of infection [8].

Traditionally, innate immunity has been considered a non-specific system whose functions included phagocytosis, the destruction of pathogens through pro-inflammatory responses, and the presentation of antigens to develop adaptive immune responses mediated by T and B lymphocytes. However, recent studies have revealed that the innate immune system does present a degree of specificity that allows distinguish between self and foreign entities. The pattern recognition receptors (PRRs) constitutively expressed by immune system cells afford this specificity. Once PRRs detect microbial patterns, innate immune cells are activated and trigger immediate alarm through the secretion of cytokines and interferons [9, 10] (**Figure 2**). PRRs will be discussed at length in **Section 2.2**.

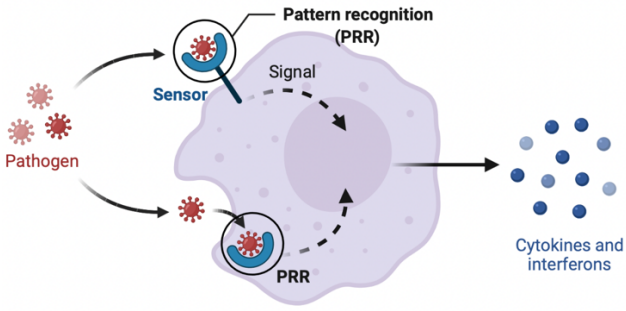

Figure 2. Pathogen Recognition by PRRs in Innate Immune Cells. Innate immune cells present sensors (PRR) that detect pathogenic or otherwise damaging stimuli (pattern recognition) and activate the secretion of cytokines and interferons to eliminate the associated threat.

Even given the efficacy of the innate immune defenses, pathogens can persist and trigger the adaptive immune system, which is highly specific to a particular antigen and provides long-lasting immunity [11, 12]. Adaptive immunity also possesses the ability to remember previous infections; this allows the magnitude of the defense response to increase with each successive exposure to a specific pathogen to improve immune outcomes.

Lymphocytes represent the primary cells of the adaptive immune system and present specific receptors against various antigens [12, 13]. Said cells include:

- **B lymphocytes** become activated and produce antibodies after recognizing their extracellular antigen. B lymphocytes can recognize soluble antigens and antigens presented on the surface of pathogens or other cells.
- **T lymphocytes** recognize antigen peptide fragments bound to specialized molecules in presenting peptides (the major histocompatibility complex or MHC) located on the surface of APCs such as dendritic cells and macrophages. T cells can be divided into **cytotoxic T lymphocytes** (CD3 + CD8 +), which recognize and eliminate infected cells that exhibit the microbial antigens presented by class I MHC molecules, and **helper T lymphocytes** (CD3 + CD4 +), which recognize microbial antigens presented by class II MHC molecules. Helper T lymphocytes release cytokines that stimulate the proliferation and activation of cytotoxic T

lymphocytes, B lymphocytes, and macrophages. **Regulatory T lymphocytes** (also called suppressor T cells) (CD4 + CD25 +) modulate the immune system to prevent excessive immune responses that could compromise homeostasis.

Overall, innate and adaptive immunity constitutes an integrated defense system. The activation of the adaptive response depends on the innate immune system, while adaptive immunity reinforces innate immunity by increasing antimicrobial ability and stimulating inflammatory responses to eliminate pathogenic threats [14] (**Figure 3**).

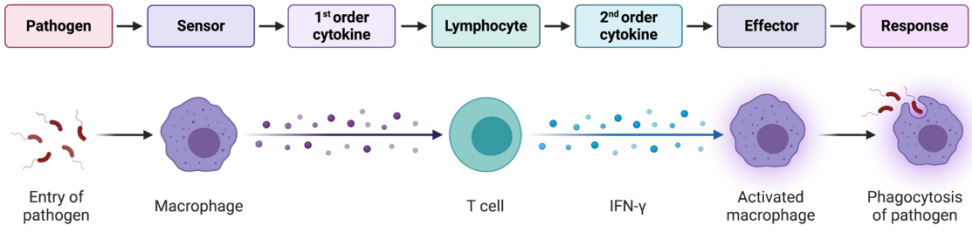

Figure 3. Summary of Immune System Feedback. Innate immune cells release pro-inflammatory cytokines in response to pathogens to activate adaptive immune cells. Adaptive immune cells then release cytokines to enhance the response of the innate immune system.

This thesis will focus on the inflammatory response, the primary mechanism of the innate immune system.

I.2 Inflammatory Response

The inflammatory response represents the primary defense mechanism of the innate immune system against a pathogenic threat [15, 16]. The inflammatory process occurs in multiple steps, including the recruitment of cells, the release of pro-inflammatory cytokines, the intracellular uptake of pathogens by phagocytes (phagocytosis), and the destruction of potentially damaging agents (**Figure 4**). Depending on the duration, the inflammatory response can be classified as acute or chronic.

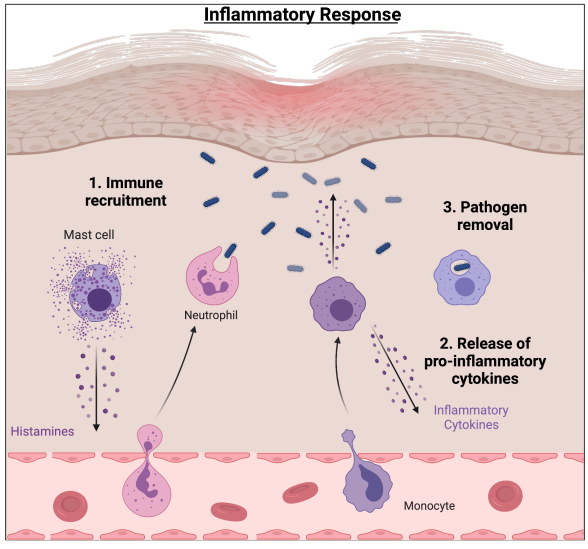

Figure 4. The Inflammatory Response. 1) The initial entry of pathogens leads to the recruitment of immune cells to the site of infection. 2) Macrophages and neutrophils release inflammatory cytokines and histamines, which serve to recruit more immune cells. 3) Immune cells eliminate pathogens as infiltrating monocytes differentiate into macrophages and release tissue healing factors. 4) After pathogen elimination, neutrophils and macrophages leave the site of inflammation and return to the bloodstream.

At the molecular level, the acute inflammatory response requires the orderly recruitment of plasma components and leukocytes (i.e., neutrophils, monocytes, basophils, and eosinophils) to the site of injury/infection (Stage 1) [15].

The initial recognition of infection by tissue-resident macrophages and mast cells leads to the production of a wide variety of inflammatory cytokines (i.e., tumor necrosis factor (TNF) and interleukin (IL)-1) and chemokines). These inflammatory mediators stimulate endothelial cells to express adhesion molecules (selectins) to promote the passage of leukocytes from the blood into the affected tissue (transmigration) (Stage 2) [17].

Neutrophils and macrophages then ingest and destroy pathogens within intracellular vesicles (Stage 3). Neutrophils become activated by direct contact with pathogens or by the action of cytokines secreted by tissue-resident cells when they reach the site of infection. Neutrophils release the cytotoxic content of their granules,

including reactive oxygen species and nitric oxide, to eliminate pathogens [18]; however, these potent effector molecules affect both pathogens and the host and induce unavoidable tissue damage.

A successful acute inflammatory response leads to the elimination of the infectious agent followed by a resolution phase that repairs the damage mediated by recruited and tissue-resident macrophages (Stage 4). An unsuccessful acute inflammatory response that fails to eliminate pathogens can prompt an ongoing inflammatory state (chronic inflammation) associate with additional tissue damage, which is the source of health problems such as, cardiovascular disease, atherosclerosis, type 2 diabetes, rheumatoid arthritis, and cancer [19-22].

Overall, the most critical components of the inflammatory response include inducers, sensors, mediators, and effectors (**Figure 5**) [23]. Inducers initiate the inflammatory response by activating specialized sensors to induce the synthesis of specific mediators that alter the function of affected tissues and organs (effectors of inflammation) so that they can adapt to and resolve the inflammatory state.

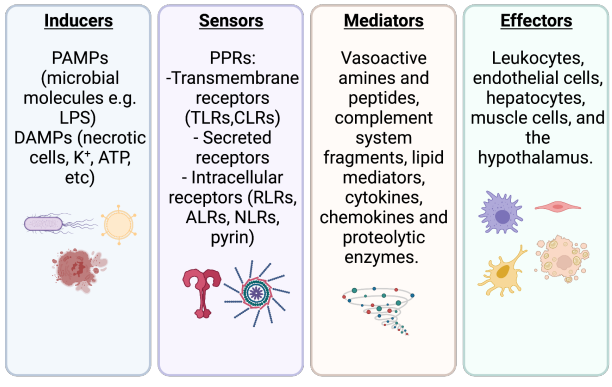

Figure 5. Principal components of the inflammatory response. Include inducers such as pathogen-associated molecular patterns (PAMPs) and damaged-associated molecular patterns (DAMPs); sensors such as Pattern recognition receptors (PRRs); mediators such as vasoactive amines and peptides, complement system, lipids, chemokines, cytokines, etc.; and effectors cells such as leukocytes, endothelial cells, hepatocytes, muscle cells and the hypothalamus.

I.2.1 Inflammation-inducing Agents (Inducers)

The innate immune system recognizes factors expressed on the surface of pathogens or molecules released by infected or damaged cells. Therefore, inflammation-inducing agents can be classified into two groups according to their origin with respect to the host: exogenous inducers and endogenous inducers [24, 25].

- **Exogenous inducers** include those with a microbial origin, such as pathogen-associated molecular patterns (PAMPs) and virulence factors, and those with a non-microbial origin, such as allergens, irritants, and toxic compounds. PAMPs, the most studied exogenous inducers, are evolutionarily conserved epitopes belonging to microorganisms (whether commensal or pathogenic) but absent on host cells [25, 26]. For example, phagocytes express receptors for bacterial endotoxin (also known as lipopolysaccharide or LPS) and peptidoglycans specifically present in the cell walls of many bacterial species.

- **Endogenous inducers** refer to metabolites released by damaged or necrotic cells, which are also called damaged-associated molecular patterns (DAMPs). Stress, damage, or loss of tissue homeostasis can prompt the release of said metabolites, which functions to activate the immune system [27]. The induced release of intracellular DAMPs by immune cells initiates the inflammatory response, with examples including heat shock proteins, purine metabolites such as ATP or uric acid, or mitochondrial DNA.

The effector mechanisms of the inflammatory response elicited by PAMPs and DAMPs include the recruitment of macrophages and neutrophils, the production of pro-inflammatory cytokines, and the induction of adaptive immune responses. The receptors of innate immunity that recognize PAMPs and DAMPs are the previously discussed PRRs [24].

I.2.2 Pattern Recognition Receptors (PRRs) (sensors)

Studies have identified distinct families of PRRs that recognize a wide variety of PAMPs and DAMPs [28]. The receptors of the innate immune system that act against pathogens and damaged cells are expressed in cell types that include phagocytes, dendritic cells, lymphocytes, endothelial cells, and epithelial cells. These PRRs can be located in different cell compartments, including the cell surface, the endoplasmic reticulum, or the cytosol. They can be classified into distinct protein families depending on their location [24, 29-33]:

I.2.2.A Transmembrane Receptors

Transmembrane receptors located in the cell plasma membrane and the membranes of endosomes and lysosomes recognize DAMPs and PAMPs in the extracellular environment. These receptors include the toll-like receptors (TLRs) and C-type lectin receptors (CLRs) [10, 31].

TLRs comprise a large family of receptors that recognize specific pathogen fragments. While TLRs present on the cell surface recognize extracellular microbe-associated factors, they are also present and can be activated on intra-cellular endosomes (**Figure 6**). Induced TLR signaling activates transcription factors that stimulate the expression of genes encoding cytokines, enzymes, and other proteins involved in the antimicrobial functions of innate cells (e.g., activated phagocytes). Nuclear factor κB (NFκB), a crucial transcription factor activated by TLRs, promotes the expression of various pro-inflammatory cytokines, endothelial adhesion molecules, and interferon regulatory factors (IRFs), among other factors [34].

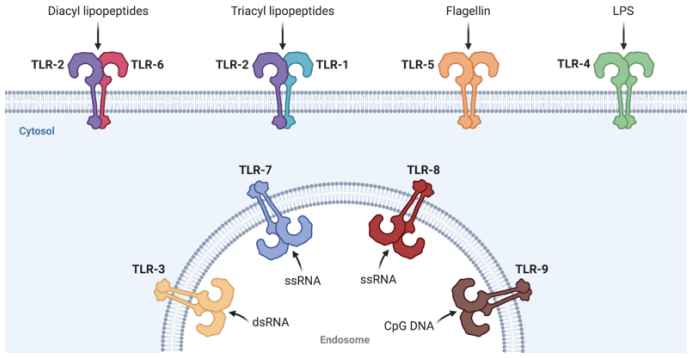

Figure 6. Detection of PAMPs and DAMPs by Toll-Like Receptors (TLRs). Several TLRs recognize different fragments of pathogens. TLRs located on the cell surface include TLR1, 2, 4, 5, and 6. TLRs located in the microbial-ingesting endosome include TLR-3,7,8, and 9.

I.2.2.B Secreted Receptors

The concentration of released receptors in tissue fluids increases during the acute inflammatory response. In general, released receptors activate the complement cascade to facilitate the opsonization of microorganisms and their subsequent phagocytosis by macrophages. Examples of secreted receptors include collectins, pentraxins, and peptidoglycan recognition proteins [31].

I.2.2.C Intracellular Receptors

Intracellular receptors allow the detection of infections or tissue damage in the cytoplasmic environment [27, 31] and include the retinoic acid-inducible gene-I (RIG1)-like receptors (RLRs), the pyrin receptor, the absent in melanoma 2 (AIM2) type receptors (ALRs), and the nucleotide-binding and oligomerization domain (NOD)-like receptors (NLRs) [35, 36]. The intracellular receptor family promotes the formation of a multiprotein complex called the inflammasome, an essential mediator for the inflammatory response.

NLRs constitute a major group of intracellular PRRs (23 cytosolic receptors in humans) that recognize DAMPs and PAMPs in the cytoplasm. All NLRs share structural features, including a C-terminal leucine-rich repeat (LRR) domain for ligand recognition, a central nucleotide-binding domain (NACHT domain) for protein oligomerization, and five variable N-terminal effector domains that propagate the

inflammatory signal (**Figure 7)** These N-terminal effector domains are used to subdivide NLRs into five groups [37] (**Table 1**).

Table 1. Classification of the NLR protein family

Subfamily	Domain	Members
NLRA	Acidic transactivation domain	CIITA
NLRB	Baculoviral inhibitory repeat-like domain	NAIP
NLRC	CARD domain for caspase recruitment and activation	NOD-1, NOD-2, NLRC3/4/5
NLRP	PYD or pyrin domain	NLRP1-14
NLRX	Contains a domain that does not show homology	NLRX1

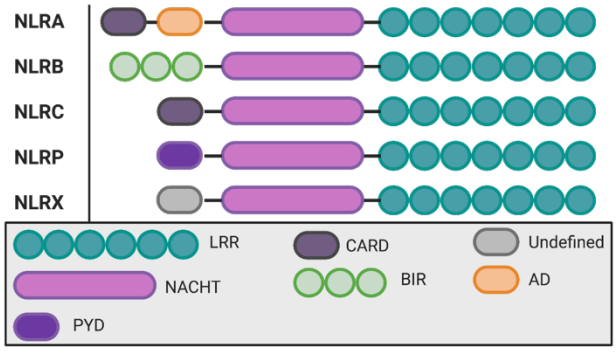

Figure 7. Structural Classification of the NLR Protein Family. All NLRs share structural features, including a C-terminal leucine-rich repeat (LRR) domain, a central nucleotide-binding domain (NACHT domain), and five variable N-terminal effector domains - CARD, BIR, AD, PYD, and an undefined domain.

Recent studies have begun to decipher the signaling pathways involved with NLR activation [29, 33, 38]. While NOD-1, NOD-2, or NLRX-1 can activate transcription factors that induce the transcription of genes involved in an inflammatory response (e.g., NF-κβ or IRF), receptors such as CIITA function as part of adaptive immunity and induce the expression of MHC molecules. Notably, the inflammasome formation represents the primary function of NLRs following the detection of their corresponding ligand in the cytoplasm [28]. Inflammasomes activate pro-caspase-1, prompting the release of the pro-inflammatory cytokines IL-1β and IL-18 to the extracellular environment [15]. **Section I.3** of this introduction will discuss inflammasomes in greater detail due to their importance as mediators of the inflammatory response and their implication in numerous diseases.

The innate immune system also contains several circulating molecules that recognize and provide defense against microbes.

I.2.3 Mediators of Inflammation

The recognition of PAMPs/DAMPs by a corresponding receptor activates the inflammation signaling pathway and induces the activity of the various cell types involved (e.g., neutrophils, macrophages, dendritic cells, mast cells, and platelets). These immune cells release inflammatory mediators (e.g., vasoactive amines and peptides, complement system fragments, lipid mediators, cytokines, chemokines and proteolytic enzymes) to modulate the target area's vasculature, recruit and activate another immune cells to combat the damage or infection [16]

I.2.4 Effectors of Inflammation

Effector components include endothelial cells, hepatocytes, leukocytes, muscle cells, and the hypothalamus. Effectors cells orchestrate a coordinated response to resolve the inflammatory event and promote homeostasis within the affected tissue [15, 39].

As a crucial component of the inflammatory response and due to their implication in numerous diseases, this thesis will focus on the study of inflammasomes.

I.3 Inflammasomes

The term "inflammasome" was originally coined by Martinon et al. [40] in 2002 to designate a multiprotein complex present in the cytoplasm of activated immune cells, responsible for the proteolytic activation of pro-inflammatory caspases, which drives subsequent systemic immune responses and inflammation. Since then, research on the inflammasome has provided information not only on its composition, but also on its activation mechanisms and its implication in the development of pathologies.

Inflammasomes are essential macromolecular complexes of the innate immune system that detect endogenous or exogenous stimuli by their PRRs [41, 42]. They coordinate inflammatory responses and the maturation and release of pro-inflammatory cytokines such as IL-1β and IL-18 [43]. There are different types of inflammasomes. The PRR family member involved provides the name for the specific inflammasome complex, such as NLRP1, NLRP3, NLRC4, NLRP6, NLRP7, NLRP12, AIM2, IFI16, pyrin, RIG-1, etc. Which inflammasome activates depends on the inflammatory stimulus.

Expression of inflammasome components were initially described in myeloid cells, such as macrophages, dendritic cells, and neutrophils [44]. Today, it has been elucidated that inflammasomes can also assemble into additional cell types, including B and T cells, keratinocytes in the skin, enterocytes and goblet cells in the intestine, hepatocytes in the liver, pigment epithelial cells in the retina, as well as neurons, astrocytes, and microglia in the central nervous system [45].

At structural level, inflammasomes comprise **sensor proteins**, which are specific cytosolic PRRs that respond to either microbe-derived PAMPs or DAMPs (e.g., NLRs, ALRs, RIG-1, or pyrin receptors), the Apoptosis-associated Speck-like Protein Containing CARD (ASC) **adaptor protein**, present in the vast majority of inflammasomes, and the **protease effector** pro-caspase-1 [46, 47]. Importantly, the last

common signaling of the inflammasome is the activation of inflammatory caspases [29]. Pro-caspase-1 together with pro-caspase-4 and pro-caspase-5 or murine pro-caspase-11 (depending on the activation pathway) are the pro-inflammatory caspases, directly or indirectly activated by the inflammasome that finally induce the maturation of the pro-inflammatory cytokines IL-1β and IL-18. [48]. Depending on the caspase stimulation pathway and the activated caspases, the inflammasome activation can be classified as canonical or non-canonical:

- **Canonical Inflammasomes activation:** Canonically-activated inflammasomes recruit and process **pro-caspase-1** into its catalytically active form (caspase-1) to induce the maturation of IL-1β and IL-18.
- **Non-canonical Inflammasome Activation**: Non-canonical activation of the inflammasome involves the recruitment and processing of murine **pro-caspase-11** or human **pro-caspase 4/5** into its catalytically active form in response to intracellular LPS [47].

In the canonical pathway, the presence of inflammatory stimuli in the intracellular environment prompts sensor receptor protein oligomerization and the recruitment of the ASC protein, in ASC-dependent inflammasomes. Inflammasome sensors typically contain a pyrin domain (PYD) or a caspase recruitment and activation domain (CARD). Upon oligomerization, inflammasome sensors engage multiple molecules of the adapter ASC, which is composed of 2 domains, the PYD (ASC^{PYD}) and the CARD (ASC^{CARD}). Depending on the recruitment domain of the sensor, ASC is involved through homotypic PYD-PYD, or CARD-CARD interactions. The initial interaction of ASC with the sensor protein triggers a process of ASC nucleation and the formation of large filaments (similar to prions), which serve as a platform for pro-caspase-1 recruitment [49-51] (**Figure 8**). ASC oligomers nucleate filaments of ASC^{PYD}, which are cross-linked by ASC^{CARD}-ASC^{CARD} interactions. The filaments, supported by the self-association of ASC^{PYD} domains, provide a rigid structural core, while ASC^{CARD} domains are exposed on the surface [52]. ASC^{CARD} domains arising from PYD-based filaments have been shown to further stabilize the filaments and condense them into specks [52]. This is believed to be accomplished through intra- and interchain

interactions between the projected ASC^{CARD} domains that serve to bind different ASC fibrils [53].

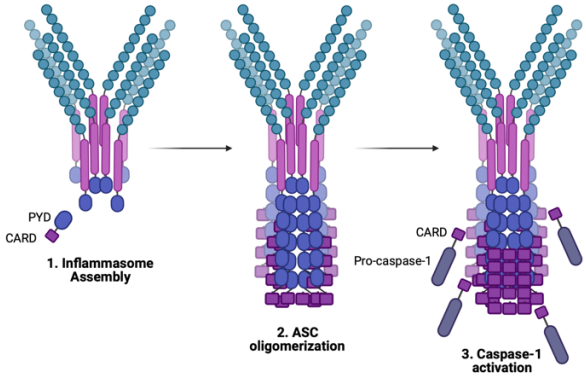

Figure 8. ASC oligomerization for caspase-1 activation. Upon inflammasome assembly (step 1), multiple molecules of the adapter ASC are recruited for sensor receptor binding. The binding of ASC with the receptors triggers a process of ASC oligomerization and the formation of large filaments (step 2), which serve as a platform for pro-caspase-1 recruitment and caspase-1 activation (step 3).

Finally, the interaction of ASC filaments and pro-caspase-1 prompts the proximity-induced processing of pro-caspase-1 into caspase-1 and the subsequent processing and release of the mature forms of IL-1β and IL-18 [54]. Caspase-1 also cleaves the pore-forming protein GSDMD into an N-terminal (GSDMD-N) and a C-terminal (GSDMD-C) fragment. The N-terminal fragment inserts into the cell membrane, generating approximately 20 nm membrane pores, which results in cell swelling and lysis to trigger pyroptotic cell death [55-57]. Pyroptosis is a lytic form of programmed cell death in response to the detection of pathogens or danger signals derived from the host. It is characterized by cellular inflammation, membrane rupture and subsequent release of inflammatory compounds into the extracellular space [58]. Pyroptotic pores also function as channels for the release of cytosolic contents, including pro-inflammatory cytokines such as IL-1β [59].

In the non-canonical pathway, the murine pro-caspase-11 or human pro-caspase 4/5 function as both sensor and effector molecules and directly detect intracellular LPS released from gram-negative bacteria by their CARD domains [56, 60]. Once activated Caspase-11 or 4/5 prompt the cleavage of the pore-forming protein GSDMD and trigger a secondary activation of the canonical NLRP3 for cytokine release. (**Figure 9** depicts the canonical and non-canonical activation of the NLRP3 inflammasome, used as an example as the most studied inflammasome.)

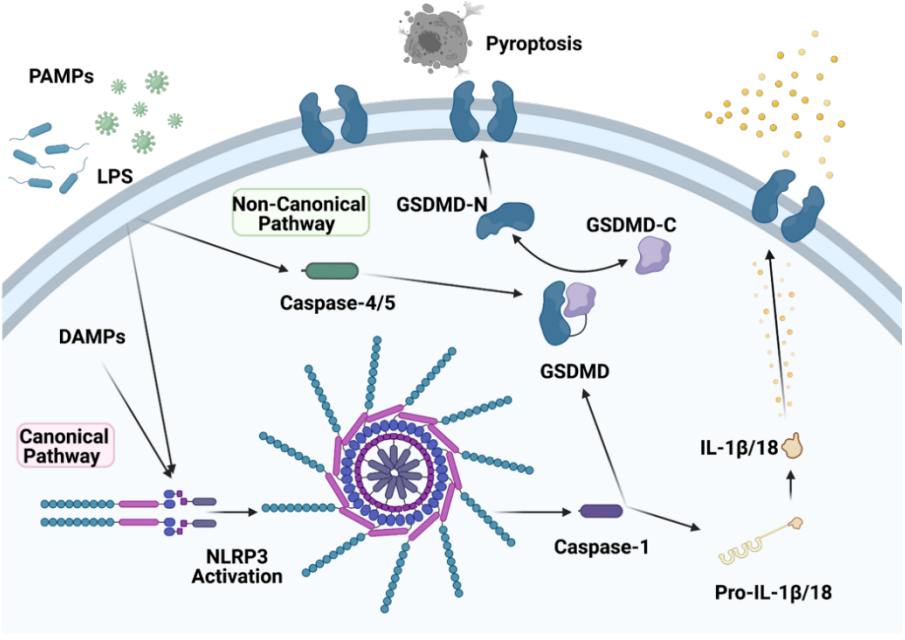

Figure 9. Canonical and Non-Canonical Activation of the NLRP3 Inflammasome. Upon canonical inflammasome activation, the inflammasome sensors initiate the inflammasome assembly by recruiting and ASC and Pro-caspase-1. The assembly of non-canonical inflammasomes involves murine pro-caspase-11 or human procaspase−4/5. Consequently, the active caspase-1 leads to the maturation and secretion of inflammatory cytokines IL-1β and IL-18. The active caspase-1 or caspase-11/4/5 triggers the cleavage of GSDMD, which can either cause pyroptosis or activate the inflammasome complex.

1.3.1 Inflammasomes as therapeutic targets

The inflammatory process triggered by the activation of inflammasomes represents a rapid response of the innate immune system to ensure the removal of harmful stimuli and repair damaged tissue [61]. Furthermore, inflammasome activation

prevents the spread of infections or the development of tumors and allows the development of an adaptive immune response [62]. However, inflammasome dysregulation has been linked to the development of several pathologies, as detailed in **section I.4.2** of this introduction [63].

Therefore, the regulation of inflammasome activity and the therapeutic targeting of inflammasome signaling and components constitute promising areas of basic and translational research.

One of the key points in controlling inflammasome-mediated inflammatory signaling is the regulation of the ASC oligomerization process. Inflammasome signaling has been associated with the all-or-nothing type of responses, whose limiting step is the arrangement of the supramolecular organizing centers, or ASC specks [64]. ASC specks appear as micron-sized points in the perinuclear region after inflammasome induction [65]. Interestingly, it has been observed that the process of ASC specks formation occurs in minutes [66] supporting the all-or-nothing response hypothesis: either the cell forms a speck followed by a strong inflammatory response or the cell remains inactive. Furthermore, it has been reported that ASC specks can be released from cells to spread inflammation in the extracellular space [67]. Importantly, overexpressed ASC in cells or purified ASC *in vitro* rapidly oligomerizes and aggregates in the absence of inflammasome sensors [68]. This indicates that both the expression levels of ASC, as well as its oligomeric state, must be strictly controlled to avoid aberrant inflammatory responses with well-documented pathological effects [45]. Moreover, the study of ASC as a molecular target is of great importance in those diseases that involve the activation of more than one inflammasome, so that inhibiting ASC would entail direct action on different inflammasomes at the same time.

In this thesis, we will focus on the study of the ASC protein, present in most inflammasomes, for the regulation of the inflammasome-mediated inflammatory response.

I.4 ASC adapter protein

ASC adapter protein (Apoptosis-associated speck-like protein containing a CARD) was initially identified by Masumoto et al. in 1999 [69] as a protein that formed specks-shaped aggregates in HL-60 cells when treated with retinoic acid or etoposide for the induction of apoptosis. Furthermore, in 2002, Srinivasa et al. described the ASC protein as a caspase-1-activating adaptor in the NLRP1 inflammasome [70].

At structural level, ASC is a 22kD and 195 amino acid protein encoded by the PYCARD gene [71]. It contains two members of the death domain superfamily: A N-terminal PYD domain (amino acids M1 to T89), and a C-terminal CARD domain (amino acids H113 to S195). Moreover, it is composed by a central region rich in glycine and prolines (H90-L112) (**Figure 10**) [72].

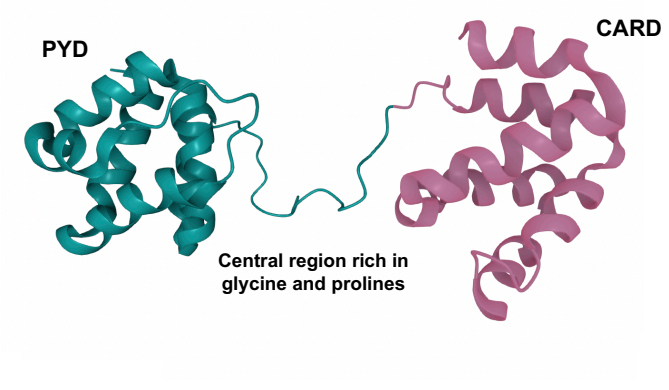

Figure 10. Structure of full-length human ASC (Apoptosis-associated speck-like protein containing a CARD). (Access number in PBD: 2KN6)

ASC interacts with other proteins via homotypic interaction by its PYD and CARD domains [73]. Four different isoforms of ASC have been described, only those that keep the PYD domain intact are functional for the formation of the inflammasome and the activation of pro-caspase-1 [74]. Structural and functional studies of the ASC protein have been limited due to its tendency to aggregate under physiological conditions. Finally, the protein structure was resolved by NMR in solution at acidic pH [72]. This study demonstrated that PYD and CARD domains are structurally

independent, while the proline-rich central region is very flexible, suggesting that it functions as a hinge to facilitate protein aggregation.

In unstimulated cultures, ASC presents a diffuse subcellular localization throughout the nucleus [75]. However, in the presence of an inflammatory signal, ASC is rapidly redistributed to the cytosol where it interacts with the sensor receptors proteins to form insoluble protein aggregates formed by ASC dimers and oligomers, with the aim of recruiting and activating pro-caspase-1. Therefore, it is widely recognized that ASC aggregate formation represents the active form of ASC-dependent inflammasomes [76]. Importantly, the generation of ASC knock-out mice ($ASC^{-/-}$) has represented a very valuable tool to elucidate the role of ASC in the secretion of pro-inflammatory cytokines and in pyroptosis cell death in response to the activation of different inflammasomes [77]. $ASC^{-/-}$ mice showed alterations in the processing of pro-caspase-1, and in the secretion of pro-inflammatory cytokines in response to AIM2, NLRP-3 and NLRC-4 inflammasomes activation.

At functional level, apart from its role in the formation of the inflammasome for the processing and activation of pro-caspase-1, and in the amplification of the inflammatory signal, a relevant role of ASC has been described in other cell signaling pathways such as in programmed cell death by apoptosis or in the activation of the NF-κβ signaling [45].

Regarding the role of ASC in the apoptotic process, functions have been described both in the extrinsic pathway of apoptosis and in the intrinsic or mitochondrial pathway. With regard to the extrinsic pathway, it has been described that ASC is capable of directly activating pro-caspase-8 [78] and causing the activation of the Bid protein for the execution of apoptosis. Regarding the intrinsic pathway of apoptosis, a direct interaction between ASC and BAX mediated by the PYD domain of ASC has been described [79], as well as a transient interaction between p53 and ASC in keratinocytes acting as a tumor suppressor gene.

In addition to the intracellular role of ASC specks, these complexes can also be found in the extracellular space. Several studies have reported that ASC particles are released by inflammasome-activated cells into the extracellular space, where they

continue to recruit and activate pro-caspase-1, in addition to catalyzing the maturation of IL-1β [67].

I.4.1 ASC-dependent inflammasomes

The most studied ASC-dependent inflammasomes are the NLRP1, NLRP3, NLRC4, AIM2, and pyrin inflammasomes (**Figure 11**).

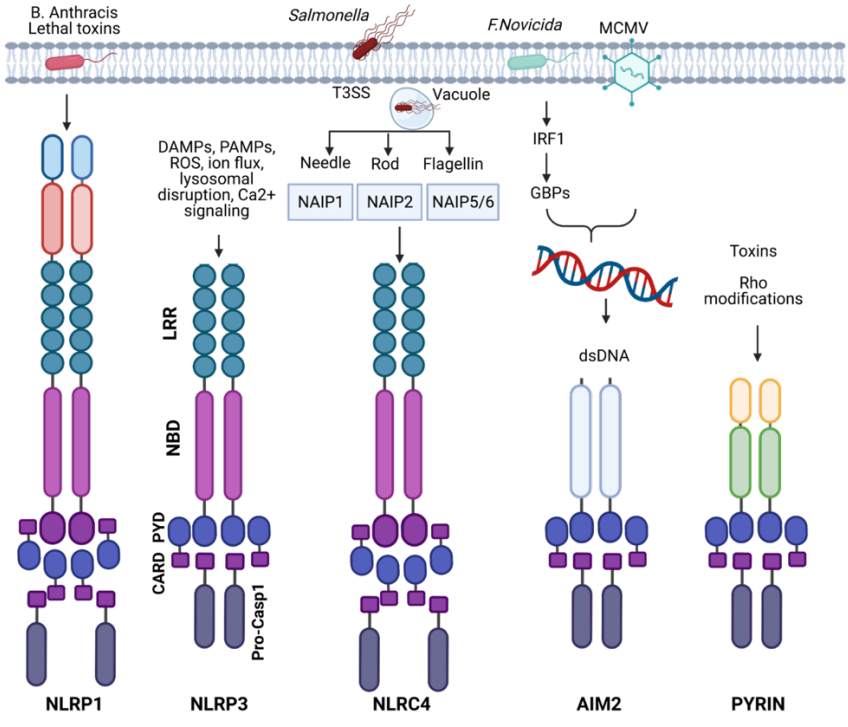

Figure 11. ASC-dependent inflammasomes activation and structure. ASC-dependent inflammasomes activation occurs through various stimuli, including microbiome-derived signals (e.g., bacteria, fungi, parasites, and viruses) and host-derived signals (e.g., ion flux, mitochondrial dysfunction, ROS, and metabolic factors).

NLRP1

The human NLRP1 (165 kDa) or murine NLRP1b (140 kDa) inflammasome was the first inflammasome described in the literature. Mouse NLRP1b activates caspase-1 in response to the lethal toxin secreted by *B. anthracis* [80], the bacterial wall component of gram-negative muramyldipeptide (MDP) and diverse picornaviruses [80].

As mentioned before, NLR proteins, except for NLRP1, have a tripartite domain organization containing a N-terminal PYD domain to bind ASC; a NACHT domain in the middle; and a C-terminal LRR domain which binds to PAMPs or DAMPs. However, human NLRP1 and murine NLRP1b are characterized by containing a C-terminal CARD domain, and a unique function-to find domain (FIIND) [29] The presence of these two domains initially suggested that the NLRP1 inflammasome could activate caspase-1 through the CARD domain without recruiting ASC. Currently, most studies indicate that caspase-1 can connect directly to the CARD C-terminal domain, but only in murine NLRP1b [29]. Regarding human NLRP1, Finger et al. [81] demonstrated that the activity of human NLRP1 depends on the binding of ASC to the C-terminal CARD domain.

NLRP3

The NLRP3 inflammasome (118 kDa) is the most studied and recognizes a wide range of pathogens (including gram-positive and gram-negative bacteria) [60, 82]. There is scientific consensus that the NLRP3 inflammasome requires a double stimulation signal for activation. The first signal, called the “priming” signal, triggers the activation of the transcription factor NF-κβ for the initiation of the expression and synthesis of pro-inflammatory proteins, including NLRP-3 and pro-IL1β; while the second signal, called the “activation” signal, causes the oligomerization of NLRP-3, the recruitment of ASC and the activation of pro-caspase-1. In the activation signal, NLRP-3 deubiquitination is essential for inflammasome formation [83]. Moreover, several molecular and cellular activation mechanisms have been proposed:

a) Ion fluxes: Ion fluxes, including K+ efflux, Ca2+ signaling, Na+ influx, and chloride efflux, have been identified as critical events in NLRP3 inflammasome activation [83]. For example, Pore-forming toxins such as nigericin, aggregating particles such as silica or calcium pyrophosphate crystals, as well as ATP through the activation of the P2X7 receptor, cause a reduction in intracellular potassium concentration prior to activation of the inflammasome [83].

b) Lysosomal disruption: Phagocytosis by macrophages of certain particles and crystals such as monosodium urate, calcium pyrophosphate, silica, or aluminum, causes the activation of the NLRP-3 inflammasome in a flow-dependent manner of intracellular K + but independent of the P2X7 receptor. In this context, it has been described that lysosomal destabilization is essential for the activation of the inflammasome [84].

c) Mitochondrial dysfunction and damage: Several inflammasome agonists such as ATP or nigericin are responsible for a drop in the mitochondrial membrane potential, as well as oxygen consumption, which produces the release of mitochondrial DNA (mtDNA) into the cytoplasm. The mtDNA can interact directly with NLRP-3 causing oligomerization and formation of the inflammasome. The translocation mechanism of NLRP-3 and ASC to this organelle in response to inflammatory stimuli occurs through microtubule-mediated transport [85].

NLRC4

The NLRC-4 (115 kDa) protein was initially identified by its homology with the apoptosis intrinsic pathway protein Apaf-1 (Apoptotic protease-activating factor-1) and its ability to bind and activate Pro-caspase-1 [86]). It lacks a PYD domain, and instead contains a N-terminal CARD domain.

Pathogenic activators of the NLRC4 inflammasome are mainly derived from Gram-negative bacteria such as *Salmonella*, *Legionella, Shigella*, and *Pseudomonas*, which possess flagellin, or a type III (T3SS) or type IV (T4SS) secretion system rod proteins that are recognized by NLR family of apoptosis inhibitory proteins (NAIP) [87]. While in humans only one NAIP protein has been described that binds to the

needle structure of the type III bacterial secretion system, in mice there are four different proteins, which recognize the needle structure (NAIP1), the basal rod structure (NAIP2) and bacterial flagellin (NAIP5/6), respectively [87] (**Figure 10**). Upon detection of these pathogenic ligands, NAIPs interact with NLRC4 and induce its oligomerization. An important aspect of NLRC4 activation is its ability to interact directly with Caspase-1. The CARD domain of NLRC4 can interact with the CARD domain of pro-Caspase-1, allowing NLRC4 to directly activate the protease. However, NLRC4-induced Caspase-1 activation is enhanced in cells by the presence of the ASC adaptor. Activated NLRC4 associates with ASC and colocalizes with ASC-containing Speck upon activation by Salmonella [86]. These findings are consistent with the ability of ASC to potentiate NLRC4-induced CASP1 activation.

AIM2

AIM-2 (39kDa) recognizes cytosolic dsDNA released from various bacterial species, including *Francisella novicida*. The inflammatory response of the AIM-2 inflammasome is not specific for viral or bacterial DNA, but also synthetic DNA such as the poly sequence (poly dA: dT), or random sequences can activate this inflammasome. Regarding the activation mechanism of the AIM-2 inflammasome, the HIN200 domain is responsible for the recognition and binding of DNA. While the HIN domain binds to DNA, activated AIM2 recruits ASC, which in turn recruits caspase-1 to form the complete AIM2 inflammasome [88].

PYRIN

Rho guanosine triphosphatase (Rho GTPases) regulate actin dynamics [89] and several pathogens modulate Rho GTPase activity as an strategy to suppress host immune responses such as phagocytosis. [35]. Pyrin (95 kDa) recognizes this Rho GTPase-inactivation, probably sensing cytoskeletal abnormalities and induces inflammasome activation as defense mechanism. Importantly, Pyrin is encoded by MEFV gene that is mutated in patients with familial Mediterranean fever (FMF), one of the most common hereditary autoinflammatory syndromes [35].

Homology studies have identified five different domains within the pyrin protein: 1) The N-terminal PYD domain, for the binding of the ASC protein. 2) the domain of transcription factor bZIP and of two superimposed nuclear localization signals. 3) The B-box and 4) the α-helical spiral domain that may play a role in the oligomerization of pyrine. 5) The C-terminal domain B30. 2, of particular importance since most FMF-associated mutations are clustered in this domain. [35].

I.4.2. ASC-dependent Inflammasomes in disease

A dysregulation of ASC-dependent inflammasomes has been implicated in the pathophysiology of several conditions (**Figure 12**) such as cardiovascular, neurodegenerative, autoimmune and metabolic diseases. Moreover, the role of ASC-dependent inflammasomes has also been described in cancer, [90] and in the development of severe acute respiratory syndromes in response to viral infections [91-94] [83, 95-97]. We will briefly discuss the evidences for the participation of ASC-dependent inflammasomes on these diseases.

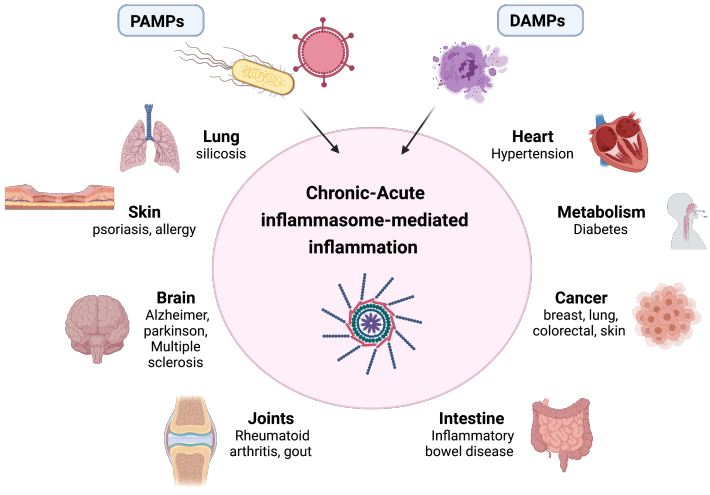

Figure 12. Inflammasome in disease. The dysregulation of the inflammasome is implicated in the development of several diseases affecting different pathologies of heart, lungs, metabolism, intestine, joints, brain, skin, and cancer.

Cardiovascular Diseases

Multiple studies have demonstrated a role for ASC-dependent inflammasomes in atherosclerosis [98], Myocardial Infarction, Heart Failure [99], and Abdominal Aortic Aneurysms (AAA) [100].

To illustrate the relevance of inflammasome in these diseases we will focus in atherosclerosis, as an example where several evidences have accumulated that demonstrate the role of the inflammasome in disease development. Historically, IL-1β was one of the first cytokines involved in the pathogenesis of atherosclerosis [101]. In fact, later studies demonstrated that human atherosclerotic lesions display an increase in the expression of inflammasome components such as NLRP3, ASC, caspase-1, and the downstream effector molecules (IL-1β and IL-18) compared to healthy arteries [102]. Moreover, a recent paper has reported an increase on the expression of other inflammasome receptors (NLRP1 and NLRC4) in atherosclerosis patients when compared to healthy controls [103]. Furthermore, Lüsebrink et al. [104] showed that in the ApoE-/- mice, a classic mice model to study cardiovascular and respiratory diseases, AIM2 stimulation promotes the development of atherosclerotic plaques, the disruption of endothelial function, higher production of ROS in the vessels, and a decrease in reendothelialization.

Neurodegenerative diseases

In neurodegenerative diseases, studies have demonstrated a role for ASC-dependent inflammasomes in Alzheimer's disease (AD), Multiple Sclerosis (MS) and Amyotrophic Lateral Sclerosis (ALS) [105].

Focusing on AD, NLRP3 inflammasome activation is described as a major contributor to neuroinflammation [105]. However, it seems, as in other diseases, that more than one inflammasome contributes to disease development. Kaushal et al. [106] demonstrated that NLRP1 and ASC mRNA was increased in AD neurons of the human brain cortex samples compared with non-AD neurons. The implication of the AIM2 and NLRC4 inflammasomes in AD has also been demonstrated; for example, Wu et al. [107] reported that AIM2 Inflammasome loss in the 5XFAD AD mouse model (a mice

model that express human b-amyloid precursor protein (APP) and Presenilin 1 (PSEN1) transgenes with a total of five AD-linked mutations), mitigates Aβ deposition and microglial activation. Meanwhile, Saadi et al. [108] observed a significant increase in the expression of NLRC4 inflammasome components, ASC, and IL-1β in an induced AD Wistar rat model. Importantly, Venegas et al. [109] demonstrated that the intra-hippocampal injection of ASC specks in transgenic double-mutant APP/PS1 mice resulted in the spread of amyloid-β pathology when compared to the contralateral hippocampus administered with vehicle control. On the contrary, homogenates from brains of ASC-knockout (ASC−/−) APP/PS1 mice injected with ASC specks displayed the reduced spread of amyloid-β pathology compared to APP/PS1 mice. Moreover, co-application of an anti-ASC antibody blocked the increase in amyloid-β pathology in APP/PS1 mice. Altogether, these studies reinforce the role of ASC in AD development.

Autoinmune diseases

Regarding autoimmune diseases, the role of ASC has been demonstrated in different disorders such as psoriasis, lupus, Rheumatoid Arthritis (RA) and peritonitis [110]. For example, Forouzandeh et al. [111] demonstrated that ASC, and not caspase-1, was increased in the serum of patients with psoriasis compared to healthy individuals. Dombrowsky et al. [112] showed increased AIM2 expression in keratinocytes from psoriasis patients compared to healthy donors. Moreover, Ekman et al. [113] reported that NLRP1 inflammasome complex genetic variations are related to elevated vulnerability to psoriasis. In the same line of evidence, peritonitis is characterized by the inflammation of the peritoneum, a membrane that lines the inner abdominal walls and the organs within the abdomen, which usually occurs due to a bacterial or fungal infection [114]. Importantly, it has been reported that during peritonitis, the peritoneal membrane undergoes structural and functional alterations that are mediated by NLRP3-IL-1β pathway [114].

Metabolic diseases

Regarding Metabolic diseases, the role of ASC has been demonstrated in different metabolic disorders such as Diabetes, or Inflammatory Bowel Disease (IBD),

where strong upregulation of different ASC-dependent inflammasomes, such as, AIM2, IFI16 and NLRP1, has been reported in the mucosa of patients with active IBD [115].

Focusing on Diabetes, several studies using genetically modified mice that lack inflammasome components NLRP3, ASC, and caspase-1 provided initial evidence that activation of the NLRP3 inflammasome is a key mechanism that induces metabolic inflammation and insulin resistance [116]. Moreover, pre-clinical studies have shown that the genetic deletion of NLPR3 and ASC in high-fat diet fed mice results in improved glucose tolerance and enhanced insulin sensitivity [116]. In addition, increased levels of other ASC-dependent inflammasomes such as AIM2 or NLRP1 have been associated with diabetes [116].

Viral infections

Inflammasome dysregulation has been related with severe acute respiratory syndromes in response to viral infections [117]. Interestingly, studies of severe acute respiratory syndrome coronavirus-2 (SARS-CoV-2) indicate that disease severity correlates with inflammatory responses, in which ASC may play a role [117]. Rodrigues et al. [118] reported that monocytes from SARS-CoV-2 infected patients showed increased ASC specks formation, as well as NLRP3 inflammasome activation and LDH release compared to monocytes from healthy donors. The authors also demonstrated that treatment with MCC950, a specific NLRP3 inhibitor, reduced NLRP3 formation in monocytes; however, MCC950 failed to inhibit ASC specks formation and LDH release, a feature that supports the hypothesis that other ASC-dependent inflammasomes may also be activated by SARS-CoV-2.

Cancer

The role of the inflammasome in tumor progression is closely linked to the concept of inflammatory tumor microenvironment (TME). TME is now recognized as an important participant or a regulator of all stages of tumor development, and is generally understood as those elements spatially located in the vicinity of the tumor that significantly influence cancer development and progression [119-124].

The concept of TME originated in 1863 when Virchow proposed the relationship between inflammation and cancer after observing that infiltrated immune cells reflect the site where cancer lesions appear in inflamed tissue [125]. In 1889, Paget presented the theory of "soil and seed" [126], which postulates that every cancer cell or “seed" required a suitable microenvironment or "soil" to grow and spread [127, 128]. In 2011, Hanahan and Weinberg expanded their proposed hallmarks of cancer from six to ten (**Figure 13**), and in doing so, recognized the emerging role of the tumor-promoting inflammation in the TME [129, 130].

Importantly, tumor cells cooperate closely with TME cells, such as stromal cells, immune cells, and Extracellular matrix (ECM) to promote chronic inflammation and immunosuppression [131]. This state of chronic inflammation is mainly mediated by the activation of the inflammasome in the immune cells of the TME and can alter the behavior of cancer cells and dictate the growth, and invasiveness of the tumor [131].

The role of inflammasome in the context of cancer can be seen as a double-edged sword because, while it can elicit and enhance an adequate immune response against cancer cells, a chronic inflammatory environment can promote pro-tumoral functions [132]. Chronic inflammation mediated by inflammasomes plays a central role in tumorigenesis by altering the microenvironment and leading to neoangiogenesis, tumor cell proliferation, and metastasis [132]. Importantly, in the same line of evidence, ASC may exert opposing functions depending on tumor type. The tumor-promoting role of ASC has been demonstrated in several types of cancer, such as breast, skin, or pancreatic cancer [133] while in other tumors such as colon cancer has a tumor suppressor role [134].

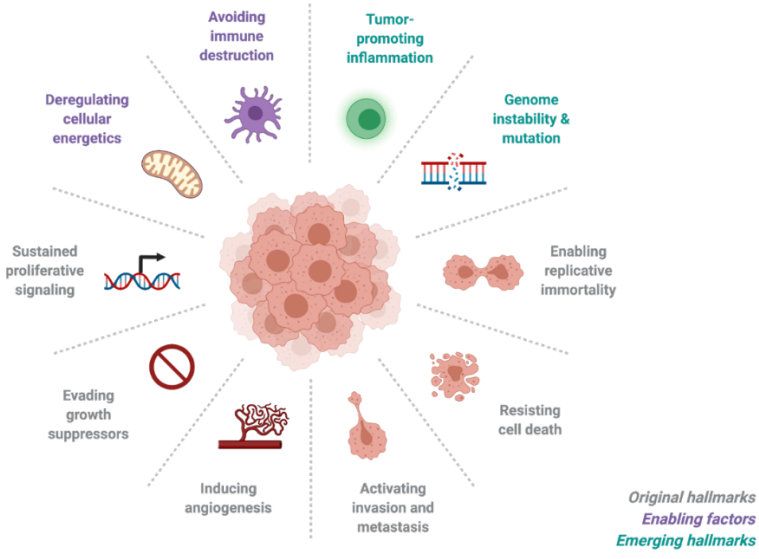

Figure 13. Hallmarks of Cancer. This illustration encompasses the ten hallmarks of cancer proposed by Hanahan and Weinberg in 2011.

In breast cancer accumulating evidence suggests that APCs, such as dendritic cells and macrophages, promote IL- 1β release in the breast TME. Moreover, breast cancer patients show highly increased serum levels of IL-1β which is dependent on tumor stage [135]. Further, significant correlation was noticed between IL-1β expression and subsequent development of metastasis [136]. Importantly, in breast cancer the expression of the inflammasome components, such as IL1β, IL18, NLRP3, ASC, and CASP1, is significantly up-regulated in most types of breast cancer compared to that in normal tissues [137]. Importantly, Guo et al. [138] demonstrated that the knock-out (KO) of various inflammasome components fostered a reduction in tumor size and metastasis in a mouse breast cancer model. The authors also reported that the NLRP3 inflammasome activation and IL-1β production promoted infiltration of myeloid cells, including tumor-associated macrophages (TAMs), to provide the inflammatory microenvironment known to support breast cancer progression. However, as we will see **in Chapter V** of this thesis, the role of the inflammasome may have contradictory functions in the progression of breast cancer.

In colorectal cancer, the overproduction of pro-inflammatory cytokines in the TME, such as tumor necrosis factor-α, IL-1β, and IL-17A, is closely associated with

the development of colitis-associated colorectal cancer. However, inflammasomes play a dual role in the development of colorectal cancer. In fact, in a mouse model of colitis, mice deficient in inflammasome components were highly susceptible to the development of colorectal cancer, suggesting a tumor-suppressor role. Allen et al. also reported suppressive effects of ASC, caspase-1 and NLRP3 on acute and recurrent colitis showing that ASC and caspase-1 were essential for survival in a murine model of colitis-associated colorectal cancer [134]. Similarly, NLRC4 and NLRP6 in epithelial and hematopoietic cells of the colon were found to play a protective role in the development of colitis-associated colorectal cancer.

In lung cancer, the scenario is different, the expression of inflammasome components in lung cancer tissues does not differ much from that in normal lung tissues. However, the Canakinumab Anti-inflammatory Thrombosis Outcome Study (CANTOS) that investigated the use of canakinumab, (a monoclonal antibody targeting IL-1β), in high-risk patients with established atherosclerotic disease who had already survived a myocardial infarction [139], showed that among the 129 lung cancer cases in the 3.7-year follow-up period, the incidence of lung cancer was significantly less frequent in the groups that received canakinumab. In line with these evidences, other studies suggested tumor-associated macrophages are the main cellular sources of IL-1β secretion, and demonstrated that macrophage depletion alleviated the development of N-methyl-N-nitroso-urea-induced lung cancer [140].

In skin cancer, it is important to note that UV radiation, one of the widely recognized skin cancer promoters, is a powerful inducer of IL-1β. The most aggressive form of skin cancer is melanoma which is characterized by upregulation of several pro-inflammatory cytokines, including IL-6, IL-8, CCL5, and IL-1β [137]. In addition, expression of the inflammasome components, such as IL-1B, ASC, and caspase-1, was detected at higher levels in squamous cell carcinoma than in normal skin tissues [137].

I.4.3 Current therapeutics approaches for inflammasome inhibition

Considering the critical role of inflammasome in autoimmune syndromes, progression of multifactorial diseases, such as cancer, and microbial defense, the

therapeutical modulation of the inflammasome represents a potential powerful tool to improve patient's prognosis in several diseases.

Current strategies that aim to avoid the consequences of pathological inflammasome activation include the inhibition of the inflammatory cascade upstream inflammasome formation (indirect inhibitors), selective inhibitors of inflammasome components (direct inhibitors), or inhibitors of inflammasome products [83, 141, 142]. **Table 2** depicts the current strategies followed for inflammasome inhibition.

As regards to downstream inhibition of inflammasomes, IL-1β targeted therapies have been stablished for the treatment of several autoimmune diseases. The three approved biologics are anakinra, canakinumab and rinolacept and they act by interrupting the inflammatory signaling cascade by either directly binding to IL-1β and IL-1α or to the interleukin 1 receptor 1 (IL-1R1). On the contrary, the development of compounds targeting caspase-1 have encountered some difficulties due to toxicity, reduced solubility, or low efficacy amongst others and thus, they are not being used in clinics. Another downstream target of great interest is the pore-forming molecule GSDMD. However, despite some interesting inhibition strategies are under study, GSDMD inhibitors are still far from being used in clinics [143].

The upstream inhibition of inflammasomes, it is being fundamentally pursed by the discovery and development of specific inflammasome receptor compounds [144]. Pharmacological research has been mainly focused on NLRP3 inhibition and indeed numerous inhibitors have shown potential for reducing inflammation (**table 2**).

A downstream sensor protein, key to prompt a complete inflammatory response is the ASC adapter protein, whose inhibition could potentially target multiple inflammasomes, as we have described above. Studies using a single domain antibody that recognizes the CARD domain of ASC and disrupts ASC assembly, have shown inhibition of inflammasome avoiding inflammatory cell death in cellular models [145]. Treatment with a recently reported anti-ASC monoclonal antibody (IC-100) prompted a clear improvement in symptoms in a mouse model of multiple sclerosis [146]. Moreover, the implementation of peptides derived from PYD and CARD domains of ASC represents another valuable strategy to modulate ASC function and have shown

activity in cellular models of inflammation. Therapeutic stapled peptides are also under development, with limitations to their widespread application including reduced cell uptake and their conformational lability, which renders them susceptible to proteolytic digestion [147].

While no specific small molecule ASC inhibitors have been identified, any compound that can interfere with ASC oligomerization would be of great interest.

In this thesis we will evaluate a new pan inflammasome inhibitor MM01, identified in our laboratory, we will disentangle the molecular mechanism of action (Chapter IV), evaluate its performance as a therapy for inflammatory-related disorders (Chapter IV), and use MM01 to explore the impact of the inflammasome inhibition in breast cancer (Chapter V and VI).

Table 2. Current strategies for Inflammasome Inhibition

INFLAMMASOME INHIBITOR	MECHANISM OF ACTION	REF.
	INDIRECT INHIBITORS	
Glyburide	FDA-approved ATP-sensitive K+ channel inhibitor	[148, 149]
Bay 11-7082	Nuclear factor kappa-B kinase subunit beta (IKK-β) and NFκB pathway inhibitor	[150, 151]
Parthenolide	Alkylates cysteine residues of caspase-1 to inhibit the activity of the NLRP1, NLRC4, and NLRP3 inflammasomes	[152]
Andrographolide	NFκB inhibitor	[153]
	DIRECT INHIBITORS	
CY-09	Binds the ATP pocket to inhibit NLRP3 assembly	[154]
MCC950	Binds to the NACHT domain of NLRP3 to interfere with ATP hydrolysis	[155, 156]
Oridonin	Inhibits the NLRP3-NEK7 interaction and compromises NLRP3 inflammasome activation	[157]
Tranilast	Target NLRP3 by binding to the NLRP3 NACHT domain and abolishing receptor oligomerization	[158]
OLT117	A β-sulfonyl nitrile compound that blocks NLRP3 ATPase activity	[159]
IC-100	Single domain antibody that recognizes the ASC CARD domain disrupted ASC assembly	[145]
VX-740	Inhibit the catalytic site of caspase-1	[160]
VX-765	Inhibit the catalytic site of caspase-1	[161, 162]
	INFLAMMASOME PRODUCTS INHIBITORS	
GSK1070806	Humanized monoclonal antibody that blocks IL18	[163]
Anakinra	A recombinant IL1 receptor antagonist	[164]
Canakinumab	An IL1β neutralizing antibody	[165, 166]
Rilonacept	A soluble decoy for the IL1 receptor	[167]

I.5 Breast Cancer at a Glance

Breast cancer involves abnormal cell growth within breast tissue, with the potential for invasion/spread to other parts of the body [168]. Female breast cancer currently represents the most commonly diagnosed cancer worldwide, with 11.7% of total cancer cases in 2020, followed by lung (11.4%) and colorectal (10.0%) cancer. In women, breast cancer is the most commonly diagnosed cancer and the leading cause of cancer death, representing 24.5% of all cancer incidence in 2020 (**Figure 14**) [169].

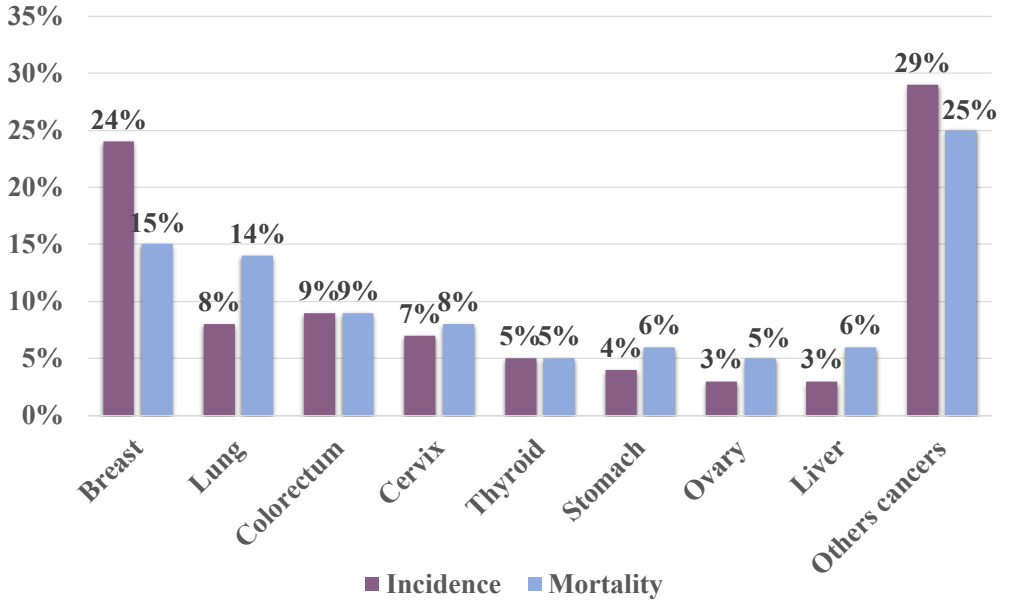

Figure 14. Estimated Breast Cancer Incidence and Mortality Rate Worldwide in Females (2020). (Purple) Estimated number of new cases of various cancer types in females in 2020. **(Blue)** Estimated number of deaths from various cancer types in females in 2020 [169].

Breast cancer originates from an *in-situ* carcinoma characterized by a complete layer of myoepithelial cells and basement membrane and by the proliferation of epithelial cells. The carcinoma progresses after disruption of the myoepithelial cell layer and the degradation of the basement membrane to allow invasion of the

neighboring tissues (invasive ductal carcinoma) and metastasis. Metastatic breast cancer is characterized by the loss of myoepithelial cell layer and basement membrane, the proliferation of stromal cells, angiogenesis, and invasion of tumorigenic epithelial cells to distant sites. After passage through the blood or lymphatic system, the main target sites for metastatic breast cancer cells are the bones, liver, lungs, and brain (**Figure 15**) [170, 171].

Breast cancer can be divided into five phases or stages (**Table 3**) based on the location of the tumor, the size of the tumor, the involvement of the lymph nodes, and metastatic progression. Together with the proliferation marker Ki67 and the status of crucial molecular markers, such as the estrogen receptor (ER), progesterone receptor (PR), and human epidermal growth factor receptor 2 (HER2) these stages currently define patient stratification: luminal A, HER2- luminal B, HER2 + luminal B, HER2-enriched breast cancer, and triple negative breast (TNBC) (**Figure 15**).

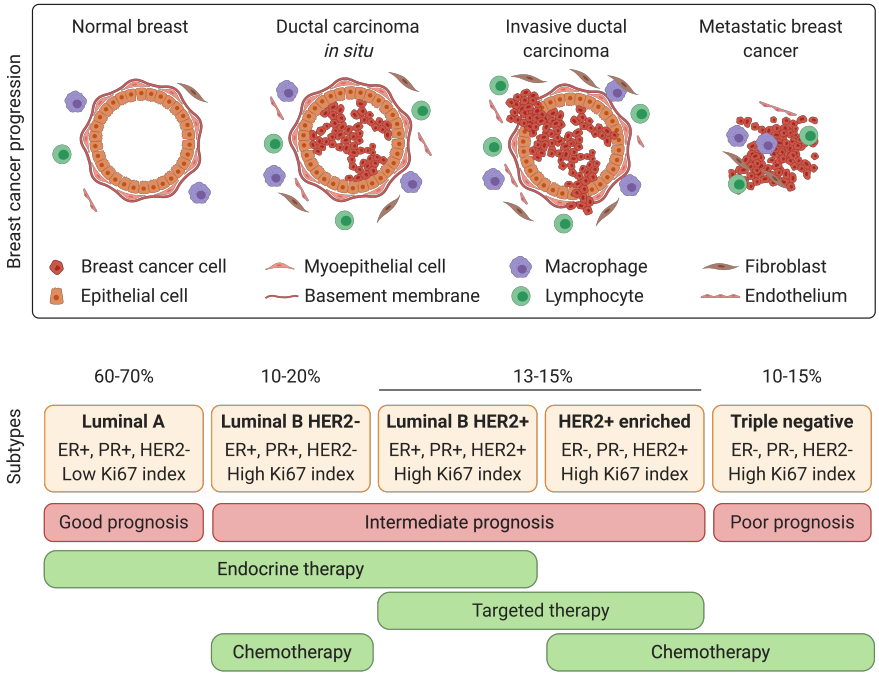

Figure 15. Breast cancer progression from the primary tumor to the metastatic stage and breast cancer subtypes, prognosis, and most common current pharmacological treatment options in each case (Adapted from [172]).

Table 3. Stages of breast cancer and clinical characteristics

Stage	Tumor size	Lymph node	Metastasis	Survival rate (5 years)
0	Small, Inside the glands	Non-affected	No	100%
I	< 2cm	Non-affected	No	98%
II	2-5 cm	Affected	No	87%
III	> 5 cm	Affected	No	61%
IV	Any size	Affected	Yes	20%

- **Luminal A** breast cancer represents the most common subtype (60-70% of all breast cancer cases) and is defined by high expression of ER and PR and low expression of HER2 and Ki67. Luminal A tumors are characterized by slow growth and better prognosis due to a more significant response to treatment [168, 173]
- **Luminal B** breast cancer is diagnosed mainly in the young and is characterized by high expression of ER and PR and Ki67 and can be HER2+ or HER2-. Luminal B tumors display a more accelerated tumor growth rate and suffer from a less favorable prognosis than luminal A tumors [168, 173, 174].
- **HER2-enriched** breast cancer is characterized by high expression of HER2 and the absence of ER and PR expression (70%). HER2-enriched breast cancers exhibit faster tumor growth, are more aggressive, and have a worse prognosis than Luminal A and B subtypes [168, 173, 174].
- **TNBC** tumors have the worst prognosis and are characterized by the lack of ER, PR, and HER2 expression and high Ki67 expression. TNBC tumors also show lymphoplasmacytic inflammatory infiltration with visceral metastases to the lungs, liver, and brain in later stages [168, 174, 175]. Importantly, the lack of hormone receptor expression in this subtype has limited the efficacy of conventional treatments and the development of effective drugs for TNBC.

Understanding the tumor stage and classifying the patient based on the histological and molecular characteristics represent crucial steps in deciding the best treatment for the patient.

I.5.1 Current Therapeutic Approaches for Breast Cancer

Conventional treatments for patients diagnosed with non-metastatic breast cancer include surgical resection, postoperative radiation therapy, and chemotherapy. For patients with metastatic breast cancer, chemotherapy represents the main treatment option, with the ultimate goal of suppressing cancer cell proliferation and slowing metastatic progression [173].

The presence of hormone receptors dictates treatment with standard endocrine therapy, including oral anti-estrogens such as tamoxifen and aromatase inhibitors such as exemestane, anastrozole, or letrozole. In some cases, patients with early-stage disease also receive chemotherapy to prevent disease recurrence, with adriamycin, docetaxel/cyclophosphamide, or cyclophosphamide/methotrexate/5-fluorouracil the primary treatment options. Patients diagnosed with HER2-enriched subtypes are treated with targeted therapies, including the monoclonal antibodies trastuzumab (also known as Herceptin) or pertuzumab (alone or in combination) with or without chemotherapy. In patients with TNBC, the most aggressive subtype with the worst response to therapy, chemotherapy currently represents the only therapeutic regimen approved by the US Food and Drug Administration (FDA) (**Figure 15**) [173].

Unfortunately, many traditional therapies suffer from limitations that decrease their efficacy, including problems related to low solubility, ineffective tumor targeting, secondary toxicities in healthy tissues, and the development of drug resistance [176]. Therefore, new advances in more specific and effective alternative treatments are needed.

Advanced drug delivery technologies, including nanomedicine, can overcome many of these limitations and improve breast cancer treatment. Importantly, nanomedicines including traditional chemotherapeutic agents, such as doxorubicin (Doxil®) and paclitaxel (Abraxane®), now represent routine first-line treatments for breast cancer [177]. **Section I.6** of this introduction will explore nanomedicine-based treatments for breast cancer in detail.

Immunotherapy represents another advanced therapeutic option that has gained recent importance as a breast cancer treatment. Immunotherapy aims to stimulate or restore the capacity of the immune system to target tumor cells [178-180]. The inhibition of the immune checkpoints that promote immunoevasion of the tumor represents an important immunotherapeutic strategy [181]. For example, programmed cell death-1 (PD-1) is an inhibitory immune checkpoint protein expressed on the surface of T, B, and natural killer cells and induces tolerance to antigens [180, 182]. Following T cell activation, simultaneous PD-1 expression offers the attacked cell a means of escaping the immune reaction. Moreover, the PD-1 ligand (programmed cell death-ligand-1 or PD-L1) is overexpressed in tumor cells and contributes to cancer immunoevasion [178]. In March 2019, the FDA approved a PD-L1 antibody (atezolizumab - Tecentriq®) as the first checkpoint inhibitor immunotherapy drug used to treat TNBC combined with chemotherapy in patients that express PD-L1 [183, 184]. Pembrolizumab (Keytruda®), a monoclonal antibody against PD-1, represents another FDA-approved immunotherapeutic agent for the treatment of PD-L1-positive TNBC in combination with chemotherapy [185].

The combination of nanomedicine and immunotherapy represents a potentially efficient means of treating advanced, metastatic breast cancers. Examples include the combination of Abraxane®, a 130 nm albumin-bound nanoparticle formulation of paclitaxel developed by Abraxis BioScience (now Celgene) with Tecentriq® [186].

Importantly, recent studies have underscored the relative importance of the inflammasome in the inflammatory TME as an important participant in tumor progression and response to treatment [120, 121, 187, 188]. As a result, due to the importance of immune infiltration within the TME and the development of a chronic inflammatory immunosuppressive state that favors tumor initiation, progression, and metastasis, **this thesis will focus on the inflammasome as an essential component of the inflammatory process that significantly impacts breast cancer. We describe the identification of a pan inflammasome inhibitor and evaluate its potential as a treatment for metastatic breast cancer. Importantly, we also explore a rationally designed nanomedicine, a polypeptide-based nanosystem, in order to improve the**

pharmacological activity of this inhibitor by improving its aqueous solubility and enhancing its capability to target the TME.

To this end, the following sections will provide a brief overview of nanomedicines in relation to breast cancer treatment and the role of polypeptide based nanosystems.

I.6 Nanomedicine for Breast Cancer Treatment: Classification and Key Design Features.

Conventional treatments for breast cancer comprise surgical resection of the tumor, radiation therapy and/or chemotherapy for non-metastatic breast cancer, and chemotherapy for metastatic breast cancer. However, chemotherapy-based treatments possess several drawbacks, such as lack of specificity, induced drug resistance, low efficacy, and low bioavailability [189]. Furthermore, the control of the pharmacokinetics of chemotherapeutics remains a problem [190]. These drawbacks have prompted research into the development of novel and personalized treatments that can improve efficiency and specificity and reduce the adverse effects associated with conventional treatment options [189, 191, 192].

Anticancer nanomedicines provide numerous advantages in comparison with their parent 'small molecule' drug, such as increased solubility and chemical stability. More remarkable is their capability, after a rational design, to fine-tune and controlled drug pharmacokinetics and pharmacodynamics, thus allows bypassing drug resistance mechanisms due to nanomedicine differential cellular internalization mechanisms [193-195]. Moreover, nanomedicines are able to increase drug target specificity and consequently therapeutic efficacy as well as to reduce drug toxicology and adverse effects in healthy cells [172]. For example, after intravenous administration, nanomedicines can be extravasated more selectively to tumor tissues by passive targeting, due to the higher permeability of blood vessels and lack of lymphatic drainage. Most nanomedicines in the clinic rely on the passive targeting effect provided

by this so-called enhanced permeability and retention effect (EPR) (**discussed in section I.6.2**). The passive tumor accumulation could even be enhanced when the nanomedicine bears active targeting moieties, named active-targeted nanosystems [196].

Modern nanomedicines are classified into three groups. The first group consists of first-generation nanomedicines that have already entered routine clinical use and includes both "blockbuster" drugs (>$1 billion in annual revenues) and certain products (e.g., targeted liposomes, PEGylated proteins, polymeric drugs) that are of such an age that they will soon begin to appear as "generics". There are already more than sixty nanomedicines in routine clinical use and around seventy-five nanosystems in clinical trials as anticancer therapies [126]. **Figure 16** shows schematically each class of nanomedicines on the market or in clinical development (e.g., Liposomes, polymer therapeutics, block copolymer micelles, nanogels, nanocrystals, nanoparticles). Second, there are a growing number of nanomedicines, mostly born in the 90s, in clinical development. Finally, the third group consists of those innovative nanotechnologies of the 21st century that may have the potential to enter clinical development and bring the expected new paradigm to diagnosis and/or therapy [193, 197].

Importantly, FDA-approved nanomedicines for cancer treatment that have provided improvements in toxicity profiles and efficacy include liposomes, protein nanoparticles, polymeric nanoparticles, antibody-drug conjugates, and recently iron nanoparticles [198].

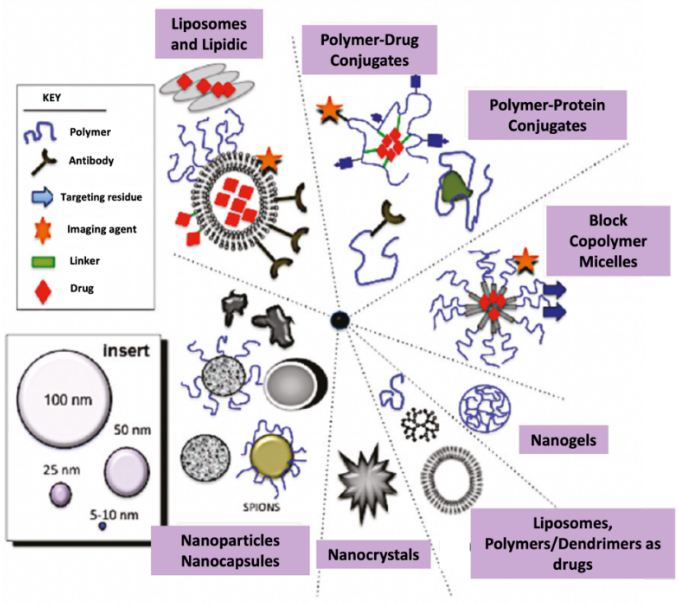

Figure 16. Schematics representation of **the Main Classes of First-Generation Nanomedicines.** (Adapted from [194]).

After proper rational design, nanomedicines can cross biological barriers and transport drugs specifically to the target sites, thus reducing any adverse effects on healthy tissues. Since biological barriers represent the main defense mechanism of the organism and block the penetration of foreign substances, the development of efficient nanodrugs requires an understanding of these barriers [199].

I.6.1 Understanding the biological Barriers

Nanomedicine formulations aim to efficiently deliver drugs to a given target site at an effective concentration; however, the "journey" taken by nanomedicines after administration proceeds through multiple biological barriers that represent the body's primary defense mechanism and block the penetration of foreign substances [200]. Biological barriers include first-level barriers (such as the skin or mucosa), second-level or circulatory barriers, third-level or tissue-specific barriers (which includes the tumor stroma), fourth-level or cell barriers, and fifth levels or subcellular barriers (**Figure 17**).

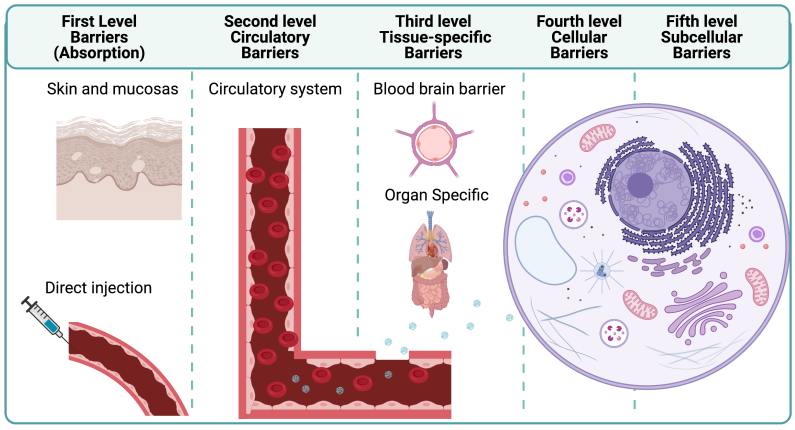

Figure 17: Biological barriers represented at five levels. (Adapted from [201])

- **First level: Absorption.** Initial strategies for the adequate distribution of nanomedicines include intravenous administration (most common), topical administration, oral administration, or administration through various mucosal barriers. Design strategies must allow nanomedicines to reach their destination and maintain their characteristics and integrity in response to different physiological conditions, including the presence of proteases, redox potential, and different pH levels. [202, 203].

- **Second level: Circulatory Barriers.** The reticuloendothelial system, the immune system, and the liver represent barriers to administered nanomedicines as they function to recognize and remove foreign objects from the circulation. The rational design of nanomedicines in terms of charge, shape, and size can modulate their interaction with these systems [204, 205]. For example, cell components appended to the surface of a nanomedicine can allow the avoidance of circulating phagocyte-mediated elimination. Furthermore, nanomedicine design must allow for better renal filtration to avoid prolonged retention in the circulation, which can cause systemic toxicity [201, 206].

- **Third level: Tissue-specific Barriers and Tumor Stroma.** Tissue-specific barriers include the blood-brain and ocular barriers, while the TME represents a

significant barrier to the uptake of nanomedicines by tumor cells. The modulation of the TME to improve tumor perfusion, facilitate tumor extravasation, or improve interstitial transport represents an important strategy to improve the delivery of nanomedicine to tumors [207-209].

- **Fourth level: Cellular Barriers.** Nanomedicines are internalized into cells using pathways that depend on molecular weight (Mw). Passive diffusion occurs when the Mw of the nanomedicine is less than 1 kDa, while nanomedicines with a higher Mw internalize through endocytic pathways. Endocytosis represents the primary cell uptake mechanism after a nanomedicine reaches the cell surface through passive or active targeting. Endocytosis can be divided into clathrin-mediated endocytosis, caveolae-mediated endocytosis, macropinocytosis, and phagocytosis [210]. Clathrin-mediated endocytosis (<120 nm) and caveolae-mediated endocytosis (<60 nm) represent the major uptake pathways used by various nanoformulations [130].

- **Fifth level: Subcellular Barriers.** Nanomedicines that enter via clathrin-mediated endocytosis pass through the early endosomes to the late endosomes and reach the lysosomal lumen, where they are degraded by hydrolases. Importantly, nanomedicines that target specific organelles rather than the cytoplasm, in general, must be designed to undergo endosomal escape [211] to avoid endosome/lysosome degradation and retain their biological activity [71]. Nanomedicines that enter via caveolae-mediated endocytosis generally do not enter the lysosomes and become transferred to the Golgi apparatus or endoplasmic reticulum. Overall, the endocytosis of antitumor nanomedicines represents a critical step in achieving therapeutic effects. Hence, a deeper understanding and exploration of endocytic pathways may foster the development of novel delivery strategies for subcellular targeting [212, 213].

I.6.2 The Enhanced Permeability and Retention (EPR) Effect

The passive accumulation of nanomedicines in tumors through the EPR effect was first described by Matsumura and Maeda in 1986 [214, 215]. The EPR effect generally allows for the enhanced tumor accumulation of nanomedicines than the "free" form of the parental drug involved [216]. The EPR effect relies on pathological alterations to the vasculature within tumors or sites of inflammation. Within these areas, the formation of the blood vessels that provide oxygen and nutrients occurs in a dysregulated manner, giving rise to a disordered vasculature formed by endothelial cells with a larger pore diameter (100-200 mm), which allows the passive accumulation of nanomedicines with an Mw between 40-800 KDa and 20-200 nm in the affected area. In addition, said areas also suffer from failures in lymphatic drainage, which also favors the retention of nanomedicines that penetrate the tumor (**Figure 18**) [103, 217, 218].

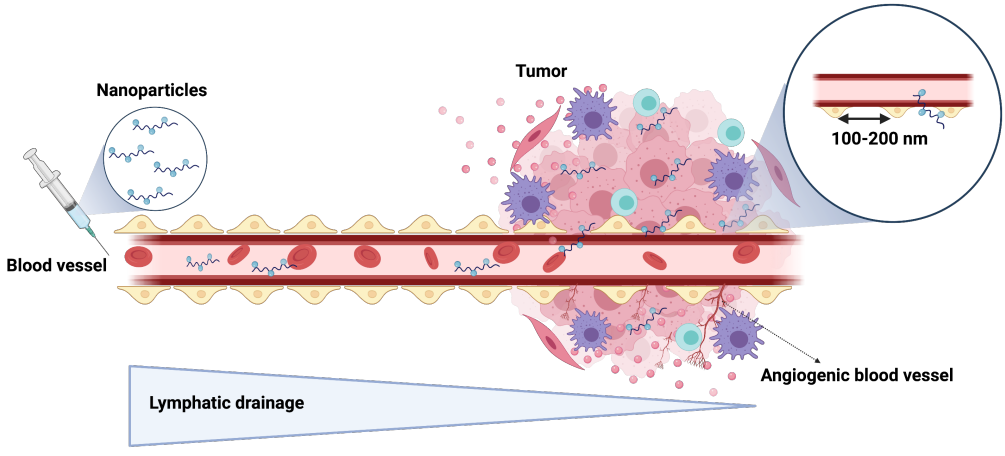

Figure 18. The Enhanced Permeability and Retention Effect. Due to inadequate lymphatic drainage and the space between endothelial cells present in the tumor vasculature, nanomedicines can preferentially accumulate in the tumor. Nanomedicines must be >5 nm in size to avoid rapid renal filtration by increasing blood circulation time and <200nm to extravasate from the vasculature.

However, the significance and behavior of therapies with respect to the EPR effect in human patients has recently been under debate [103]. For example, it has been shown that nanomedicine entry into tumors is more complex than simple extravasation through

gaps in the endothelial lining [219]. In addition, studies now show that the immune cells of the TME play critical roles in the passive accumulation, retention, and intratumoral distribution of nanomedicines [103]. Another point to note is that the effect of EPR is significantly more pronounced in the small animal xenograft tumor models typically used to evaluate nanomedicines compared to human tumor growth [103]. Although nanomedicine accumulation in human tumors exists, the degree varies greatly between patients and tumor types. Consequently, further work is needed to study strategies to enhance the effect of EPR and enhance the efficacy of nanomedicine therapy. This can be done through pharmacological strategies to modulate vessel permeabilization, vessel normalization, vessel disruption or vessel promotion, and physical strategies, such as hyperthermia, radiotherapy, sonoporation and phototherapy. In addition, the optimization of the physicochemical properties of nanomedicines, which include surface charge, size, and size distribution, can promote enhanced tumor accumulation via the EPR effect [103, 220]. Furthermore, active targeting can be used as a complementary strategy to EPR-based passive targeting to enhance the accumulation and retention of nanomedicines in tumors, or employ combined treatments based on nanomedicines or combination between immunotherapy and nanomedicines [172].

I.6.3 Currently used Nanomedicines in Breast Cancer Treatment

Nanomedicines implemented in breast cancer treatment include liposomal nanoformulations of doxorubicin, such as **Doxil®**, **Lipodox®**, and **Myocet®**, which provide reduced side effects by inhibiting off-target toxicity and improved tumor specificity [186]. Additional liposomal nanomedicines include nanoformulations of paclitaxel (**Lipusu®**, approved in China [221]) or daunorubicin (DaunoXome®), which are currently in advanced clinical trials for metastatic breast cancer [222]. Other advanced therapies include nanoparticle formulations of paclitaxel (**Abraxane®** [223]), polymeric micelles (e.g., **Genexol-PM®** [224] or **Nanoxel®** [225]), and the antibody-drug conjugate **Kadcyla®** (trastuzumab emtansine) [226] (**Figure 19**).

All nanomedicines demonstrated improvement in efficacy, reduction in tumor size and survival, specificity for targeting the target site, and reduction in side effects compared to the associated free drugs. For example, **Doxil®,** a liposome modified with polyethylene glycol (PEGylated) of approximately 80-90 nm in diameter containing approximately 15,000 encapsulated doxorubicin molecules, reduces the cardio-cardiotoxic effects associated with free doxorubicin [227]. Meanwhile, **Abraxane®,** a 130 nm albumin-bound form of paclitaxel, promoted higher tumor accumulation of paclitaxel and demonstrated a superior overall response rate (34%) compared to free paclitaxel (19%) in patients with advanced breast cancer [228, 229]. Notably, a combination of **Abraxane®** and atezolizumab, a PD-L1 inhibitor, has been established as a first-line treatment for patients with unresectable, locally advanced, or metastatic TNBC.

This thesis focuses on the use of Polymers Therapeutics as the strategy to rationally design a bioresponsive nanomedicine capable to improve the therapeutic output of the inflammasome inhibitor MM01 in preclinically relevant breast cancer models.

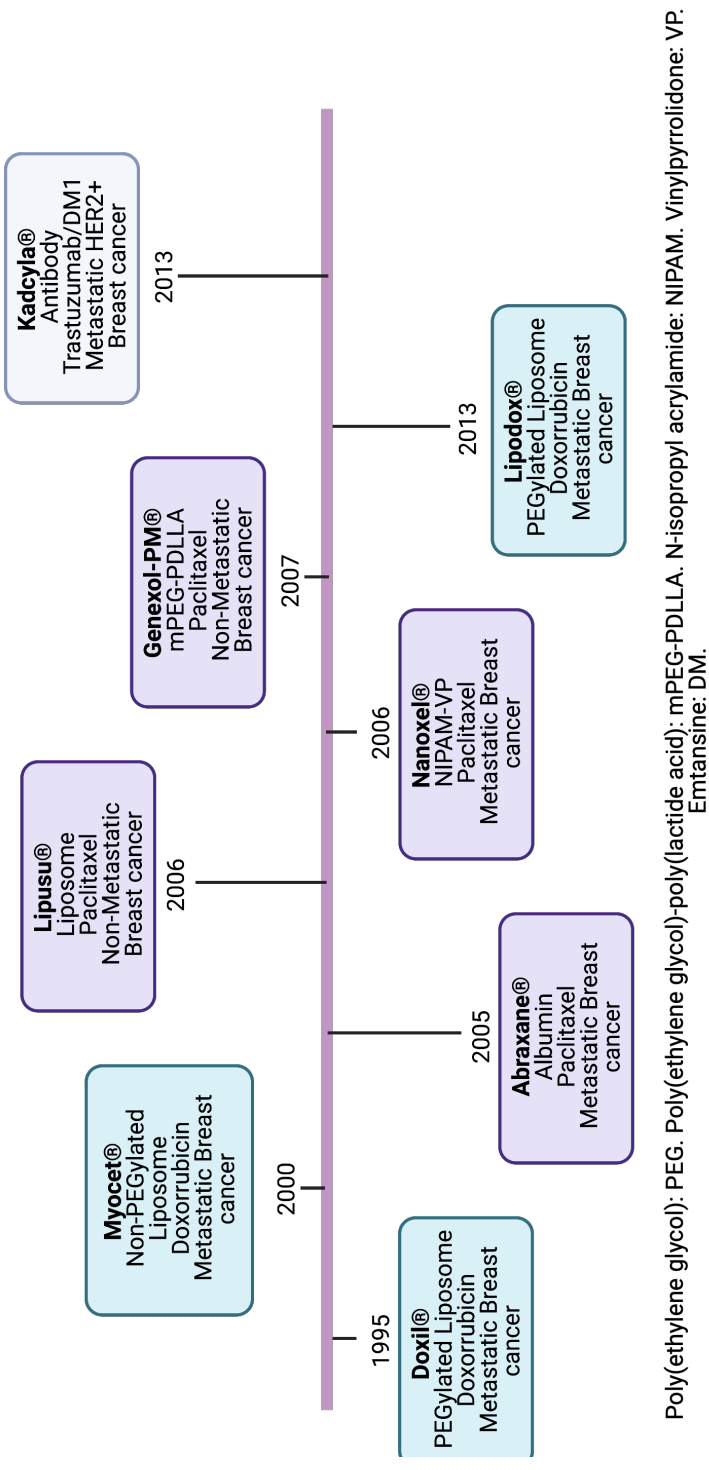

Figure 19. FDA-Approved Nanomedicines in Routine Clinical Use for Breast Cancer Treatment.

I.7 Polymer Therapeutics

Polymer therapeutics represent one of the most successful areas contributing to the first generation of nanomedicines. The term "Polymer Therapeutics", coined by Prof. Ruth Duncan, includes an extensive family of nano-sized medicines (5 - 100 nm in diameter) with more than twenty-five products in routine clinical use [230]. Examples include the polymeric drug glatiramer acetate for multiple sclerosis (Copaxone®) and the polymer conjugate PEG-filgrastim for the treatment of neutropenia (Neulasta®), that even appeared in the US list of Top 10 bets-selling drugs in 2013 [230].

Treatments based on Polymer Therapeutics have demonstrated their suitability in several diseases/disorders, such as cancer [231], neurodegenerative disorders, hepatitis and autoimmune diseases reflecting the enormous potential of these nanomedicines [232].

I.7.1 Definition and Classification of Polymer Therapeutics

The classical definition of Polymer therapeutics encompasses various macromolecular systems composed of a rationally designed covalent bond between a water-soluble polymeric carrier (with or without inherent activity) and the bioactive molecule(s). They include polymeric drugs, polymer-drug conjugates, polymer-protein conjugates, polymeric micelles (where drug attachment occurs via covalent bonding) and polyplexes (multi-component systems used as non-viral vectors for gene/small interfering RNA delivery) (**Figure 20**) [233]. However, this is an evolving concept and hybridized, supramolecular and self-assembled nanoconstructs are an increasing number within this successful family [233].

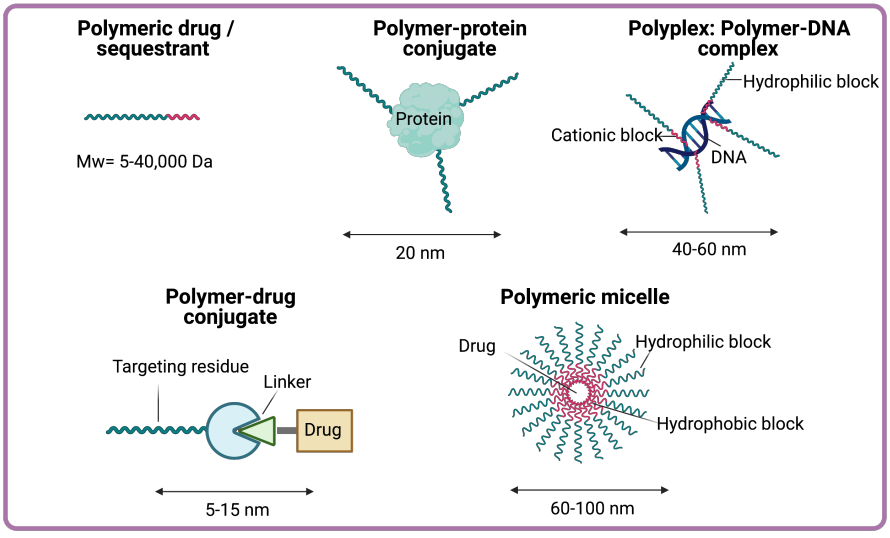

Figure 20. Overview of the Classical Classification of the Polymer Therapeutics Family

Polymer therapeutics represent 'new chemical entities' that differ from conventional drug delivery systems or formulations that simply trap, solubilize, or control drug release without resorting to chemical conjugation [233]. Through the versatility of synthetic chemistry and chemical conjugations, polymer therapeutics can play a critical role by changing drug distribution or by providing more targeted drug delivery to specific tissues or cells within those tissues. This spatiotemporal control of the administered drug leads to improved therapeutic effects and/or reduced side effects.

Therefore, the advantages of the use of rationally-designed Polymer Therapeutics are related to their controllable size and macromolecular properties.

In this doctoral thesis, we focused on the development of a novel polymer-based nanoconjugate of our newly identified inflammasome inhibitor MM01 as a means to improve breast cancer treatment and tumor accumulation. Therefore, in the following sections, we will go deeper into the main characteristics of the use of polymer-drug conjugates and Polypeptide-Based drug Conjugates as therapeutics.

I.8 Polymer Conjugates as Therapeutics

Depending on the nature of the conjugated bioactive molecule, polymer conjugates could be classified in polymer-drug and polymer-protein conjugates. Depending the location of the molecular target to reach each case would require a different rational design, however in general terms one could say that conjugation of a therapeutic agent to a polymeric backbone offers several advantages over other nanomedicines, including (1) controlled size and size-dependent properties; (2) prevention or reduction of aggregation, immunogenicity and antigenicity; (3) improved plasma half-life due to increased hydrodynamic volume and decreased renal clearance; (4) protection of the therapeutic agent against degradation by proteolytic enzymes or nonspecific cellular uptake (5) increased water solubility; (6) modification of pharmacokinetics at both cellular and even subcellular levels [201].

The following table shows the marketed Polymer conjugates with a clear prevalence of polymer-protein conjugates (mainly PEG) if compared to polymer-drug conjugates with only one marketed product, Movantik® approved by the FDA in 2014 for the treatment of opioid-induced constipation in adult patients with chronic non-oncologic pain (**Table 4)** [234].

Table 4: Marketed polymer conjugates. *Adapted* [234]).

Name (company)	Polymer carrier	Drug	Indication(s)	Year approved[a]
Adagen (Enzon Pharmaceuticals)	PEG	ADA	ADA-SCID	1990
SMANCS (Astellas Pharma)	Poly(styrene-co-maleic acid)	Neocarzinostatin	Liver and renal cancer	1993 (Japan)
Oncaspar (Enzon Pharmaceuticals)	PEG	L-asparaginase	Acute lymphoblastic leukemia	1994
PegIntron (Merck & Co.)	PEG	Interferon α2b	Hepatitis C	2001
Pegasys (Genentech)	PEG	Interferon α2a	Hepatitis B and C	2002
Neulasta (Amgen)	PEG	G-CSF	Chemotherapy-induced neutropenia	2002
Somavert (Pfizer)	PEG	HGF receptor antagonist	Acromegaly	2003
Macugen (Baush& Lomb)	PEG	Anti-VEGF aptamer	Neovascular age-related macular degeneration	2004
Mircera (Roche)	PEG	Epoetin beta	Anemia associated with chronic kidney disease	2007

Table 4: Marketed polymer conjugates (continuation). *Adapted* [234].

Name (company)	Polymer carrier	Drug	Indication(s)	Year approved[a]
Cimzia (UCB Pharma)	PEG	Anti-TNF Fab´	Crohn´s disease, rheumatoid arthritis, psoriatic arthritis and ankylosing spondylitis	2008
Krystexxa (Horizon Pharma)	PEG	Uricase	Chronic gout	2010
Plegridy (Biogen)	PEG	Interferon β1a	Relapsing multiple sclerosis	2014
Movantik (AstraZeneca)	PEG	Naloxone	Opioid-induced constipation	2014
Adynovate (Baxalta)	PEG	Factor VIII	Haemophilia A	2015
Palynziq (BioMarin)	PEG	Phenylalanine ammonia lyase	Phenylketonuria	2018
Jivi (Bayer)	PEG	Factor VIII	Haemophilia A	2018

I.8.1 Polymer-drug Conjugates as Therapeutics

Polymer-drug conjugates, described by Ringsdorf in 1975, are a subtype of Polymer therapeutics [234]. Ringsdorf described the four main features necessary for the design of polymer-drug conjugates: (i) a hydrophilic, ideally biodegradable, multivalent polymeric carrier with a high loading capacity; (ii) a suitable selection of drugs with appropriate potency and structural functionality to enable conjugation; (iii) bioresponsive polymer-drug linkers that allow controlled release of drugs at the site of action under selected endogenous or exogenous triggers; and (iv) the possibility of implementing targeting elements to enhance accumulation at the pathological site [234] (**Figure 21**). Considering these four features, the rational design of polymer-drug conjugates has gained attention primarily for their ability for precise and controlled release of bioactive agents in specific biological environments [234]. Importantly, the multivalency of polymers allows the conjugation of more than one compound to the polymeric backbone, enabling the introduction of more than one drug (polymer-based combination therapy), diagnostic elements, or targeting residues (promoting receptor-mediated endocytosis to target therapy) [233].

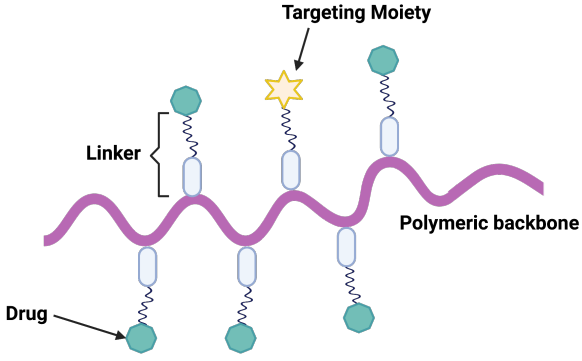

Image 21. Schematic illustration of polymer-drug conjugates.

Regarding internalization pathways, polymer-drug conjugates primarily require lysosomotropic intracellular transport, in which the bioactive agent must be stable under proteolytic degradation. In this case, the nanoconjugate is internalized through endocytosis and directed to the early and late endosomes, and finally to the

lysosome, where the presence of proteolytic enzymes (such as cathepsin B) or the acidic pH allows the release of the drug from the polymer by degradation of the polymer itself or a cleavable linking moiety [235, 236]. Lysosomes present ion channels and transmembrane proteins to transport the drug to the cytosol to access the therapeutic target [237] (**Figure 22**).

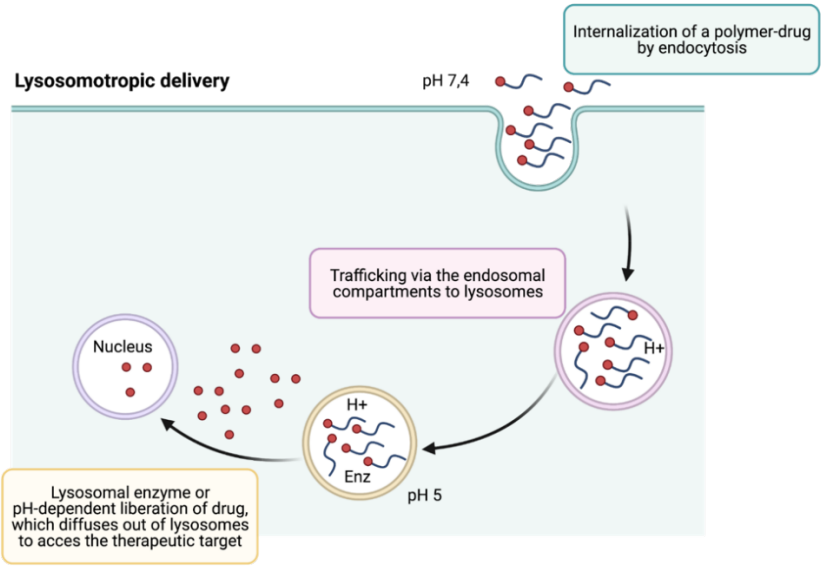

Figure 22. Overview of Lysosomotropic Route Employed for the Delivery of Nanomedicines. Lysosomotropic transport (release through the lysosome) is suitable for bioactive agents protected from proteolytic degradation.

The therapeutic application of polymer-drug conjugates spans numerous conditions including cancer treatment. For example, PK1 or HPMA-DOX was the first clinically evaluated anticancer drug-polymer conjugate developed by Kopecek and Duncan in 1994 [233]. PK1 is composed of the conjugation of poly-N-hydroxypropylmethacrylamide (HPMA) copolymer and doxorubicin (DOX) via a cleavable peptidyl linker in the lysosome [236]. However, although PK1 was shown to improve antitumor efficacy, tumor accumulation, safety profile and plasma circulation time compared to unconjugated doxorubicin, the development of PK1 was discontinued due to economic decisions by the parent company [238].

The limitations on molecular weight and the lack of biodegradability in the first generation of PEG and HMPA conjugates produce deficient pharmacokinetics. Hence,

current research efforts focus on the evaluation of conjugates employing new biodegradable and backbone-degradable water-soluble polymers (see section I.9.2).

As mentioned above, so far, only one polymer-drug conjugate has reached the market, Movantik® [234] that was approved by the FDA in 2014 for the treatment of opioid-induced constipation in adult patients with chronic non-oncologic pain, and other examples currently under evaluation in clinical/preclinical studies [234]. However, there are many in advanced clinical stages as it is reflected in **Table 5** showing the increasing use of multivalent, biodegradable polymeric carriers.

Table 5: Polymer-drug conjugate. *Adapted from* [234]

Name (company)	Polymer carrier	Drug	Indication(s)	Stage (ClinicalTrials.gov identifier)
Onzeald (Nektar Therapeutics)	PEG	Irinotecan	Breast cancer	Pre-registration (NCT02915744)
NKTR-181 (Nektar Therapeutics)	PEG	μ-Opioid receptor agonist	Chronic low back pain and chronic non-cancer pain	Pre-registration (NCT03486899)
PEX168 (Jiangsu-Hansoh Pharmaceutical)	PEG	Loxenatide	Type 2 diabetes	Phase II (NCT02367820)
NC-6004 (NanoCarrier)	PEG-b-poly(glutamic acid) micelle	Cisplatin	Pancreatic cancer	Phase III (NCT02477969)
Opaxio (CTI BioPharma)	Polyglutamic acid	Paclitaxel	Ovarian cancer, peritoneal cancer and fallopian tube cancer	Phase III (NCT02043288)
APL-2 (Apellis Pharmaceuticals)	PEG	Cyclic peptide complement C3 inhibitor	Paroxysmal nocturnal haemoglobinuria	Phase III (NCT00108745)
CRLX101(BlueLink Pharmaceuticals)	Cyclodextrin-PEG that self-assembles into nanoparticle	Camptothecin	Ovarian cancer, peritoneal cancer and fallopian tube cancer	Phase II (NCT01652079)
NK012 (Nippon Kayaku)	PEG-b-poly(glutamic acid) micelle	SN-38	Breast cancer	Phase II (NCT00951574)
OsteoDex (Dextech Medical)	Dextran	Alendronate	Prostate cancer	Phase II (NCT02825628)
Somadex (DexTech Medical)	Dextran	Somastostatin	Neuroendocrine tumorus and acromegaly	Phase II (NA)
BP-C1 (Meabco A/S)	Benzo-polycarbonic acid polymer	Pt(II)	Breast cancer	Phase II (NCT02783794)

Table 5: Polymer-drug conjugate (continuation). *Adapted from* [234]

Name (company)	Polymer carrier	Drug	Indication(s)	Stage (ClinicalTrials.gov identifier)
Pegcantratinib (Sienna Biopharmaceuticals)	PEG	TrkA inhibitor	Pruritus	Phase II (NCT03322137)
DEP docetaxel (Starpharma)	PEG-polylysine dendrimer	Docetaxel	Solid tumors	Phase II (NA)
NC-6300 (NanoCarrier)	PEG-b-poly(aspartic acid) micelle	Epiribicin	Solid tumors and soft tissue sarcoma	Phase I/II (NCT03168061)
CRLX301 (BlueLink Pharmaceuticals)	Cyclodextrin-PEG that self-assembles into nanoparticles	Docetaxel	Solid tumors	Phase I/II (NCT02380677)
DEP cabazitaxel (Starpharma)	PEG-polylysine dendrimer	Cabacitaxel	Solid tumors	Phase I/II (NA)
NKTR-262 (Nektar Therapuetics)	PEG	TLR7/TLR8 agonist	Solid tumors	Phase I/II (NCT03435640)
CriPec docetaxel (Cristal Therapeutics)	Core-crosslinked PEG-polymer micelle	Docetaxel	Solid tumors	Phase I (NCT02442531)
NC-4016 (NanoCarrier)	PEG-b-poly(glutamic acid) micelle	Oxaliplatin	Solid tumors and lymphoma	Phase I (NCT03168035)
RadProtect (Original BioMedicals)	PEG-b-poly(glutamic acid) chelating complex micelle	Amifostine	Acute radiation syndrome	Phase I (NCT02587442)
SER-214 (Serina Therapeutics)	Poly(2-ethyl-2-oxazoline)	Rotigotine	Parkinson disease	Phase I (NCT02579473)
DFP-13318 (ProLynx)	PEG	SN-38	Solid tumors	Phase I (NCT02646852)

I.8.2 Rational Design of Polymer-Drug Conjugates

As mentioned above, the use of polymer-drug conjugates is gaining interest due to their precise and controlled release capability and the multivalency of the polymers. Therefore, it is necessary to keep in mind that it is necessary to control the rational design of the conjugates in order to obtain effective polymer-drug conjugates for the treatment of a given disease or disorder [239].

First, the physicochemical characteristics of the polymer-drug conjugates will determine their ability to cross the necessary biological barriers, as well as their biological activity. In addition, the success of the conjugates' activity depends primarily on their response to the specific physiological environments encountered in the organism. Therefore, the rational design of polymer-drug conjugates begins with a thorough understanding of the biological barriers that each conjugate must circumvent to reach the selected cellular/molecular target. In addition, other components to consider in the rational design of polymer-drug conjugates are the biodegradable polymeric carrier itself and the bioreactive linker between the polymer and the therapeutic agent involved.

I.8.2.A Polymeric Carriers

One of the key features in the design of Polymer Therapeutics is the chosen polymeric nanocarrier. Most employed polymeric carriers can be composed of varied materials with different geometries and sizes and can be chemically conjugated with targeting ligands to allow specific targeting of individual organs, tissues, and cells. Furthermore, different architectures (including linear, graft, star, dendrimer, and dendronized polymers) allow for multivalency (the ability to carry multiple moieties) and potentially longer blood circulation times (**Figure 23)** [236, 240].

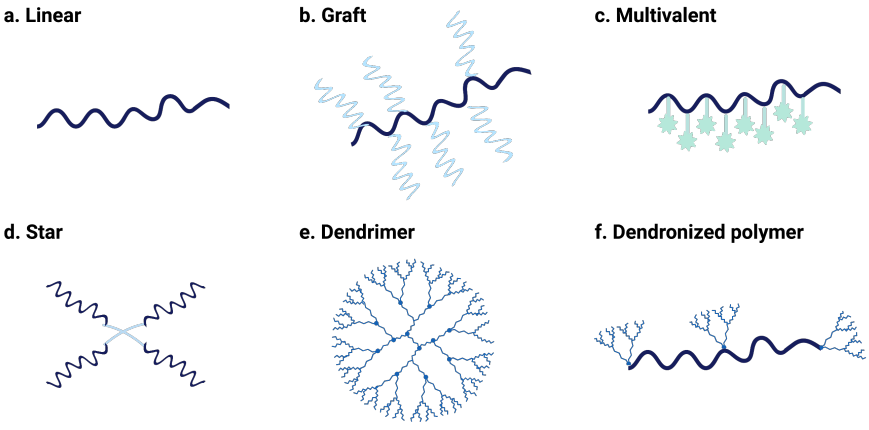

Figure 23. An Overview of Polymeric Architectures [236]

In general, the main properties that the polymeric carrier of choice must meet are [239]:

i. Biodegradability or a suitably small molecular weight to facilitate excretion *in vivo*.
ii. Prolonged half-life in blood, which favors adequate biodistribution and accumulation in body compartments.
iii. Low polydispersity, providing homogeneity to the final conjugate.
iv. Multivalency, allowing adequate drug loading, combined drug loading or application of targeting/diagnostic elements.

Biodegradability represents one of the most important characteristics that polymeric carriers must have, since this avoids accumulation in the organism and possible side effects. For example, the lack of biodegradability of first-generation PEG and HPMA conjugates presents limitations in pharmacokinetics and systemic toxicity [239]. Therefore, new biodegradable and biocompatible water-soluble polymers are being developed. Polymeric carriers include natural polymers such as dextran (α-1,6 polyglucose), dextrin (α-1,4 polyglucose), cyclodextrin and hyaluronic acid, and synthetic polymers such as polyacetals and polypeptides.

Moreover, the structural versatility of the polymers should also be taken into account [239]. For example, branched polymers may exhibit greater responsiveness to

stimuli and conjugation of a large number of different bioactive agents versus their linear polymer analogues. In addition, branched polymers have demonstrated superior biodistribution, pharmacokinetic profiles, and in vivo biodistribution in healthy mice [239].

I.8.2.B Bioresponsive Linkers

Finally, it is important to consider for the rational design of polymer-grug conjugates the use of linkers that respond to stimuli, both endogenous (e.g., pH, redox environments or reactive oxygen species) and exogenous (e.g., magnetic field, temperature, light).

Linker chemistry can optimize drug release profiles in specific microenvironments or in the presence of specific enzymes, thus ensuring the release of the active agent(s) within the target site and enhancing biological activity. Different types of linkers have been described according to their susceptibility [239]:

i. pH-responsive linkers: including acetal or ester linkers, N-cis-aconityl acid or hydrazone linkers.
ii. Lysosomal enzyme-responsive linkers: usually oligopeptides cleaved by lysosomal enzymes such as cathepsin B or D, or metalloproteinases. Examples of these linkers are GFLG (Gly-Phe-Leu-Gly) and GLFG (Gly-Leu-Phe-Gly).
iii. Self-immolative linkers: These linkers can disassemble into constitutive fragments, causing rapid disassembly of the polymer.
iv. Reduction-sensitive linkers: Drug release occurs in reducing environments, mainly due to the presence of glutathione.
v. Drug release by anchorage-assisted hydrolysis: first, drug linkers are released from the polymer after hydrolysis (first prodrug), activating the linker (second prodrug) that releases the free and active form of the drug.

The nanoconjugates synthesized, characterized, and evaluated throughout this Thesis have been based on polypeptides, in particular polyglutamates (PGA).

I.9 Polypeptide-Based drug Conjugates as therapeutics

Many examples polymer-drug conjugates use copolymers of N- (2-hydroxypropyl) -methacrylamide (HPMA), PEG, or, more recently, polyglutamic acid (PGA) as carrier molecules [239]. However, biopersistent carriers such as HPMA and PEG can cause lysosomal storage disease and do not allow combination therapy. Moreover, evidence of clinically reported hypersensitivity reactions with specific PEG-protein conjugates has raised awareness of the benefits of alternative biodegradable polymers.

Biodegradable polymers such as PGA have benefits due to their similarities to native proteins, which include safety, low immunogenicity, biocompatibility, and biodegradability [241]. In addition, polypeptides also have advantages due to their structural versatility, which allows the formation of multiple architectures with different physicochemical characteristics (charge, polarity, and hydrophilicity) [237, 242]. Moreover, the possibility of using carriers with a higher Mw allows optimization of pharmacokinetics and improves EPR-mediated tumor targeting.

Biodegradable polymers currently employed at the preclinical and clinical levels include polypeptides, dextrins, polysialic acids, polyacetals, and hydroxyethyl starch. In addition, promising clinical results and lessons learnt with Opaxio® (PGA-paclitaxel (PTX) conjugate) have underscored the high potential of synthetic polypeptides within nanomedicine [236].

In this work, we developed a new strategy by means of a novel polyglutamate-based nanocarrier derivatized with discrete cyclodextrin moieties capable to entrap the inhibitor in a highly efficient manner.

I.10 References

1. Gasteiger, G., et al., *Cellular Innate Immunity: An Old Game with New Players.* J Innate Immun, 2017. **9**(2): p. 111-125.
2. Travis, J., *Origins. On the origin of the immune system.* Science, 2009. **324**(5927): p. 580-2.
3. Smith, N.C., M.L. Rise, and S.L. Christian, *A Comparison of the Innate and Adaptive Immune Systems in Cartilaginous Fish, Ray-Finned Fish, and Lobe-Finned Fish.* Front Immunol, 2019. **10**: p. 2292.
4. Turvey, S.E. and D.H. Broide, *Innate immunity.* J Allergy Clin Immunol, 2010. **125**(2 Suppl 2): p. S24-32.
5. Bernareggi, D., S. Pouyanfard, and D.S. Kaufman, *Development of innate immune cells from human pluripotent stem cells.* Exp Hematol, 2019. **71**: p. 13-23.
6. Pasupuleti, M., A. Schmidtchen, and M. Malmsten, *Antimicrobial peptides: key components of the innate immune system.* Crit Rev Biotechnol, 2012. **32**(2): p. 143-71.
7. Vivier, E., et al., *Functions of natural killer cells.* Nat Immunol, 2008. **9**(5): p. 503-10.
8. Lubbers, R., et al., *Production of complement components by cells of the immune system.* Clin Exp Immunol, 2017. **188**(2): p. 183-194.
9. McComb, S., et al., *Introduction to the Immune System.* Methods Mol Biol, 2019. **2024**: p. 1-24.
10. Takeuchi, O. and S. Akira, *Pattern recognition receptors and inflammation.* Cell, 2010. **140**(6): p. 805-20.
11. Boehm, T., N. Iwanami, and I. Hess, *Evolution of the immune system in the lower vertebrates.* Annu Rev Genomics Hum Genet, 2012. **13**: p. 127-49.
12. Bonilla, F.A. and H.C. Oettgen, *Adaptive immunity.* J Allergy Clin Immunol, 2010. **125**(2 Suppl 2): p. S33-40.
13. Marshall, J.S., et al., *An introduction to immunology and immunopathology.* Allergy Asthma Clin Immunol, 2018. **14**(Suppl 2): p. 49.
14. Nicholson, L.B., *The immune system.* Essays Biochem, 2016. **60**(3): p. 275-301.
15. Chen, L., et al., *Inflammatory responses and inflammation-associated diseases in organs.* Oncotarget, 2018. **9**(6): p. 7204-7218.
16. Abdulkhaleq, L.A., et al., *The crucial roles of inflammatory mediators in inflammation: A review.* Vet World, 2018. **11**(5): p. 627-635.
17. *A current view on inflammation.* Nat Immunol, 2017. **18**(8): p. 825.
18. Mantovani, A., et al., *Neutrophils in the activation and regulation of innate and adaptive immunity.* Nat Rev Immunol, 2011. **11**(8): p. 519-31.
19. Lawrence, T. and D.W. Gilroy, *Chronic inflammation: a failure of resolution?* Int J Exp Pathol, 2007. **88**(2): p. 85-94.
20. Dregan, A., et al., *Chronic inflammatory disorders and risk of type 2 diabetes mellitus, coronary heart disease, and stroke: a population-based cohort study.* Circulation, 2014. **130**(10): p. 837-44.
21. DeMizio, D.J. and L.B. Geraldino-Pardilla, *Autoimmunity and Inflammation Link to Cardiovascular Disease Risk in Rheumatoid Arthritis.* Rheumatol Ther, 2020. **7**(1): p. 19-33.
22. Rogovskii, V., *Modulation of Inflammation-Induced Tolerance in Cancer.* Front Immunol, 2020. **11**: p. 1180.
23. Gallo, J., et al., *Particle disease: biologic mechanisms of periprosthetic osteolysis in total hip arthroplasty.* Innate Immun, 2013. **19**(2): p. 213-24.
24. Zindel, J. and P. Kubes, *DAMPs, PAMPs, and LAMPs in Immunity and Sterile Inflammation.* Annu Rev Pathol, 2020. **15**: p. 493-518.
25. Tang, D., et al., *PAMPs and DAMPs: signal 0s that spur autophagy and immunity.* Immunol Rev, 2012. **249**(1): p. 158-75.
26. Herwald, H. and A. Egesten, *On PAMPs and DAMPs.* J Innate Immun, 2016. **8**(5): p. 427-8.
27. Gong, T., et al., *DAMP-sensing receptors in sterile inflammation and inflammatory diseases.* Nat Rev Immunol, 2020. **20**(2): p. 95-112.
28. Takeda, K. and S. Akira, *Toll-like receptors in innate immunity.* Int Immunol, 2005. **17**(1): p. 1-14.
29. Bai, L., et al., *Promising targets based on pattern recognition receptors for cancer immunotherapy.* Pharmacol Res, 2020. **159**: p. 105017.

30. Agier, J., J. Pastwinska, and E. Brzezinska-Blaszczyk, *An overview of mast cell pattern recognition receptors.* Inflamm Res, 2018. **67**(9): p. 737-746.
31. Zhu, G., et al., *Targeting pattern-recognition receptors to discover new small molecule immune modulators.* Eur J Med Chem, 2018. **144**: p. 82-92.
32. Zhu, Y., et al., *The Interplay Between Pattern Recognition Receptors and Autophagy in Inflammation.* Adv Exp Med Biol, 2019. **1209**: p. 79-108.
33. Amarante-Mendes, G.P., et al., *Pattern Recognition Receptors and the Host Cell Death Molecular Machinery.* Front Immunol, 2018. **9**: p. 2379.
34. Zeromski, J., et al., *Significance and Role of Pattern Recognition Receptors in Malignancy.* Arch Immunol Ther Exp (Warsz), 2019. **67**(3): p. 133-141.
35. Schnappauf, O., et al., *The Pyrin Inflammasome in Health and Disease.* Front Immunol, 2019. **10**: p. 1745.
36. Nakaya, Y., et al., *AIM2-Like Receptors Positively and Negatively Regulate the Interferon Response Induced by Cytosolic DNA.* mBio, 2017. **8**(4).
37. Takagi, M., et al., *Danger of frustrated sensors: Role of Toll-like receptors and NOD-like receptors in aseptic and septic inflammations around total hip replacements.* J Orthop Translat, 2017. **10**: p. 68-85.
38. McKernan, D.P., *Pattern recognition receptors as potential drug targets in inflammatory disorders.* Adv Protein Chem Struct Biol, 2020. **119**: p. 65-109.
39. Cronkite, D.A. and T.M. Strutt, *The Regulation of Inflammation by Innate and Adaptive Lymphocytes.* J Immunol Res, 2018. **2018**: p. 1467538.
40. Martinon, F., K. Burns, and J. Tschopp, *The inflammasome: a molecular platform triggering activation of inflammatory caspases and processing of proIL-beta.* Mol Cell, 2002. **10**(2): p. 417-26.
41. Zheng, D., T. Liwinski, and E. Elinav, *Inflammasome activation and regulation: toward a better understanding of complex mechanisms.* Cell Discov, 2020. **6**: p. 36.
42. Amin, J., D. Boche, and S. Rakic, *What do we know about the inflammasome in humans?* Brain Pathol, 2017. **27**(2): p. 192-204.
43. Guo, H., J.B. Callaway, and J.P. Ting, *Inflammasomes: mechanism of action, role in disease, and therapeutics.* Nat Med, 2015. **21**(7): p. 677-87.
44. Palazon-Riquelme, P. and G. Lopez-Castejon, *The inflammasomes, immune guardians at defence barriers.* Immunology, 2018. **155**(3): p. 320-330.
45. Franklin, B.S., E. Latz, and F.I. Schmidt, *The intra- and extracellular functions of ASC specks.* Immunol Rev, 2018. **281**(1): p. 74-87.
46. Yerramothu, P., A.K. Vijay, and M.D.P. Willcox, *Inflammasomes, the eye and anti-inflammasome therapy.* Eye (Lond), 2018. **32**(3): p. 491-505.
47. Broz, P. and V.M. Dixit, *Inflammasomes: mechanism of assembly, regulation and signalling.* Nat Rev Immunol, 2016. **16**(7): p. 407-20.
48. Martinon, F. and J. Tschopp, *Inflammatory caspases and inflammasomes: master switches of inflammation.* Cell Death Differ, 2007. **14**(1): p. 10-22.
49. Yang, Y., et al., *Recent advances in the mechanisms of NLRP3 inflammasome activation and its inhibitors.* Cell Death Dis, 2019. **10**(2): p. 128.
50. Song, N. and T. Li, *Regulation of NLRP3 Inflammasome by Phosphorylation.* Front Immunol, 2018. **9**: p. 2305.
51. Gavrilin, M.A., et al., *Inflammasome Adaptor ASC Is Highly Elevated in Lung Over Plasma and Relates to Inflammation and Lung Diffusion in the Absence of Speck Formation.* Front Immunol, 2020. **11**: p. 461.
52. Dick, M.S., et al., *ASC filament formation serves as a signal amplification mechanism for inflammasomes.* Nat Commun, 2016. **7**: p. 11929.
53. Hoss, F., J.F. Rodriguez-Alcazar, and E. Latz, *Assembly and regulation of ASC specks.* Cell Mol Life Sci, 2017. **74**(7): p. 1211-1229.
54. Chen, G. and J.H. Pedra, *The inflammasome in host defense.* Sensors (Basel), 2010. **10**(1): p. 97-111.
55. Liu, X., et al., *Inflammasome-activated gasdermin D causes pyroptosis by forming membrane pores.* Nature, 2016. **535**(7610): p. 153-8.
56. Downs, K.P., et al., *An overview of the non-canonical inflammasome.* Mol Aspects Med, 2020. **76**: p. 100924.

57. Wang, X., W.J. Eagen, and J.C. Lee, *Orchestration of human macrophage NLRP3 inflammasome activation by Staphylococcus aureus extracellular vesicles.* Proc Natl Acad Sci U S A, 2020. **117**(6): p. 3174-3184.
58. Yu, P., et al., *Pyroptosis: mechanisms and diseases.* Signal Transduct Target Ther, 2021. **6**(1): p. 128.
59. Man, S.M., R. Karki, and T.D. Kanneganti, *Molecular mechanisms and functions of pyroptosis, inflammatory caspases and inflammasomes in infectious diseases.* Immunol Rev, 2017. **277**(1): p. 61-75.
60. Elizagaray, M.L., et al., *Canonical and Non-canonical Inflammasome Activation by Outer Membrane Vesicles Derived From Bordetella pertussis.* Front Immunol, 2020. **11**: p. 1879.
61. Medzhitov, R., *Origin and physiological roles of inflammation.* Nature, 2008. **454**(7203): p. 428-35.
62. Lamkanfi, M. and V.M. Dixit, *Inflammasomes and their roles in health and disease.* Annu Rev Cell Dev Biol, 2012. **28**: p. 137-61.
63. Li, Y., et al., *Inflammasomes as therapeutic targets in human diseases.* Signal Transduct Target Ther, 2021. **6**(1): p. 247.
64. Kagan, J.C., V.G. Magupalli, and H. Wu, *SMOCs: supramolecular organizing centres that control innate immunity.* Nat Rev Immunol, 2014. **14**(12): p. 821-6.
65. Qiao, Q. and H. Wu, *Supramolecular organizing centers (SMOCs) as signaling machines in innate immune activation.* Sci China Life Sci, 2015. **58**(11): p. 1067-72.
66. Cheng, J., et al., *Kinetic properties of ASC protein aggregation in epithelial cells.* J Cell Physiol, 2010. **222**(3): p. 738-47.
67. Franklin, B.S., et al., *The adaptor ASC has extracellular and 'prionoid' activities that propagate inflammation.* Nat Immunol, 2014. **15**(8): p. 727-37.
68. Lu, A., et al., *Unified polymerization mechanism for the assembly of ASC-dependent inflammasomes.* Cell, 2014. **156**(6): p. 1193-1206.
69. Masumoto, J., et al., *ASC, a novel 22-kDa protein, aggregates during apoptosis of human promyelocytic leukemia HL-60 cells.* J Biol Chem, 1999. **274**(48): p. 33835-8.
70. Srinivasula, S.M., et al., *The PYRIN-CARD protein ASC is an activating adaptor for caspase-1.* J Biol Chem, 2002. **277**(24): p. 21119-22.
71. Agrawal, I. and S. Jha, *Comprehensive review of ASC structure and function in immune homeostasis and disease.* Mol Biol Rep, 2020. **47**(4): p. 3077-3096.
72. de Alba, E., *Structure and interdomain dynamics of apoptosis-associated speck-like protein containing a CARD (ASC).* J Biol Chem, 2009. **284**(47): p. 32932-41.
73. Sahillioglu, A.C., et al., *Structural and dynamics aspects of ASC speck assembly.* Structure, 2014. **22**(12): p. 1722-1734.
74. Bryan, N.B., et al., *Differential splicing of the apoptosis-associated speck like protein containing a caspase recruitment domain (ASC) regulates inflammasomes.* J Inflamm (Lond), 2010. **7**: p. 23.
75. Bryan, N.B., et al., *Activation of inflammasomes requires intracellular redistribution of the apoptotic speck-like protein containing a caspase recruitment domain.* J Immunol, 2009. **182**(5): p. 3173-82.
76. Fernandes-Alnemri, T., et al., *The pyroptosome: a supramolecular assembly of ASC dimers mediating inflammatory cell death via caspase-1 activation.* Cell Death Differ, 2007. **14**(9): p. 1590-604.
77. Mariathasan, S., et al., *Differential activation of the inflammasome by caspase-1 adaptors ASC and Ipaf.* Nature, 2004. **430**(6996): p. 213-8.
78. Lee, B.L., et al., *ASC- and caspase-8-dependent apoptotic pathway diverges from the NLRC4 inflammasome in macrophages.* Sci Rep, 2018. **8**(1): p. 3788.
79. Ohtsuka, T., et al., *ASC is a Bax adaptor and regulates the p53-Bax mitochondrial apoptosis pathway.* Nat Cell Biol, 2004. **6**(2): p. 121-8.
80. Ciazynska, M., et al., *NLRP1 and NLRP3 inflammasomes as a new approach to skin carcinogenesis.* Oncol Lett, 2020. **19**(3): p. 1649-1656.
81. Finger, J.N., et al., *Autolytic proteolysis within the function to find domain (FIIND) is required for NLRP1 inflammasome activity.* J Biol Chem, 2012. **287**(30): p. 25030-7.
82. Pellegrini, C., et al., *Canonical and Non-Canonical Activation of NLRP3 Inflammasome at the Crossroad between Immune Tolerance and Intestinal Inflammation.* Front Immunol, 2017. **8**: p. 36.

83. Lee, H.E., et al., *Inhibition of NLRP3 inflammasome in tumor microenvironment leads to suppression of metastatic potential of cancer cells.* Sci Rep, 2019. **9**(1): p. 12277.
84. Kinnunen, K., et al., *Lysosomal destabilization activates the NLRP3 inflammasome in human umbilical vein endothelial cells (HUVECs).* J Cell Commun Signal, 2017. **11**(3): p. 275-279.
85. Gong, Z., et al., *Mitochondrial dysfunction induces NLRP3 inflammasome activation during cerebral ischemia/reperfusion injury.* J Neuroinflammation, 2018. **15**(1): p. 242.
86. Duncan, J.A. and S.W. Canna, *The NLRC4 Inflammasome.* Immunol Rev, 2018. **281**(1): p. 115-123.
87. Zhao, Y., et al., *The NLRC4 inflammasome receptors for bacterial flagellin and type III secretion apparatus.* Nature, 2011. **477**(7366): p. 596-600.
88. Lugrin, J. and F. Martinon, *The AIM2 inflammasome: Sensor of pathogens and cellular perturbations.* Immunol Rev, 2018. **281**(1): p. 99-114.
89. Ridley, A.J., *Rho GTPases and actin dynamics in membrane protrusions and vesicle trafficking.* Trends Cell Biol, 2006. **16**(10): p. 522-9.
90. Ahmed, S., et al., *Andrographolide suppresses NLRP3 inflammasome activation in microglia through induction of parkin-mediated mitophagy in in-vitro and in-vivo models of Parkinson disease.* Brain Behav Immun, 2021. **91**: p. 142-158.
91. Heymann, M.C. and A. Rosen-Wolff, *Contribution of the inflammasomes to autoinflammatory diseases and recent mouse models as research tools.* Clin Immunol, 2013. **147**(3): p. 175-84.
92. Masters, S.L., *Specific inflammasomes in complex diseases.* Clin Immunol, 2013. **147**(3): p. 223-8.
93. Moll, M. and J.B. Kuemmerle-Deschner, *Inflammasome and cytokine blocking strategies in autoinflammatory disorders.* Clin Immunol, 2013. **147**(3): p. 242-75.
94. Olsen, I. and S.K. Singhrao, *Inflammasome Involvement in Alzheimer's Disease.* J Alzheimers Dis, 2016. **54**(1): p. 45-53.
95. Masters, S.L., et al., *Activation of the NLRP3 inflammasome by islet amyloid polypeptide provides a mechanism for enhanced IL-1beta in type 2 diabetes.* Nat Immunol, 2010. **11**(10): p. 897-904.
96. Hamarsheh, S. and R. Zeiser, *NLRP3 Inflammasome Activation in Cancer: A Double-Edged Sword.* Front Immunol, 2020. **11**: p. 1444.
97. Moossavi, M., et al., *Role of the NLRP3 inflammasome in cancer.* Mol Cancer, 2018. **17**(1): p. 158.
98. Duewell, P., et al., *NLRP3 inflammasomes are required for atherogenesis and activated by cholesterol crystals.* Nature, 2010. **464**(7293): p. 1357-61.
99. Mezzaroma, E., et al., *The inflammasome promotes adverse cardiac remodeling following acute myocardial infarction in the mouse.* Proc Natl Acad Sci U S A, 2011. **108**(49): p. 19725-30.
100. Dihlmann, S., et al., *Increased expression and activation of absent in melanoma 2 inflammasome components in lymphocytic infiltrates of abdominal aortic aneurysms.* Mol Med, 2014. **20**: p. 230-7.
101. Grebe, A., F. Hoss, and E. Latz, *NLRP3 Inflammasome and the IL-1 Pathway in Atherosclerosis.* Circ Res, 2018. **122**(12): p. 1722-1740.
102. Paramel Varghese, G., et al., *NLRP3 Inflammasome Expression and Activation in Human Atherosclerosis.* J Am Heart Assoc, 2016. **5**(5).
103. Borborema, M.E.A., et al., *Inflammasome activation by NLRP1 and NLRC4 in patients with coronary stenosis.* Immunobiology, 2020. **225**(3): p. 151940.
104. Lusebrink, E., et al., *AIM2 Stimulation Impairs Reendothelialization and Promotes the Development of Atherosclerosis in Mice.* Front Cardiovasc Med, 2020. **7**: p. 582482.
105. Duan, Y., N. Kelley, and Y. He, *Role of the NLRP3 inflammasome in neurodegenerative diseases and therapeutic implications.* Neural Regen Res, 2020. **15**(7): p. 1249-1250.
106. Kaushal, V., et al., *Neuronal NLRP1 inflammasome activation of Caspase-1 coordinately regulates inflammatory interleukin-1-beta production and axonal degeneration-associated Caspase-6 activation.* Cell Death Differ, 2015. **22**(10): p. 1676-86.
107. Wu, P.J., et al., *Deletion of the Inflammasome Sensor Aim2 Mitigates Abeta Deposition and Microglial Activation but Increases Inflammatory Cytokine Expression in an Alzheimer Disease Mouse Model.* Neuroimmunomodulation, 2017. **24**(1): p. 29-39.
108. Saadi, M., et al., *Involvement of NLRC4 inflammasome through caspase-1 and IL-1beta augments neuroinflammation and contributes to memory impairment in an experimental model of Alzheimer's like disease.* Brain Res Bull, 2020. **154**: p. 81-90.

109. Venegas, C., et al., *Microglia-derived ASC specks cross-seed amyloid-beta in Alzheimer's disease.* Nature, 2017. **552**(7685): p. 355-361.
110. Shaw, P.J., M.F. McDermott, and T.D. Kanneganti, *Inflammasomes and autoimmunity.* Trends Mol Med, 2011. **17**(2): p. 57-64.
111. Forouzandeh, M., et al., *The Inflammasome Signaling Proteins ASC and IL-18 as Biomarkers of Psoriasis.* Front Pharmacol, 2020. **11**: p. 1238.
112. Dombrowski, Y., et al., *Cytosolic DNA triggers inflammasome activation in keratinocytes in psoriatic lesions.* Sci Transl Med, 2011. **3**(82): p. 82ra38.
113. Ekman, A.K., et al., *Genetic variations of NLRP1: susceptibility in psoriasis.* Br J Dermatol, 2014. **171**(6): p. 1517-20.
114. Hautem, N., et al., *The NLRP3 Inflammasome Has a Critical Role in Peritoneal Dialysis-Related Peritonitis.* J Am Soc Nephrol, 2017. **28**(7): p. 2038-2052.
115. Vanhove, W., et al., *Strong Upregulation of AIM2 and IFI16 Inflammasomes in the Mucosa of Patients with Active Inflammatory Bowel Disease.* Inflamm Bowel Dis, 2015. **21**(11): p. 2673-82.
116. Volpe, C.M., P.M. Anjos, and J.A. Nogueira-Machado, *Inflammasome as a New Therapeutic Target for Diabetic Complications.* Recent Pat Endocr Metab Immune Drug Discov, 2016. **10**(1): p. 56-62.
117. Tiwari-Heckler, S., et al., *Dysregulated Host Response in Severe Acute Respiratory Syndrome Coronavirus 2-Induced Critical Illness.* Open Forum Infect Dis, 2021. **8**(3): p. ofab019.
118. Rodrigues, T.S., et al., *Inflammasomes are activated in response to SARS-CoV-2 infection and are associated with COVID-19 severity in patients.* J Exp Med, 2021. **218**(3).
119. Maman, S. and I.P. Witz, *A history of exploring cancer in context.* Nat Rev Cancer, 2018. **18**(6): p. 359-376.
120. Mittal, S., N.J. Brown, and I. Holen, *The breast tumor microenvironment: role in cancer development, progression and response to therapy.* Expert Rev Mol Diagn, 2018. **18**(3): p. 227-243.
121. Deepak, K.G.K., et al., *Tumor microenvironment: Challenges and opportunities in targeting metastasis of triple negative breast cancer.* Pharmacol Res, 2020. **153**: p. 104683.
122. Choi, J., et al., *The role of tumor-associated macrophage in breast cancer biology.* Histol Histopathol, 2018. **33**(2): p. 133-145.
123. Annaratone, L., et al., *The Multifaceted Nature of Tumor Microenvironment in Breast Carcinomas.* Pathobiology, 2020. **87**(2): p. 125-142.
124. Jin, M.Z. and W.L. Jin, *The updated landscape of tumor microenvironment and drug repurposing.* Signal Transduct Target Ther, 2020. **5**(1): p. 166.
125. Korniluk, A., et al., *From inflammation to cancer.* Ir J Med Sci, 2017. **186**(1): p. 57-62.
126. Akhtar, M., et al., *Paget's "Seed and Soil" Theory of Cancer Metastasis: An Idea Whose Time has Come.* Adv Anat Pathol, 2019. **26**(1): p. 69-74.
127. Paget, S., *The distribution of secondary growths in cancer of the breast. 1889.* Cancer Metastasis Rev, 1989. **8**(2): p. 98-101.
128. Langley, R.R. and I.J. Fidler, *The seed and soil hypothesis revisited--the role of tumor-stroma interactions in metastasis to different organs.* Int J Cancer, 2011. **128**(11): p. 2527-35.
129. Hanahan, D. and R.A. Weinberg, *Hallmarks of cancer: the next generation.* Cell, 2011. **144**(5): p. 646-74.
130. Fu, X., et al., *Precise design strategies of nanomedicine for improving cancer therapeutic efficacy using subcellular targeting.* Signal Transduct Target Ther, 2020. **5**(1): p. 262.
131. Yang, Q., et al., *The role of tumor-associated macrophages (TAMs) in tumor progression and relevant advance in targeted therapy.* Acta Pharm Sin B, 2020. **10**(11): p. 2156-2170.
132. Kolb, R., et al., *Inflammasomes in cancer: a double-edged sword.* Protein Cell, 2014. **5**(1): p. 12-20.
133. Kantono, M. and B. Guo, *Inflammasomes and Cancer: The Dynamic Role of the Inflammasome in Tumor Development.* Front Immunol, 2017. **8**: p. 1132.
134. Allen, I.C., et al., *The NLRP3 inflammasome functions as a negative regulator of tumorigenesis during colitis-associated cancer.* J Exp Med, 2010. **207**(5): p. 1045-56.
135. Jang, J.H., et al., *Breast Cancer Cell-Derived Soluble CD44 Promotes Tumor Progression by Triggering Macrophage IL1beta Production.* Cancer Res, 2020. **80**(6): p. 1342-1356.
136. Nutter, F., et al., *Different molecular profiles are associated with breast cancer cell homing compared with colonisation of bone: evidence using a novel bone-seeking cell line.* Endocr Relat Cancer, 2014. **21**(2): p. 327-41.

137. Jang, J.H., D.H. Kim, and Y.J. Surh, *Dynamic roles of inflammasomes in inflammatory tumor microenvironment.* NPJ Precis Oncol, 2021. **5**(1): p. 18.
138. Guo, B., et al., *Targeting inflammasome/IL-1 pathways for cancer immunotherapy.* Sci Rep, 2016. **6**: p. 36107.
139. Kong, H., et al., *Differential expression of inflammasomes in lung cancer cell lines and tissues.* Tumour Biol, 2015. **36**(10): p. 7501-13.
140. Terlizzi, M., et al., *IL-1alpha and IL-1beta-producing macrophages populate lung tumor lesions in mice.* Oncotarget, 2016. **7**(36): p. 58181-58192.
141. Xu, S., et al., *Inflammasome inhibitors: promising therapeutic approaches against cancer.* J Hematol Oncol, 2019. **12**(1): p. 64.
142. Perrichet, A., F. Ghiringhelli, and C. Rebe, *Understanding Inflammasomes and PD-1/PD-L1 Crosstalk to Improve Cancer Treatment Efficiency.* Cancers (Basel), 2020. **12**(12).
143. Cao, X. and J. Xu, *Insights into inflammasome and its research advances in cancer.* Tumori, 2019. **105**(6): p. 456-464.
144. Lahooti, B., et al., *Therapeutic role of inflammasome inhibitors in neurodegenerative disorders.* Brain Behav Immun, 2021. **91**: p. 771-783.
145. Schmidt, F.I., et al., *A single domain antibody fragment that recognizes the adaptor ASC defines the role of ASC domains in inflammasome assembly.* J Exp Med, 2016. **213**(5): p. 771-90.
146. Desu, H.L., et al., *IC100: a novel anti-ASC monoclonal antibody improves functional outcomes in an animal model of multiple sclerosis.* J Neuroinflammation, 2020. **17**(1): p. 143.
147. Pal, A., et al., *Inhibition of NLRP3 inflammasome activation by cell-permeable stapled peptides.* Sci Rep, 2019. **9**(1): p. 4913.
148. Carvalho, A.M., et al., *Glyburide, a NLRP3 Inhibitor, Decreases Inflammatory Response and Is a Candidate to Reduce Pathology in Leishmania braziliensis Infection.* J Invest Dermatol, 2020. **140**(1): p. 246-249 e2.
149. Lamkanfi, M., et al., *Glyburide inhibits the Cryopyrin/Nalp3 inflammasome.* J Cell Biol, 2009. **187**(1): p. 61-70.
150. Lee, J., et al., *BAY 11-7082 is a broad-spectrum inhibitor with anti-inflammatory activity against multiple targets.* Mediators Inflamm, 2012. **2012**: p. 416036.
151. Garcia, M.G., et al., *Inhibition of NF-kappaB activity by BAY 11-7082 increases apoptosis in multidrug resistant leukemic T-cell lines.* Leuk Res, 2005. **29**(12): p. 1425-34.
152. Juliana, C., et al., *Anti-inflammatory compounds parthenolide and Bay 11-7082 are direct inhibitors of the inflammasome.* J Biol Chem, 2010. **285**(13): p. 9792-9802.
153. Coon, J.T. and E. Ernst, *Andrographis paniculata in the treatment of upper respiratory tract infections: a systematic review of safety and efficacy.* Planta Med, 2004. **70**(4): p. 293-8.
154. Jiang, H., et al., *Identification of a selective and direct NLRP3 inhibitor to treat inflammatory disorders.* J Exp Med, 2017. **214**(11): p. 3219-3238.
155. Coll, R.C., et al., *MCC950 directly targets the NLRP3 ATP-hydrolysis motif for inflammasome inhibition.* Nat Chem Biol, 2019. **15**(6): p. 556-559.
156. Tapia-Abellan, A., et al., *MCC950 closes the active conformation of NLRP3 to an inactive state.* Nat Chem Biol, 2019. **15**(6): p. 560-564.
157. He, H., et al., *Oridonin is a covalent NLRP3 inhibitor with strong anti-inflammasome activity.* Nat Commun, 2018. **9**(1): p. 2550.
158. Huang, Y., et al., *Tranilast directly targets NLRP3 to treat inflammasome-driven diseases.* EMBO Mol Med, 2018. **10**(4).
159. Marchetti, C., et al., *OLT1177, a beta-sulfonyl nitrile compound, safe in humans, inhibits the NLRP3 inflammasome and reverses the metabolic cost of inflammation.* Proc Natl Acad Sci U S A, 2018. **115**(7): p. E1530-E1539.
160. Wannamaker, W., et al., *(S)-1-((S)-2-{[1-(4-amino-3-chloro-phenyl)-methanoyl]-amino}-3,3-dimethyl-butanoy l)-pyrrolidine-2-carboxylic acid ((2R,3S)-2-ethoxy-5-oxo-tetrahydro-furan-3-yl)-amide (VX-765), an orally available selective interleukin (IL)-converting enzyme/caspase-1 inhibitor, exhibits potent anti-inflammatory activities by inhibiting the release of IL-1beta and IL-18.* J Pharmacol Exp Ther, 2007. **321**(2): p. 509-16.
161. Flores, J., et al., *Caspase-1 inhibition alleviates cognitive impairment and neuropathology in an Alzheimer's disease mouse model.* Nat Commun, 2018. **9**(1): p. 3916.
162. Bialer, M., et al., *Progress report on new antiepileptic drugs: a summary of the Eleventh Eilat Conference (EILAT XI).* Epilepsy Res, 2013. **103**(1): p. 2-30.

163. McKie, E.A., et al., *A Study to Investigate the Efficacy and Safety of an Anti-Interleukin-18 Monoclonal Antibody in the Treatment of Type 2 Diabetes Mellitus.* PLoS One, 2016. **11**(3): p. e0150018.
164. Granowitz, E.V., et al., *Pharmacokinetics, safety and immunomodulatory effects of human recombinant interleukin-1 receptor antagonist in healthy humans.* Cytokine, 1992. **4**(5): p. 353-60.
165. Dinarello, C.A. and J.W. van der Meer, *Treating inflammation by blocking interleukin-1 in humans.* Semin Immunol, 2013. **25**(6): p. 469-84.
166. Rondeau, J.M., et al., *The molecular mode of action and species specificity of canakinumab, a human monoclonal antibody neutralizing IL-1beta.* MAbs, 2015. **7**(6): p. 1151-60.
167. Hoffman, H.M., et al., *Efficacy and safety of rilonacept (interleukin-1 Trap) in patients with cryopyrin-associated periodic syndromes: results from two sequential placebo-controlled studies.* Arthritis Rheum, 2008. **58**(8): p. 2443-52.
168. Feng, Y., et al., *Breast cancer development and progression: Risk factors, cancer stem cells, signaling pathways, genomics, and molecular pathogenesis.* Genes Dis, 2018. **5**(2): p. 77-106.
169. Sung, H., et al., *Global cancer statistics 2020: GLOBOCAN estimates of incidence and mortality worldwide for 36 cancers in 185 countries.* CA Cancer J Clin, 2021.
170. Kumar, S., et al., *Change in the microenvironment of breast cancer studied by FTIR imaging.* Analyst, 2013. **138**(14): p. 4058-65.
171. Khamis, Z.I., Z.J. Sahab, and Q.X. Sang, *Active roles of tumor stroma in breast cancer metastasis.* Int J Breast Cancer, 2012. **2012**: p. 574025.
172. Boix-Montesinos, P., et al., *The past, present, and future of breast cancer models for nanomedicine development.* Adv Drug Deliv Rev, 2021. **173**: p. 306-330.
173. Waks, A.G. and E.P. Winer, *Breast Cancer Treatment: A Review.* JAMA, 2019. **321**(3): p. 288-300.
174. Harbeck, N., et al., *Breast cancer.* Nat Rev Dis Primers, 2019. **5**(1): p. 66.
175. Peddi, P.F., M.J. Ellis, and C. Ma, *Molecular basis of triple negative breast cancer and implications for therapy.* Int J Breast Cancer, 2012. **2012**: p. 217185.
176. O'Reilly, E.A., et al., *The fate of chemoresistance in triple negative breast cancer (TNBC).* BBA Clin, 2015. **3**: p. 257-75.
177. Hartshorn, C.M., et al., *Nanotechnology Strategies To Advance Outcomes in Clinical Cancer Care.* ACS Nano, 2018. **12**(1): p. 24-43.
178. Basu, A., et al., *Immunotherapy in breast cancer: Current status and future directions.* Adv Cancer Res, 2019. **143**: p. 295-349.
179. Thakur, V. and R.V. Kutty, *Recent advances in nanotheranostics for triple negative breast cancer treatment.* J Exp Clin Cancer Res, 2019. **38**(1): p. 430.
180. Bayraktar, S., et al., *Immunotherapy in breast cancer.* J Carcinog, 2019. **18**: p. 2.
181. Polk, A., et al., *Checkpoint inhibitors in breast cancer - Current status.* Cancer Treat Rev, 2018. **63**: p. 122-134.
182. Cyprian, F.S., et al., *Targeted immunotherapy with a checkpoint inhibitor in combination with chemotherapy: A new clinical paradigm in the treatment of triple-negative breast cancer.* Bosn J Basic Med Sci, 2019. **19**(3): p. 227-233.
183. Gupta, G.K., et al., *Perspectives on Triple-Negative Breast Cancer: Current Treatment Strategies, Unmet Needs, and Potential Targets for Future Therapies.* Cancers (Basel), 2020. **12**(9).
184. Reddy, S.M., E. Carroll, and R. Nanda, *Atezolizumab for the treatment of breast cancer.* Expert Rev Anticancer Ther, 2020. **20**(3): p. 151-158.
185. Vaddepally, R.K., et al., *Review of Indications of FDA-Approved Immune Checkpoint Inhibitors per NCCN Guidelines with the Level of Evidence.* Cancers (Basel), 2020. **12**(3).
186. Adams, S., et al., *Atezolizumab Plus nab-Paclitaxel in the Treatment of Metastatic Triple-Negative Breast Cancer With 2-Year Survival Follow-up: A Phase 1b Clinical Trial.* JAMA Oncol, 2019. **5**(3): p. 334-342.
187. Frankel, T., M.P. Lanfranca, and W. Zou, *The Role of Tumor Microenvironment in Cancer Immunotherapy.* Adv Exp Med Biol, 2017. **1036**: p. 51-64.
188. Murciano-Goroff, Y.R., A.B. Warner, and J.D. Wolchok, *The future of cancer immunotherapy: microenvironment-targeting combinations.* Cell Res, 2020. **30**(6): p. 507-519.
189. Senapati, S., et al., *Controlled drug delivery vehicles for cancer treatment and their performance.* Signal Transduct Target Ther, 2018. **3**: p. 7.

190. Kayl, A.E. and C.A. Meyers, *Side-effects of chemotherapy and quality of life in ovarian and breast cancer patients.* Curr Opin Obstet Gynecol, 2006. **18**(1): p. 24-8.
191. Arruebo, M., et al., *Assessment of the evolution of cancer treatment therapies.* Cancers (Basel), 2011. **3**(3): p. 3279-330.
192. Navya, P.N., et al., *Current trends and challenges in cancer management and therapy using designer nanomaterials.* Nano Converg, 2019. **6**(1): p. 23.
193. Wicki, A., et al., *Nanomedicine in cancer therapy: challenges, opportunities, and clinical applications.* J Control Release, 2015. **200**: p. 138-57.
194. Duncan, R. and R. Gaspar, *Nanomedicine(s) under the microscope.* Mol Pharm, 2011. **8**(6): p. 2101-41.
195. Danhier, F., *To exploit the tumor microenvironment: Since the EPR effect fails in the clinic, what is the future of nanomedicine?* J Control Release, 2016. **244**(Pt A): p. 108-121.
196. Maso, K., et al., *Molecular platforms for targeted drug delivery.* Int Rev Cell Mol Biol, 2019. **346**: p. 1-50.
197. He, H., et al., *Survey of Clinical Translation of Cancer Nanomedicines-Lessons Learned from Successes and Failures.* Acc Chem Res, 2019. **52**(9): p. 2445-2461.
198. Zhang, Y., et al., *Nanotechnology in cancer diagnosis: progress, challenges and opportunities.* J Hematol Oncol, 2019. **12**(1): p. 137.
199. Lehr, C.M., *Biological barriers and nanomedicine--timely challenges in advanced drug delivery research.* Eur J Pharm Biopharm, 2009. **72**(2): p. 287-8.
200. Barua, S. and S. Mitragotri, *Challenges associated with Penetration of Nanoparticles across Cell and Tissue Barriers: A Review of Current Status and Future Prospects.* Nano Today, 2014. **9**(2): p. 223-243.
201. Zagorodko, O., et al., *Polypeptide-Based Conjugates as Therapeutics: Opportunities and Challenges.* Macromol Biosci, 2017. **17**(1).
202. Meng, H., et al., *Walking the line: The fate of nanomaterials at biological barriers.* Biomaterials, 2018. **174**: p. 41-53.
203. Riehemann, K., et al., *Nanomedicine--challenge and perspectives.* Angew Chem Int Ed Engl, 2009. **48**(5): p. 872-97.
204. Blanco, E., H. Shen, and M. Ferrari, *Principles of nanoparticle design for overcoming biological barriers to drug delivery.* Nat Biotechnol, 2015. **33**(9): p. 941-51.
205. Lin, J., et al., *Understanding the synergistic effect of physicochemical properties of nanoparticles and their cellular entry pathways.* Commun Biol, 2020. **3**(1): p. 205.
206. Ma, N., et al., *Influence of nanoparticle shape, size, and surface functionalization on cellular uptake.* J Nanosci Nanotechnol, 2013. **13**(10): p. 6485-98.
207. Miao, L., C.M. Lin, and L. Huang, *Stromal barriers and strategies for the delivery of nanomedicine to desmoplastic tumors.* J Control Release, 2015. **219**: p. 192-204.
208. Valkenburg, K.C., A.E. de Groot, and K.J. Pienta, *Targeting the tumour stroma to improve cancer therapy.* Nat Rev Clin Oncol, 2018. **15**(6): p. 366-381.
209. Zhang, B., Y. Hu, and Z. Pang, *Modulating the Tumor Microenvironment to Enhance Tumor Nanomedicine Delivery.* Front Pharmacol, 2017. **8**: p. 952.
210. Hoshyar, N., et al., *The effect of nanoparticle size on in vivo pharmacokinetics and cellular interaction.* Nanomedicine (Lond), 2016. **11**(6): p. 673-92.
211. Xu, S., et al., *Targeting receptor-mediated endocytotic pathways with nanoparticles: rationale and advances.* Adv Drug Deliv Rev, 2013. **65**(1): p. 121-38.
212. Zhou, Q., et al., *Enzyme-activatable polymer-drug conjugate augments tumour penetration and treatment efficacy.* Nat Nanotechnol, 2019. **14**(8): p. 799-809.
213. Du, W. and O. Elemento, *Cancer systems biology: embracing complexity to develop better anticancer therapeutic strategies.* Oncogene, 2015. **34**(25): p. 3215-25.
214. Matsumura, Y. and H. Maeda, *A new concept for macromolecular therapeutics in cancer chemotherapy: mechanism of tumoritropic accumulation of proteins and the antitumor agent smancs.* Cancer Res, 1986. **46**(12 Pt 1): p. 6387-92.
215. Dai, Y., et al., *Nanoparticle design strategies for enhanced anticancer therapy by exploiting the tumour microenvironment.* Chem Soc Rev, 2017. **46**(12): p. 3830-3852.
216. Shi, Y., et al., *The EPR effect and beyond: Strategies to improve tumor targeting and cancer nanomedicine treatment efficacy.* Theranostics, 2020. **10**(17): p. 7921-7924.
217. Fang, J., W. Islam, and H. Maeda, *Exploiting the dynamics of the EPR effect and strategies to improve the therapeutic effects of nanomedicines by using EPR effect enhancers.* Adv Drug Deliv Rev, 2020. **157**: p. 142-160.

218. Maeda, H., *Polymer therapeutics and the EPR effect.* J Drug Target, 2017. **25**(9-10): p. 781-785.
219. Sindhwani, S., et al., *The entry of nanoparticles into solid tumours.* Nat Mater, 2020. **19**(5): p. 566-575.
220. Bor, G., I.D. Mat Azmi, and A. Yaghmur, *Nanomedicines for cancer therapy: current status, challenges and future prospects.* Ther Deliv, 2019. **10**(2): p. 113-132.
221. Zhang, Q., X.E. Huang, and L.L. Gao, *A clinical study on the premedication of paclitaxel liposome in the treatment of solid tumors.* Biomed Pharmacother, 2009. **63**(8): p. 603-7.
222. O'Byrne, K.J., et al., *A phase I dose-escalating study of DaunoXome, liposomal daunorubicin, in metastatic breast cancer.* Br J Cancer, 2002. **87**(1): p. 15-20.
223. Li, Y., et al., *Pharmacologic sensitivity of paclitaxel to its delivery vehicles drives distinct clinical outcomes of paclitaxel formulations.* Mol Pharm, 2015. **12**(4): p. 1308-17.
224. Lim, W.T., et al., *Phase I pharmacokinetic study of a weekly liposomal paclitaxel formulation (Genexol-PM) in patients with solid tumors.* Ann Oncol, 2010. **21**(2): p. 382-388.
225. Ranade, A.A., et al., *Clinical and economic implications of the use of nanoparticle paclitaxel (Nanoxel) in India.* Ann Oncol, 2013. **24 Suppl 5**: p. v6-12.
226. von Minckwitz, G., et al., *Trastuzumab Emtansine for Residual Invasive HER2-Positive Breast Cancer.* N Engl J Med, 2019. **380**(7): p. 617-628.
227. Safra, T., et al., *Pegylated liposomal doxorubicin (doxil): reduced clinical cardiotoxicity in patients reaching or exceeding cumulative doses of 500 mg/m2.* Ann Oncol, 2000. **11**(8): p. 1029-33.
228. Gradishar, W.J., et al., *Phase III trial of nanoparticle albumin-bound paclitaxel compared with polyethylated castor oil-based paclitaxel in women with breast cancer.* J Clin Oncol, 2005. **23**(31): p. 7794-803.
229. Yuan, H., et al., *Albumin Nanoparticle of Paclitaxel (Abraxane) Decreases while Taxol Increases Breast Cancer Stem Cells in Treatment of Triple Negative Breast Cancer.* Mol Pharm, 2020. **17**(7): p. 2275-2286.
230. Duro-Castano, A., J. Movellan, and M.J. Vicent, *Smart branched polymer drug conjugates as nano-sized drug delivery systems.* Biomater Sci, 2015. **3**(10): p. 1321-34.
231. Arroyo-Crespo, J.J., et al., *Tumor microenvironment-targeted poly-L-glutamic acid-based combination conjugate for enhanced triple negative breast cancer treatment.* Biomaterials, 2018. **186**: p. 8-21.
232. Rodriguez-Otormin, F., et al., *Envisioning the future of polymer therapeutics for brain disorders.* Wiley Interdiscip Rev Nanomed Nanobiotechnol, 2019. **11**(1): p. e1532.
233. Duncan, R. and M.J. Vicent, *Polymer therapeutics-prospects for 21st century: the end of the beginning.* Adv Drug Deliv Rev, 2013. **65**(1): p. 60-70.
234. Ekladious, I., Y.L. Colson, and M.W. Grinstaff, *Polymer-drug conjugate therapeutics: advances, insights and prospects.* Nat Rev Drug Discov, 2019. **18**(4): p. 273-294.
235. El-Sayed, M.E., A.S. Hoffman, and P.S. Stayton, *Smart polymeric carriers for enhanced intracellular delivery of therapeutic macromolecules.* Expert Opin Biol Ther, 2005. **5**(1): p. 23-32.
236. Duncan, R., *The dawning era of polymer therapeutics.* Nat Rev Drug Discov, 2003. **2**(5): p. 347-60.
237. Patel, S., et al., *Brief update on endocytosis of nanomedicines.* Adv Drug Deliv Rev, 2019. **144**: p. 90-111.
238. Stirland, D.L., et al., *Mind the gap: a survey of how cancer drug carriers are susceptible to the gap between research and practice.* J Control Release, 2013. **172**(3): p. 1045-64.
239. Melnyk, T., et al., *Therapeutic potential of polypeptide-based conjugates: Rational design and analytical tools that can boost clinical translation.* Adv Drug Deliv Rev, 2020. **160**: p. 136-169.
240. Duro-Castano, A., et al., *Well-Defined Star-Shaped Polyglutamates with Improved Pharmacokinetic Profiles As Excellent Candidates for Biomedical Applications.* Mol Pharm, 2015. **12**(10): p. 3639-49.
241. Chow, D., et al., *Peptide-based Biopolymers in Biomedicine and Biotechnology.* Mater Sci Eng R Rep, 2008. **62**(4): p. 125-155.
242. Dobrovolskaia, M.A., *Pre-clinical immunotoxicity studies of nanotechnology-formulated drugs: Challenges, considerations and strategy.* J Control Release, 2015. **220**(Pt B): p. 571-83.

Ch.II

Objectives

The hypothesis of this work is that our inflammasome inhibitor, MM01, is a potential chemical tool to study the role of the inflammasome in inflammation and metastatic breast cancer models that currently represent an unmet clinical need.

The long-term objective of this doctoral thesis is the characterization of the molecular mechanism of action and pharmacological activity of a novel pan-inflammasome inhibitor, MM01, and its validation as potential anti-inflammatory and anticancer treatment. In this work, MM01 will be explored as small molecule as well as the active component of a rationally designed polypeptide-based nanomedicine.

These main objectives will be achieved through the following specific objectives:

1. The identification of the mechanism of action of MM01 – we will demonstrate the ability of MM01 to inhibit ASC oligomerization using recombinant human ASC protein and in cellular assays.
2. The demonstration of the ability of MM01 to inhibit different ASC-dependent inflammasomes in different cellular models and *in vivo* – we will evaluate inhibitory activity by studying the expression/secretion of pro-inflammatory proteins and pyroptotic cell death
3. The study of the role of inflammasome-mediated inflammation in breast cancer cell migration – we will study the impact of MM01 on the migration of human/murine breast cancer cells in response to the secretome of M1 macrophages
4. The evaluation of the antitumor and antimetastatic activity of MM01 in the 4T1 and EO771 orthotopic *in vivo* murine models
5. The identification of biomarkers to predict tumor responses to inflammasome inhibitors through proteomics
6. The development, synthesis, and chemical characterization of a polymer-based nanomedicine using a biodegradable, multivalent and newly develop polymeric carrier (poly-L-glutamic acid or PGA derivatized with cyclodextrines) capable to complex MM01 (L-PGA-βCD-MM01)
7. The characterization of L-PGA-βCD-MM01 and the study of inflammasome inhibition efficacy in cellular models of inflammation
8. The study of the antitumor efficacy of L-PGA-βCD-MM01 in the EO771 orthotopic *in vivo* model of murine breast cancer.

Ch.III

Materials & Methods

III.1. Materials

III.1.1 Chemical and biological agents.

Phorbol 12-myristate 13-acetate (PMA), dimethyl sulfoxide (DMSO), lipopolysaccharides (LPS) from Escherichia coli 055: B55, nigericine sodium salt, poly(deoxyadenylic-deoxythymidylic) acid sodium salt (poly(dA:dT)), Cholera Toxin from Vibrio cholerae, RPMI-1640, fetal bovine serum (FBS) and Dulbecco's phosphate-buffered saline (PBS) were purchased from Sigma-Aldrich (St. Louis, Missouri, USA). Monosodium Urate Crystals (MSU) were purchased from Invivogen (St. Diego, California, USA). Lipofectamine 2000 Transfection Reagent, disuccinimidyl suberate (DSS), 4′,6-diamidino-2-phenylindole (DAPI) and Wheat Germ Agglutinin, Alexa Fluor™ 488 Conjugate (WGA) were purchased from ThermoFisher Scientific (Waltham, Massachusetts, USA). VX-765 and MCC950 were provided by AdooQ Bioscience (Irvine, California, USA). Lactate Dehydrogenase (LDH) activity was measured by the Lactate Assay Kit III by BioVision (Milpitas, California, USA). The human IL-1β ELISA Set III and skin milk powder were purchased from BD Biosciences (St. Jose, California, USA). ECL Western blotting detection reagents were purchased from Amersham Pharmacia Biotech (Amersham, UK). Mouse IL-1β ELISA was purchased from R&D Systems (Minneapolis, Minnesota, USA). Poly-L-glutamic acid (PGA, acid form, 200 glutamic acid units) was purchased from Polypeptide Therapeutics Solutions (PTS) (Valencia, Spain). Anhydrous N,N-dimethylformamide (DMF, ≥99.8% anhydrous) was purchased from Scharlab SL (Sentmenat, Spain). T75 flasks, sterile 24-well plates, 12-well plates, and 6-well plates were provided by Sarstedt (Nümbrecht, Germany). ELISA 96-well plate and white 96-well plates were from Corning Costar® (New York, USA). Luciferase (Luc2) Lentiviral Vector was provided by Innoprot (Vizcaya, Spain). Bright-GloTM Luciferase Assay System and Tetrazolium (MTS) were purchased from Promega (Madison, Wisconsin, USA). Geneticin (G418) and Sodium Dodecyl Sulfate (SDS) were purchased from Fisher (Loughborough, UK). Paraformaldehyde (PFA) was provided by Electron Microscopy Sciences (Hatfield, Pennsylvania, USA). Black 96-well plates and XenoLight D-luciferin potassium salt were purchased from Perkin

Elmer (Waltham, Massachusetts, USA). Acrylamide/Bisacrylamide was provided by VWR Live Science (Radnor, Pennsylvania, USA). Mowiol® 4-88 was provided by Carl Roth (Karlsruhe, Germany). 0.22µm filters were purchased from Jet Biofil (Guangzhou, China). Insulin syringes (29G), absorbable sutures 6/0, and isoflurane were purchased form B. Braun VetCare (Barcelona, Spain). Reusable straight 20 gauge feeding needles were provided by InterFocus (Linton, UK). Ultrapure water with a resistivity of 18 MΩ.cm was used in all aqueous preparations (Milli-Q® ultrapure).

III.1.2 Cell lines and culture conditions

The human embryonic kidney HEK293 cells were obtained from Sigma Aldrich (St. Louis, Missouri, USA) and grown in DMEM – high glucose medium supplemented with inactivated 10% FBS. The human monocytic THP-1 cell line was obtained from the American Type Culture Collection (ATCC (Virginia, USA)) and grown in RPMI medium supplemented with inactivated 10% FBS. THP1-ASC-GFP cells were obtained from Invitrogen (Waltham, Massachusetts, USA) and cultured in RPMI medium supplemented with 10% FBS and supplemented with 100 µg/mL of Zeocin. The human breast cancer cell lines MDA-MB-231, MDA-MB-468, MCF7, MDA-MB-453, HCC1954 and ZR-751, were purchased from ATCC and grown in RPMI medium supplemented with inactivated 10% FBS. The murine breast cancer cell lines EO771 and 4T1 were also purchased from ATCC and grown in RPMI medium and DMEM – high glucose, respectively, supplemented with inactivated 10% FBS. Finally, the murine macrophages J744A.1 were purchased from American ATCC and grown in DMEM – high glucose. All cultures were maintained at 37°C in a 5% CO2 atmosphere. **Table 1** depicts the different cell lines, the growth media used, and the main characteristics of each cell line.

Table 1. Summary of the origin and growth medium of the different Cell Lines. FBS: Heat-inactivated fetal bovine serum.

Cell line	Origin	Growth Medium
HEK293	Human embryonic kidney	DMEM, 10% FBS
THP-1	Monocytes from Leukemia patient	RPMI, 10% FBS
THP-1-GFP-ASC	Monocytes from Leukemia patient transfected with ASC-GFP	RPMI, 10% FBS, Zeocin
MDA-MB-231	Human breast adenocarcinoma	RPMI, 10% FBS
MDA-MB-468	Human breast adenocarcinoma	RPMI, 10% FBS
MCF7	Human breast adenocarcinoma	RPMI, 10% FBS
MDA-MB-453	Human breast metastatic carcinoma	RPMI, 10% FBS
HCC1954	Human breast carcinoma	RPMI, 10% FBS
ZR-751	Human breast carcinoma	RPMI, 10% FBS
EO771	Murine breast carcinoma of C57BL/6 mice	RPMI, 10% FBS
4T1	Murine breast carcinoma of BALB/c mice	DMEM, 10% FBS
J744A.1	Murine macrophages	DMEM, 10% FBS

III.1.3 Antibodies

Table 2 depicts the antibodies employed in this thesis.

Table 2. Primary antibodies used for immunoblotting

Antibody	Purchased	Source	Dilution
Pro-caspase-1	Cell signaling	Rabbit	1:1000
Caspase-1	Cell signaling	Rabbit	1:1000
Pro-IL-1β	Cell signaling	Mouse	1:1000
IL-1β	Cell signaling	Rabbit	1:1000
ASC	Santa Cruz	Rabbit	1:1000
NLRP3	Cell signaling	Rabbit	1:1000
GAPDH	Sigma	Mouse	1:3000
Tubulin	Cell signaling	Rat	1:3000

III.1.4 Animals

The immunocompetent C57BL/6 and BALB/c mice were provided by Envigo Laboratories Inc. (Gannat, France) at 6-8 weeks of age were used for all animal experiments. All mice were kept in a specific-pathogen-free facility under constant temperature and humidity using a 12 h light-dark cycle. Food pellets and water were supplied ad-libitum during the whole experiment in all cases. Additionally, to ensure animal well-being, general aspects such as grooming conduct, tumor size, body weight, and behavior were evaluated daily.

III.2. Methods

III.2.1 *In vitro* assays

III.2.1.A Purification of the apoptosis-associated speck-like protein (ASC).

Human His-tagged-ASC was previously cloned into the vector pET28a for expression in E. coli. Afterward, pET28a vector containing the human His-tagged-ASC sequence was inoculated in a preculture of BL21 (DE3) pLysSCodon+ *E. coli* bacteria, in 150 mL of LB medium supplemented with 30 µg/mL of kanamycin and 25 µg/mL of chloramphenicol, at 37◦C under orbital shaking at 160 rpm overnight. The next day, the culture was scaled up to a volume of 8 L under the same conditions until reaching an optical density (OD) 600nm of 0.6-0.7. Then, the induction of ASC expression was carried out with the addition of 1mM isopropyl-β-D-1-thiogalactopyranoside (IPTG) and incubating at 28◦C at 160rpm for 4h. After this time, the culture was centrifuged at 6000 rpm at 4◦C for 15 min and frozen at -80◦C until further processing. The cell pellet obtained was resuspended in 300mL of lysis buffer (50 mM NaH2PO4, 300 mM NaCl, pH = 8), supplemented with protease inhibitors (10 µg/ml leupeptin, 10 µg/ml pepstatin A, 100 µM phenylmethylsulfonyl fluoride (PMSF)), lysozyme 1mg/ mL and DNase 5 µg/mL, and it was incubated for 30 min at 4◦C while shaking. To complete cell lysis, the bacteria were sonicated in a BRANSON S-450D digital sonicator with an amplitude of 40% for 5 min with pauses on ice every minute to avoid overheating the sample. The cell lysate was centrifuged at 11000 rpm for 1h at 4◦C, and the supernatant was discarded because, under these conditions, ASC is localized in bacterial inclusion

bodies. To solubilize the inclusion bodies, the pellet obtained was resuspended in 100mL of resuspension buffer (50 mM NaH2PO4, 300 mM NaCl, 8M Urea, pH = 8), sonicated under the same conditions described, and centrifuged at 11000 rpm for 45 min at 4ºC. The supernatant was purified by affinity chromatography using a 4mL cobalt-sepharose BD Talon column (635502, Clontech) after overnight incubation with shaking at room temperature (RT). The following day, a first column wash of 5 column volumes was carried out in wash buffer (50 mM NaH2PO4, 300 mM NaCl, 8 M Urea, pH = 8), and the protein folding was subsequently carried out in the own column utilizing a descending urea gradient until its complete elimination. Finally, it was eluted with 15 mL of elution buffer (50 mM NaH2PO4, 300 mM NaCl, 500mM Imidazole pH = 8). Next, desalting of the eluate was performed with PD-10 desalting columns (GE Healthcare). Finally, the protein was concentrated to 9-10 µM by centrifugation using an Amicon Ultra-4 10000Mw CO concentrator (Millipore). The protein concentration was determined by UV spectroscopy, and it was stored at -80ºC, previously passing through liquid nitrogen. The recombinant ASC construct has an approximate molecular weight of 25458 Da and a molar extinction coefficient of 25440 M-1 cm-1 measured at 280 nm.

III.2.1.B ASC filament formation *in vitro.*

Recombinant ASC protein was eluted from the PD-10 column as described above in an acidic pH buffer to avoid protein precipitation. Then, the formation of filaments is achieved at neutral pH by adding 3M Tris buffer (ph8.0) in a ratio of 1: 5 (vol/vol). The samples were incubated overnight at room temperature (RT). Finally, for analysis by electron microscopy (EM), a drop of 10 µl sample at 1mg/ml was placed on clean Parafilm, and a mesh copper pure carbon-coated grid was floated on top of it for 10 min. Then, the grids were transferred and contrasted with 1 % uranyl acetate for 5 min. Excess fluid was removed and allowed to dry before examining a transmission electron microscope FEI Tecnai G2 Spirit (ThermoFisher Scientific Company, Oregon, USA). All images were acquired using Radius software with a digital camera Xarosa (EMSIS GmbH, Münster, Germany) (**Figure 1**).

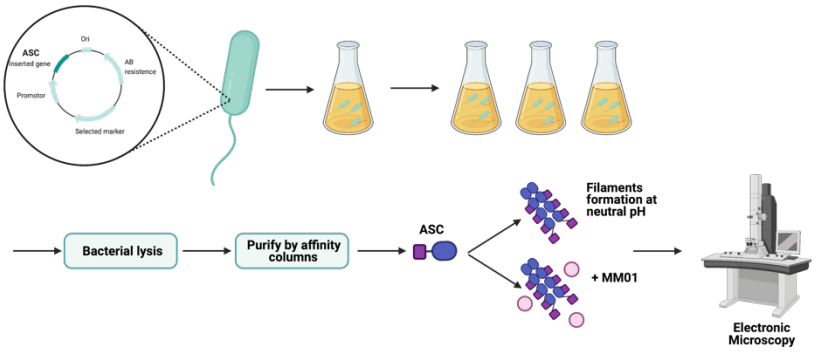

Figure 1. ASC purification and filament formation in vitro procedure.

III.2.2 Cellular assays

III.2.2.A ASC speck assay.

THP1-ASC-GFP cells were seeded at 1×10⁶/ml the day before use in six-well plates and differentiated to macrophages with 50 ng/mL of PMA. The following day, the culture medium was replaced with fresh medium containing 20 µM MM01 inhibitor or vehicle for 30 mins. Cells were then primed with 100 ng/ml LPS for 3 h and stimulated with 10 µM nigericin for 30 min for NLRP3 inflammasome activation. For confocal analysis, cells were incubated with DAPI and WGA. Image acquisition used a Leica SP8 confocal microscope, and image processing was performed using FiJi software. For cytometry analysis, samples were detached and analyzed in a CytoFlex Flow Cytometer (Beckman Coulter).

III.2.2.B ASC oligomerization assays.

THP-1 cells were seeded at $1x10^6$ cells/ml in six-well plates and differentiated with PMA 50 ng/mL. The following day, the medium was replaced with fresh medium supplemented with FBS 1%. Then, cells were treated with 20 µM MM01 inhibitor for 30 min, primed with 100 ng/ml LPS for 3 h, and then stimulated with 10 µM nigericin for 30 min. Next, the supernatants were removed, cells were rinsed in ice-cold PBS and then lysed in NP-40 buffer (20 mM HEPES-KOH pH 7.5, 150 mM KCL, 1% NP-40 plus protease inhibitors). Lysates were centrifuged at 330 × g for 10 min at 4 °C. Next, the pellets were washed and resuspended in PBS plus 2 mM DSS and incubated at RT for 10 min. Samples were then centrifuged at 330 × g for 10 min at 4 °C. The

supernatant was removed, and the cross-linked pellets were then resuspended in sample buffer (60 mM Tris pH 6.8, 10% glycerol, 2% SDS, 5% 2-mercaptoethanol, and 0.1% bromophenol blue), boiled, and analyzed by immunoblotting.

HEK293 cells were seeded at 3.0 x10^5 cells/ml in six-well plates and transfected with ASC-YFP construct [1] according to standard procedure for Lipofectamine 2000 reagent (Invitrogen). Then, cells were treated with 20 μM MM01 inhibitor for 6 h and oligomers purified as described above. Bafilomycin A1 (InvivoGen) is a selective inhibitor of vacuolar-type H^+ ATPase (V-ATPase) that inhibits autophagosome and lysosome fusion [2]. Bafilomycin (200 nM) treatment for 2 h was used as an inhibitor of protein degradation.

III.2.2.C ASC mutant analysis.

ASC mutants in the active site predicted by MM01 molecular docking were generated by using QuikChange Site-Directed Mutagenesis Kit (Agilent Technologies) in the ASC-YFP plasmid. These mutations include H118A, F163A, W169A, K174A, W169A, K174A, L192A, and the double mutant L177A L178A. In addition, the mutant R119A was used as a negative control due to the already existing literature about its inability to form specks. All molecular biology techniques were performed according to standard procedures.

To assess the effect of ASC mutants on speck formation, HEK293 cells were seeded at a concentration of 4.0x10^5 cells/ml in 12-well plates. The next day, LipofectamineTM 2000 (Invitrogen) was used according to the manufacturer's instructions to transfect the cells with the ASC-YFP plasmid. After 18 h, HEK293 cells were harvested to analyze the speck formation by flow cytometry and confocal microscopy and the oligomerization formation by chemical crosslinking. In addition, whole-cell extracts were obtained to check the presence of the fusion protein in every sample (**Figure 2**).

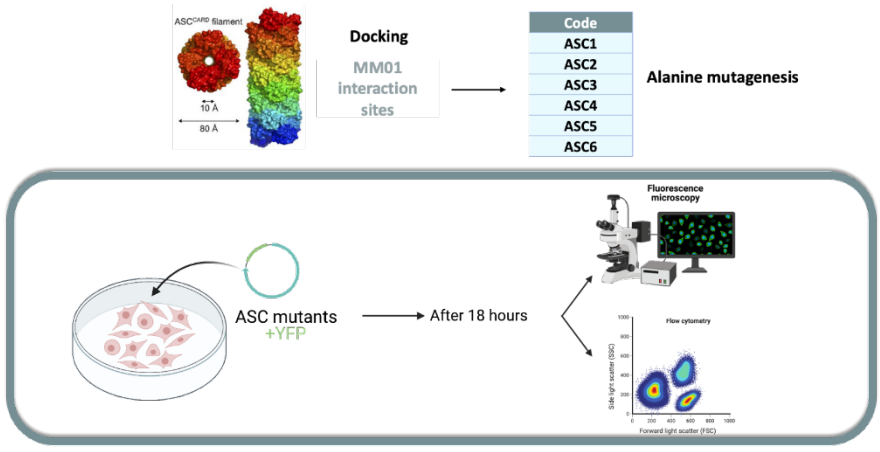

Figure 2. ASC mutant analysis procedure

III.2.2.D Docking Calculations with GOLD 5.2.

The crystal structures of caspase-1 (PDB ID: 2FQQ1 and 2BHQ1) were downloaded from the protein data bank2 and subjected to docking calculations using GOLD 5.2 software (CCDC, Cambridge, UK). The internal energy of the compounds was first minimized using the MM2 protocol and submitted to GOLD in SDF format. Docking experiments were performed three times using the default docking settings and ChemScore as the scoring function. A total of thirty genetic algorithms (GA) runs were set for each compound. The program was allowed to stop the GA runs when the top three solutions were within 1.5 Å root mean square deviation to accelerate the calculations. Intermolecular interactions were described using Discovery Studio 4.0 (Accelrys Inc, San Diego, CA, USA).

III.2.2.E Cellular assay for macrophages polarization

Monocyte to macrophage (M0) differentiation. THP-1 cells were seeded at $1x10^6$ cells/ml in six-well plates and differentiated to macrophages (M0) by treating cells for 24 hours with 50 ng/ ml PMA.

Monocyte to pro-inflammatory macrophage (M1) differentiation. THP-1 cells were seeded at $1x10^6$ cells/ml in six-well plates and treated for 24 hours with 50 ng/mL of PMA (M0 differentiation). At 24 hours the differentiated adherent cells were washed once with PBS and cultured in 1% FBS RPM1 medium. Cells were treated simultaneously with 20 ng/mL IFN-ϒ and 10 pg/ml of LPS for a further 24 hours in

complete PMA-free medium to obtain M1 macrophages. For murine macrophages, J744A.1 cell line was seeded at $1x10^6$ cells/mL in 6-well cell culture plates in 10% FBS DMEM medium for 24h (M0). The next day the medium was replaced to 1% FBS DMEM and cells were stimulated with 25 ng/mL IFN-ϒ and 10 pg/ml of LPS for a further 24 hours to obtain M1 polarization.

To characterize the proper macrophage polarization, pro-inflammatory IL-1β cytokine levels and LDH activity were analyzed in cell supernatants by ELISA assay and Lactatase Assay Kit III respectively following the supplier's instructions. Moreover, gene expression of common protein markers of polarized macrophages was studied via RT-qPCR analysis. CCR7 and CXCL10 markers were associated to pro-inflammatory human M1 macrophages and IL-6 and IL-1β markers were associated to pro-inflammatory murine M1 macrophages. Moreover, Immunoblotting was employed for specific antibody detection.

III.2.2.F Cellular assay for inflammasome inhibition.

The inflammasome inhibitor, MM01, was evaluated in PMA-differentiated THP-1 cells (50 ng/mL PMA for 24h) (M0).

NLRP3 inflammasome. $1x10^6$ of THP-1 cells were seeded in six-well plates in 1 mL RPMI media that contained 1% FBS and stimulated with 50 ng/mL PMA for 24 h to polarize into M0 macrophages. The next day, medium was replaced to 1% FBS RPM1 medium and M0 cells were treated with 20 μM MM01 inhibitor for 30 min, followed by treatment with 100 ng/mL LPS for 3 h and 10 μM nigericin for 30 min at 37ºC.

AIM2 inflammasome. PMA-differentiated cells (M0) were treated in the same conditions as before (20 μM MM01 inhibitor for 30 min) and transfected with poly(dA:dT) (0.5 μg/ml) overnight using Lipofectamine 2000.

Pyrin inflammasome. PMA-differentiated cells (M0) cells were treated with 20 μM MM01 inhibitor for 30 min and primed with LPS 100 ng/mL 3 h followed by Cholera toxin treatment overnight.

Non-canonical inflammasome. PMA-differentiated cells (M0) cells were treated with 20 μM MM01 inhibitor for 30 min and transfected with ultrapure LPS 300 ng (Sigma) overnight using Lipofectamine 2000.

Cellular extracts were collected, and supernatants were harvested and clarified by centrifugation at 1,500 rpm at room temperature for further analysis. IL-1β secretion and the release of IL-18 were monitored by ELISA assay (BD OptEIA™ Human IL-1β ELISA Kit and Human IL-18 Module Set eBioscience). Cell viability was analyzed in parallel by evaluating the release of lactate dehydrogenase (LDH) (CytoTox-ONE™ Homogeneous Membrane Integrity Assay; Promega). Immunoblotting was employed for specific antibody detection.

III.2.2.G Cellular assays for inflammasome inhibition in pro-inflammatory M1 macrophages.

Human macrophages. $1x10^6$ of THP-1 cells were seeded in six-well plates in 1 mL RPMI media that contained 1% FBS and stimulated with 50 ng/mL PMA for 24 h to polarize into M0 macrophages. The next day, medium was replaced to 1% FBS RPM1 medium. M0 cells were treated with 20 μM MM01 inhibitor for 30 min, followed by M1 differentiation 20 ng/mL IFN-ϒ and 10 pg/ml of LPS for a further 24 hours at 37ºC.

Murine macrophages. J744A.1 cells were seeded in six-well plates in 1 mL DMEM media that contained 10% FBS 24 h. The next day, medium was replaced to 1% FBS RPM1 medium. Cells were treated with 20 μM MM01 inhibitor for 30 min, followed by M1 differentiation 25 ng/mL IFN-ϒ and 10 pg/ml of LPS for a further 24 hours at 37ºC.

Cellular extracts were collected, and supernatants were harvested and clarified by centrifugation at 1,500 rpm at room temperature for further analysis. IL-1β secretion was monitored by ELISA assay. Cell viability was analyzed in parallel by evaluating the release of LDH. Immunoblotting was employed for specific antibody detection. Moreover, gene expression of common protein markers of polarized macrophages was studied via RT-qPCR analysis. CCR7 and CXCL10 markers were associated to pro-inflammatory human M1 macrophages and IL-6 and IL-1〈 markers were associated to pro-inflammatory murine M1 macrophages.

III.2.2.H Assays to determine the secretion of pro-inflammatory cytokines.

Pro-inflammatory cytokines were analyzed from the supernatants of the cell cultures stimulated with the different inflammasome inducers using the ELISA kit (BD OptEIA™ Human IL-1β ELISA Kit and Human IL-18 Module Set eBioscience y') technique in 96-well plates. Briefly, in this assay, the wells are coated with a first capture antibody of the cytokine to be quantified resulting from hydrophobic interactions. After eliminating the excess of antibodies, the supernatants of the treatments are added where the immobilized antibodies specifically capture the cytokines present in them. Specific biotin-conjugated antibodies then detect the bound cytokines (detection antibody), recognized after an incubation step with the peroxidase enzyme conjugated to avidin or streptavidin. Finally, a chromogenic substrate is added that can be quantified in a spectrophotometer with a plate reader. The quantification of the cytokines of the supernatants can be carried out by interpolating the absorbance data in a calibration curve with standards of known concentrations of the cytokine to be quantified. The absorbance was determined using the Wallac Victor 1420 spectrofluorimeter (PerkinElmer) at a wavelength of 450nm. When required, the samples were diluted in culture medium until obtaining total absorbance values within the linear range of the calibration curve. Each sample was analyzed in duplicate for each independent experiment, and the results were expressed as interleukin concentration in pg/mL.

III.2.2.I Cell toxicity tests by lactate dehydrogenase activity.

To evaluate the cellular integrity of the cell cultures, the Cytotox-ONE Homogeneous Membrane Integrity Assay Kit (Promega) was used. The test is based on the release into the culture medium of the cytosolic enzyme lactate dehydrogenase by cells that have damaged the plasma membrane, characteristic of the necrotic or pyroptotic types of cell death. This assay measures the enzymatic conversion of the resazurin compound to the fluorescent resorufin compound. The amount of resorufin formed is directly proportional to the amount of LDH released into the medium [3]. This assay was performed in 96-well black plates; 50 µL of the supernatants were mixed with 50 µL of the commercial substrate and incubated in the dark for approximately 30 min. After this time, the fluorescence was measured at λexc = 560 nm and λem = 590 nm in the

Wallac Victor 1420 spectrofluorimeter (PerkinElmer). Each sample was analyzed in duplicate for each independent experiment, and the results were expressed as a percentage of the release of the enzyme lactate dehydrogenase from the treated samples with respect to a positive control (100% release) obtained by lysis with 0.1% Triton. X-100 from a cell culture seeded with the same number of cells as the treatments. The applied formula was the following:

$$\text{LDH release } \% = 100 \times (\text{Abs treated cells} - \text{Abs untreated cells} / \text{Abs untreated lysed cells})$$

III.2.2.J Immunoblotting.

The supernatants of the treated cells were lyophilized, and cellular extracts were obtained by lysing cells in 25 mM of Tris-HCl pH 7.4, 1 mM EDTA, 1 mM EGTA, and 1% SDS, plus protease and phosphatase inhibitors. The BCA protein assay determined the protein concentration. Both lyophilized supernatants and quantified cellular extracts were then resuspended in sample buffer (60 mM Tris pH 6.8, 10% glycerol, 2% SDS, 5% 2-mercaptoethanol, and 0.1% bromophenol blue) for immunoblotting analysis.

Proteins were separated by electrophoresis on polyacrylamide gels (SDS-PAGE, 12-14%), using the vertical electrophoresis system (Mini Protejan-3, Bio-Rad Laboratories) in electrophoresis buffer (25 mM Tris pH 8.0, 200 mM glycine, and 0.1% SDS). A molecular weight marker (EZ-RUN, Fisher) was used in all experiments. Then, the proteins separated on the polyacrylamide gels were electrophoretically transferred to 0.45 μm nitrocellulose membranes (Bio-Rad) using the Mini-Transblot system (Bio-Rad) using the transfer buffer (25 mM Tris pH 7.5, 192 mM glycine, and 20% (v/v) methanol for 3h at 400mA. The membranes were then blocked for 1h in blocking buffer (5% milk in TBS-T ("Tris -Buffered Saline" 20 mM Tris pH 8.0, 500 mM NaCl, 0.1% (w/v) Tween-20). The incubation of the membranes with the primary antibody was carried out in the blocking buffer at 4 ° C overnight (Table 1). The membranes were then washed three times with TBS-T and incubated with the corresponding peroxidase-conjugated secondary antibody in blocking solution for 1 h at room temperature. Finally, after washing three times with TBS -T, the Western blot

was developed by ECL according to the manufacturer's instructions (ECL Western Blotting Detection Reagents), and the membranes were exposed to Amersham Hyperfilm ECL film (GE Healthcare). As a loading control, the α-tubulin antibody was used. When required, the area of the bands obtained was quantified using the Image J1.46r program (Wayne Rasband, National Institute of Health, USA).
Some membranes of the Western blots were reused to re-incubate them with a primary antibody other than the initial one, so they were stripped. Briefly, the membranes were incubated in the stripping buffer (2% (w/v) SDS, 0.7% (v/v) β-mercaptoethanol and 65 mM Tris-HCl pH 6.8) at 65oC for 30min. The membranes were then washed three times with TBS-T, and the Western blot was performed as previously indicated.

III.2.2.K Analysis of mRNA by Real-Time quantitative Polymerase Chain Reaction (RT-qPCR)

Total RNA was extracted from cells using the RNA isolation RNeasy Mini Kit (Qiagen). mRNA was obtained by reverse transcription (RT) using super script first strand synthesis system for RT-PCR (Invitrogen). PCR amplification was performed with equal amounts of cDNA from each RT reaction. qPCR was performed on the Roche Light Cycler 480 using the SYBR Green Reagent Kit. GAPDH was used as the control gene for normalization. In addition, scrambled controls were added for each primer pair to discard contaminants and the specificity of the. PCR products was confirmed by meting-curve analysis. Finally, the mRNA expression was quantified using Roche Applied Science software by the threshold cycle (CT) method and the abundance was expressed as relative-fold change front GAPDH expression.

III.2.2.L Evaluation of the migratory capacity of breast cancer cells in response to inflammatory stimuli by transwell assays

Human/Mouse macrophages were treated with MM01 and stimulated to M1 phenotype as described before (**Materials and methods III.2.2.G**). The supernatant of cells was collected and centrifuged at 1,500 rpm for 5 min. Then, breast cancer cells were seeded in the upper part of the transwell (Sigma Aldrich), containing a permeable membrane,

at 25.000 cells/transwell in 10% FBS medium. Next, 600 µL of M1 supernatant, treated or untreated with MM01, were added to the lower part of the transwell for cell stimulation. Finally, following an incubation period of 6 hours, the migrated cells were stained with DAPI and WGA for confocal microscopy visualization. 10% FBS medium was employed to evaluate the basal migration of each cell line.

III.2.2.M Development of stable luciferase expressing EO771 cells by lentiviral infection

EO771 cell line was virally infected with the Luciferase (Luc2) Lentiviral Vector (Photinus Pyralis Cumate) to express luciferase. 1x 10^6 EO771 cells were seeded in a 6-well plate in 2 ml of complete medium per well. The cells were incubated at 37ºC in a 5% CO^2 atmosphere. Once the cells were at 80% confluence, the medium was removed, and the cells were washed with sterile PBS. Luc2 stock contains 1-2 x 10^7 particles forming units (pfu)/m. The lentiviral solution was prepared by adding 240 µl of each lentivirus to 960 µl of complete medium. After PBS washing, the lentiviral virus was incubated for 24 h at 37ºC in a 5% CO^2 atmosphere, after which point the solutions was replaced by 2 ml of complete medium. 500 µg/ml of the antibiotic geneticin (G418) was added in the complete medium to select positive cells for lentiviral infection. To detect stable luciferase-expressing cells (EO771-Luc2), 10,000 cells in 100 µl of complete medium was added to a well in a white 96-well plate. 20µl of Bright-GloTM Luciferase Assay System was next added, and the fluorescence was immediately evaluated in relative luminescence units (RLU) in the spectrophotometer.

III.2.3 *In vivo* assays

III.2.3.A Ethical considerations

All the animal experiments performed were planned following the European Communities Council Directive (86/609/ECC) guidelines and by the Spanish Royal Decree 1201/2005. All experimental procedures were approved by the Institutional 171

Animal Care and Use Committee and carried out by accredited and trained staff, meeting the animal care rules.

III.2.3.B MSU-induced peritonitis mouse model.

In vivo model was performed as described in Bioprotocols (Spalinger, 2018) using an approach approved by the Institutional Animal Ethical Committee of the CIPF. C57BL/6 mice were injected intraperitoneally with 10 mg/kg MM01 or vehicle (PBS + 0.1% DMSO) 30 min before intraperitoneal injection of MSU (2 mg MSU crystals in 200 µl sterile PBS). After 6 h, mice were sacrificed, and peritoneal lavage with 5 ml of PBS was performed. Cytokine IL-1β secretion was determined by ELISA (#DY401 R&D Systems), and neutrophil content was measured by flow cytometry in ACVLAB Laboratory Valencia. Each group condition included twelve animals (**Figure 3**).

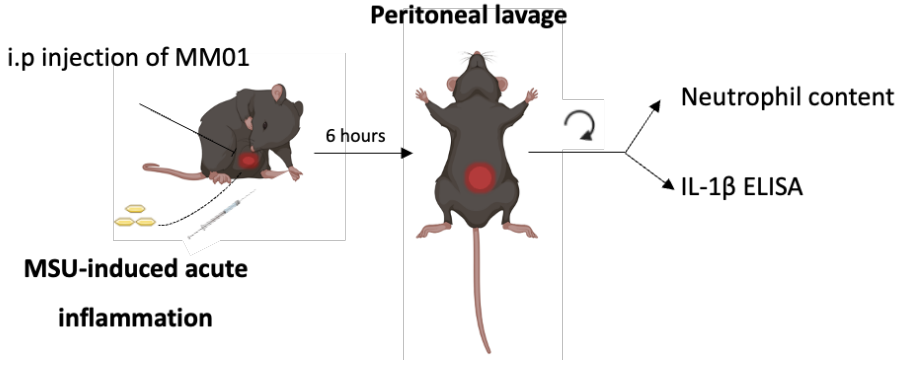

Figure 3. MSU-induced peritonitis mouse model procedure.

III.2.3.C Development of orthotopic EO771-luc2 breast cancer mouse model

The orthotopic EO771-Luc2 breast cancer mice model was performed employing the C57BL/6J female strain at 6-8 weeks of age. Before cell injection, mice were anesthetized by isoflurane inhalation with (2-5%). Then $1x10^6$ and $1x10^6$ EO771-Luc2 cells, prepared within 1:3 (v/v) of Matrigel and RPM1 complete medium in a final volume of 100 µl, were orthotopically implanted in the fourth mammary pat pad using an insulin syringe (29G). Tumor growth was measured three times per week via in vivo bioluminescence by Xenogen IVIS® Spectrum (Caliper Life Sciences; Hopkinton,

Massachusetts, USA) for five weeks, at which point the tumors reached a maximum size permitted [4]. To be able to visualize the tumor luminescence, 150 mg/kg of XenoLight D-luciferin Potassium Salt in sterile PBS was administered subcutaneously as a bioluminescent substrate. Immediately, mice were anesthetized, and 10 mins after injection mice were introduced in the IVIS® Spectrum. Tumor images were acquired using the following parameters: Exposure time: Automatic, Binning: 8, F/Stop: 1, Emission Filter: Open and Field of View: C. With these parameters, the luminescent tumor signal will be acquired within 20 mins post luciferin injection. In the following animal experiments, we used this schedule. Finally, the luminescence in the tumors was analyzed with the Living Image® (64-bit) program.

III.2.3.D Development of orthotopic 4T1 breast cancer mouse model

The orthotopic 4T1 breast cancer mice model was performed employing the BALB/c female strain at 6-8 weeks of age. Before cell injection, mice were anesthetized by isoflurane inhalation with (2-5%). Then $1x10^6$ 4T1 cells, prepared within 1:3 (v/v) of Matrigel and DMEM complete medium in a final volume of 100 µl, were orthotopically implanted in the fourth mammary pat pad using an insulin syringe (29G). Tumor growth was measured three times per week via caliper for four weeks, at which point the tumors reached a maximum size permitted [4].

III.2.3.5 Antitumor analysis

MM01 was administered once tumors reached a size of 0,02 cm3 with at least 5 animals used in each group. MM01 was i.v. administered starting from at 10 mg/kg three timpes per week for 4-5 weeks. MM01 was previously dissolved in PBS + 5% DMSO. At the end of the experiment (corresponding the week 4-5), all animals were euthanized via carbon dioxide (CO2) inhalation, and tumors were weighed and measured by caliper after extraction. Blood was also extracted from the heart employing 21G x 1” needles (Ø 0.80 x 25 mm), and insulin syringes 10 µl 0.1% (w/v), heparin was added in the insulin syringes to avoid clotting. 100 µl of each sample was centrifuged for 10 mins at 4000 rpm at 4◦C to obtain the plasma used to hematological studies.

III.2.4 Proteomic studies

The proteomic analysis was performed in the proteomics facility of SCSIE University of Valencia.

III.2.4.1 Cellular assays for proteomic studies

$0{,}5x10^{6}$ of EO771 and 4T1 breast cancer cells were seeded in six-well plates in 1 mL of complete RPMI and DMEM media, respectively. J744A.1 murine macrophages were polarized to M1 macrophaes as detailed in the section **III.2.2.7.** The next day, the media of EO771 and 4T1 cells was replaced and 800 µL of J744A.1 M1 supernatant was added to the cells for 6h. At 6h, cells lysated in 25 mM of Tris-HCl pH 7.4, 1 mM EDTA, 1 mM EGTA, and 1% SDS, plus protease and phosphatase inhibitors for proteomic studies.

III.2.4.2 Sample preparation.

Aliquots with an equivalent amount of all the samples were mixed to make a pool (20 µg) for build the spectral library from a 1D_SDS_PAGE gel. Appropriate volumen of 4x Laemmli Sample Buffer with β-mercaptoethanol was added to 20 ug of the samples. The samples were denatured at 95ºC during 5 min. The electrophoresis was performed using an 12% precast gel (Bio-Rad) at 200V 5 min. The gel was fixed with 40% ethanol/10% acetic acid for one hour. The gel was stained with colloidal Coomassie (Bio-Rad) for one hour. The gel was distained with H2O milliQ. Every sample run was into 5 pieces and then were digested with sequencing grade trypsin (Promega). 500 ng of trypsin were used for each sample, and digestion was set to 37 ºC on. The trypsin digestion was stopped with 10% TFA and the supernatant was removed, and the library gel slides dehydrated with pure ACN. The new peptide solutions were combined with the corresponding supernatant. The peptide mixtures were dried in a speed vacuum and re suspended with 15 µL of 2 % ACN; 0.1% TFA (20 µL). Then, 5 µl of peptide mixture sample was loaded onto a trap column (3µ C18-CL, 350 µm x 0.5mm; Eksigent) and desalted with 0.1% TFA at 5 µl/min during 5 min. The peptides were then loaded onto an analytical column (3µ C18-CL 120 Ă, 0.075 x 150 mm; Eksigent) equilibrated in 5% acetonitrile 0.1% FA (formic acid). Elution was carried out with a linear gradient of 7-40% B in A for 20 min. (A: 0.1% FA; B: ACN, 0.1% FA) at a flow rate of 300

nL/min. Peptides were analysed in a mass spectrometer nanoESI qQTOF (6600plus TripleTOF, ABSCIEX). Sample was ionized in a Source Type: Optiflow < 1 uL Nano applying 3.0 kV to the spray emitter at 200 ºC. Analysis was carried out in a data-dependent mode. Survey MS1 scans were acquired from 350–1400 m/z for 250 ms. The quadrupole resolution was set to 'LOW' for MS2 experiments, which were acquired 100–1500 m/z for 25 ms in 'high sensitivity' mode. Following switch criteria were used: charge: 2+ to 4+; minimum intensity; 250 counts per second (cps). Up to 100 ions were selected for fragmentation after each survey scan. Dynamic exclusion was set to 15 s. The rolling collision energies equations were set for all ions as for 2+ ions according to the following equations: |CE|=(slope)x(m/z)+(intercept).

III.2.4.3 Protein Identification.

ProteinPilot default parameters were used to generate peak list directly from 6600 plus TripleTOF wiff files. The Paragon algorithm of ProteinPilot v 5.0 was used to search the mammalia_200218.fasta database with the following parameters: trypsin specificity, cys-alkylation, taxonomy restricted to mus musculus (70419 proteins), and the search effort set to through with FDR analysis. The protein grouping was done by Pro group algorithm.

III.2.4.4 Bioinformatic analysis.

The statistical analysis was performed in collaboration with the bioinformatics facilities in the Príncipe Felipe research center. Differential expression was carried out using the moderate t statistic of the limma package. To minimize the number of false positives, the p-values will be adjusted using the method proposed by Benjamini-Hochberg.

The functional enrichment analysis was performed with the ORA (Over-representation Analysis) method implemented in the clusterProfiler package. This method makes it possible to determine whether, in a biological process or function, the number of proteins associated with that function in a list of interest is greater than would be expected by chance. To determine whether or not a function is over-represented, the one-sided version of Fisher's exact test is used. The p-values were corrected using the method proposed by Benjamini-Hochberg. Finally, the protein-protein interaction analysis was performed with STRING database. For the protein-protein interaction analysis, the gene identifiers are first found to STRING's own identifiers. To build the

network, the first 200 genes whose p-value in the differential expression analysis is closer to 0 were selected. This was carried out for each of the comparisons proposed in the study, using version 11 of STRING. Moreover, using the "fastgreedy" algorithm, a cluster analysis was performed with each network, with the aim of detecting possible functional groupings within it.

III.2.5 PGA-MM01 synthesis

III.2.5.1 Physico-chemical characterization methods

III.2.5.1.A Nuclear Magnetic Resonance (NMR) Spectroscopy.

NMR spectra were recorded at 27°C (300K) on a 300 Ultrashield^{TM} from Bruker (Billerica MA, USA). Data were processed with the software Mestrenova (Bruker GmbH, Karlsruhe, Germany). Samples were prepared at the desired concentration in D_2O.

III.2.5.1.B UV-Vis

UV-VIS analysis were performed using JASCO V-630 spectrophotometer 20 at 25°C with a 1.0 cm quartz cells and with spectral bandwidth of 0.5 nm. Spectra analysis were recorded 3 times in the range of 200 – 350 nm.

III.2.5.1.C Dynamic Light Scattering (DLS).

Size measurements were performed using a Malvern ZetasizerNanoZS instrument, equipped with a 532nm laser at a fixed scattering angle of 173°. CSS-PGA-peptide solutions were freshly prepared in Phosphate Buffered Saline (PBS, 10 mM phosphate, 150 mM NaCl) and filtered through a 0.45 µm cellulose membrane filter and measured. Size distribution was measured (diameter, nm) for each polymer in triplicate with n> 3 measurements. Automatic optimization of beam focusing and attenuation was applied for each sample.

III.2.5.1.D Nuclear magnetic resonance (NMR).

During synthesis the structure of compounds was verified using Nuclear Magnetic Resonance (NMR). All experiments were conducted using a Bruker 300 MHz NMRspectrometer (Billerica, U.S.A.) unless specified. Sample

preparation was done bydissolving around 5 mg of compound in 700 µL of suitable deuterated solvent before transfer in a 5 mm NMR tube.

III.2.5.2 Synthetic procedure

III.2.5.2.A Synthesis of L-PGA- 6-MONODEOXY-6-MONOAMINO-BETA-CYCLODEXTRIN (βCD).

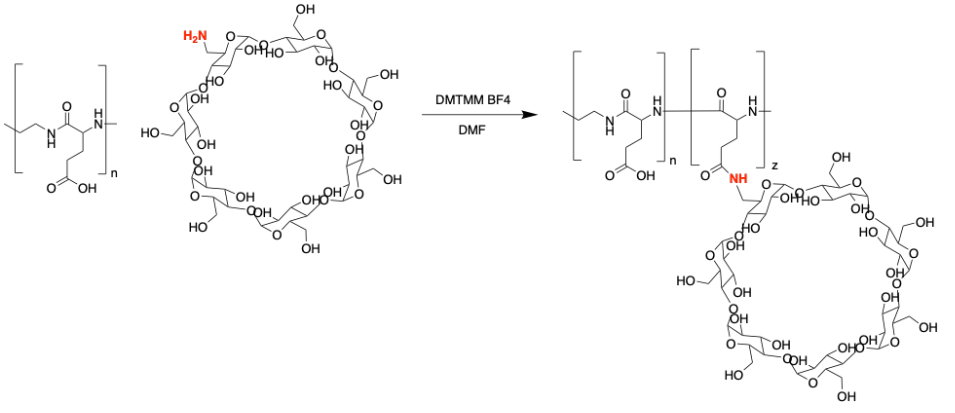

Figure 4. Synthetic route for the preparation of L-PGA-6-MONODEOXY-6-MONOAMINO-CD.

L-PGA was dissolved in anhydrous N,N'-dimtheylformamide under inert atmosphere. The solution was added of 4-(4,6-dimethoxy-1,3,5-triazin-2-yl)-4-methyl-morpholinium tetrafluoroborate salt (DMTMM BF_4, 0.1 eq per Glutamic Acid Unit - GAU) and the mixture was stirred for 30 min. Following the time, 6-monodeoxy-6-monoamino-CD was added to the solution, the pH was increased to 8 by adding N,N-diIsopropylethylamine (DIEA) and the resulting solution was allowed to react for 24 hours at room temperature. Following the time, the work-up was performed by precipitation in cold diethyl ether (3*100 mL). The resulting white powder was dried under vacuum to remove the dithyl ether traces for 3 hours. The resulting L-PGA-CD were dissolved in 1.0 M deuterated sodium hydrogen carbonate ($NaDCO_3$) and analyzed by ^{1}H-NMR to ensure purity and to calculate the percentage of modification. The withe powder was converted into salt form by adding 5 mL of 0.5 M $NaHCO_3$ solution and further purified using Vivaspin 3 kDa. The final product was lyophilized and an amorphous white solid was obtained.

The product was analyzed by ^{1}H NMR. Yield: 80 %.

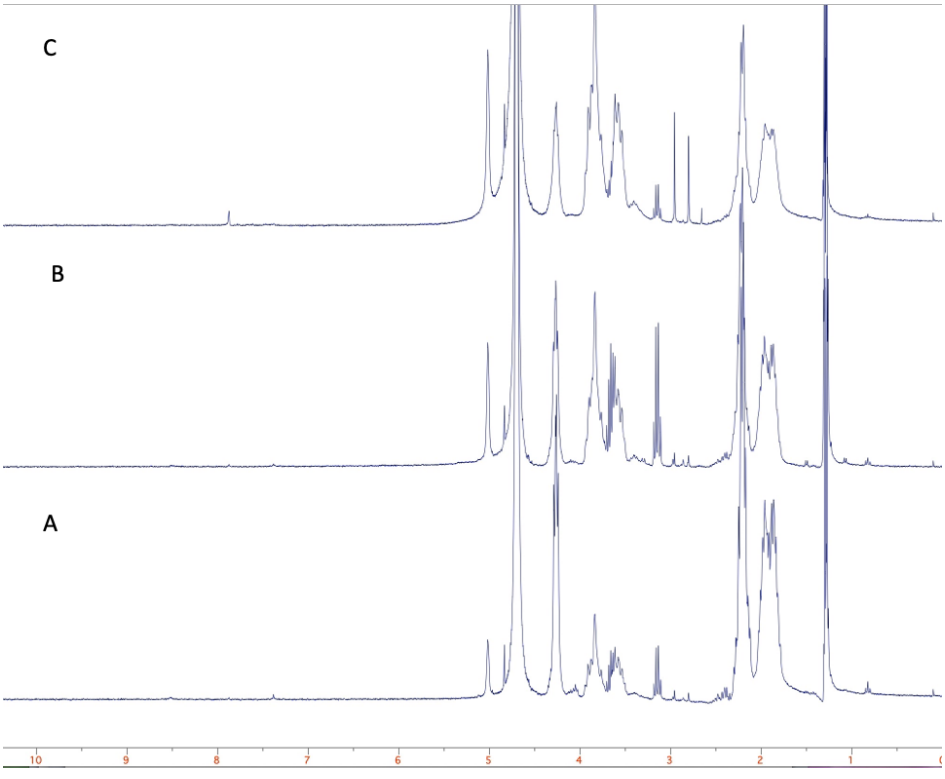

Figure 5. ^{1}H NMR spectrum of L-PGA-6-MONODEOXY-6-MONOAMINO-CD with a) 1% b) 5% and c) 10% of functionalization of 6-MONODEOXY-6-MONOAMINO-CD (300MHz, D_2O).

III.2.5.2.B General Procedure for the encapsulation using dialysis.

L-PGA was dissolved in milliQ water and MM01 in dry DMF in 1:1 proportion. The solution was added into a dialysis membrane of cellulose ester (cut off 100-500Da) and the mixture was stirred inside a mixture of H2O/DMF in different proportions for 24h. Following the mixture pass through a celite column and the final mixture was lyophilized and an amorphous orange solid was obtained.

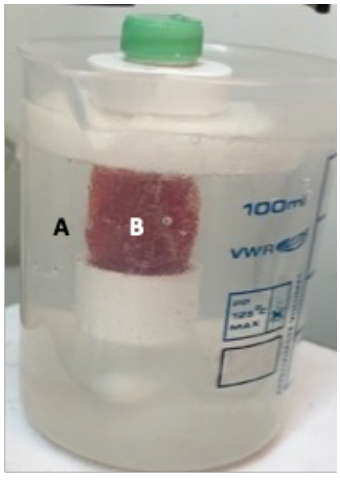

Figure 6. Dialysis membrane example: a) Mixture outside of H2O/DMF in different proportions and b) Mixture inside of L-PGA was dissolved in milliQ water and MM01 in dry DMF in 1:1 proportion.

III.2.5.2.C Scale-up of L-PGA(200)-10% of -CD; 50:50 H_2O/DMF and 3mg of MM01

L-PGA was dissolved in milliQ water and MM01 in dry DMF in 1:1 proportion. The solution was added into a dialysis membrane of cellulose ester (cut off 100-500Da) and the mixture was stirred inside a mixture of H2O/DMF in different proportions for 24h. Following the mixture pass through a celite column and the final mixture was lyophilized and an amorphous orange solid was obtained.

Yield: 90.4%.

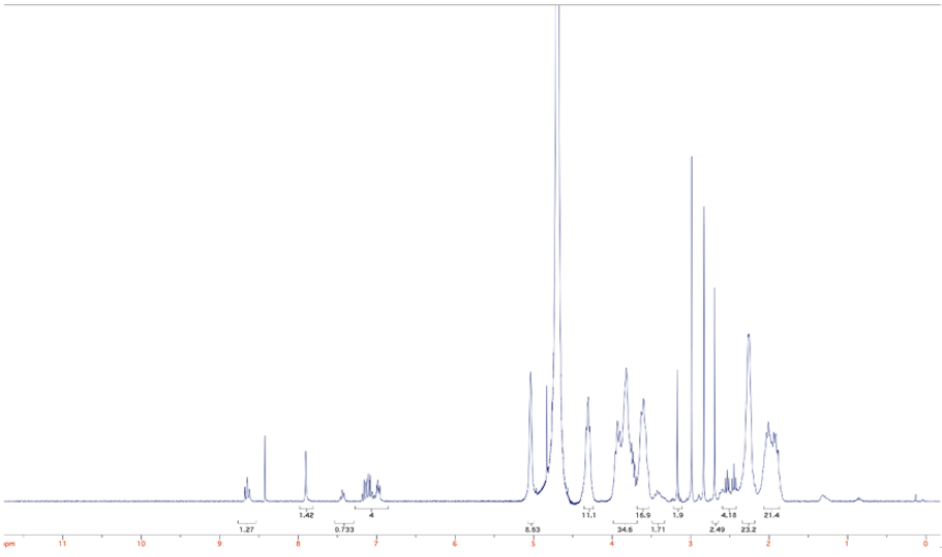

Figure 7. ^{1}H NMR spectrum of encapsulation of L-PGA(200)-10% of -CD; 50:50 H_2O/DMF and 6mg of MM01 (300MHz, D_2O).

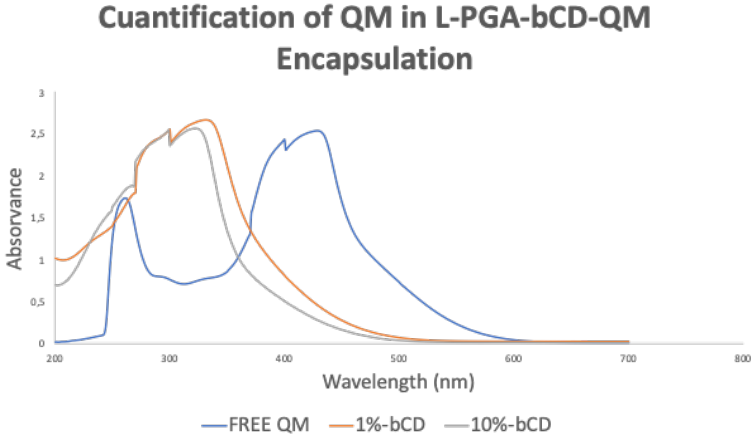

Figure 8. UV-VISible spectrum of encapsulation of L-PGA(200)-10% of -CD; 50:50 H_2O/DMF and 6mg of MM01 (grey); L-PGA(200)-1% of -CD; 50:50 H_2O/DMF (orange) and free MM01 in PBS (2mg/ml).

III.2.6 Statistical analysis

All values obtained were plotted, displayed as ± SEM from n ≥ 3 assays. Animals' experiments were performed using 6-10 animals per group. Statistical significance was evaluated using a paired t-test, two-way ANOVA, test t, or ANOVA test depending on the type of test performed; comparisons with $p<0.0001$ (****), $p<0.001$ (***), $p<0.01$ (**), and $p<0.05$ (*) were considered statistically significant with a 95% confidence interval. GraphPad Prism 8 software was used to performed statistical analyses.

References

1. Baroja-Mazo, A., et al., *The NLRP3 inflammasome is released as a particulate danger signal that amplifies the inflammatory response.* Nat Immunol, 2014. **15**(8): p. 738-48.
2. Yoshimori, T., et al., *Bafilomycin A1, a specific inhibitor of vacuolar-type H(+)-ATPase, inhibits acidification and protein degradation in lysosomes of cultured cells.* J Biol Chem, 1991. **266**(26): p. 17707-12.
3. Kabakov, A.E. and V.L. Gabai, *Cell Death and Survival Assays.* Methods Mol Biol, 2018. **1709**: p. 107-127.
4. Workman, P., et al., *Guidelines for the welfare and use of animals in cancer research.* Br J Cancer, 2010. **102**(11): p. 1555-77.

Molecular mechanism of action and pharmacological activity of the novel inflammasome inhibitor MM01

Graphical Abstract

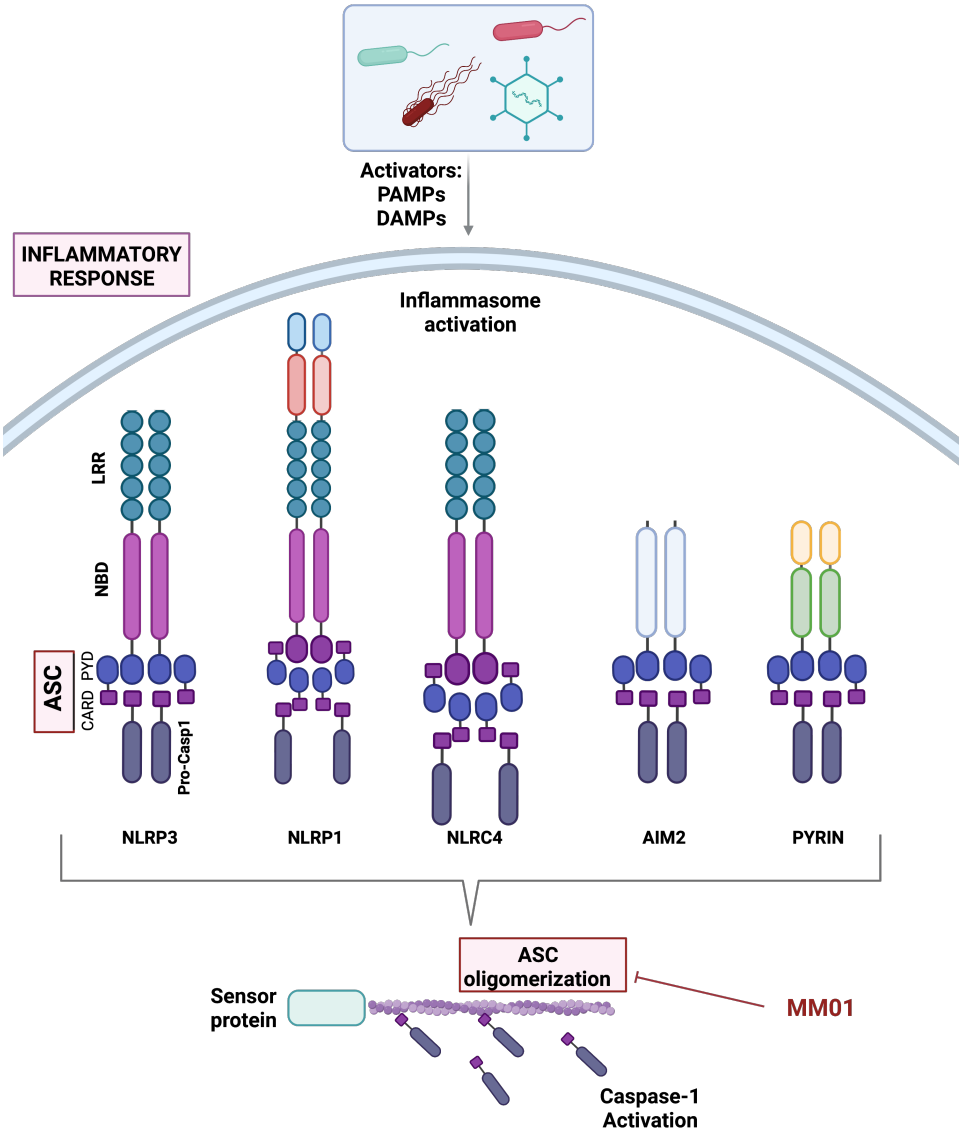

MM01, novel ASC oligomerization inhibitor
ASC-dependent targeting of multiple inflammasomes
Treatment of multifactorial diseases
Decreases release of pro-inflammatory cytokines,
Decrease the extracellular accumulation of ASC specks
Inhibits pyroptotic cell death

Antecedents and Background

As stated in the **general introduction**, the inflammasome plays a dual role during inflammatory responses [1]; [2]; [3] - although activation prevents the spread of infection and tumor development and promotes the activation of adaptive responses, over-activation, and dysregulation of the inflammasome have been implicated in numerous pathologies ([4]; [5]; [6]. In these cases, the targeted inhibition of inflammasome activity may represent an effective treatment strategy.

Currently reported inhibitors of inflammation [7]) focus on the inhibition of inflammatory cascade end products, such as caspase-1 inhibitors (VX-765) [8] or Il-1b inhibitors (Anakinra) [9], or the inhibition of specific inflammasomes, such as the NLRP3 inflammasome inhibitor MCC950 [10]. However, as inflammatory responses depend on the activation of more than a single inflammasome in various multifactorial diseases [11]; [12]; [13]; [14], any small molecule with the potential to inhibit different inflammasome complexes simultaneously would be of great interest.

Prior to this work, Dr. Orzáez's laboratory proposed the search for new *pan*-inflammasome modulators. To this end, the proposed molecular target was the inhibition of ASC-dependent pro-caspase-1 activation, a common step in the activation of multiple inflammasomes.

In the search for new inflammasome inhibitors, our laboratory employed a screening assay based on the *in vitro* reconstitution of the ASC-pro-caspase-1 interaction using purified proteins [15]. The incubation of recombinant ASC and pro-caspase-1 triggers pro-caspase-1 autoprocessing and the formation of the active caspase-1 protein [16]. Caspase-1 activity can be quantified using the caspase-1-specific fluorogenic peptide substrate Ac-WEHD-AFC [16, 17].

This screen identified MM01 as an inhibitor of ASC-associated caspase-1 activity with an IC50 value in the nanomolar range. Furthermore, this study highlighted that MM01 did not target the active site of caspase-1, as is the case with the known caspase inhibitor zVAD or VX-765 **[16].** Importantly, docking studies performed in

collaboration with Dr. Irmgard Merfort's laboratory in Freiburg, Germany, revealed possible interactions of MM01 with the protein ASC.

The work described in this thesis deepens in the characterization of the molecular mechanism of action and activity of MM01 using *in vitro*, *ex vivo* and *in vivo* models of inflammation.

Abstract

In this chapter, we delineate a novel mechanism of action for MM01, a recently identified modulator of inflammasome activity - the inhibition of ASC oligomerization and the subsequently reduced processing of pro-caspase-1 and inhibited caspase-1 activity. We demonstrate that MM01 disrupts the ASC oligomerization process associated with the activity of various inflammasomes and inhibits downstream IL-1β release and pyroptosis in various cellular models of inflammation. MM01 also reduces neutrophil infiltration and pro-inflammatory cytokine accumulation in an *in vivo* model of peritonitis, used as a proof-of-concept for the therapeutic capabilities of this ASC inhibitor. Given the involvement of ASC function in multiple inflammasome complexes, treatment with MM01 may represent an effective therapeutic approach to treat those diseases where the activation of multiple inflammasomes is involved.

Results and Discussion

IV.1 Identification of a Novel ASC Oligomerization Inhibitor

Following the identification of MM01 as an inhibitor of ASC-associated caspase-1 activity **[16]**, we explored potential mechanisms of action.

Following inflammasome activation, ASC oligomerizes into large filaments to form ASC specks, which recruit pro-caspase-1. This results in pro-caspase-1 auto-processing and the formation of the catalytically active caspase-1 heterotetramer comprising the p10 and p20 subunits [18].

Given the results obtained from previous *in vitro* evaluations, we anticipated two possible mechanisms for the MM01 inhibitor (**Figure 1**):

1) Interference in the formation of ASC oligomers to inhibit the recruitment and subsequent auto-processing of pro-caspase-1

2) The inhibition of the interaction between ASC and pro-caspase-1 to inhibit auto-processing and the formation of active caspase-1

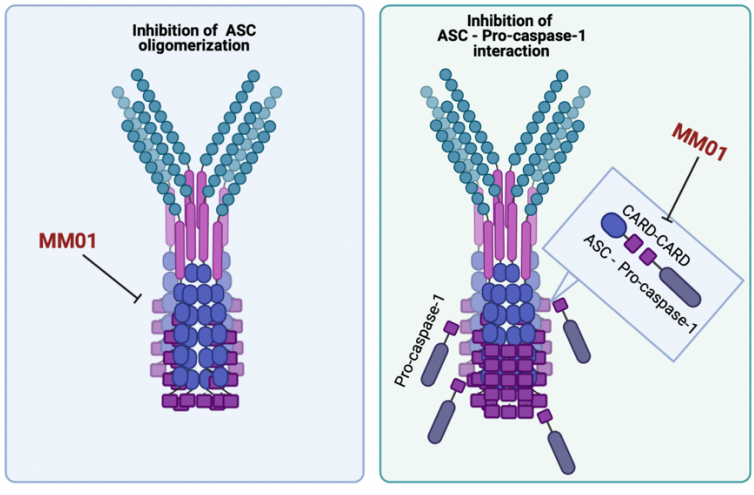

Figure 1. Possible Mechanisms of Action of MM01. (Left panel) MM01-mediated inhibition of ASC oligomerization. (Right panel) MM01-mediated inhibition of the ASC-pro-caspase-1 interaction.

IV.1.1 MM01 Prevents ASC Oligomerization *in vitro*

To study the effect of MM01 on ASC oligomerization, we purified human recombinant ASC protein and reconstituted ASC filaments *in vitro* in the presence or absence of MM01 as detailed in **Materials and Methods Sections III.2.1.A** and **III.2.1.B.** We employed electron microscopy for the structural characterization of ASC filaments, a strategy supported by a previous study that successfully visualized ASC oligomers [19]. This method involves the purification and solubilization of human recombinant ASC protein in 50 mM NaH_2PO_4, 100 mM NaCl buffer at acidic pH, the induction of ASC oligomerization into filaments at physiological pH, and the visualization of filaments by electron microscopy in negatively stained samples.

This evaluation demonstrated that ASC oligomerization prompts the formation of long, well-defined filaments (**Figure 2 –** compare ASC to buffer only sample). Furthermore, we demonstrated that MM01 treatment severely impacts ASC oligomerization by significantly reducing filaments formation. (**Figure 2 –** compare ASC and ASC+MM01).

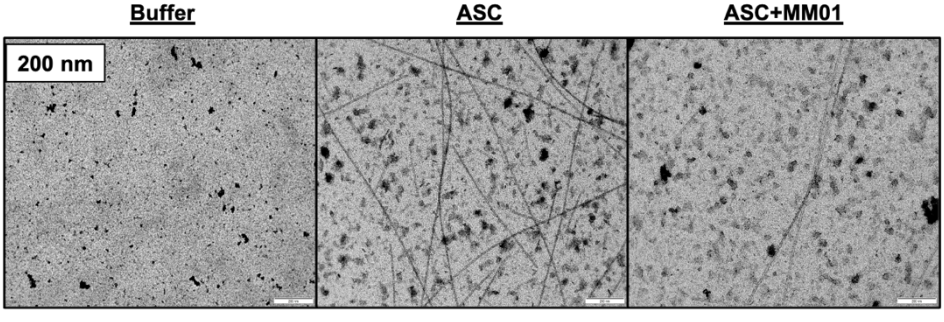

Figure 2. Structural Characterization of ASC Oligomerization as Filaments. Electron microscopy images of negatively stained preparations of ASC filaments at physiological pH. (Scale bars 200 nm).

IV.1.2 MM01 Inhibits ASC Oligomerization in a Cellular Context

After demonstrating the ability of MM01 to disrupt ASC filament formation *in vitro*, we next corroborated the mechanism of action of MM01 in a cellular environment.

The transfection of a plasmid coding for the protein ASC fused with the yellow fluorescent protein (ASC-YFP) leads to the formation of spontaneous ASC filaments/specks in HEK293 human embryonic kidney cells [20]. ASC-YFP levels can be evaluated by techniques such as Western blot, confocal microscopy, or flow cytometry. Importantly, HEK293 cells lack the expression of all inflammasome components, which permits an understanding of how MM01 impacts individual transfected inflammasome proteins.

We transiently transfected HEK293 cells with the plasmid coding for ASC-YFP in the presence or absence of 20 μM MM01 treatment for 6 h (as detailed in the **Materials and Methods III.2.2.A** and **III.2.2.B**) and analyzed the formation of ASC oligomers by Western blot after lysing cells and crosslinking proteins using disuccinimidyl suberate (DSS) (**Figure 3**). Chemical crosslinking inhibits ASC filament/speck disassembly during protein denaturation and represents a crucial step in the visualization of ASC by immunoblotting [21].

The upper panel of **Figure 3** depicts ASC expression in HEK293 cells after ASC-YFP transfection and 20μM MM01 treatment for 6 h without crosslinking, while the lower panel employs crosslinking to detect oligomerization. As expected, after ASC-YFP transfection (+ASC), the overall levels of ASC increase compared to untreated cells; furthermore, a small number of monomers appear at 55 kDa, an increased number of dimers at 110 kDa, and a large number of higher-order ASC oligomers at around 250 kDa.

Interestingly, while MM01 treatment in the presence of ASC (+ASC+MM01) inhibited ASC oligomerization into dimers or higher-order oligomers (Lower part of **Figure 3**), MM01 also significantly reduced overall ASC protein levels, as evidenced by reduced ASC protein levels in the uncrosslinked sample (Upper part of **Figure 3**).

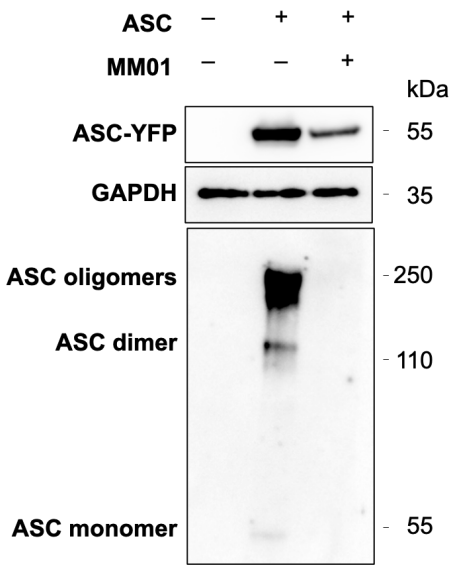

Figure 3. ASC Oligomerization in a Cellular Context. (Upper panel) Western blot analysis of ASC expression levels following MM01 treatment (20 μM, 6 h) in ASC-YFP transfected HEK293 cells in the absence of crosslinking. (Lower panel) Western blot analysis of ASC oligomerization following MM01 treatment (20 μM, 6 h) in ASC-YFP transfected HEK293 cells in the presence of a crosslinking agent. GAPDH functioned as a loading control (Central panel).

Given these results, we measured the possible impact of MM01 treatment on *ASC* mRNA expression by quantitative reverse transcription PCR (RT-qPCR). The results depicted in **Figure 4** demonstrate the expected significant increase in *ASC* mRNA levels after transfection with the ASC-YFP plasmid (+ASC); however, MM01 treatment failed to significantly alter *ASC* mRNA levels (+ASC+MM01), suggesting that MM01 does not impact the transcription of *ASC*.

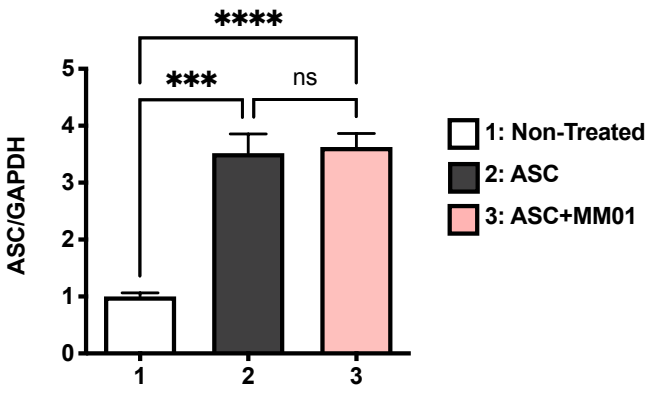

Figure 4. *ASC* mRNA Expression in HEK293 Cells. RT-qPCR analysis of *ASC* levels in HEK293 in the presence or absence of ASC-YFP plasmid transfection (+ASC) and MM01 treatment (+MM01). GAPDH used as a housekeeping gene. Data represent the mean ± SD of three independent experiments. Asterisks represent significant differences determined by one-way analysis of variance (ANOVA) test with Tukey's multiple post-test comparisons ***p<0.001; ****p<0.0001.

Given these results, we wondered if the inhibition of ASC oligomerization would give rise to an increased degradation of free ASC protein. We evaluated the potential of MM01 to induce ASC degradation via the ubiquitin-proteasome system (UPS) or the autophagy-lysosome pathway [22]. The UPS degrades misfolded and damaged proteins and, more importantly, short-lived regulatory proteins that control critical cellular processes [23]. The attachment of multiple ubiquitin moieties (polyubiquitination) to the side chain amino group of a lysine residue marks a protein for degradation by the proteasome [22]. Meanwhile, the autophagy-lysosome pathway, primarily a stress response mechanism, degrades proteins and larger cellular structures such as organelles under conditions of starvation and other types of stress [24]. Notably, the lysosomal pathway also plays a role in innate and adaptive immunity, and several lines of evidence have established that autophagy contributes to the inhibition of inflammasomes and excessive inflammation [25]; [26].

We first studied whether the proteasome pathway regulates ASC protein degradation by treating ASC-YFP-transfected HEK293 cells with the MG132 proteasome inhibitor, which reduces the degradation of ubiquitin-conjugated proteins.

We pretreated HEK293 cells with MM01 at 20μM for 30 min and then transfected cells with the ASC-YFP plasmid. After 4 h, we replaced the medium and treated cells with 1 μM MG132 for 2 h and then collected cells in the absence and presence of the DSS crosslinking agent to study ASC expression and oligomerization respectively.

The upper panel of **Figure 5** (uncrosslinked) depicts the expected reduction in ASC protein levels with the treatment of MM01 (compare +ASC to +ASC+MM01); however, co-treatment with MG132 (+ASC+MM01+MG132) failed to recover protein levels to that observed in ASC-YPF transfected cells (+ASC). Indeed, MM01 and MG132 treatment combined appeared to reduce levels of the ASC protein further. The evaluation of ASC oligomerization (crosslinked) in the lower panel of **Figure 5** depicts the expected reduction in ASC oligomerization following MM01 treatments (compare +ASC to +ASC+MM01). Again, the addition of MG132 (+ASC+MM01+MG132) failed to recover oligomerization levels to that observed in ASC-YPF transfected cells (+ASC).

Overall, these findings suggest that protein degradation by the UPS does not regulate ASC protein levels in response to MM01 treatment.

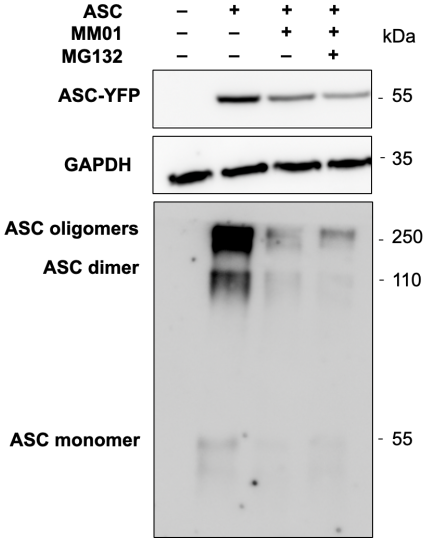

Figure 5. Impact of MM01 on ASC Expression and Oligomerization in HEK293 Cells following UPS Inhibition. Western blot analysis of ASC expression levels following MM01 (+MM01) (20 μM) and MG132 treatment (+MG132) in ASC-YFP (+ASC) transfected HEK293 cells in the absence of

crosslinking (Upper panel) and the presence of crosslinking (Lower panel). GAPDH functioned as a loading control (Central panel).

Previous studies had suggested the involvement of the lysosomal pathway in inflammasome degradation [25]. Therefore, we pretreated HEK293 cells with MM01 at 20μM for 30 min, transfected cells with ASC-YFP for 4 h, and then treated cells with 200 nM bafilomycin (an inhibitor of autophagosome-lysosome fusion) for 2 h and collected cells in the absence and presence of the DSS crosslinking agent.

The upper panel of **Figure 6** (uncrosslinked) depicts the expected reduction in ASC protein levels after the addition of MM01 (compare +ASC to +ASC+MM01); however, co-treatment with bafilomycin (ASC+MM01+Bafilomycin) recovers ASC protein to the level observed in ASC-YPF transfected cells (+ASC).

The evaluation of ASC oligomerization (crosslinked) in the lower panel of **Figure 6** depicts the expected reduction in ASC oligomerization following MM01 treatments (compare +ASC to +ASC+MM01); however, cotreatment with bafilomycin (+ASC+MM01+Bafilomycin) does not induce the recovery of ASC oligomerization to that observed in ASC-YPF transfected cells (+ASC). Furthermore, bafilomycin treatment in the absence of MM01 (+ASC + bafilomycin) does not negatively impact ASC oligomerization.

Overall, these findings suggest that MM01 interferes with ASC oligomer formation and facilitates ASC degradation in HEK293 cells via the autophagy-lysosome pathway.

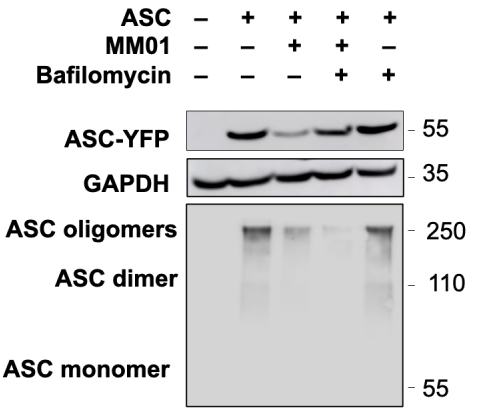

Figure 6. Impact of MM01 on ASC Expression and Oligomerization in HEK293 following Autophagy-lysosome Pathway Inhibition. Western blot analysis of ASC expression levels following treatment with 20 μM MM01 (+MM01) and bafilomycin (+Bafilomycin) in ASC-YFP (+ASC) transfected HEK293 cells in the absence (upper panel) and presence of crosslinking (lower panel). GAPDH functioned as a loading control (central panel).

IV.1.3 MM01 inhibits ASC Speck Formation in Macrophages Expressing ASC-GFP

Our *in vitro* assays in HEK293 cells provided evidence that MM01 inhibits ASC oligomerization; however, we lacked an understanding of MM01's mechanism in a cellular environment that naturally contains inflammasome components.

Therefore, to confirm the mechanism of action of MM01 and to rule out interactions with other proteins, we studied the ability of MM01 to inhibit ASC speck formation using monocytic THP-1 leukemia cells expressing an ASC-green fluorescent protein (GFP) fusion protein (THP-1-ASC-GFP), which provides similar advantages to the previously described ASC-YFP protein regarding detection. THP-1-ASC-GFP cells stably express ASC-GFP fusion protein under the control of the nuclear factor kappa B (NFκB) binding promoter.

We first studied the ability of MM01 to reduce ASC speck formation in NLRP3, the most studied inflammasome. Classical or canonical NLRP3 inflammasome activation represents a two-step process - the priming step comprises NFκB pathway

activation, which prompts the upregulated expression of NLRP3 and pro-IL-1β proteins and induces post-translational modifications of NLRP3 that promote inflammasome assembly. The priming step also comprises the upregulation of ASC-GFP expression in THP-ASC-GFP cells. The priming step can be initiated by different PAMPs or DAMPs that bind to TLRs, including lipopolysaccharide (LPS) [27] - a component of the outer membrane of Gram-negative bacteria - or the binding of IL-1β and TNF-α to their respective receptors. The subsequent activation step prompts changes in the conformation of NLRP3 to allow oligomerization and the activation of the inflammasome. A wide range of factors can induce the activation step, including PAMPs and DAMPs such as nigericin - a microbial toxin derived from the Gram-positive bacterium *Streptomyces hygroscopicus* [28], extracellular ATP, and lysosomal destabilizing agents such as silica and cholesterol crystals [27].

Hence, we employed phorbol 12-myristate 13-acetate (PMA)-differentiated macrophages derived from THP-1-ASC-GFP cells, a common cellular model to study the activation of inflammasomes [29]; [30], to study the impact of MM01 pretreatment on ASC speck formation after inflammasome priming and activation with LPS and nigericin, respectively (**Material and methods III.2.2.F**).

We pretreated PMA-differentiated cells with 20 μM MM01 for 30 min, primed cells with 100 ng/mL LPS for 3 h, and then activated the canonical NLRP3 inflammasome with 10 μM nigericin treatment for 30 min.

We analyzed ASC specks formation in cells by confocal microscopy **(Figure 7)**. As expected**,** in resting cells (untreated) we failed to observe any ASC-GFP expression; however, inflammasome priming with LPS induced NFκB-dependent ASC-GFP expression, resulted in cells exhibiting diffuse ASC expression. Inflammasome activation by co-treatment with LPS and nigericin (LPS/Nig) prompted the formation of ASC aggregates as bright fluorescent specks in the perinuclear region (white arrows highlight ASC specks). Finally, MM01 pretreatment reduced ASC speck formation following LPS and nigericin treatment (LPS/Nig+MM01), demonstrating that MM01 can inhibit ASC oligomerization in a cellular environment with multiple inflammasome components.

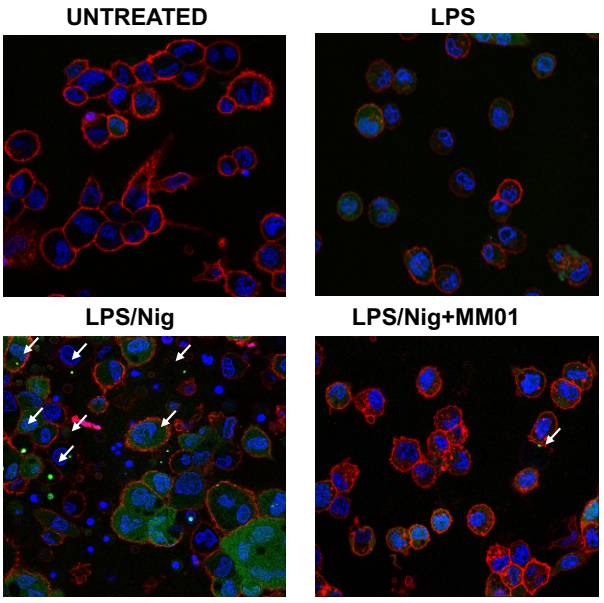

Figure 7. Impact of MM01 on ASC Speck Formation in THP-1-ASC-GFP Cells. Live-cell imaging of PMA-differentiated THP-1-ASC-GFP cells pretreated with 20 μM MM01 and then stimulated with 100 ng/mL LPS and 10 μM nigericin. DAPI (blue) staining marks cell nuclei and wheat germ agglutinin (WGA – red) staining marks the cell membrane.

We next employed flow cytometry to quantitatively evaluate ASC speck formation using a recently described approach [20]. Unlike image-based assays, flow cytometry enables the quantitative analysis of a large number of cells and recognizes inflammasome-activated cells. This technique relies on detecting a signal pulse formed after speck formation in cells. While non-stimulated cells display a more distributed ASC pattern that results in a low signal pulse with a width corresponding to the cell size, inflammasome-activated cells display concentrated ASC clusters (specks) that result in a high signal pulse of small width [20] (**Figure 8**).

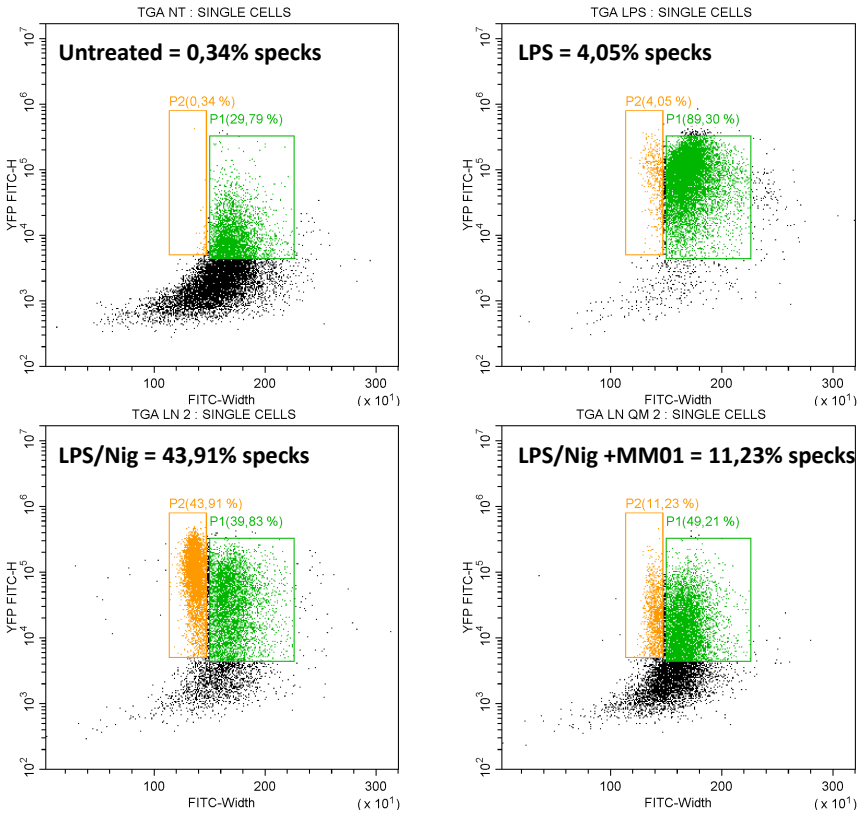

Figure 8. Detection of ASC Speck Formation within Cells by Flow Cytometry. PMA-differentiated THP-1-ASC-GFP cells primed with 100 ng/mL LPS for 3 h and activated with 10 µM nigericin for 30 min were evaluated for ASC speck formation in the presence and absence of 20 µM MM01 pretreatment. Each graph represents signal width on the X-axis and signal intensity (YFP-FITCH) on the Y-axis – the green signal represents the percentage of induced ASC expressed in cells, and the orange signal represents the percentage ASC speck formation.

Flow cytometry technique allows the distinction of ASC specks from monomeric ASC in cells because the light emissions from the fluorescent reporter differ significantly from state to state. The diffuse localization of ASC throughout the cytosol, which is verified when the GFP signal is homogeneously distributed in an area the size of a cell, is interpreted as a broad signal with a flattened peak (↓ Height-Width ratio). In contrast, ASC specks show the highest levels of fluorescence intensity in a very limited space in the cytoplasm due to the organization of ASC in supramolecular

structures, which are perceived as much narrower GFP pulses with higher intensity values. (↑ height-width ratio)

As shown in **Figure 8**, inflammasome priming with LPS induced an increase in NFκB-dependent ASC-GFP expression (89.30%) compared to untreated cells (29.79%) (compare green signal of LPS to Untreated). We failed to detect high levels of ASC speck formation after LPS priming (4.05%) compared to untreated cells (0.34%) (compare the orange signal of LPS and NT). Notably, LPS and nigericin (LPS/Nig) treatment induced a significant increase in speck formation within cells (43.91%) when compared to LPS treatment only (4.05%). Finally, MM01 pretreatment before LPS and nigericin treatment (LPS/Nig+MM01) reduced speck formation (11.23%) when compared to stimuli LPS and nigericin (LPS/Nig) treatment (43.91%).

Finally, the quantification of ASC specks formation by flow cytometry (**Figure 9),** demonstrated the significant formation of ASC specks in THP-1-GPF-ASC cells upon the treatment with LPS and nigericin (+LPS/Nig) compared to untreated cells. However, MM01 pretreatment prompted a significant reduction in ASC speck formation compared to LPS and nigericin treatment (compare +LPS/Nig to +LPS/Nig+MM01). Overall, these findings provide further evidence that MM01 reduces ASC speck formation in an inflammasome competent cellular environment after the LPS and nigericin-mediated activation of the NLRP3 inflammasome.

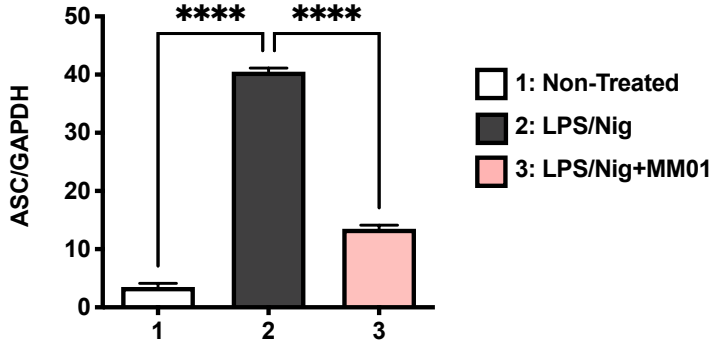

Figure 9. Quantification of ASC Speck Formation. Percentage of ASC speck formation in THP-1-ASC-GFP cells following treatment with LPS and nigericin (+LPS/Nig) with and without pretreatment with

MM01 (+MM01). Data represent the mean ± SD of three independent experiments. Asterisks represent significant differences determined by one-way ANOVA test with Tukey's multiple post-test comparisons ***p<0.001.

Finally, we chemically crosslinked THP-1-ASC-GFP cell pellets and analyzed the formation of ASC oligomers by Western blot in response to the various treatments (**Figure 10**). The evaluation of ASC oligomerization (crosslinked) in the lower panel of **Figure 10** demonstrates the expected formation of ASC oligomers following LPS and nigericin treatment (+LPS+Nig) compared to untreated cells and cells primed with LPS (+LPS). Pretreatment of cells with MM01 (+LPS+Nig+MM01) prompted the inhibition of oligomer formation in response to LPS and nigericin treatment (+LPS+Nig).

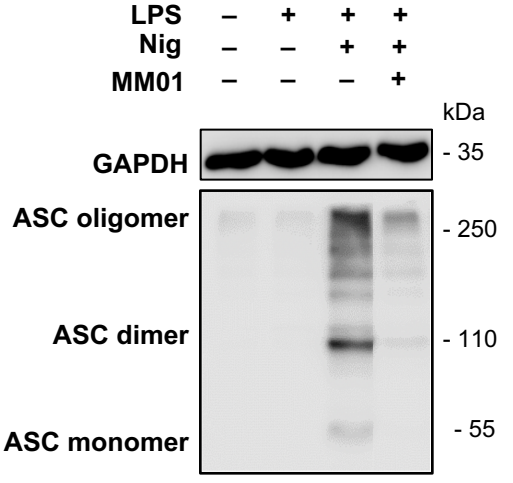

Figure 10. ASC Oligomerization Profile in THP-1-ASC-GFP Cells (Lower panel) Western blot analysis of crosslinked pellets of PMA-differentiated THP-1-GFP-ASC cells following pretreatment with 20 μM MM01 and LPS (+LPS) and nigericin (+Nig) treatments. (Upper panel) GAPDH functions as a loading control.

In conclusion, we identified the inhibition of ASC oligomerization as the mechanism of action of MM01 both *in vitro* and in cellular models. Electron microscopy imaging *in vitro* analysis demonstrated the ability of MM01 to prevent

ASC filament formation after incubating the drug with recombinant human ASC protein. We studied the ASC oligomerization process and ASC speck formation in cell models - HEK293 and THP-1-ASC-GFP cell lines. In both lines, we demonstrated the ability of MM01 to inhibit ASC oligomers formation by Western blot and ASC speck formation by confocal microscopy. Finally, we demonstrated that MM01 interferes with the formation of ASC oligomers and facilitates the degradation of ASC through the autophagy-lysosome pathway.

IV.2 Identification of MM01 Binding Sites in ASC

Once delineated the molecular mechanism of action of MM01, we aimed to study the role of the interaction sites between MM01 and ASC, previously identified by docking, in the ASC oligomerization process.

The multi-inflammasome adapter protein ASC possesses a simple structure comprising two domains (N-terminal ASC^{PYD}, C-terminal ASC^{CARD}) [31], making it a straightforward candidate for structural studies. Understanding the structure of the studied protein, as well as investigating drug-protein binding represents one of the most critical parameters in early-stage drug discovery [32].

Prior to this work, to identify interaction sites between ASC and MM01, docking studies were carried out in collaboration with the laboratory of Dr. Irmgard Merfort in Freiburg (Germany).

Computational approaches for drug-protein docking studies include GOLD, Glide, AutoDock Vina, and DOCK [33]. Docking studies were performed with the GOLD 5.2 protein-ligand coupling software (CCDC, Cambridge, UK) using the default docking settings to obtain data regarding critical interactions between ASC and MM01 (**Figure 11** and **12**). As noted in the **Material and Methods Section III.2.2.C,** the docking predictions were carried out employing the crystal structures of ASC downloaded from the protein data bank2.

The critical interactions between MM01 and ASC identified involve His-118, Phe-136, Trp-169, Lys-174, Leu-177, Leu-178, and Leu-192, which correspond to amino acids located in the ASC^{CARD} domain (**Figure 11**).

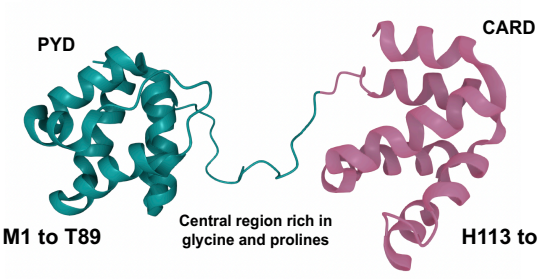


```
        10         20         30         40         50
MGRARDAILD ALENLTAEEL KKFKLKLLSV PLREGYGRIP RGALLSMDAL
        60         70         80         90        100
DLTDKLVSFY LETYGAELTA NVLRDMGLQE MAGQLQAATH QGSGAAPAGI
       110        120        130        140        150
QAPPQSAAKP GLHFIDQHRA ALIARVTNVE WLLDALYGKV LTDEQYQAVR
       160        170        180        190
AEPTNPSKMR KLFSFTPAWN WTCKDLLLQA LRESQSYLVE DLERS
```

Figure 11. Predicted ASC and MM01 Interaction Sites. ASC contains two members of the death domain superfamily: A N-terminal PYD domain (amino acids M1 to T89), marked in blue, and a C-terminal CARD domain (amino acids H113 to S195), marked in pink. The interaction amino acids between MM01 and ASC correspond to amino acids located in the ASC^{CARD} domain and are marked in yellow.

Moreover, the docking results suggested how MM01 interacts with the identified amino acids (**Figure 12**). The results proposed an interaction of MM01 through i) van der Waals interactions with His-118, Leu-192, Leu-178, Leu-177, and Lys-174 at different points in the molecule, III) π interactions between MM01 and Phe-163 and Trp-169, and IV) hydrogen bonds between MM01 and Lys-174.

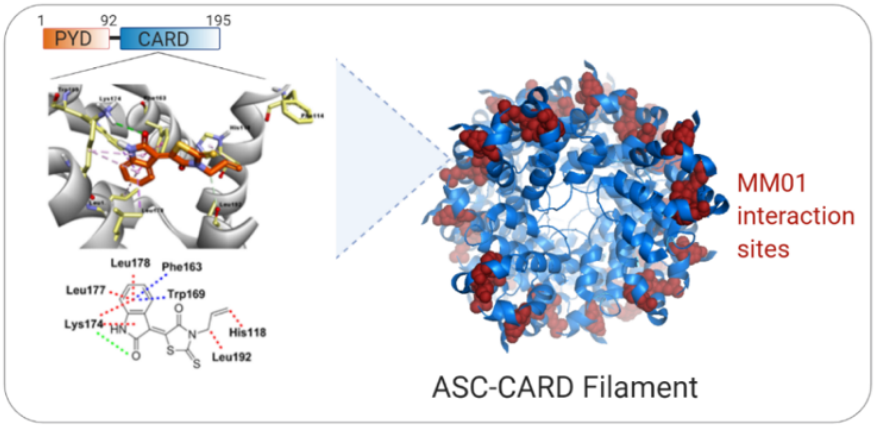

Figure 12. Characterization of Binding Sites Associated with the ASC-MM01 Interaction. Docking model of ASC with MM01. Green lines represent hydrogen bonds, red lines show van der Waals interactions, and blue lines depict π interactions.

IV.2.1 Study of the MM01 ASC Binding site

To investigate the relevance of the suggested interaction sites in the ASC oligomerization process, we generated site-directed mutants in the YFP-fused ASC construct (ASC-YFP) employing an alanine mutagenesis strategy to determine the contribution of a specific residue to the stability or function of a given protein. Alanine has a non-bulky, chemically inert, methyl functional group [34]. that does not alter the conformation of the backbone (as glycine or proline can), nor does it impose extreme electrostatic or steric effects [35].

We replaced the amino acids identified as ASC and MM01 interactions sites with alanine to study their potential role in ASC oligomerization.

Overall, site-directed mutagenesis produced single mutants (ASC^{H118A}-YFP, ASC^{F136A}-YFP, ASC^{W169A}-YFP, $ASCK^{174A}$-YFP, and ASC^{L192A}-YFP) and a double mutant ($ASC^{L177A\text{-}L178A}$-YFP) designed due to the proximity of amino acids.

Additionally, a complete binding site mutant at the six residues (ASC^{ALL}-YFP) was generated.

Interestingly, a previous study noted that mutations in residues Trp-169 and Arg-119 (close to His-118) (which play a fundamental role in the formation of ASC filaments) interrupt ASC oligomerization [36]. Therefore, we employed the ASC^{R119}-YFP mutation as a positive control for the inhibition of speck formation [16]. Drugs such as MM01 may target these residues, or nearby sites, to impair oligomer formation and interfere with pro-caspase-1 activation.

We then transfected HEK293 cells with the ASC-YFP mutants at 1 μg/mL for 24 h and analyzed speck formation by flow cytometry and Western blot (**Figure 13** and **14**).

As detailed above, the levels of ASC oligomerization were assessed by plotting the height and width of the recorded fluorescent signals by flow cytometry. Furthermore, in this experiment, to distinguish different ASC-YFP+ subpopulations, the height of the signal pulse vs. width cytograms were divided into four polygonal regions (R-1, R-2, R-3, and R-4) (**Figure 13**). R-1 and R-2 polygonal regions correspond to ASC specks (green dots) or cytosolic ASC (yellow dots), respectively. A third minor subpopulation in the medium (R-2), indicated in red, corresponds to cells with high levels of expression of ASC-YFP that do not complete the formation of ASC specks. Finally, the cellular events coupled to the low width and low height fluorescent emissions are collected in R-4. These are associated with low expression of the recombinant protein and are therefore no longer considered for future comparative studies.

Visually comparing the distribution of fluorescence emissions as a function of the height and width of the YFP pulses (**Figure 13**), we observe a significative increase of ASC speck formation in HEK293 cells upon the transfection with wildtype ASC (ASC^{wt}). Importantly, the ASC mutant used as a positive control for its inability to complete ASC specks formation (ASC^{R119A}) shows a decreased positive population of specks compared to ASC^{wt} that appear to move along the width axis (X-axis). Consequently, the R-2 region that acts as a bridge between speck-positive cells and

cytosolic ASC-YFP cells is more densely populated. This distribution pattern is shown in the single amino acid ASC mutants ASC^{F136A}, ASC^{W169A}, $ASCK^{174A}$, ASC^{L192A}, as well as by the mutant with the six altered positions ASC^{ALL}. In contrast, this change in high intensity fluorescence events along the broad axis is not as obvious for the ASC^{H118A} mutant and appears insignificant for $ASC^{L177A-L178A}$, whose distribution more closely resembles the wild-type phenotype.

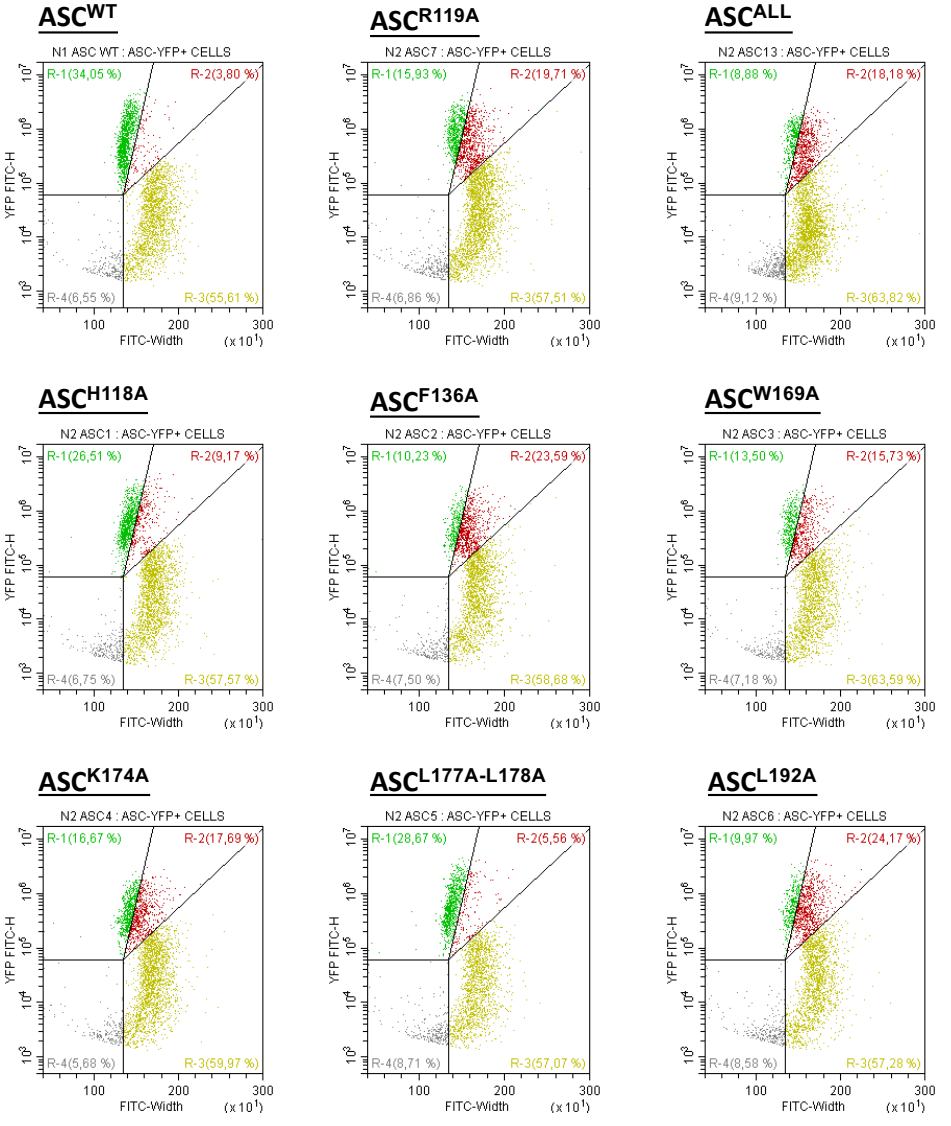

Figure 13. Influence of Specific Amino Acids on ASC Speck Formation in HEK293 Cells Evaluated by Flow Cytometry. The cytograms Y-axis (YFP FITC-H) represent the height of the ASC-YFP signal (a.u.), while the cytograms X-axis represent the width of the ASC-YFP signal (a.u.). Green events in the

polygonal region R-1 represent ASC specks, red events represent undefined intermediate species, yellow events represent cytosolic distribution of ASC and grey events are associated with cellular populations with residual or low expression of ASC.

Moreover, the quantification of the formation of ASC specks by flow cytometry (**Figure 14A**) demonstrates the expected increase in ASC speck formation with ASC^{WT} transfection in HEK293; however, all mutants (except for the double mutant $ASC^{177A\text{-}L178A}$) produced a highly significant reduction in the number of ASC specks compared to ASC^{WT} cells (**Figure 14A**). In addition, Western blot analysis demonstrated that all mutants expressed ASC to a similar degree (**Figure 14B**). Overall, these data provide evidence for the critical nature of the MM01 binding pocket in ASC for speck formation and represent a new site for therapeutic intervention.

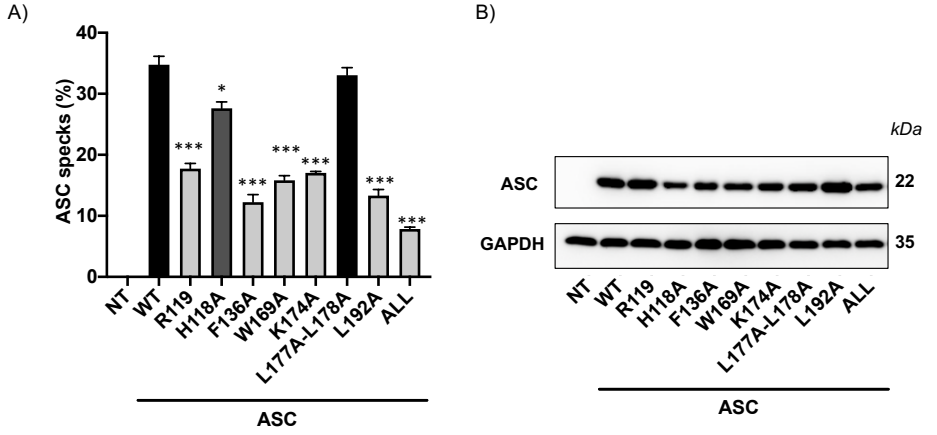

Figure 14. Speck Formation in HEK293 Cells Following Mutation to Amino Acids Involved in the MM01-ASC Interaction A) Percentage of ASC speck formation in HEK293 cells transfected with the ASC mutants measured by flow cytometry. **B**) (Upper panel) Western blot of uncrosslinked cellular extracts from transfected HEK293 cells. (Lower panel) GAPDH as a loading control. Data represent the mean ± SD of three independent experiments. Asterisks represent significant differences to the wildtype transfection determined by one-way ANOVA test with Tukey's multiple post-test comparisons, ***$p<0.001$.

Finally, to complement the flow cytometry-mediated quantification of ASC speck formation, we evaluated ASC oligomers by confocal microscopy, following the ASC speck formation through YFP. **Figure 15** demonstrates the expected formation of small, tight ASC specks (green punctae) in HEK293 cells transfected with the ASC^{WT}-YFP control plasmid; however, all mutants except for the double mutant $ASC^{177A-L178A}$ reduced/disrupted ASC speck formation when compared to ASC^{WT}.

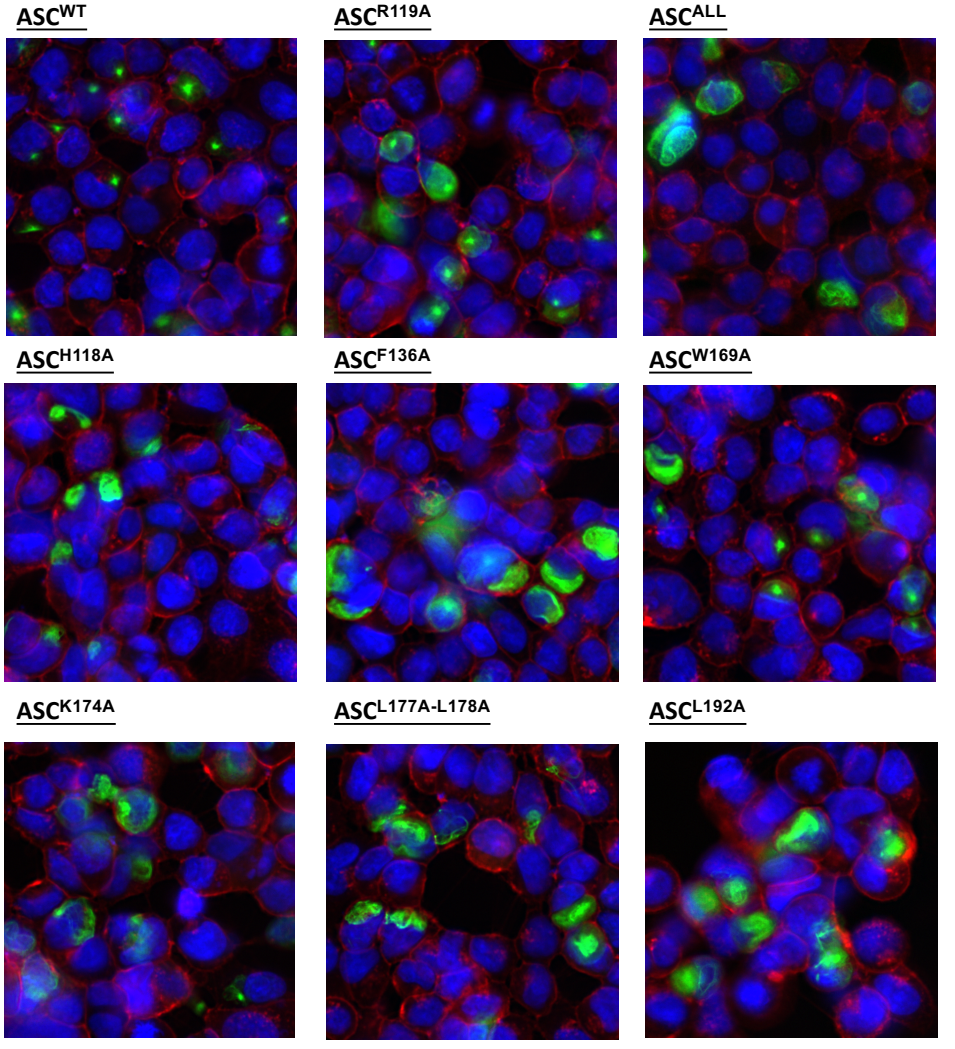

Figure 15. Live Cell Imaging of HEK293 Cells Transfected with ASC Mutants. Cell membranes were stained with Wheat Germ Agglutinin Alexa Fluor 647 Conjugate (red), nuclei were stained with Hoechst 33342 (blue) and the intracellular ASC-YFP distribution is represented in green. BS_1 to BS_6 refers to single amino acid binding site ASC mutants, BS_ALL refers to the mutant with the six residues altered and specks- is a described control for its inability to form specks.

In conclusion, we demonstrated the importance of the interaction sites identified by docking between MM01 and ASC in the ASC oligomerization process. Moreover, by doing so, we have identified new drug binding sites in ASC for inflammasome inhibition.

IV.3. MM01 Inhibits ASC-mediated Inflammatory Signaling *in vitro*

The ability of MM01 to target the ASC adapter protein, which is common to diverse types of inflammasomes, suggest that MM01 should be able to inhibit different ASC-dependent inflammasomes concomitantly activated in multifactorial diseases [37]; [38]; [39]. For this reason, we aimed to evaluate the ability of MM01 to inhibit different inflammasomes in cellular models.

IV.3.1 MM01 Prevents NLRP3 Activation in THP-1 -derived Monocytes and Macrophages

Monocytes and macrophages are the main cells expressing the inflammasome genes. They are capable to adapt to their surrounding microenvironment towards a pro-inflammatory M1 phenotype that promotes inflammation [40]**.** For this reason, we employed THP-1-derived monocytes and macrophages as a cellular model of inflammation for MM01 evaluation.

We first evaluated MM01 activity in undifferentiated monocytic THP-1 cells to optimize activation conditions for the NLRP3 inflammasome (as the most studied and characterized inflammasome with implications to numerous disease states [41]. We selected LPS and nigericin as activation stimuli for THP-1 cells and analyzed the impact of MM01 on inflammasome activity.

The bacterial component LPS initiates the priming process that induces NLRP3 and pro-IL-1β expression through activation of NF-κB. Moreover, the bacterial toxin nigericin, derived from the gram-positive bacterium *Streptomyces hygroscopicus*, is a

K + efflux agonist capable of activating NLRP3 in a second signal step [42]. The drop in intracellular K + causes conformational changes of NLRP3 that lead to the activation of the inflammatory process.

We evaluated the inhibitory capacity of MM01 through the quantification of IL-1β secretion, pyroptotic cell death by the quantification of lactate dehydrogenase (LDH) release, and the analysis of inflammatory proteins by Western Blot in THP-1 monocytes following a 30 min pretreatment with 20 μM MM01 and then NLRP3 inflammasome activation with 100 ng/ml of LPS for 3 h and 20 μM nigericin for 30 min (**Figure 16**).

As expected, LPS and nigericin stimuli (+ LPS/Nig) increased IL-1β secretion and pyroptosis compared to untreated cells; however, MM01 pretreatment (+MM01) led to a significant reduction in IL-1β and pyroptosis (compare + LPS/Nig to + LPS/Nig + MM01) (**Figure 16A**).

Pyroptotic cell death, characterized by the release of the cell content [43], contributes to the amplification of pro-inflammatory signaling to neighboring cells [44]. Therefore, the inhibition of MM01-mediated pyroptosis could significantly slow the inflammatory spread (**Figure 16B**).

Finally, we analyzed protein expression of the inflammasome components in cell supernatants (SN) and cell lysates (pellet). This analysis (**Figure 16C**) demonstrated that treatment with MM01 reduced levels of active caspase-1 and processed IL-1β in cell supernatants without affecting the protein expression in cells. Thus, MM01 effectively inhibits NLRP3 inflammasome activity in the monocytic THP-1 cell line.

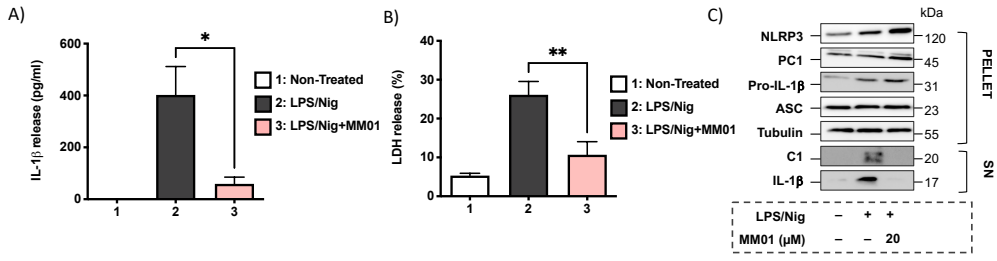

Figure 16. MM01 Inhibits NLRP3 Activation in monocytic THP-1 Cells. A) IL-1β secretion evaluated by ELISA following activation of the NLRP3 inflammasome with LPS (100 ng/ml) and nigericin (10 μM). Cells were pretreated with MM01 at 20 μM. **B**) Measurement of LDH release under the above-described conditions. **C**) THP-1 cells were stimulated as described above, and cell supernatants (SN) and pellets analyzed by immunoblotting for IL-1β and cleaved caspase-1 (C1) identification in SN, and NLRP3, pro-caspase-1 (PC1), pro- IL-1β and ASC expression in pellets. A representative blot is shown. Data represent the mean ± SD of three independent experiments. Asterisks represent significant differences determined by one-way ANOVA test with Tukey's multiple post-test comparisons *p<0.05; **p<0.01.

We next evaluated MM01 activity in macrophages generated by the PMA-induced differentiation of THP-1 cells, the most common cellular model for inflammasome studies, using the same conditions as for THP-1 monocytes (**Figure 17**). In a comparable manner to the THP-1 monocyte experiments, **Figure 17** depicts the MM01-dependent reduction in the levels of IL-1β (**Figure 17A**) and pyroptosis (**Figure 17B**) in NLRP3 activated cells macrophages. MM01 treatment also reduced the presence of caspase-1 and processed IL-1β in THP-1 secretome without affecting the expression of NLRP3, pro-caspase-1, pro-IL-1β and ASC in the cells (**Figure 17C**). Overall, these findings confirm that MM01 prevents NLRP3 inflammasome activation in a cellular context.

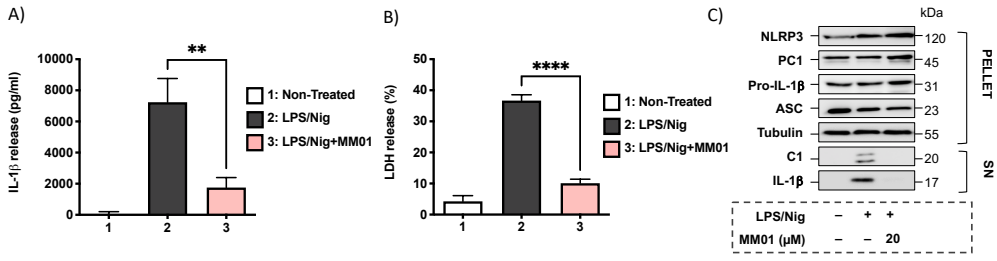

Figure 17. MM01 Inhibits NLRP3 Activation in THP-1- derived Macrophages. A) IL-1β secretion evaluated by ELISA following activation of the NLRP3 inflammasome with LPS (100 ng/ml) and nigericin (10 μM). Cells were pretreated with MM01 at 10 μM. **B**) Measurement of LDH release under the above-described conditions. **C**) THP-1-derived macrophages cells were stimulated as described above, and cell supernatants (SN) and pellets were analyzed by immunoblotting for IL-1β and cleaved caspase-1 (C1) identification in SN, and NLRP3, pro-caspase-1 (PC1), pro- IL-1β and ASC expression in pellets. A representative blot is shown. Data represent the mean ± SD of three independent experiments. Asterisks represent significant differences determined by one-way ANOVA test with Tukey's multiple post-test comparisons **p<0.01; ***p<0.0001.

IV.3.2 MM01 Prevents AIM2 Inflammasome Activation in THP-1-ASC-GFP-derived Macrophages

The AIM2 innate immune sensor detects altered or mislocated DNA and the presence of foreign DNA in the cytosol that occurs during the life cycle of intracellular pathogens, including viruses, bacteria, and parasites [45].

We employed cytosolic double-stranded DNA (poly (dA:dT)) [46] to activate AIM2 inflammasome in PMA-differentiated THP-1-ASC-GFP macrophages.

We first differentiated THP-1-ASC-GFP cells with PMA for 24 h, pretreated cells with 20μM MM01 for 30 min, and then transfected cells with 0.5μg/mL poly (dA:dT) (as detailed in **Materials and Methods Section III.2.2.F**).

Figure 18 demonstrates that sensing cytosolic DNA produces alterations to levels of cellular IL-1β release (**Figure 18A**) and a low degree of pyroptosis in macrophages in response to AIM2 inflammasome activation (**Figure 18B**). MM01 pretreatment (+MM01) significantly inhibits the increase in IL-1β release while a non-significant tendency to decrease cell death is observed, that could be explained by the

very low cell death percentages observed upon AIM2 activation. Overall, these results suggest the ability of MM01 to also prevent AIM2 inflammasome activation.

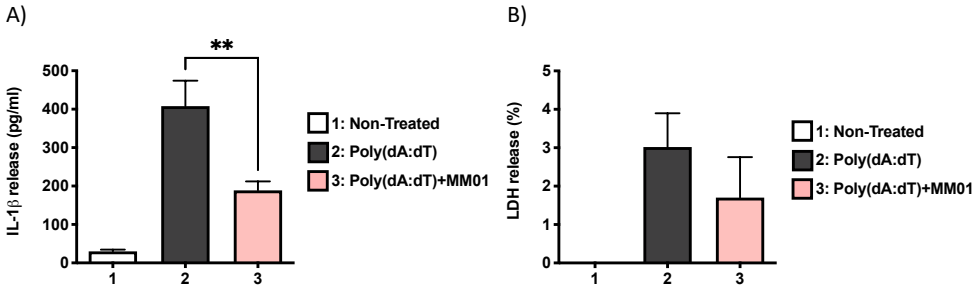

Figure 18. MM01 Inhibits AIM2 Activation in THP-1-ASC-GFP-derived Macrophages. A) IL-1β secretion evaluated by ELISA following activation of the AIM2 inflammasome with 0.5 μg/ml poly (dA:dT). Cells were pretreated with 20 μM MM01. **B**) Measurement of LDH release under the above-described conditions. Data represent the mean ± SD of three independent experiments. Asterisks represent significant differences determined by one-way ANOVA test with Tukey's multiple post-test comparisons, **p<0.01.

We also studied the effect of MM01 on ASC speck formation induced by AIM2 activation by confocal microscopy using THP-1-ASC-GFP-derived macrophages (**Figure 19**).

As expected, in untreated THP-1-ASC-GFP macrophages, we did not observe any speck formation; however, AIM2 activation (poly(dA:dT)) induced significant levels of ASC specks (green punctae marked by white arrows), which MM01 pretreatment significantly inhibited (poly(dA:dT)+MM01) (**Figure 19A** and **B**). Overall, these findings suggest that MM01 can robustly inhibit ASC speck formation following the activation of the AIM2 inflammasome.

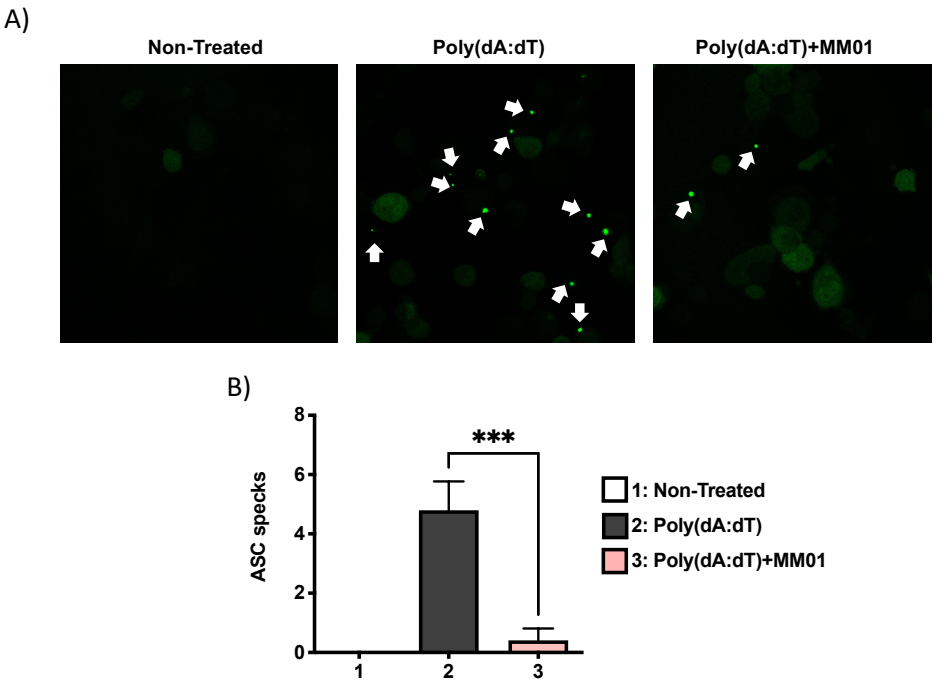

Figure 19. MM01 Inhibits ASC Speck Formation following AIM2 Inflammasome Activation. A) Live-cell imaging of THP-1-ASC-GFP cells pretreated with 20 μM MM01 and then stimulated with poly (dA: dT) to activate the AIM2 inflammasome. **B**) Quantification of intracellular speck formation. Data represent the mean ± SD of three independent experiments. Asterisks represent significant differences determined by one-way ANOVA test with Tukey's multiple post-test comparisons, ***p<0.001.

IV.3.3 MM01 Inhibits Pyrin Inflammasome Activation in THP-1-ASC-GFP-derived Macrophages

We next evaluated the ability of MM01 to inhibit the pyrin ASC-dependent inflammasome. The pyrin inflammasome has evolved as an innate immune sensor that detects the inactivation of guanosine triphosphatase Rho (Rho GTPase) by bacterial toxins. Rho GTPases function as molecular switches to regulate a variety of signal transduction pathways, including cytoskeletal organization. Pathogens modulate Rho GTPase activity to suppress host immune responses such as phagocytosis. Thus, the pyrin inflammasome detects alterations to Rho GTPases activity by pathogen virulence factors [47].

We selected LPS (100 ng/mL) priming for 3 h followed by 18 h treatment with cholera toxin, a bacterial enterotoxin secreted by *Vibrio cholerae,* to activate the pyrin

inflammasome in PMA-differentiated THP-1-ASC-GFP cells (**Materials and method III.2.2.F**) [48].

Figure 20 shows the expected induction of IL-1β release (**Figure 20A)** and pyroptotic cell death (**Figure 20B**) following pyrin inflammasome activation (+LPS/Cholera.T); however, MM01 pretreatment significantly inhibited the induction of IL-1β release (compare + LPS/Cholera.T to + LPS/Cholera.T + MM01) and pyroptotic cell death. These findings suggest the ability of MM01 to prevent activation of the pyrin inflammasome in a cellular context.

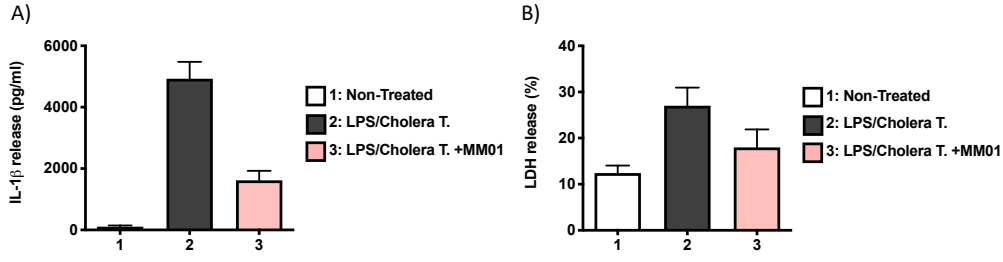

Figure 20. MM01 Inhibits Pyrin Inflammasome Activation in THP-1-ASC-GFP-derived Macrophages. A) IL-1β secretion evaluated by ELISA following activation of the pyrin inflammasome with 100 ng/ml LPS and 5 mM Cholera toxin. Cells were pretreated with 20 μM MM01. **B**) Measurement of LDH release under the above-described conditions. Data represent the mean ± SD of three independent experiments. Asterisks represent significant differences determined by one-way ANOVA test with Tukey's multiple post-test comparisons, ***$p<0.001$.

Moreover, as expected**,** pyrin inflammasome activation (LPS/Cholera T.) robustly induced ASC speck formation (**Figure 21**); however, MM01 pretreatment significantly inhibited the appearance of ASC oligomers (Cholera T.+MM01). Overall, these findings suggest that MM01 can also inhibit the ASC-dependent Pyrin inflammasome activation.

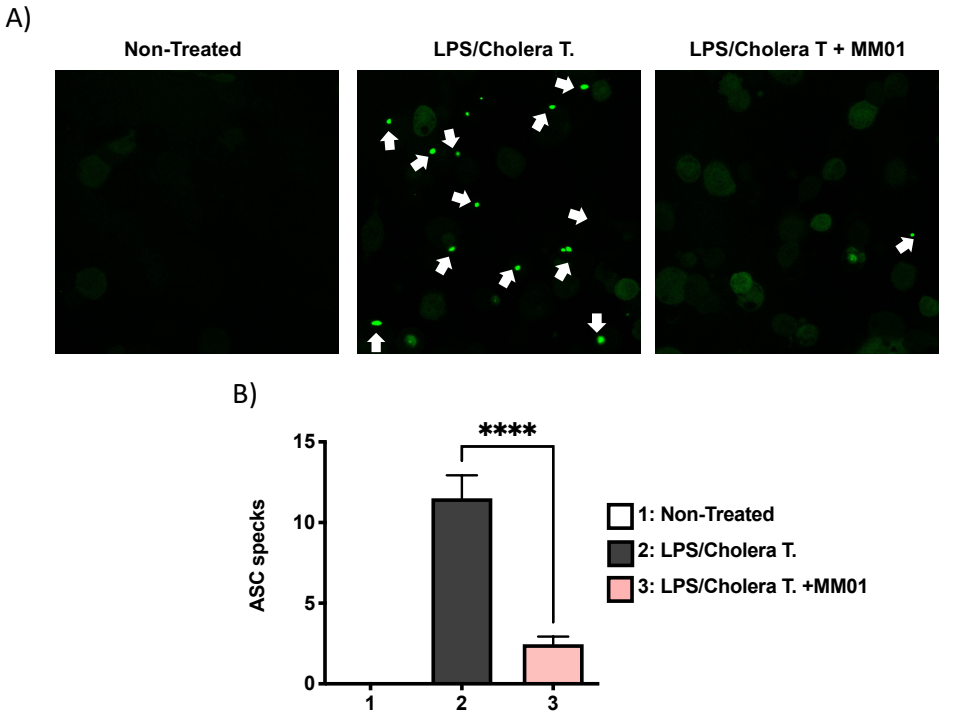

Figure 21. MM01 inhibits pyrin speck formation. A) Live-cell imaging of THP-1-ASC GFP cells treated with MM01 (10 μM) and stimulated with LPS and Cholera toxin for the activation of pyrin inflammasome. B) Count of speck formation in cells. Data represent the mean ± SD of three independent experiments. Asterisks represent significant differences determined by one-way ANOVA test with Tukey's multiple post-test comparisons ****$p<0.0001$.

IV.3.4 MM01 Fails to Inhibit Non-canonical Inflammasome Activation in THP-1-ASC-GFP-derived Macrophages

To reinforce the mechanism of action of MM01, we studied the effect of MM01 in the non-canonical inflammasome pathway, which does not depend on ASC.

The non-canonical inflammasome activation pathway does not require the formation of the conventional inflammasome complex. Instead, the activation of human caspases 4/5 occurs in response to intracellular LPS [49]. Therefore, caspase-4/5 or murine caspase-11 directly recognize intracellular LPS by their CARD domains to prompt the cleavage of the pore-forming protein GSDMD and trigger a secondary activation of the canonical NLRP3 inflammasome for cytokine release.

Caspases-4/5 and caspase-11, in the same way as caspase-1, are initiator caspases composed of an N-terminal CARD domain, responsible for their oligomerization, and the caspase domains p10 and p20. Importantly, the idea that caspase-11 itself could act as a direct receptor for LPS was reported from the observation that caspase-11 purified from *E. coli*, but not from insect cells, was oligomerized under non-denaturing conditions. This demonstration suggested that bacterial components can induce caspase-11 oligomerization, which is necessary for its activation. In fact, it was shown that LPS was responsible for this oligomerization since the insect cells incubated with LPS produced the oligomerization of caspase-11.

Overall, the consequences of canonical and non-canonical inflammasome activation are similar - while caspase-1 promotes the processing and release of pro-inflammatory cytokines (IL-1β and IL-18) and pyroptotic cell death, caspase-4/5 directly promotes pyroptosis through the cleavage of GSDMD [50].

We pretreated THP-1-ASC-GFP-derived macrophages with 20 μM MM01 for 30 min and stimulated non-canonical inflammasome activation by transfecting 300 ng of ultrapure LPS (**Material and Methods III.2.2.F**). **Figure 23** depicts alterations to the levels of IL-1β (**Figure 23 A**) and pyroptosis (**Figure 23 B**) in PMA-stimulated THP-1-ASC-GFP cells following non-canonical inflammasome activation. The induction of non-canonical inflammasome (+LPS) increases both IL-1β release and pyroptosis compared to untreated cells. In this case, the pretreatment with MM01 (+MM01) fails to inhibit induced IL-1β release and pyroptosis, thereby reinforcing the ASC-specific mechanism of action of MM01. Overall, these results suggest the inability of MM01 to inhibit non-canonical inflammasome activation.

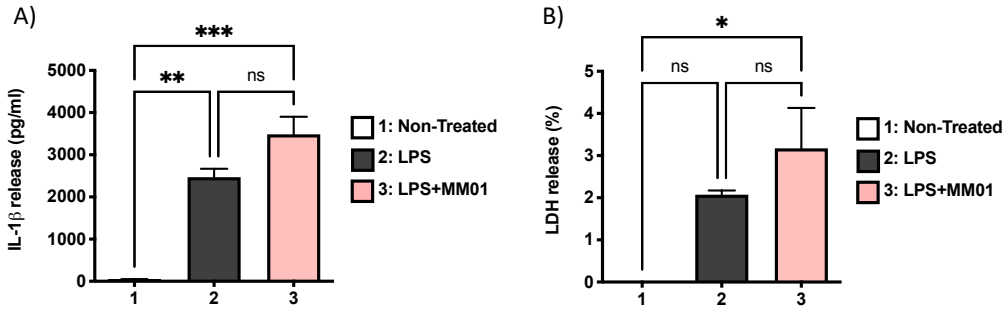

Figure 23. MM01 Fails to Inhibit Non-canonical Inflammasome Activation in THP-1-ASC-GFP-derived Macrophages. A) IL-1β secretion evaluated by ELISA following activation of the non-canonical inflammasome by transfection of 300 ng ultrapure LPS. Cells were pretreated with 20 μM MM01. **B**) Measurement of LDH release under the above-described conditions. Data represent the mean ± SD of three independent experiments.

Overall, these data provide evidence for MM01 as a specific inhibitor of ASC-dependent inflammasome activation in a cellular context.

IV.4 MM01 Inhibits ASC-mediated Inflammatory Signaling *in vivo*

We next aimed to evaluate the efficacy of MM01 *in vivo* in a murine model of peritonitis.

Peritonitis is inflammation of the peritoneum, the membrane that lines the inner abdominal walls and the organs within the abdomen, and generally occurs as the cause of a bacterial or fungal infection. There are two types of peritonitis: spontaneous bacterial peritonitis, or secondary peritonitis caused by a rupture or perforation in the abdomen. Peritonitis requires urgent medical attention to fight the infection [51]. During peritonitis, the peritoneal membrane undergoes structural and functional alterations that are mediated by IL-1β. Importantly, Hautem et al. reported the implication of NLRP3 inflammasome during peritonitis disease [51]. They demonstrated that the NLRP3 inflammasome is activated during peritonitis and directly involved in the deleterious inflammatory response in patients on peritoneal dialysis and in mouse models of peritonitis, leading to structural and functional impairment in the

peritoneal membrane. They showed that genetic and pharmacologic blockade of the NLRP3/IL-1β axis rescued morphologic alterations and transport defects during acute peritonitis, revealing novel therapeutic perspectives for this complication.

To evaluate the efficacy of MM01 in vivo, we selected a murine model of monosodium urate (MSU)-induced peritonitis [52] in which MSU crystals potently activate NLRP3 [53].

In this experimental model, the intraperitoneal injection of MSU crystals induces peritoneal inflammation accompanied by increased levels of IL-1β and neutrophil infiltration into the intraperitoneal fluid [52].

IV.4.1 MM01 Inhibits NLRP3 Activation in a Mouse Model of MSU-induced Peritonitis

Prior to the *in vivo* analysis, we confirmed the ability of MM01 to inhibit the inflammatory response caused by MSU crystals in macrophages derived from the THP-1-ASC-GFP cell line. For this purpose, we pretreated macrophages with 10 μM MM01 for 30 min and then stimulated cells with 300 μg/mL MSU crystals for 6 hours to activate the NLRP3 inflammasome and evaluated the secretion of IL-1β [52].

Figure 24 demonstrates the ability of MSU crystals (MSU) to robustly induce IL-1β release in macrophages, suggesting the activation of the NLRP3 inflammasome and the ability of MM01 (+MM01) to inhibit this induction.

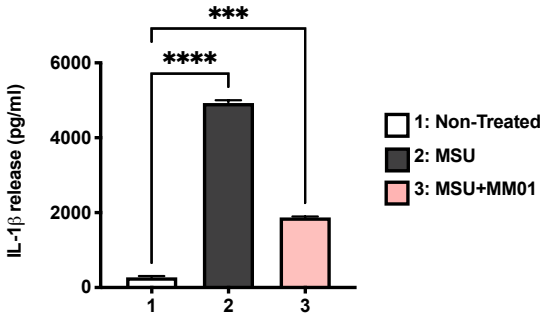

Figure 24. MM01 Pretreatment Inhibits IL-1β Release after MSU-treatment of THP-1-ASC-GFP-derived Macrophages. IL-1β secretion evaluated by ELISA following activation of the NLRP3 inflammasome with 300 μg/ml MSU. Cells were pretreated with 20 μM MM01. Data represent the mean ± SD of three independent experiments. Asterisks represent significant differences determined by one-way ANOVA test with Tukey's multiple post-test comparisons ****p<0.0001.

IV.4.2 MM01 Inhibits NLRP3 Inflammasome Activation in a Mouse Model of MSU-induced Peritonitis

We next studied the activity of MM01 in a mouse model of MSU-induced peritonitis. In this model, the number of infiltrating neutrophils and the release of IL-1β into the peritoneal cavity correlates with the extent of inflammasome activation [54].

At a functional level, peritonitis is characterized by an infiltration of leukocytes in the peritoneal membrane [51]. This immune infiltration consists of a rapid accumulation of neutrophils, which are progressively eliminated and are replaced by a population of mononuclear cells, monocytes and / or macrophages and lymphocytes. These cells contribute to the release of pro-inflammatory cytokines that stimulate the nearby microvasculature and attract large numbers of immune cells to migrate through the vascular wall and infiltrate the tissues [51]. Although these innate activities are important for host defense, their adverse effects are also evident, as demonstrated in numerous inflammatory diseases. In these cases, the low target specificity of inflammatory immune cells results in severe tissue and organ damage, often leading to rapid progression of the pathophysiological condition [55]. Thus, effective control of immune cell infiltration would greatly alleviate inflammatory disease.

For the *in vivo* experiment, we pretreated animals with an intraperitoneal injection of 10 mg/kg MM01 for 1 h and stimulated them with 10 mg/kg MSU crystals

for 6 hours. At 6 hours, we injected 5 mL of PBS to perform an intraperitoneal lavage and evaluate IL-1β and neutrophil content.

As represented in **Figure 25,** pretreatment with MM01 (10 mg/kg) efficiently suppressed MSU-induced IL-1β release and peritoneal neutrophil recruitment than activated animals (compare +LPS/MSU+MM01 to +LSP/MSU), thereby providing evidence for the *in vivo* anti-inflammatory activity of the ASC speck inhibitor MM01.

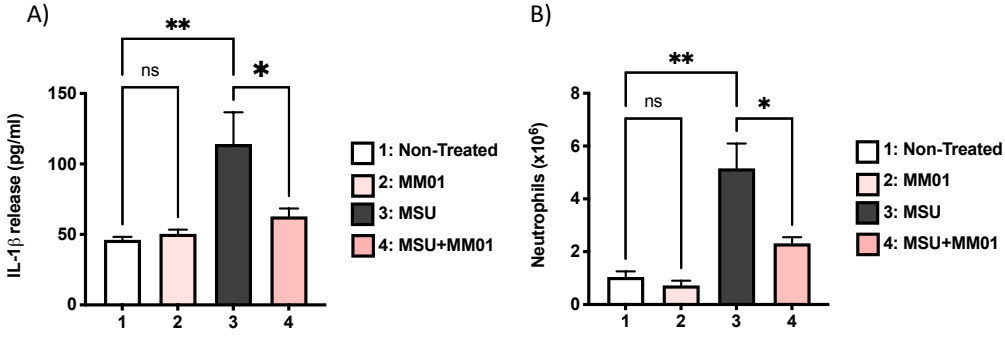

Figure 25. MM01 Inhibits ASC-dependent Inflammasome Activation in stimulated murine peritoneal macrophages and the MSU-induced peritonitis mouse model. A) ELISA for IL-1β in the peritoneal cavity of C57BL/6 mice injected with MSU crystals with or without MM01 (10 mg/kg) treatment. Data are representative of two independent experiments (mean and SD of n=12). B) Neutrophil numbers in the peritoneal cavity of C57BL/6 mice treated as in the above-described. Data represent the mean ± SD of eight animals per group. Asterisks represent significant differences determined by one-way ANOVA test with Tukey's multiple post-test comparisons *p<0.05.

Conclusions

We have shown that MM01, the first-in class small molecule inhibitor of ASC, inhibits the in vitro formation of specks from recombinant human ASC protein. We have identified MM01-ASC potential interaction sites by docking and showed that they are crucial to ASC oligomerization by site-directed mutagenesis. In a cellular context, MM01 inhibited ASC oligomer formation in HEK293 overexpressing ASC-YFP and in inflammasome-competent THP1 cells. Additional cell assays have confirmed the ability of MM01 to inhibit the activation of various ASC-dependent inflammasomes, decreasing both cytokine release and pyroptotic cell death. Finally, MM01 inhibits inflammasome activity in vivo in an MSU-induced mouse model of peritonitis.

References

1. Protti, M.P. and L. De Monte, *Dual Role of Inflammasome Adaptor ASC in Cancer.* Front Cell Dev Biol, 2020. **8**: p. 40.
2. Gorfu, G., et al., *Dual role for inflammasome sensors NLRP1 and NLRP3 in murine resistance to Toxoplasma gondii.* mBio, 2014. **5**(1).
3. Fais, R.S., et al., *The inflammasome NLRP3 plays a dual role on mouse corpora cavernosa relaxation.* Sci Rep, 2019. **9**(1): p. 16224.
4. Olsen, I. and S.K. Singhrao, *Inflammasome Involvement in Alzheimer's Disease.* J Alzheimers Dis, 2016. **54**(1): p. 45-53.
5. Masters, S.L., et al., *Activation of the NLRP3 inflammasome by islet amyloid polypeptide provides a mechanism for enhanced IL-1beta in type 2 diabetes.* Nat Immunol, 2010. **11**(10): p. 897-904.
6. Hamarsheh, S. and R. Zeiser, *NLRP3 Inflammasome Activation in Cancer: A Double-Edged Sword.* Front Immunol, 2020. **11**: p. 1444.
7. Xu, S., et al., *Inflammasome inhibitors: promising therapeutic approaches against cancer.* J Hematol Oncol, 2019. **12**(1): p. 64.
8. Wannamaker, W., et al., *(S)-1-((S)-2-{[1-(4-amino-3-chloro-phenyl)-methanoyl]-amino}-3,3-dimethyl-butanoy l)-pyrrolidine-2-carboxylic acid ((2R,3S)-2-ethoxy-5-oxo-tetrahydro-furan-3-yl)-amide (VX-765), an orally available selective interleukin (IL)-converting enzyme/caspase-1 inhibitor, exhibits potent anti-inflammatory activities by inhibiting the release of IL-1beta and IL-18.* J Pharmacol Exp Ther, 2007. **321**(2): p. 509-16.
9. Dinarello, C.A., A. Simon, and J.W. van der Meer, *Treating inflammation by blocking interleukin-1 in a broad spectrum of diseases.* Nat Rev Drug Discov, 2012. **11**(8): p. 633-52.
10. Yang, Y., et al., *Recent advances in the mechanisms of NLRP3 inflammasome activation and its inhibitors.* Cell Death Dis, 2019. **10**(2): p. 128.
11. Freeman, L., et al., *NLR members NLRC4 and NLRP3 mediate sterile inflammasome activation in microglia and astrocytes.* J Exp Med, 2017. **214**(5): p. 1351-1370.
12. Ravi Kumar, S., et al., *Emerging Roles of Inflammasomes in Acute Pneumonia.* Am J Respir Crit Care Med, 2018. **197**(2): p. 160-171.
13. Saresella, M., et al., *Multiple inflammasome complexes are activated in autistic spectrum disorders.* Brain Behav Immun, 2016. **57**: p. 125-133.
14. Jang, J.H., D.H. Kim, and Y.J. Surh, *Dynamic roles of inflammasomes in inflammatory tumor microenvironment.* NPJ Precis Oncol, 2021. **5**(1): p. 18.
15. Garcia-Lainez, G., et al., *Identification and validation of uterine stimulant methylergometrine as a potential inhibitor of caspase-1 activation.* Apoptosis, 2017. **22**(10): p. 1310-1318.
16. Soriano-Teruel, P.M., et al., *Identification of an ASC oligomerization inhibitor for the treatment of inflammatory diseases.* Cell Death Dis, 2021. **12**(12): p. 1155.
17. Komoriya, A., et al., *Assessment of caspase activities in intact apoptotic thymocytes using cell-permeable fluorogenic caspase substrates.* J Exp Med, 2000. **191**(11): p. 1819-28.
18. Boucher, D., et al., *Caspase-1 self-cleavage is an intrinsic mechanism to terminate inflammasome activity.* J Exp Med, 2018. **215**(3): p. 827-840.
19. Sborgi, L., et al., *Structure and assembly of the mouse ASC inflammasome by combined NMR spectroscopy and cryo-electron microscopy.* Proc Natl Acad Sci U S A, 2015. **112**(43): p. 13237-42.
20. Hoss, F., et al., *Detection of ASC Speck Formation by Flow Cytometry and Chemical Cross-linking.* Methods Mol Biol, 2018. **1714**: p. 149-165.
21. Fernandes-Alnemri, T., et al., *The pyroptosome: a supramolecular assembly of ASC dimers mediating inflammatory cell death via caspase-1 activation.* Cell Death Differ, 2007. **14**(9): p. 1590-604.
22. Wang, X. and J. Robbins, *Proteasomal and lysosomal protein degradation and heart disease.* J Mol Cell Cardiol, 2014. **71**: p. 16-24.
23. Lecker, S.H., A.L. Goldberg, and W.E. Mitch, *Protein degradation by the ubiquitin-proteasome pathway in normal and disease states.* J Am Soc Nephrol, 2006. **17**(7): p. 1807-19.
24. Wu, T., et al., *Targeted protein degradation as a powerful research tool in basic biology and drug target discovery.* Nat Struct Mol Biol, 2020. **27**(7): p. 605-614.
25. Yuk, J.M. and E.K. Jo, *Crosstalk between autophagy and inflammasomes.* Mol Cells, 2013. **36**(5): p. 393-9.

26. Biasizzo, M. and N. Kopitar-Jerala, *Interplay Between NLRP3 Inflammasome and Autophagy.* Front Immunol, 2020. **11**: p. 591803.
27. Gritsenko, A., et al., *Priming Is Dispensable for NLRP3 Inflammasome Activation in Human Monocytes In Vitro.* Front Immunol, 2020. **11**: p. 565924.
28. He, Y., H. Hara, and G. Nunez, *Mechanism and Regulation of NLRP3 Inflammasome Activation.* Trends Biochem Sci, 2016. **41**(12): p. 1012-1021.
29. Kim, J.H., et al., *NLRP3 Inflammasome Activation in THP-1 Target Cells Triggered by Pathogenic Naegleria fowleri.* Infect Immun, 2016. **84**(9): p. 2422-8.
30. Mortimer, L., et al., *The NLRP3 Inflammasome Is a Pathogen Sensor for Invasive Entamoeba histolytica via Activation of alpha5beta1 Integrin at the Macrophage-Amebae Intercellular Junction.* PLoS Pathog, 2015. **11**(5): p. e1004887.
31. de Alba, E., *Structure and interdomain dynamics of apoptosis-associated speck-like protein containing a CARD (ASC).* J Biol Chem, 2009. **284**(47): p. 32932-41.
32. Verdonk, M.L., et al., *Improved protein-ligand docking using GOLD.* Proteins, 2003. **52**(4): p. 609-23.
33. Zhang, W., et al., *EDock: blind protein-ligand docking by replica-exchange monte carlo simulation.* J Cheminform, 2020. **12**(1): p. 37.
34. Gray, V.E., R.J. Hause, and D.M. Fowler, *Analysis of Large-Scale Mutagenesis Data To Assess the Impact of Single Amino Acid Substitutions.* Genetics, 2017. **207**(1): p. 53-61.
35. Lefevre, F., M.H. Remy, and J.M. Masson, *Alanine-stretch scanning mutagenesis: a simple and efficient method to probe protein structure and function.* Nucleic Acids Res, 1997. **25**(2): p. 447-8.
36. Li, Y., et al., *Cryo-EM structures of ASC and NLRC4 CARD filaments reveal a unified mechanism of nucleation and activation of caspase-1.* Proc Natl Acad Sci U S A, 2018. **115**(43): p. 10845-10852.
37. Conforti-Andreoni, C., P. Ricciardi-Castagnoli, and A. Mortellaro, *The inflammasomes in health and disease: from genetics to molecular mechanisms of autoinflammation and beyond.* Cell Mol Immunol, 2011. **8**(2): p. 135-45.
38. Karki, R., S.M. Man, and T.D. Kanneganti, *Inflammasomes and Cancer.* Cancer Immunol Res, 2017. **5**(2): p. 94-99.
39. Fernandes, F.P., et al., *Inflammasome genetics and complex diseases: a comprehensive review.* Eur J Hum Genet, 2020. **28**(10): p. 1307-1321.
40. Awad, F., et al., *Impact of human monocyte and macrophage polarization on NLR expression and NLRP3 inflammasome activation.* PLoS One, 2017. **12**(4): p. e0175336.
41. Kelley, N., et al., *The NLRP3 Inflammasome: An Overview of Mechanisms of Activation and Regulation.* Int J Mol Sci, 2019. **20**(13).
42. Katsnelson, M.A., et al., *K+ efflux agonists induce NLRP3 inflammasome activation independently of Ca2+ signaling.* J Immunol, 2015. **194**(8): p. 3937-52.
43. Bergsbaken, T., S.L. Fink, and B.T. Cookson, *Pyroptosis: host cell death and inflammation.* Nat Rev Microbiol, 2009. **7**(2): p. 99-109.
44. Schneider, K.S., et al., *The Inflammasome Drives GSDMD-Independent Secondary Pyroptosis and IL-1 Release in the Absence of Caspase-1 Protease Activity.* Cell Rep, 2017. **21**(13): p. 3846-3859.
45. Lugrin, J. and F. Martinon, *The AIM2 inflammasome: Sensor of pathogens and cellular perturbations.* Immunol Rev, 2018. **281**(1): p. 99-114.
46. Chiu, Y.H., J.B. Macmillan, and Z.J. Chen, *RNA polymerase III detects cytosolic DNA and induces type I interferons through the RIG-I pathway.* Cell, 2009. **138**(3): p. 576-91.
47. Schnappauf, O., et al., *The Pyrin Inflammasome in Health and Disease.* Front Immunol, 2019. **10**: p. 1745.
48. Orimo, T., et al., *Cholera toxin B induces interleukin-1beta production from resident peritoneal macrophages through the pyrin inflammasome as well as the NLRP3 inflammasome.* Int Immunol, 2019. **31**(10): p. 657-668.
49. Elizagaray, M.L., et al., *Canonical and Non-canonical Inflammasome Activation by Outer Membrane Vesicles Derived From Bordetella pertussis.* Front Immunol, 2020. **11**: p. 1879.
50. Downs, K.P., et al., *An overview of the non-canonical inflammasome.* Mol Aspects Med, 2020. **76**: p. 100924.
51. Hautem, N., et al., *The NLRP3 Inflammasome Has a Critical Role in Peritoneal Dialysis-Related Peritonitis.* J Am Soc Nephrol, 2017. **28**(7): p. 2038-2052.

52. Spalinger, M.R. and M. Scharl, *Mono Sodium Urate Crystal-induced Peritonitis for in vivoAssessment of Inflammasome Activation.* Bio Protoc, 2018. **8**(5): p. e2754.
53. Martinon, F., et al., *Gout-associated uric acid crystals activate the NALP3 inflammasome.* Nature, 2006. **440**(7081): p. 237-41.
54. Spalinger, M.R., et al., *NLRP3 tyrosine phosphorylation is controlled by protein tyrosine phosphatase PTPN22.* J Clin Invest, 2016. **126**(5): p. 1783-800.
55. Chen, L., et al., *Inflammatory responses and inflammation-associated diseases in organs.* Oncotarget, 2018. **9**(6): p. 7204-7218.

Ch.V

The Role of the Inflammasome in Breast Cancer

Graphical Abstract

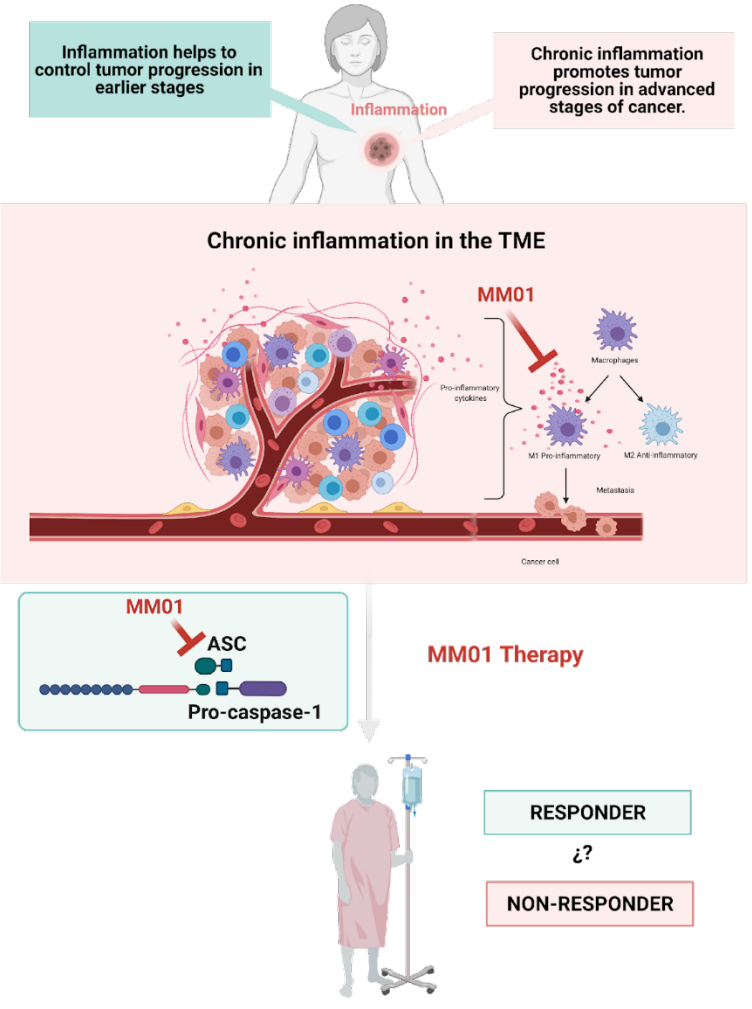

Antecedents and Background

The inflammatory tumor microenvironment (TME), driven by the presence of immune cells and inflammatory mediators in proximity to cancer cells, plays fundamental roles in all stages of tumor development [1];[2]; [3].

Inflammasome activation represents a central mechanism contributing to inflammation by immune cells [4]. Cancer cell necrosis and persistent tissue damage

ensure a high concentration of damage-associated molecular patterns (DAMPs) in the TME, leading to inflammasome activation in immune cells [5]. However, the role of immune cell-derived inflammasome signaling in tumors remains controversial, as this pathway can display both pro-tumorigenic and anti-tumor activities depending on the tumor type [4, 6].

Aberrant activation of the inflammasomes and overexpression/overproduction of effector molecules occurs in several types of human malignancies [4]. Most breast tumor subtypes overexpress inflammasome components such as NLRP3, ASC, Caspase-1, IL-1β, or IL-18 (**Figure 1**) compared to normal tissue [4]. Moreover, breast cancer patients possess increased serum levels of IL-1β, which correlates with tumor stage and cancer progression [7]; [8].

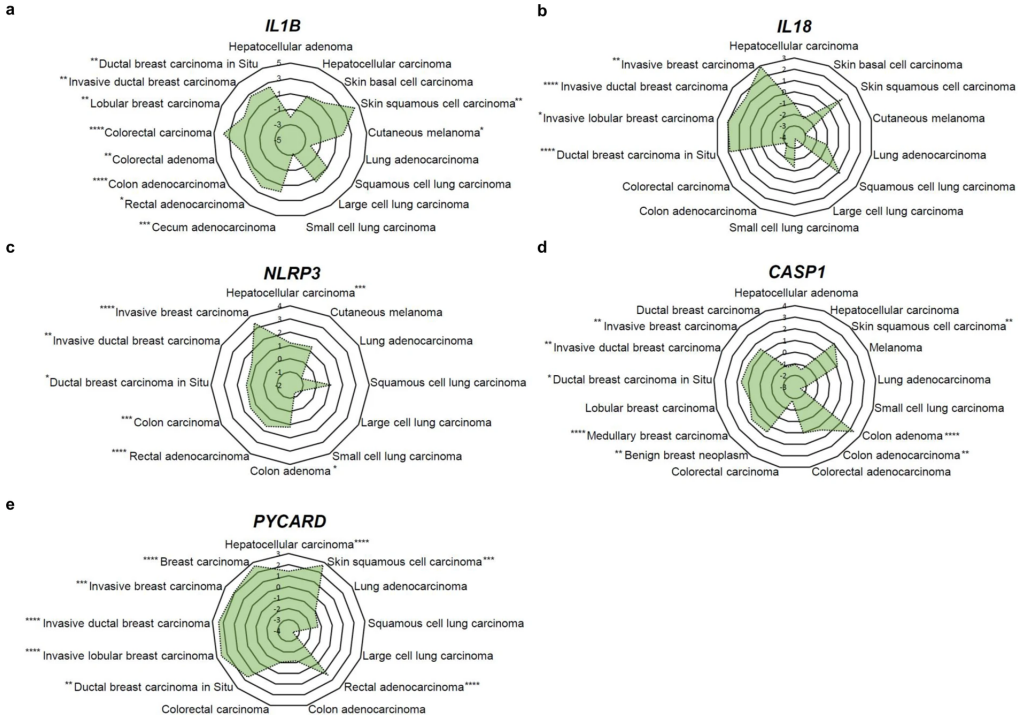

Figure 1. Relative expression of inflammasome components in different tumors. Relative mRNA expression of IL-1β, IL-18, NLRP3, Caspase-1, ASC (PYCARD) in breast cancer (from the "ONCOMINE database"). http://creativecommons.org/licenses/by/4.0/. [4]

Interestingly, studies have underscored a significant correlation between the activity/expression of inflammasomes components and subsequent metastasis [9]; [10]. Guo et al. [9] demonstrated that the knock-out (KO) of various inflammasome components fostered a reduction in tumor size and metastasis in a mouse breast cancer model. The authors also reported that the NLRP3 inflammasome Activation and IL-1β production promoted infiltration of myeloid cells, including tumor-associated macrophages (TAMs), to provide the inflammatory microenvironment known to support breast cancer progression. Jang et al. [8] reported macrophages as the primary source of IL-1β production in the breast cancer TME and demonstrated that triple negative breast cancer (TNBC) cells induced the ASC oligomerization and speck formation associated with inflammasome activation in macrophages. Notably, the depletion of macrophages decreased serum levels of IL-1β and slowed breast cancer progression in a syngeneic orthotopic breast cancer mouse model [8]. Weichand et al. [10] reported that sphingolipid sphingosine-1-phosphate receptor 1 (S1pr1) KO in mouse breast tumor-infiltrating TAMs prevented pulmonary metastasis and tumor lymphangiogenesis. Transcriptome analysis of isolated TAMs revealed reduced expression of NLRP3 in S1pr1-deficient TAMs, demonstrating that NLRP3 inflammasome promotes metastasis through the lymphatic system and favors breast cancer development [10]. Zhang et al. demonstrated that expression of the miR-223-3p microRNA, which inhibits the NLRP3 pathway, increased apoptosis and reduced human breast cancer cell proliferation and the expression of ASC, IL-1β, and IL-18. Furthermore, the authors demonstrated that miR-223-3p expression reduced tumor growth and increased survival in an MCF-7 breast cancer mouse model [11].

Taken together, these data indicate that therapeutically targeting the inflammasome/IL-1β pathway could effectively suppress breast cancer cell growth and metastasis in patients.

However, several studies have also provided evidence of the contribution of inflammasome Activity to breast cancer inhibition. Chen et al. [12] reported that AIM2 inflammasome expression suppressed the proliferation and tumorigenicity of human breast cancer cells. Moreover, AIM2 gene therapy inhibited mammary tumor growth

in orthotopic MDA-MB-435 and AIM2-inducible MCF-7 tumor models, suggesting AIM2 as a tumor suppressor in specific breast cancer models.

IL-1β release upon inflammasome activation induces tumor progression; however, studies have suggested a tumor-suppressive function for IL-1β in the breast TME. For example, the blockade of IL-1β receptor (IL-1R) in combination with paclitaxel reduced primary breast tumor growth but potentiated pulmonary metastasis in the orthotopic 4T1 model [13]. In agreement with the differential effects of IL-1β, Kaplanov et al. demonstrated that Il-1β-deficient mice exhibited a profound regression of primary tumor growth in a 4T1 orthotopic breast cancer mouse model [14]. Il-1β-deficient mice lacked tumor-infiltrating inflammatory monocytes; however, CD11b+ dendritic cells and activated CD8+ T cells predominated in tumor tissues compared to wild-type mouse breast tissue [14].

Given the differential effects of the inflammasome and the increasing relevance of inflammasome inhibitors as a cancer treatment, distinguishing which patients/tumors will benefit from inflammasome inhibition represents an important task.

In this chapter, we describe the application of the ASC oligomerization inhibitor MM01 as a chemical tool to study the role of the inflammasome in breast cancer models. Furthermore, we also aimed to identify biomarkers to stratify patients as responders and non-responders to MM01 treatment.

Abstract

In this chapter, we employed our inflammasome inhibitor, MM01, to study the role of the inflammasome in tumor progression in different breast cancer models both *in vitro* and *in vivo*. We demonstrated that different breast cancer cell lines respond differently to MM01 treatment. We developed a functional assay comprising the evaluation of breast cancer cell migration in response to the pro-inflammatory M1 macrophage secretome (inflammatory stimulus) in the presence of MM01. Certain cell lines (such as the EO771 cell line) displayed increased migration in response to the inflammatory stimulus and decreased migration in response to treatment with MM01; however, we also identified cell lines that respond negatively to MM01 treatment (such as the 4T1 cell line). Finally, we demonstrated the efficacy of this functional experiment *in vivo* by demonstrating that MM01 treatment reduced tumor size in the EO771 orthotopic model but increased tumor size and lung metastasis in the 4T1 orthotopic model. These two models, which recapitulate contradictory responses to treatment with our inflammasome inhibitor, may be used in the future to determine biomarkers that predict the response of breast cancer models to treatment with an inflammasome inhibitor.

Results and Discussion

V.1 Characterization of Inflammasome Inhibition in Breast Cancer Models

Inflammatory signaling within the tumor depends greatly on TAMs, which comprise a significant cell population in the breast cancer TME contributing to tumor growth and angiogenesis [15]; [16].

In a simplified view, TAMs are characterized as classically pro-inflammatory (M1) or alternatively anti-inflammatory (M2) activated macrophages [17]. The presence of M2 macrophages in the tumor associates with poor prognosis [18]; however, excessive/prolonged pro-inflammatory signaling by M1 macrophages contribute to tissue damage, which promotes angiogenesis and tumor spread [19]; [20].

These findings underscore the need for personalized functional assays to predict patient response to the inflammatory TME.

This chapter describes the application of M1 macrophage and breast cancer cells cocultures to reproduce a pro-inflammatory microenvironment and allow the study of inflammasome inhibition as a therapy for breast cancer.

V.1.1 Characterization of Human and Murine Macrophage-based Models

Blood monocytes differentiate into macrophages after recruitment to the TME [21]. To study the activation of the inflammasome in pro-inflammatory M1 macrophages and its influence in breast cancer progression, we employed human macrophages differentiated from the human monocytic THP-1 cell line. As described in the Material and Methods, we established THP-1-derived basal M0 macrophages by treatment with 50 ng/mL PMA for 24 h, and pro-inflammatory M1 macrophages through treatment with 10 pg/mL LPS and 25 ng/mL IFN-γ for 24 h.

Recent studies have grouped M1 stimuli according to their ability to induce prototypical inflammatory responses and biomarkers expression [22];[23]. IFN-γ is the major cytokine associated with M1 activation, and LPS activates macrophages to produce pro-inflammatory mediators [24].

The gene expression signature of THP-1-derived M1 macrophages stimulated with LPS and IFN-γ includes genes involved in chemotaxis and cell migration [25]; [26]; [27]. Genes expressed in M1 human macrophages include the chemokine receptor CCR7 [28], which promotes the recruitment of lymphocytes and mature dendritic cells to lymphoid tissues, and the chemokine interferon-γ inducible protein 10 kDa (CXCL10), which is involved in chemotaxis, apoptosis, cell growth regulation, and angiogenesis [29]. The profile of M1 macrophages *in vitro* also includes inflammasome activation and the expression of well-known cytokines such as IL-1α, IL1β, IL-6, and TNF [27]. Therefore, we employed these markers to characterize the differentiation of M1 macrophages derived from the THP-1 cell line.

Moreover, to discriminate pro-inflammatory macrophages at the functional level, we assessed M1 polarization by measuring the release of the inflammatory

cytokine IL-1β, the expression of inflammasomal proteins (NLRP3, pro-caspase-1, pro-IL-1β, and ASC), and the expression of pro-inflammatory marker genes (CCR7 and CXCL10) (**Figure 2**).

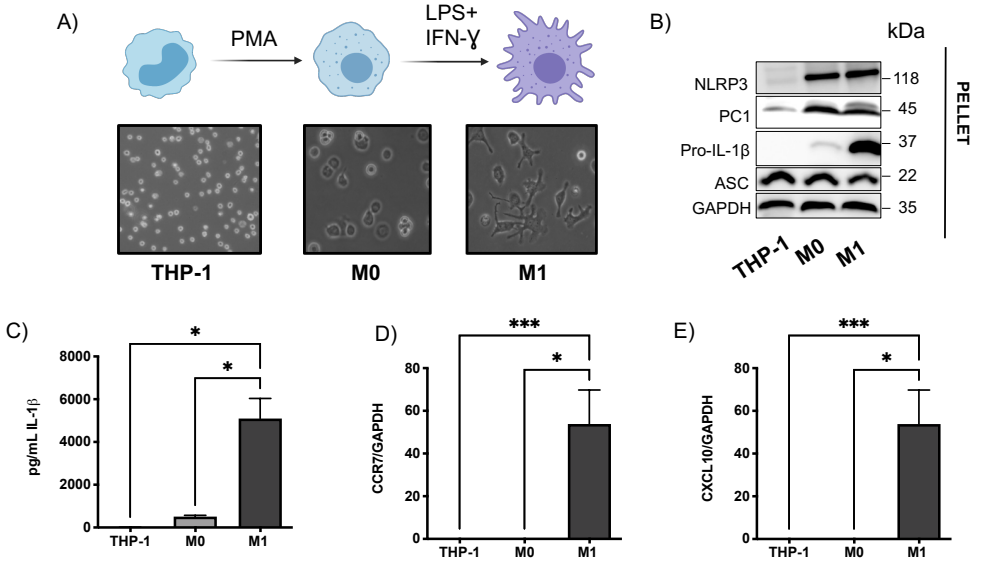

Figure 2. Human macrophage differentiation from THP-1 monocyte cells and their polarization. (**A**) (Upper) Schematic representation of THP-1 derived macrophage differentiation and polarization. (Lower) Phase-contrast microscope image of THP-1 monocytes, differentiated M0 macrophages, and polarized M1 macrophages. (**B**) Western blot for inflammatory proteins (pro-caspase-1 (PC1), NLPR3, Pro-IL-1β, and ASC) in cell lysates using GAPDH as a reference protein. (**C**) ELISA quantification of IL-1β secretion. (**D**) Relative gene expression of CCR7 and CXCL10 by RT-qPCR. Data represent the means ± SEM of at least three independent experiments. Statistical significance determined using one-way ANOVA (one-way Anova, Dunnett's test * $p < 0.05$; and *** $p < 0.001$).

As shown in **Figure 2A**, the monocytic THP-1 cell line presents a non-adherent rounded basal morphology that changes upon treatment with PMA, acquiring an adherent phenotype with an elongated morphology (M0). These alterations become enhanced following exposure to LPS and IFN-γ for M1 polarization.

IFN-γ and LPS treatment produced an expected pro-inflammatory profile of M1 macrophages. **Figure 2B** demonstrates an increase in the expression of pro-

inflammatory proteins such as pro-IL-1β and pro-caspase-1 in M1 macrophages compared to M0 macrophages and undifferentiated THP-1 monocytes. M0 macrophages also displayed increased expression of pro-caspase-1, pro-IL-1β and NLRP3 compared to THP-1 monocytes. Moreover, we observed an increased release of IL-1β in M1 macrophages compared to both M0 macrophages and THP-1 monocytes (**Figure 2C)**. Finally, we observed a significant increase in CCR7 and CXCL10 gene expression in M1 macrophages compared to both M0 macrophages and THP-1 monocytes (**Figure 2D**).

Overall, these results demonstrate that PMA-stimulation followed by IFN-γ and LPS treatment induced the differentiation of THP-1 monocytes into M0 macrophages and their pro-inflammatory polarization into M1 macrophages, respectively. Moreover, M1 macrophages displayed increased signs of inflammasome activation, which supports their inflammatory profile.

We also characterized M1 pro-inflammatory macrophages derived from the murine J744A.1 macrophage cell line (M0) with future *in vivo* experiments in mind. As for human macrophages, we polarized murine macrophages to M1 using LPS and IFN-γ and, in this case, we analyzed the release of the inflammatory cytokine IL-1β and the expression of inflammatory genes (IL-6, IL-1α, and IL-1β) (**Figure 3**).

Figure 3 demonstrates the expected increased release of IL-1β by murine M1 macrophages compared to M0 macrophages (J744A.1) (**Figure 3A**). Moreover, M1 polarization also induced a significant increase in IL-1β, IL-6, and IL-1α gene expression (**Figure 3B**) compared to M0 macrophages.

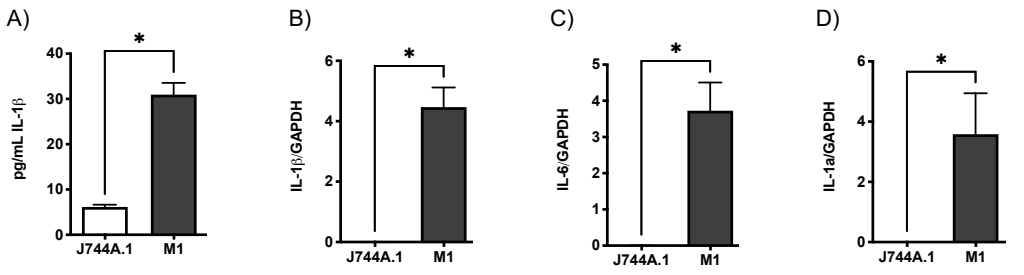

Figure 3. Characterization of J744A.1 mouse macrophage polarization (**A**) ELISA quantification of IL-1β secretion. (**B**) Relative expression of IL-1β, IL-6, and IL-1α mRNA by RT-qPCR. Data represent the means ± SEM of at least three independent experiments. Statistical significance assessed using Student's t-test (* $p < 0.05$).

In summary, we established effective differentiation protocols to generate human and murine pro-inflammatory M1 macrophages to study our inflammasome inhibitor MM01.

V.1.2 MM01 Prevents Inflammasome Activation in Pro-inflammatory Macrophages

Inflammasome activation characterizes M1 macrophages, with the higher expression of inflammasome components in M1 macrophages (e.g., NLRP3, pro-Caspase-1, pro-IL-1β, and ASC) and an increase in IL-1β secretion (**Figure 2**). Therefore, to study the effect of the MM01 ASC oligomerization inhibitor on M1 macrophages, we analyzed the ability of MM01 to prevent inflammasome activation in M1 macrophages.

We first differentiated THP-1 monocytes with PMA to produce M0 macrophages and then evaluated the impact of a 30 min pretreatment with 20 μM MM01 on M1 macrophage polarization with LPS and IFN-γ (**Figure 4**).

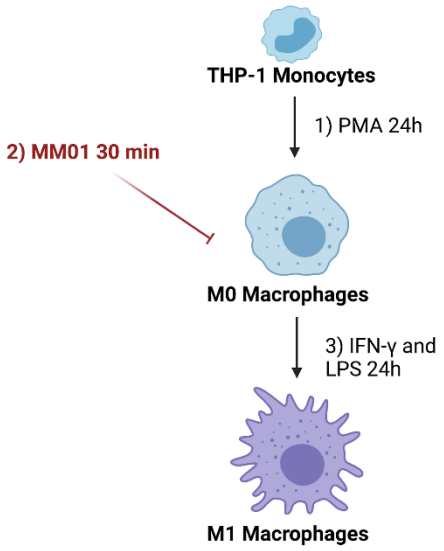

Figure 4. Scheme describing the treatment with MM01 inhibitor in pro-inflammatory M1 macrophages differentiation procedure.

We also evaluated the effect of MM01 on inflammasome activation in M1 macrophages by analyzing the release of the pro- inflammatory cytokine IL1β, levels of pyroptotic cell death, and expression and/or release of inflammatory proteins (**Figure 5**).

We observed the expected increase in IL-1β release in M1 macrophages compared to M0 macrophages; furthermore, we found that MM01 pretreatment prevented inflammasome activation after exposure to LPS and IFN-γ, as evidenced by the decrease in IL-1β release (compare M1 to M1+MM01) (**Figure 5A**). We also discovered that MM01 treatment inhibited the pyroptotic cell death (LDH release) observed in M1 macrophages (compare M1 to M1+MM01) (**Figure 5B**). Moreover, in **Figure 5C,** which presents the expression of inflammasome-related proteins in cell lysates (Pellet), we demonstrated that M1 macrophages presented the expected increase of inflammasome-related proteins (e.g., NLRP3, pro-caspase-1, and pro-IL-1β) compared to M0 macrophages, demonstrating the activation of the NLRP3 inflammasome. Moreover, to study whether the MM01 inhibitor influenced the activity of inflammasome-related proteins, we detected activated caspase-1 and IL-1β in the

supernatants of M1 cells (SN) compared to M0 macrophages. We demonstrated that MM01 treatment failed to influence the expression of inflammasome-related proteins in the cellular lysates; however, MM01 pretreatment reduced the levels of activated caspase-1 and IL-1β in the supernatant of M1 macrophages (compare M1 to M1+MM01), demonstrating that treatment with MM01 prevents the activation of inflammatory proteins caspase-1 and IL-1β without affecting expression levels.

Overall, these results suggest that MM01 pretreatment prevents inflammasome activation in M1 pro-inflammatory macrophages and maintains a polarization profile similar to the M0 basal state.

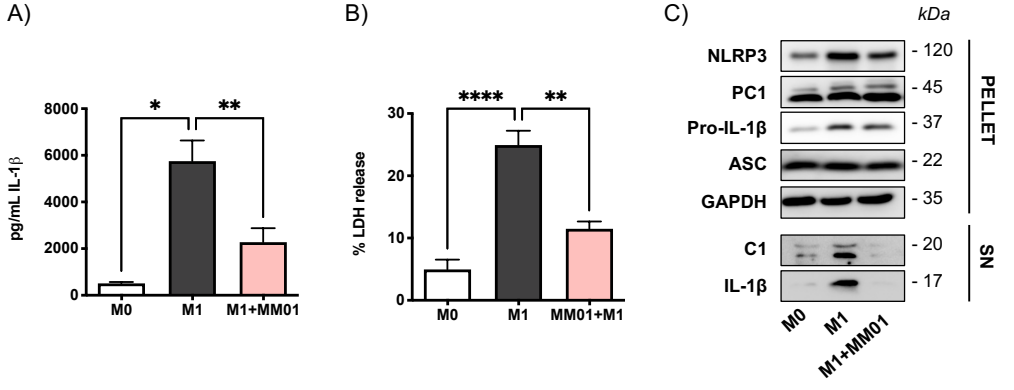

Figure 5. Inflammasome inhibition by MM01 in human pro- inflammatory M1 macrophages. (**A**) ELISA quantification of IL-1β secretion. (**B**) Percentage of pyroptosis cell death as a measure of LDH activity in culture supernatants. (**C**) Western blot analysis of inflammatory proteins (pro-caspase-1 (PC1), NLPR3, pro-IL-1β, and ASC) in cell lysates (pellet) and supernatants (SN) using GAPDH as a reference protein. Data represent the means ± SEM of at least three independent experiments. Statistical significance determined using a one-way ANOVA (one-way Anova, Dunnett's test * $p < 0.05$; ** $p < 0.01$ and **** $p < 0.0001$).

Moreover, to confirm the ability of MM01 to prevent inflammasome activation in murine macrophages, we pre-treated J744A.1 macrophages with 20 μM MM01 for 30 min before polarization of M0 macrophages into an M1 inflammatory state via a 24 h treatment with IFN-γ and LPS. We failed to observe an effect of MM01 on IL-1β

cytokine release (**Figure 6A**), possibly due to the low amount of protein released by M1 macrophages compared to THP-1 derived M0 macrophages (compare **Figure 5A** (THP-1) to **Figure 6A** (J744A.1)). **Figure 6B** shows that MM01 pretreatment reduced pyroptotic cell death induced by M1 polarization, as evidenced by decreased LDH release (compare M1 to M1+MM01). **Figure 6C** shows the increased protein expression of NLPR3 in the cellular lysates (pellet) of M1 macrophages compared to M0; however, we also observed the reduced expression of pro-caspase-1 and pro-IL-1β in M1 cell lysates (pellet), which may be due to increased protein processing and activation. MM01 pretreatment returned pro-caspase-1 and pro- IL-1β expression levels to a basal-like level, perhaps to their inhibited activation. We also observed activated caspase-1 in the supernatants of M1 macrophages (SN) (previously absent in the basal state); however, MM01 pretreatment inhibited this increase in caspase-1 protein levels. These results confirm that MM01 prevented inflammasome activation in murine macrophages.

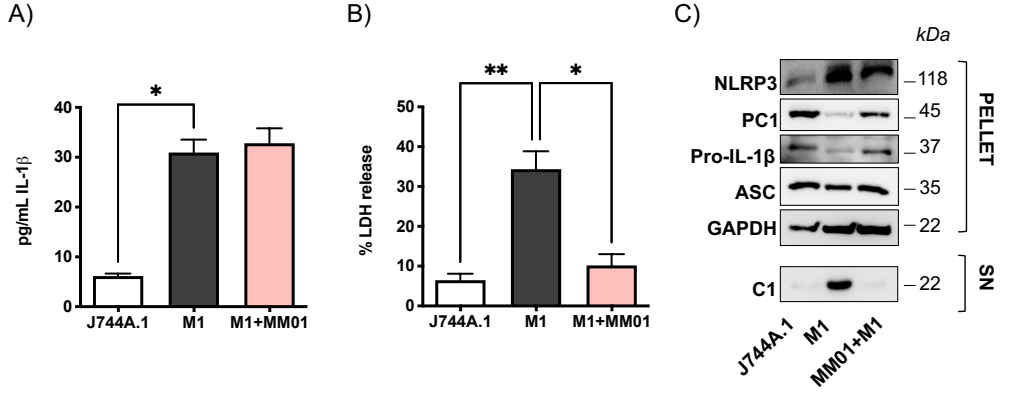

Figure 6. Inflammasome Inhibition by MM01 in Murine Pro-inflammatory M1 Macrophages derived from J744A.1 monocytes. (**A**) ELISA quantification of IL-1β secretion (**B**) Cell viability measured by LDH actVity in culture supernatants. (**C**) Western blot detection of inflammatory proteins such as pro-caspase-1, NLPR3, IL-1β, and ASC detected in cell lysates and supernatants using GAPDH as reference protein. Data represent the means ± SEM of at least three independent experiments. Statistical significance determined using a one-way ANOVA (one-way Anova, Dunnett's test * $p < 0.05$; and *** $p < 0.001$).

V.1.3 Pro-inflammatory M1 Macrophages Influence Breast Cancer Cell Migration in a Subtype-dependent Manner

The presence of pro-inflammatory macrophages in the TME can promote metastasis in multiple breast cancer types [8]. Moreover, recent studies have shown that conditioned media from LPS-stimulated macrophages can increase the transmigration of MDA-MB-231 and MCF-7 cells across both the blood and lymphatic endothelium *in vitro* [30]. Therefore, to study and characterize the effect of pro-inflammatory M1 macrophages and inflammasome inhibition in breast cancer progression, we next studied the effect of the secretome of pro-inflammatory M1 macrophages and MM01 pretreatment on the migration of mouse and human breast cancer cells *in vitro*, a characteristic linked to their tumorigenic potency.

We first collected the supernatants (secretome) of macrophages polarized into an M1 state in the presence/absence of MM01 pretreatment and employed them as a migratory stimulus for breast cancer cells in a transwell assay. We seeded human breast cancer cells in the upper part of the transwell (25,000 cells/transwell), added the cell secretomes to the well below, and analyzed the number of migrating cells at 6 h by confocal microscopy (**Figure 7**). We employed human TNBC cells (MDA-MB-231 and MDA-MB-468), ER+/PR+/HER2- cells (MCF7), ER-/PR-/HER2+ cells (MDA-MB-453 and HCC1954), and ER+/PR+/HER2+ cells (ZR-751 cells).

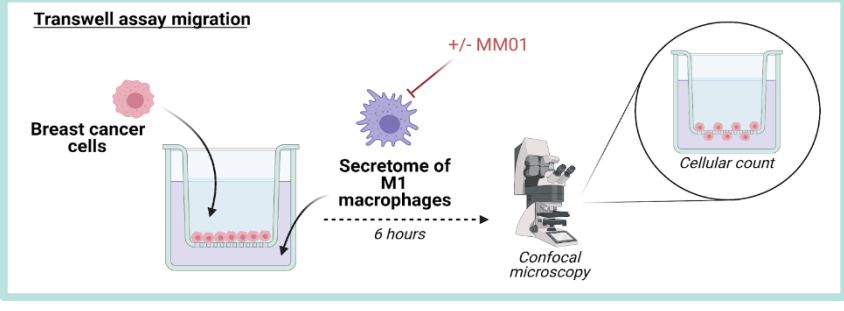

Figure 7. Scheme of the migration experiment

As shown in **Figures 8** (confocal analysis) and **9** (quantification), these results demonstrated cell-type-specific responses following exposure to the various secretome samples. We observed an increase in the migration of MDA-MB-231, MDA-MB-468, MCF7, and ZR-75 cells following treatment with M1 macrophage secretome compared to untreated cells (compare NT to M1 in **Figure 8** and **9**). However, the MDA-MB-453 and HCC1954 cell lines (both ER-/PR-/HER2+) failed to migrate after treatment with the M1 macrophage secretome. Thus, we classify cells that migrate in response to the M1 secretome as responders and those that do not migrate as non-responders.

Interestingly, the secretome of macrophages pre-treated with MM01 before exposure to M1 polarizing stimuli reduced the level of migration in the previously responding cells (MDA-MB-231, MDA-MB-468, MCF7, and ZR-75) (compare M1+MM01 to M1 in **Figure 8** and **9**). The non-responding MDA-MB-453 and HCC1954 cell lines did not present any changes in their migration following the inclusion of MM01 pretreatment before secretome isolation (compare M1+MM01 to M1) (**Figure 8** and **9**).

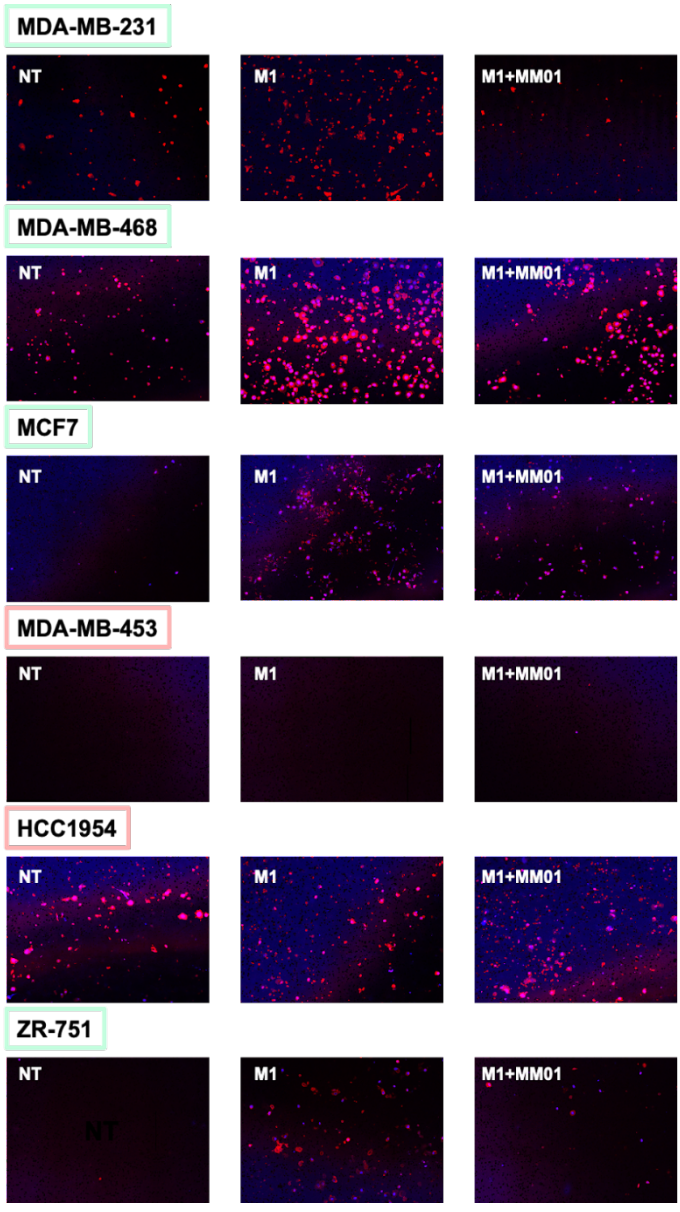

Figure 8. Migration of Human Breast Cancer Cells in Response to the M1 Macrophage Secretome in the presence/absence of MM01 pretreatment. Confocal microscopy images of the migration of human breast cancer cell lines MDA-MB-231, MDA-MB-468, MCF7, ZR-751 (responders) and MDA-MB-453 and HCC1954 (Non-responders). DAPI (blue) staining marks cell nuclei and wheat germ agglutinin (WGA – red) staining marks the cell membrane.

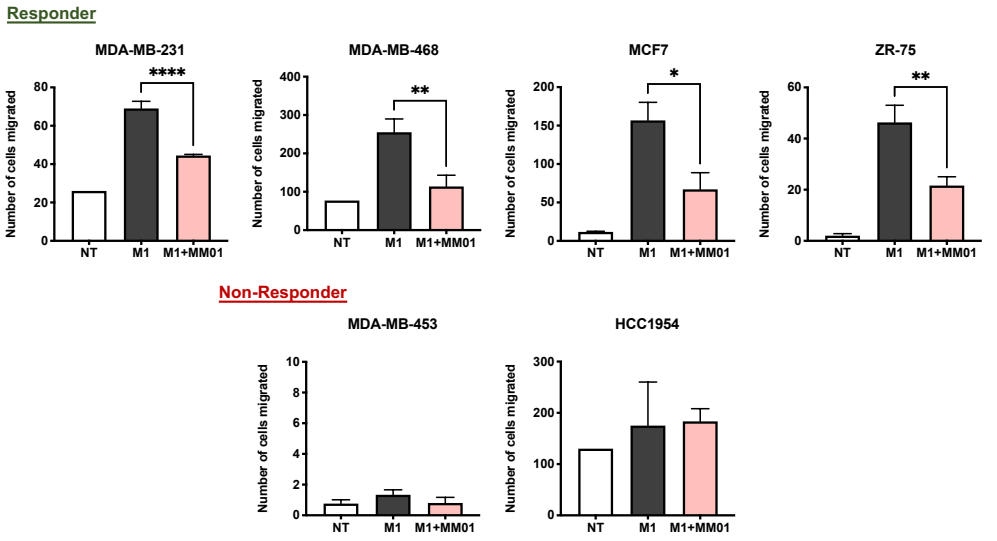

Figure 9. Migratory Potential of Human Breast Cancer Cells in Response to the M1 Macrophage Secretome and the Influence of MM01 Pretreatment. Number of migrated breast cancer cells in response to the M1 macrophage secretome (M1) and MM01 treatment (M1+MM01). Green and red bars signify responding and non-responding cell lines, respectively. Data represent the means ± SEM of at least three independent experiments. Statistical significance determined using one-way ANOVA (one-way Anova, Dunnett's test * $p < 0.05$; ** $p < 0.01$ and **** $p < 0.0001$).

Overall, we discovered that the pro-inflammatory stimuli provided by the M1 macrophage secretome provide for cell-type/sub-type-specific alterations to breast cancer cell migration (as a proxy for tumorigenicity/metastatic potential). Furthermore, we demonstrated that MM01 pretreatment reduces the ability of the secretome derived from macrophages exposed to M1 polarizing stimuli to increase breast cancer cell migration, suggesting that MM01 treatment may help to reduce the tumorigenicity or metastatic potential of breast cancer cells.

We next evaluated the effect of the M1 macrophage secretome and MM01 pretreatment on the migration of the murine 4T1 and EO771 TNBC lines. As for human macrophages, we collected the supernatants of murine J744A.1-derived macrophages after exposure to M1 polarizing stimuli in the presence/absence of MM01 pretreatment and employed them as a migratory stimulus for murine breast cancer cells in a transwell assay. Again, we seeded the murine 4T1 and EO771 breast cancer cells in the upper

part of the transwell (25,000 cells/transwell), added the M1 macrophage secretome to the well below, and then analyzed the number of migrating cells at 6 h by confocal microscopy (**Figure 10**).

The results demonstrated that the exposure to the M1 secretome increased the migration of EO771 cells (compare M1 to NT in **Figure 10A**), but that the secretome of macrophages pre-treated with MM01 before exposure to M1 polarization stimuli induced a significantly lower increase in the migratory potential of EO771 cells (compare M1+MM01 to M1 in **Figure 10A**).

Interestingly, the supernatant of M1 macrophages failed to modify the 4T1 migration (compare M1 to NT **Figure 10B**); however, exposure to the secretome of macrophages pre-treated with MM01 before exposure to M1 polarization stimuli produced an unexpected and significant increase in migration (compare M1+MMO1 to M1 in **Figure 10B**).

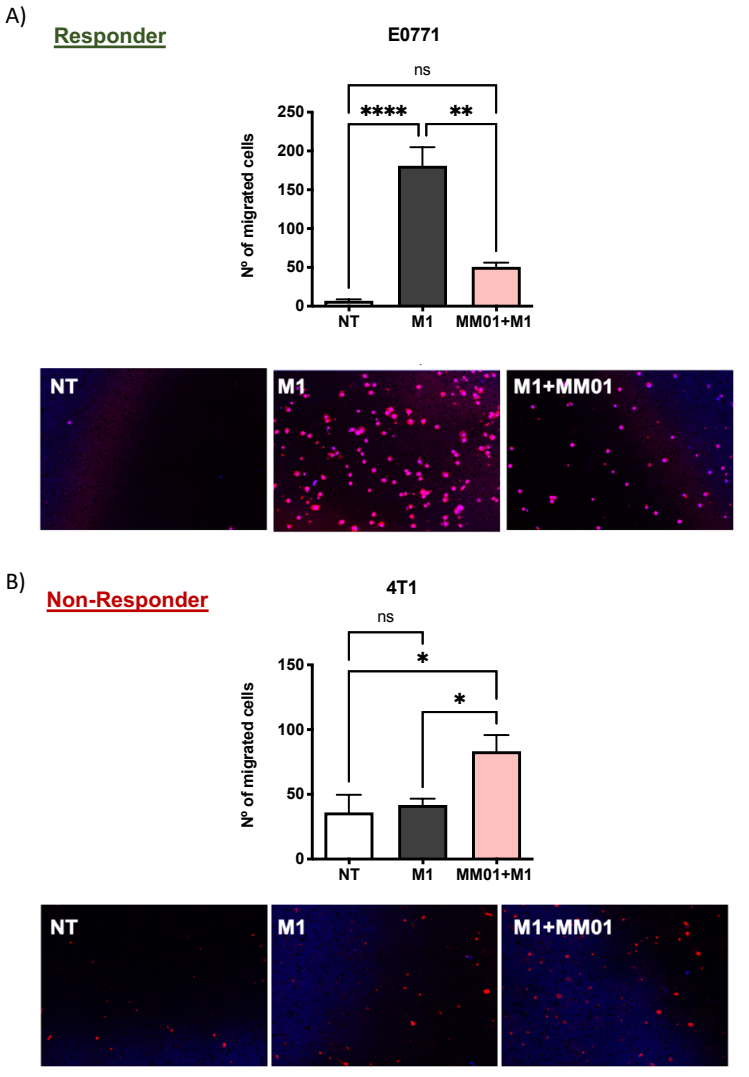

Figure 10. Murine Breast Cancer Cell Migration in Response to the M1 macrophage secretome and the Influence of MM01. Graphs showing the quantification of E0771 (**A**) and 4T1 (**B**) mouse TNBC line migration in response to the M1 macrophage secretome with and without exposure to MM01. Associated confocal microscopy images depict the migration of breast cancer cell lines. Data represent the means ± SEM of at least three independent experiments. Statistical significance determined using one-way ANOVA (one-way Anova, Dunnett's test * $p < 0.05$; **** $p < 0.0001$).

These results reinforce the findings from the human models, suggesting that intrinsic differences in breast cancer cells condition their migration towards pro- inflammatory stimuli. In the case of mouse TNBC cells, we classify EO771 cells as responders and 4T1 cells as non-responders.

In conclusion, we developed a functional assay to characterize the influence of the M1 macrophage secretome on breast cancer cell migration and, in doing so, demonstrated that this pro-inflammatory stimulus has a cell-type/subtype-specific influence. Furthermore, we demonstrated that pre-treating macrophages with the inflammasome inhibitor MM01 before exposure to M1 polarizing stimuli reduces the impact on responder breast cancer cell migration.

V.2. *In vivo* Validation of Inflammasome Inhibition in Breast Cancer

We next sought to confirm our *in vitro* findings (suggesting that inflammasome inhibition by MM01 reduced tumorigenic/metastatic potential) *in vivo* by studying the impact of MM01 treatment on tumor progression in immunocompetent 4T1 and EO771 *in vivo* mouse breast cancer models.

V.2.1 Development of Stable Luciferase-expressing EO771 Cells

To allow us to monitor *in vivo* tumor growth using minimally invasive procedures (such as VIS® Spectrum technology), we transfected EO771 cells with lentiviral particles containing a plasmid coding for luciferase (Luc) and an antibiotic resistance cassette (G418) to positively select transfected cells (**Figure 11**).

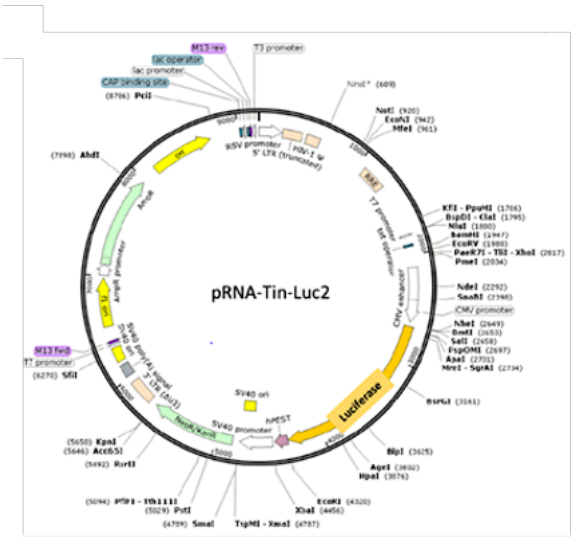

Figure 11: pRNA-Tin-Luc2 Plasmid. The T3 promoter regulates the luciferase transgene. The pRNA-Tin-Luc2 plasmid also contains a G418 (geneticin) antibiotic resistance cassette.

After lentiviral transduction with the pRNA-Tin-Luc2 plasmid and antibiotic selection with G418, we observed stable high levels of luciferase expression (**Figure 12**).

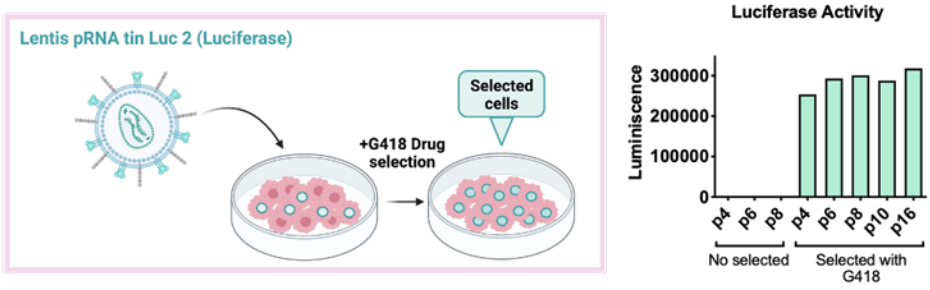

Figure 12: Schematic Representation of Lentiviral infection of VCaP Cells. EO771 cells were infected with lentiviral particles containing plasmids encoding luciferase and luciferase-positive cells selected with G418. Luminescence analysis demonstrates efficient and stable transfection and maintained expression during cell passaging.

We next sought to confirm that lentivirally infected EO771 cells (designated EO771-Luc2) did not display aberrations in essential cell characteristics, such as their

growth rate or migration in response to pro-inflammatory stimuli. To evaluate the growth rate of EO771-Luc2, we seeded 50,000 cells in a P24 well and analyzed the number of cells at 24, 48, 72, and 96 hours. The data shown in **Figure 13A** confirms a similar growth rate of EO771-Luc2 cells to parental EO771 cells. Furthermore, EO771-Luc2 cells displayed a similar migratory profile in response to M1 secretome stimulation in the presence/absence of MM01 pretreatment as parental EO771 cells (**Figure 13B**). We observed the expected increase in EO771-Luc2 migration following treatment with the M1 macrophage secretome and the decrease in migration following MM01 treatment (compare M1+MM01 to M1). These findings suggest the suitability of EO771-Luc2 cells for the development of the orthotopic breast cancer mouse model.

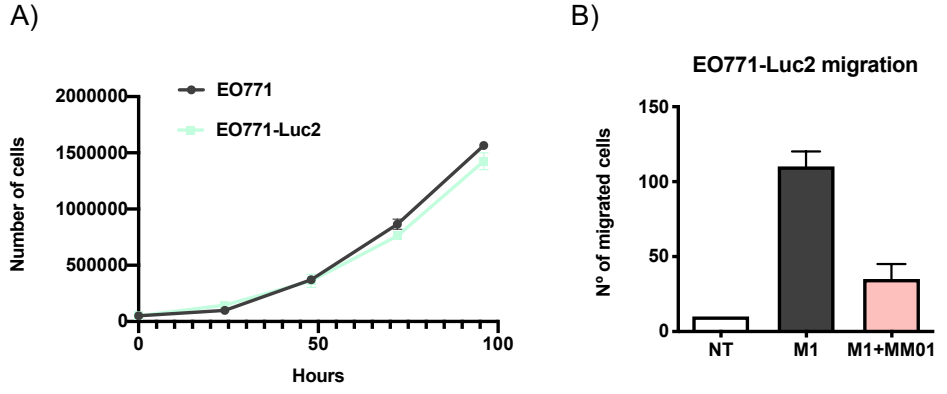

Figure 13. Growth rate and cell migration of EO771-Luc2 cells. A) Growth rate of EO771-Luc compared with EO771. **B**) Migration of EO771-Luc2 cells in response to various stimuli.

V.2.2 Optimization of the Orthotopic Luciferase-expressing E0771 Mouse Model

We optimized the orthotopic mouse model by first determining the appropriate number of cells to inject and the required time for the tumor to reach the maximum allowed size (approximately 1.2 cm^2). We injected $1x10^6$ and $2x10^6$ EO771-Luc2 cells into the fourth mammary fat pad of seven female C57BL/6 mice between 6-8 weeks of age. We evaluated the weight of the animals and the tumor growth weekly by caliper measurements (**Figure 14**) and through the VIS® Spectrum after subcutaneous luciferin administration (150 mg/kg) (**Figure 15**).

Relative body weight measurements made over time suggest the maintenance of mouse body weight throughout the whole experiment (**Figure 14A**). Moreover, from a safety point of view, daily monitoring of the general aspect of mice failed to reveal any deterioration in animal welfare.

Figure 14B shows exponential tumor growth, as measured by caliper three times a week for five weeks in both groups; of note, highly heterogeneous tumor growth represented a significant limitation of this model. **Figure 14C**, which depicts tumor volume (cm^3) at the endpoint, demonstrates a slight increase in the tumor size of the animals inoculated with $1x10^6$ cells compared to $2x10^6$. Notably, only four of the seven animals inoculated with $2x10^6$ cells presented with tumors; however, all animals inoculated with $1x10^6$ cells presented a tumor in the mammary gland. This fact may be the consequence of immune response activation against the tumor of those animals injected with higher cell numbers.

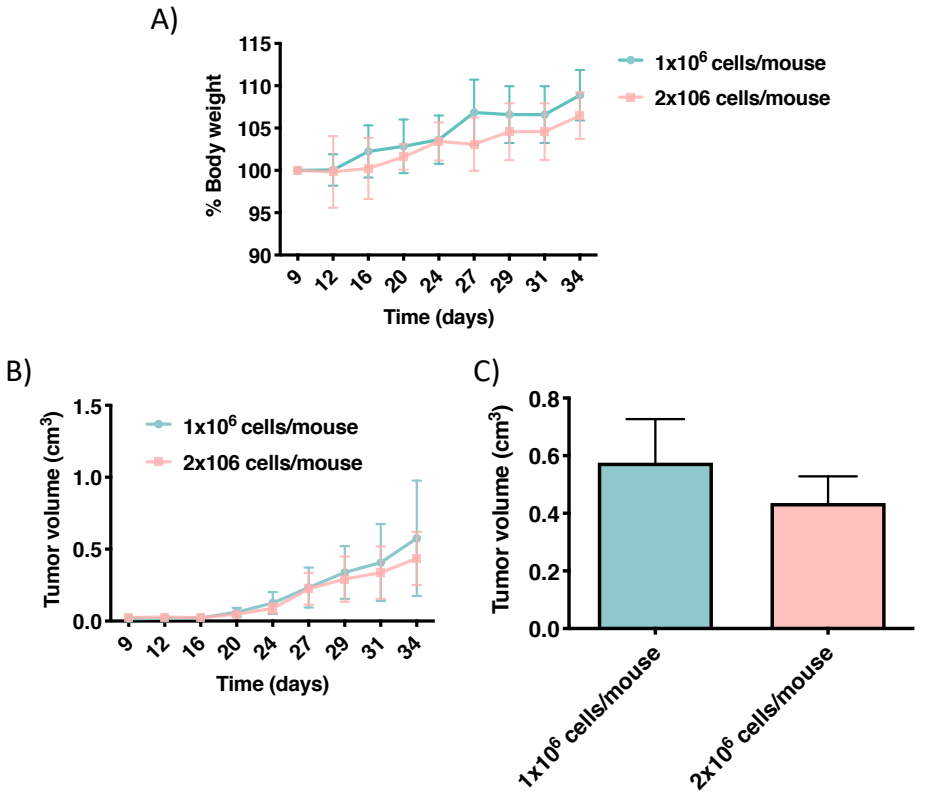

Figure 14. Optimization of the Orthotopic EO771-Luc2 Mouse Model. C57BL/6 mice injected into the fourth mammary fat pad with $1x10^6$ (blue) and $2x10^6$ (orange) EO771-Luc2 cells. **A**) Relative body weight (as a percentage) over time. **B**) Tumor volume expressed in cm^3 over time, measured with a caliper. **C**) Tumor volume expressed in cm^3 at the experimental endpoint (N=7).

Luminescence measurements corroborated the homogeneous and exponential tumor growth localized to the fourth mammary fat pad (**Figure 15**) . **Figure 15A**, which shows tumor progression followed by VIS of mice injected with $1x10^6$ cells/mice and $2x10^6$ cells/mice, demonstrates an increasing luminescence signal that corresponds to the increasing size of the breast tumor. We failed to observe any metastasis in this model throughout the experimental timeframe (**Figure 15A**). **Figures 15B** and **15C,** which show luminescence quantification (photons/sec) in mice injected with $1x10^6$ and $2x10^6$ cells /mice, respectively, confirm an increase in luminescence and hence tumor volume throughout the experimental timeframe.

However, since not all mice injected with $2x10^6$ cells/mice presented tumors, we selected $1x10^6$ cells as the optimal concentration for tumor development in the EO771-Luc2 model.

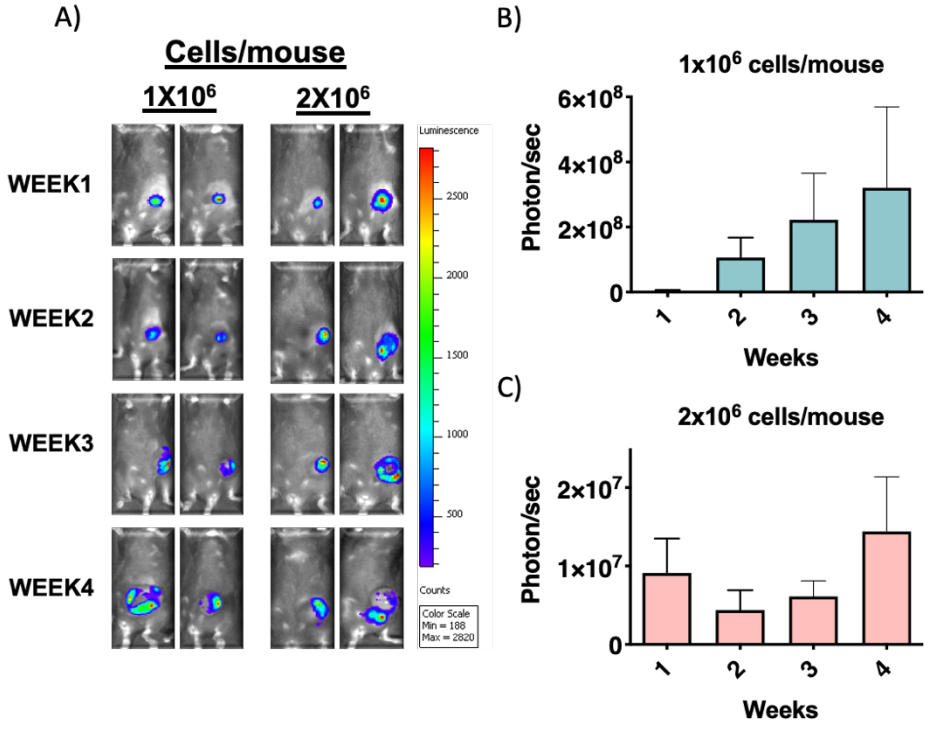

Figure 15. Optimization of the Orthotopic EO771-Luc2 Mouse Model. A) Topographic tumor growth images displaying tumor growth evaluated using VIS® Spectrum in animals inoculated with $1x10^6$ and $2x10^6$ cells. **B-C**) Tumor growth over time evaluated as photons per second. Data derived from VIS® Spectrum analysis in animals inoculated with $1x10^6$ and $2x10^6$ cells, respectively.

V.2.3 Study of MM01 Antitumor Activity and Safety in the EO771 Murine Model

We next investigated the anti-tumorigenic potential and safety of MM01 treatment in female C57BL/6 mice between 6-8 weeks of age injected with $1x10^6$ EO771-Luc2 cells in the fourth mammary. When tumors reach a size of approximately 0.02 cm^3 (day 15), we randomly divided mice into two groups (n=8, both groups):

i) control vehicle-treated group intravenously treated with PBS+5%DMSO three times per week

ii) experimental group intravenously injected with 10 mg/kg MM01 three times a week.

We evaluated animal weight and tumor growth weekly using a caliper until the experimental endpoint (33 days). Relative body weight measurements suggest the maintenance of mouse body weight throughout the experimental timeframe (**Figure 16A**). Furthermore, daily monitoring of the general aspect of mice failed to reveal any deterioration in animal welfare.

Figure 16B shows images of representative tumors dissected from mice at the experimental endpoint; encouragingly, MM01 treatment induced a notable decrease in tumor size

In the same line of evidence, **Figure 16C** which depicts the fold change (final tumor volume/initial tumor volume in cm^3 measured by caliper) in tumor growth throughout the experimental time frame, demonstrate a significative reduction of tumor growth in treated animals with MM01. **Figure 16D** depicts the quantification of fold change in tumor growth as analyzed at the experimental endpoint, demonstrating that MM01 treatment induces a significant decrease in tumor growth. Overall, these results suggest that MM01 may represent a safe and effective means of reducing tumor growth in an orthotopic EO771-Luc2 mouse breast cancer model.

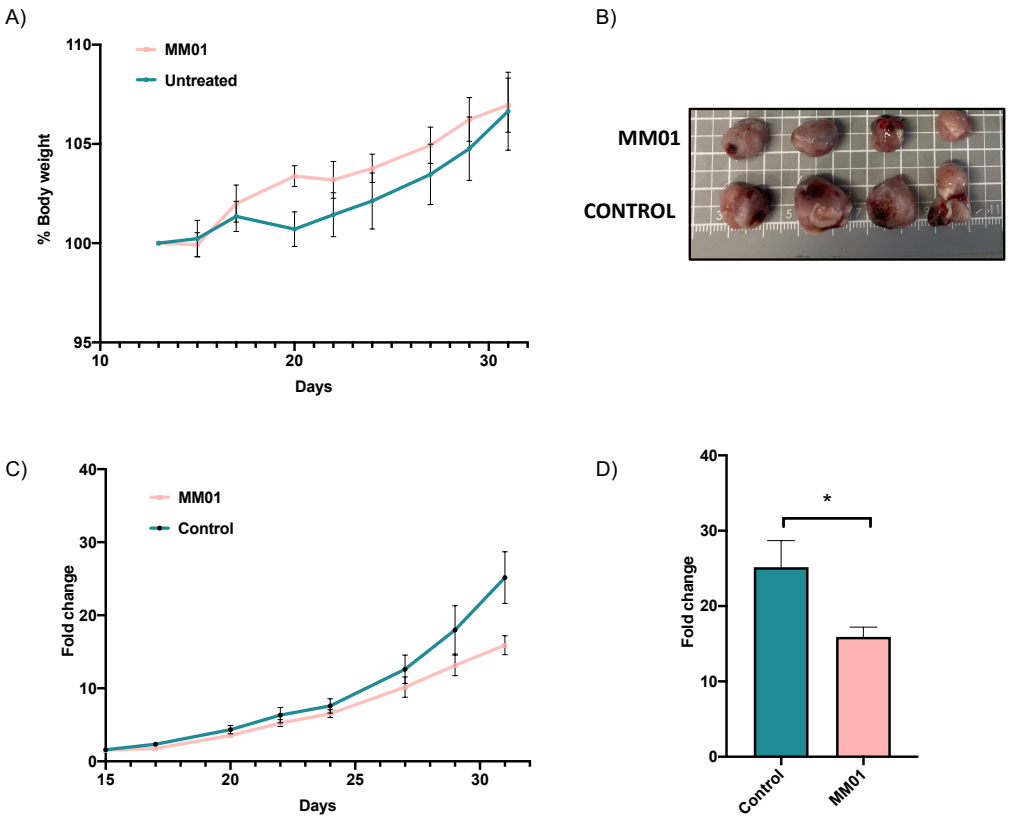

Figure 16. Analysis of MM01 Treatment in the Orthotopic EO771-Luc2 Mouse Breast Cancer Model. Mice were treated with MM01 at 10 mg/kg or PBS+5%DMSO vehicle control. **A**) Relative body weight (as a percentage) over time. **B**) Representative images of tumors at the experimental endpoint. **C**) Fold change tumor volume over time, as measured by caliper. **D**) Fold change in tumor volume at the experimental endpoint. Data expressed as mean±SEM, n>3. Statistical significance determined using one-way ANOVA (one-way Anova, Dunnett's test * p <0.05).

After sacrificing animals at the experimental endpoint, we isolated blood and carried out hematological studies to identify the development of systemic pathologies during tumor growth, such as marked inflammatory response derived from the tumor, anemia, thrombocytosis, reticulocytosis, leukocytosis, or lymphocytosis.

Figure 17 shows the count in g/L of leukocytes, erythrocytes, thrombocytes, neutrophils, monocytes, and lymphocytes present in the blood at the experimental

endpoint in the EO771-Luc2 model. We failed to observe any significant changes between the three different groups of mice.

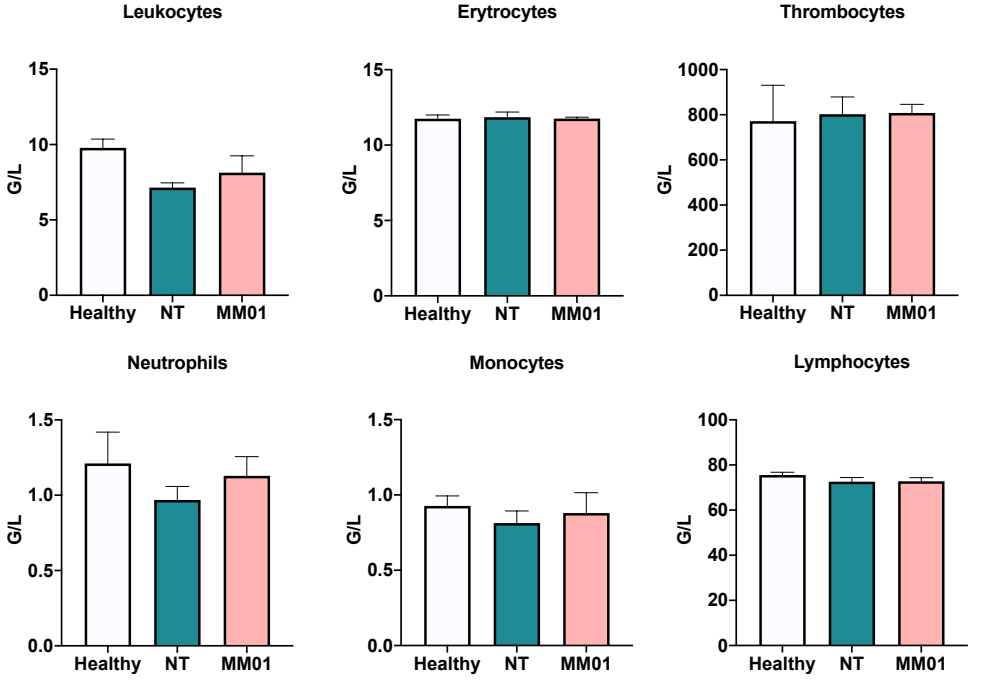

Figure 17. Complete Hemogram of EO771-Luc2 model. Counts in g/L of leukocytes, erythrocytes, thrombocytes, neutrophils, monocytes, and lymphocytes present in the blood at the experimental endpoint in the EO771-Luc2 model. Data expressed as mean±SEM, n>3. Statistical significance determined using one-way ANOVA.

V.2.4 Study of MM01 Antitumor Activity and Safety in the orthotopic 4T1 model.

We next studied the safety and efficacy of MM01 treatment in the orthotopic 4T1 metastatic TNBC murine model, which develops elevated levels of lung and axillary lymph node metastasis [31].

We injected $1x10^6$ 4T1 cells into the fourth mammary fat pad of female BALB/c mice between 6-8 weeks of age. We evaluated animal weight and tumor growth by caliper three times a week during the experimental timeframe. As in the

EO771 model, when tumors reached a size of approximately 0.02 cm^3 (day 7), we randomly divided mice into two groups (n=5, both groups):

i) control vehicle-treated group intravenously injected with PBS+5%DMSO three times per week.

ii) experimental group intravenously injected with 10 mg/kg MM01 three times per week.

Relative body weight measurements made over time suggest the maintenance of mouse body weight throughout the experimental timeframe (**Figure 18A**). Moreover, from a safety point of view, daily monitoring of the general aspect of mice failed to reveal any deterioration in animal welfare.

In contrast to the EO771 model, representative images of tumors (**Figure 18B**) and tumor volume measurements (**Figure 18C**) made at the experimental endpoint failed to provide evidence of significant alterations to tumorigenic potential after MM01 treatment. Furthermore, analysis of lung metastasis demonstrated that MM01 treatment induced a significant *increase* in incidence (**Figure 18C**). Together, these data suggest the unsuitable nature of MM01 treatment in this mouse model of breast cancer.

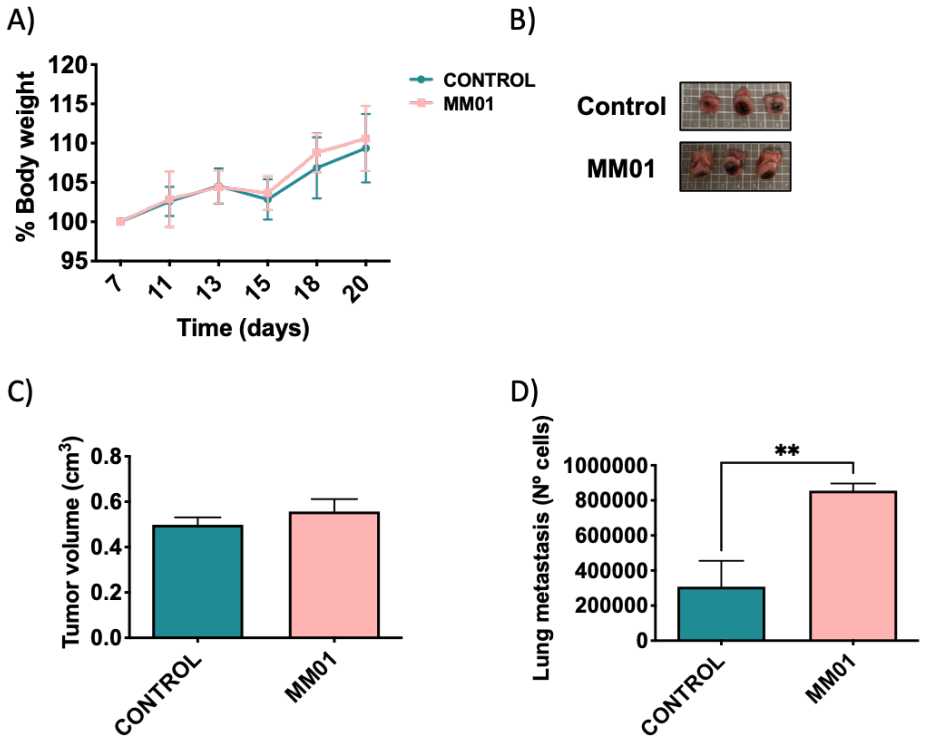

Figure 18. Analysis of MM01 Treatment in the Orthotopic 4T1 Mouse Breast Cancer Model. Mice were treated with MM01 at 10 mg/kg or PBS+5%DMSO vehicle control. **A**) Alterations to relative body weight (as a percentage) over time. **B**) Representative images of tumors at the experimental endpoint. **C**) Tumor volume (cm^3) over time, measured with a caliper. **D**) Lung metastasis incidence measured by the number of cells in lungs at the experimental endpoint. Data expressed as mean±SEM, n>3. Statistical significance determined using one-way ANOVA (one-way Anova, Dunnett's test ** $p < 0.01$).

We also carried out hematological studies in the 4T1, as for the EO771 model (**Figure 19**). Unlike the EO771-Luc2 model, the 4T1 model presented significant differences in the cell populations of the hematological count between the healthy animals (non-induced tumor mice) and the 4T1 control animals (NT) (orthotopically induced tumor mice) and the 4T1 animals treated with MM01 (Compare Healthy to NT and/or Healthy to MM01 in **Figure 19**). However, we failed to observe significant differences between the control animals of the 4T1 model (NT) and those treated with MM01 (Compared NT to MM01 in **Figure 19**). For example, the 4T1 model, treated or not with MM01, exhibited an increased number of neutrophils, leukocytes, thrombocytes, and monocytes compared to healthy animals (compare

neutrophils, leukocytes, thrombocytes and monocytes in Healthy to NT and/or Healthy to MM01 in **Figure 19**). In addition, we observed a non-significative increasing trend in the number of these cells (neutrophils, leukocytes, thrombocytes, and monocytes) in the 4T1 animals treated with MM01 compared to control animals (compare neutrophils, leukocytes, thrombocytes and monocytes in MM01 to NT in **Figure 19**). The presence of these cells represents an increase in inflammation levels. This trend of increased inflammation in the animals of the 4T1 model treated with MM01 with respect to the untreated animals may correlate with the increase in metastasis observed.

The 4T1 animals also displayed decreased erythrocyte levels compared to healthy animals (Compare erythrocytes in Healthy to NT and/or healthy to MM01 in **Figure 19**). This reduction in erythrocyte levels may signify the presence of anemia in the 4T1 model.

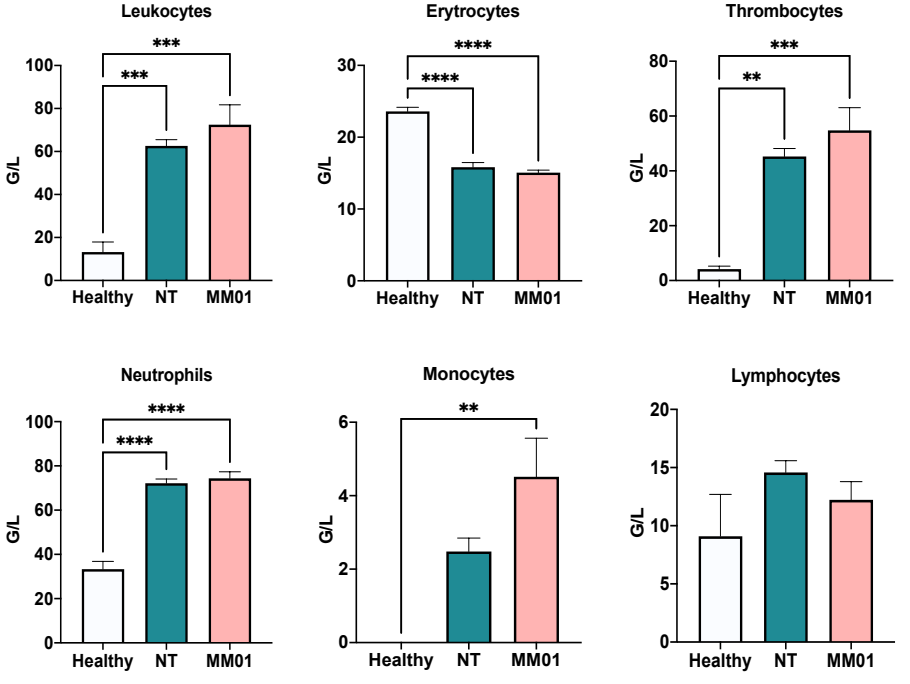

Figure 19. Complete Hemogram of 4T1 model. Counts in g/L of leukocytes, erythrocytes, thrombocytes, neutrophils, monocytes, and lymphocytes present in the blood at the endpoint of the 4T1 model**.** Data expressed as mean±SEM, n>3. Statistical significance determined using one-way ANOVA (one-way Anova, Dunnett's test **p <0.01; *** p <0.001 and ****p <0.0001).

These results from the EO771-Luc2 and 4T1 models provide contradictory responses to treatment with an inflammasome inhibitor. These results correlate well with the *in vitro* migration experiment, in which we observed an increase in migration in 4T1 cells after MM01 treatment. This correlation between *in vivo* experiments and migration assays confirms the efficacy of the predictive *in vitro* assay (migration experiment) for the subsequent behavior of metastasis *in vivo*. Importantly, these two models may provide an opportunity to study predictive biomarkers of treatment response in breast cancer models.

V.3 Identification of Biomarkers of Response to MM01 Treatment

Considering the contradictory roles of the inflammasome in cancer progression, understanding which tumors will respond to inflammasome inhibitor treatment remains an important consideration. We have identified two murine breast cancer models that respond differently to the inflammatory environment. The next chapter describes the application of the EO771 (responder) and 4T1 (non-responder) models to identify sensitivity biomarkers that can predict responses to inflammasome inhibitor treatment.

V.3.1 Inflammasome-related Proteins Fail to Impact EO771 and 4T1 Migration

To better understand the dual role of the inflammasome in cancer, we first studied the factors present in the M1 secretome that may increase breast cancer cell migration. As previously demonstrated in **section V.1.1**, a pro- inflammatory profile comprised of elevated levels of inflammasome-related proteins such as caspase-1 and IL-1β characterizes M1 macrophages. Therefore, we performed a transwell assay to study the migration of 4T1 and EO771 cells in response to the presence of caspase-1, IL-β, and ASC as migratory stimuli to evaluate whether inflammasome-related proteins have a role in breast cancer cell migration.

Apart from a hypothesized activity as migratory stimuli, recent studies have indicated that the spontaneous activation of caspases in many cancer cells plays a fundamental role in maintaining their tumorigenicity and metastasis [32]. For example, a recent meta-analysis revealed a correlation between increased caspase-3 expression and worse prognosis in breast cancer patients [33]. Huang et al. [34] found that breast, head and neck cancer patients with higher levels of activated caspase-3 in tumor tissues demonstrated a significantly higher rate of recurrence and deaths. Moreover, Zhou et al. [35] provided experimental evidence for the pro-metastatic role of caspases by demonstrating a reduced level of invasiveness and an increased sensitivity to *in vitro* and *in vivo* radiotherapy in caspase-3-knockout colon cancer cells. Related studies have also described the protumoral function of caspase-8 and caspase-3 as regulators of cell migration. For example, Gdynia et al. [36] reported that inhibition of caspase-3 and 8 through peptide inhibitors decreased glioblastoma cell migration.

Therefore, due to the described pro-metastatic role of caspases in cancer progression, we also implemented the universal caspase inhibitor, Z-vad, to study the role of caspases in breast cancer cell migration.

First, to study the effect of inflammasome-related proteins in breast cancer cell migration, we seeded 4T1 or EO771 cells in the upper part of the transwell (25,000 cells/transwell) and added medium complemented with caspase-1, IL-1β, or the protein ASC as migratory stimuli. To study the effect of caspases in breast cancer cell migration, we pre-treated EO771 and 4T1 cells with 1 μM Zvad for 30 min, seeded treated cells in the upper part of the transwell and added the secretome of M1 macrophages as migratory stimuli in the lower part of the transwell. We also used the secretome from M1 macrophage with and without MM01 treatment as a control for both cell lines.

As shown in **Figure 20**, the EO771 model (responder) presents the expected increase in migration with the M1 macrophage secretome (compare NT with M1) and decrease after the addition of MM01 (M1 + MM01). Surprisingly, we observed the inhibition of cell migration following treatment of the breast cancer cells with the caspase inhibitor Z-vad. This fact indicates that the presence of activated caspases in

cells could play a role in migration. Furthermore, we failed to observe any increase in migration towards stimulation with the inflammasome-related proteins, such as ASC, Caspase-1, and IL-1β, demonstrating that these proteins in the M1 macrophage secretome do not induce EO771 migration. Finally, for the 4T1 model, we failed to observe any increase in migration with the M1 macrophage secretome compared to untreated cells (NT). Furthermore, we observed no change in migration following MM01 treatment (M1 + MM01). As for EO771 cells, we also observed an inhibition in migration when we treated the cells with the caspase inhibitor Zvad. The cells also do not show migration in the presence of proteins related to the inflammasome.

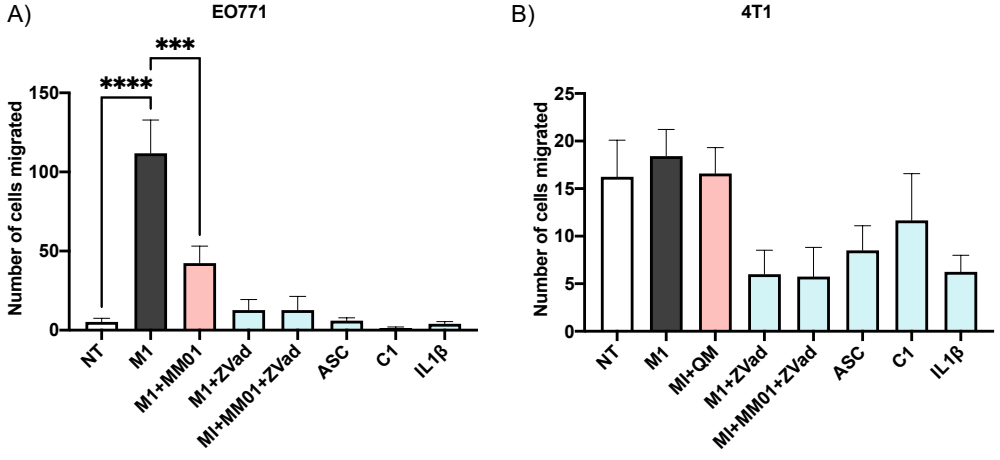

Figure 20. Migration of Murine Breast Cancer Cell Lines in Response to Inflammasome-related Proteins. Quantification of EO771 and 4T1 cell migration in response to stimuli: The M1 macrophage secretome +/- MM01 (M1+MM01), cells treated with ZVad and migrated in response to the M1 macrophage secretome +/- MM01, protein ASC, Caspase-1, and IL-1β. Data expressed as mean±SEM, n>3. Statistical significance determined using one-way ANOVA (one-way Anova, Dunnett's test *** p <0.001).

Overall, these results demonstrated that inflammasome-related proteins (Caspase-1, IL-1β, and ASC) failed to induce EO771 and 4T1 cell migration, although we highlighted a potential role of caspases in migration.

V.3.2 Proteomic Analysis of Responder and Non-responder Breast Cancer Cells

The identification of possible protein biomarkers distinguishing the responder (EO771) and non-responder (4T1) models to the inflammatory stimuli (M1 secretome) represents a primary objective of the chapter. Biomarkers could help to identify which breast cancer patients would benefit from treatment with inflammasome inhibitors such as MM01. Therefore, we performed differential proteomic studies in EO771 and 4T1 cells to identify differentially expressed proteins.

We first treated EO771 and 4T1 cells with the M1 macrophage secretome as detailed in **Chapter III, Materials and Methods section III.2.2.L.** After six hours, we collected cells and analyzed the proteome present in cell lysates.

The functional proteomic analysis aimed to answer two main questions:

1) What proteomic changes take place in breast cancer cells after treatment with the M1 macrophage secretome?.

2) What proteomic differences exist between the M1-stimulated responding (EO771) and non-responding (4T1) breast cancer cells?

To address these questions and identify biomarkers that predict responses to the inflammatory stimulus, we selected the following groups of samples:

- EO771 Non-treated (NT)
- EO771 + M1 secretome
- 4T1 Non-treated (NT)
- 4T1 +M1 secretome

Proteomic studies carried out in the SCSIE University of Valencia proteomics facility in collaboration with the "Bioinformatics unit of the Principe Felipe Research Center" identified differentially expressed proteins using the moderate t statistic of the limma package (The moderated t-statistic [t] is the ratio of the M-value to its standard error, while the M-value [M] is the log2-fold change).

To answer the first question noted above, we performed differential proteomics analysis for EO771+M1 vs. EO771 NT and 4T1+M1 vs. 4T1 NT. To answer the second question, we performed differential proteomics analysis for EO771+M1 secretome vs. 4T1+M1 secretome. We also analyzed differences in untreated cells to identify basal biomarkers that anticipate cellular response to pro- inflammatory stimuli - EO771 NT vs. 4T1 NT.

Table 2 depicts the differential expressed proteins obtained from these comparisons. For the first question, the EO771 + M1 vs. EO771 NT proteomic comparison revealed nine overexpressed and one underexpressed protein. Meanwhile, the same comparison in 4T1 cells produced four differential overexpressed proteins.

For the second question, a proteomic analysis of stimulated and unstimulated breast cancer cell lines generated a large number of differentially expressed proteins: 486 and 421 upregulated proteins for the EO771+M1 vs. 4T1+M1 and EO771-NT vs. 4T1-NT comparisons, respectively, suggesting a significant difference between the cell lines (**Table 2).**

Table 2. Differentially expressed proteins identified between the proteome comparisons of EO771 and 4T1 cell lines

	Differentially expressed proteins		
	Underexpressed	***Non diff. expressed***	***Overexpressed***
EO771+M1 vs EO771 NT	*1*	*2127*	*9*
4T1+M1 vs 4T1 NT	*0*	*2133*	*4*
EO771 NT vs 4T1 NT	*320*	*1396*	*421*
EO771+M1 vs 4T1+M1	*312*	*2137*	*486*

Figure 21 shows a schematic representation of the dysregulated proteins in EO771 and 4T1 cells after pro- inflammatory stimulation compared to untreated cells. In EO771 responder cells, we identified the overexpression of Platelet factor 4 (Pf4),

Serine protease inhibitor clade E member 1 (Serpine1), Ras Homolog Family Member B (RhoB), Interferon-gamma inducible protein 47 (Ifi47), Immunity-related GTPase family M protein 1 (Irgm1), Intercellular Adhesion Molecule 1 (Icam1), and nuclear factor-kappaB (Nfkb2) proteins. Meanwhile, we found the downregulated expression of the EIF-2-alpha kinase activator Gcn1 in EO771 responder cells.

In 4T1 non-responder cells, we identified the overexpression of Immunity Related GTPase M (Irgm1), Platelet Factor 4 (Pf4), CXC motif chemokine ligand 10 (Cxcl10), and Interferon-gamma inducible protein 47 (Ifi47).

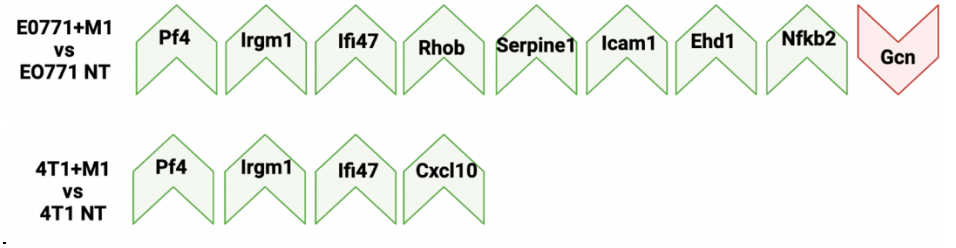

Figure 21. Differentially expressed proteins identified (Upper) Differentially expressed proteins identified between EO771+M1 vs. EO771 NT. (Lower) Differentially expressed proteins identified between 4T1+M1 vs. 4T1 NT. Green and red identify over- and under-expressed proteins, respectively.

Both EO771 and 4T1 cells exhibited the shared overexpression of three proteins after stimulation with the M1 macrophage secretome (Pf4, Irgm1, and Ifi47). Notably, these proteins play critical roles in tumor progression and metastases.

The **chemokine Pf4** (also known as Cxcl4) is normally released from activated platelet alpha granules and binds with high affinity to heparin-like molecules to promote coagulation [37]; however, Pf4 also appears to possess pro-tumor Activity in lung cancer cells [38]. The authors [38] described Pf4 as an endocrine factor whose overexpression in tumors correlates with decreased patient survival. The overproduction of Pf4 in a Kras-driven lung adenocarcinoma mouse genetic model increased platelet accumulation in the lungs and accelerated de novo adenocarcinogenesis [38]. Jiang et al. reported that platelet release could support breast cancer cell proliferation and induce tumor growth in vivo [39].

Franci et al. noted the upregulation of **Ifi47**, a residual disease marker after breast cancer therapy [40], in the tumor invasive front of squamous cell carcinomas [41].

Tian et al. observed the upregulation of **Irgm1**, a GTPase family member that regulates immune cell motility, in melanoma cells; furthermore, Irgm1 knock-down reduced migratory and invasive potential [42].

The significant increase in **Cxcl10** expression in 4T1+M1 cells compared to untreated cells correlates with shortened survival of human breast cancer patients with metastatic disease, with Cxcl10 implicated in the activation of dormant hepatic metastases [43].

Serpine1, RhoB, Icam1, Nfkb2, displayed over-expression in the EO771 responder cell line. Studies have highlighted elevated **Serpine1** expression in various tumor tissues [44]; furthermore, this protein plays a particular role in breast cancer cell adhesion, migration, invasion, and tumor metastasis [44]. A recent study reported the role of Serpine1 in the development of taxane resistance in TNBC cells and that Serpine1 silencing downregulated the expression of the angiogenic factor vascular endothelial growth factor A (VEGFA) and markedly attenuated tumor growth in vivo [45]. Related studies have also identified Serpine1 as a prognostic biomarker associated with epithelial-to-mesenchymal transition and poor prognosis in gastric cancer [46].

RhoB has both pro-tumor and anti-tumor functions depending on the type of cancer. However, RhoB overexpression in breast cancer correlates with advanced-stage disease and poor prognosis [47].

Figenschau et al. reported that pro-inflammatory cytokines induce the expression of **Icam1**, which supports the intratumoral formation of tertiary lymphoid structures in aggressive breast cancer subtypes, including MCF7, MDA-MB-468, and SK-BR-3 cells [48]. These results agree with our migration studies, where MCF7 and MDA-MB-468 respond to the M1 macrophage secretome migratory stimulus comparably to EO771.

The overexpression of the pro-inflammatory transcription factor **Nfkb2** has been noted in breast cancer [49] and facilitates the development of invasive, high-grade, and late-stage tumor phenotype [49].

To answer the second question of the study (the proteome differences between the M1-stimulated responding [EO771] and non-responding [4T1] breast cancer cells), we next analyzed the results of the EO771 NT vs. 4T1 NT and EO771+M1 vs. 4T1+M1 comparison. **Figure 21** depicts a Venn diagram between EO771 NT vs. 4T1 NT (Group A) and EO771+M1 vs. 4T1+M1 (Group B). The left side of the diagram (Group A) shows the upregulated proteins in EO771 NT vs. 4T1 NT (68 proteins). The right side (Group B) shows the upregulated proteins in EO771 + M1 vs. 4T1 + M1 (143 proteins), while the center represents the common proteins between the groups (353). We had a particular interest in those proteins overexpressed in the responder EO771 cells treated with M1, compared to the 4T1+M1 cells (Group B), suppressing the differential proteins due to intrinsic differences because they are two different cell lines.

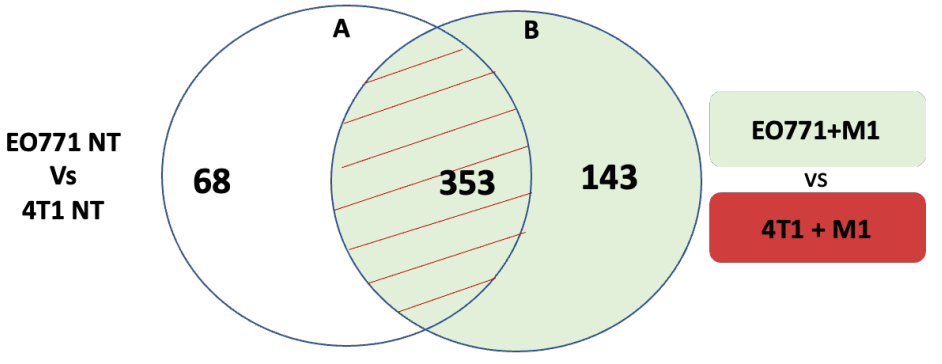

Figure 21. Bioinformatic characterization of overexpressed proteins from the EO771 NT vs. 4T1 NT (A) and EO771+M1 vs. 4T1+M1 (B) categories. Venn diagram showing the number of identified proteins. Common shown in the center of the figure**.**

We performed a functional enrichment analysis using the ORA (Over-representation Analysis) method implemented in the clusterProfiler package [50] to determine whether the number of proteins associated with that function in a list of interest is more frequent than that expected by chance in a biological process or function.

Using this approach, we identified three groups of proteins classified in the GO.MolecularFunction (GO.MF) upregulated in Group B (**Figure 22**). These three groups of proteins include twelve RNA binding proteins (Eif4g2/Prpf8/Rnaseh2a/Rbm39/Pabpc1/Ssb/Ewsr1/Krr1/Pabpc4/Hnrnpl/Eif3b/Lrrc47), four translation initiation factor activity proteins (Eif2a/Eif3d/Eif3b/Eif3l) and two with ATP-dependent peptidase activity (Afg3l2/Lonp1).

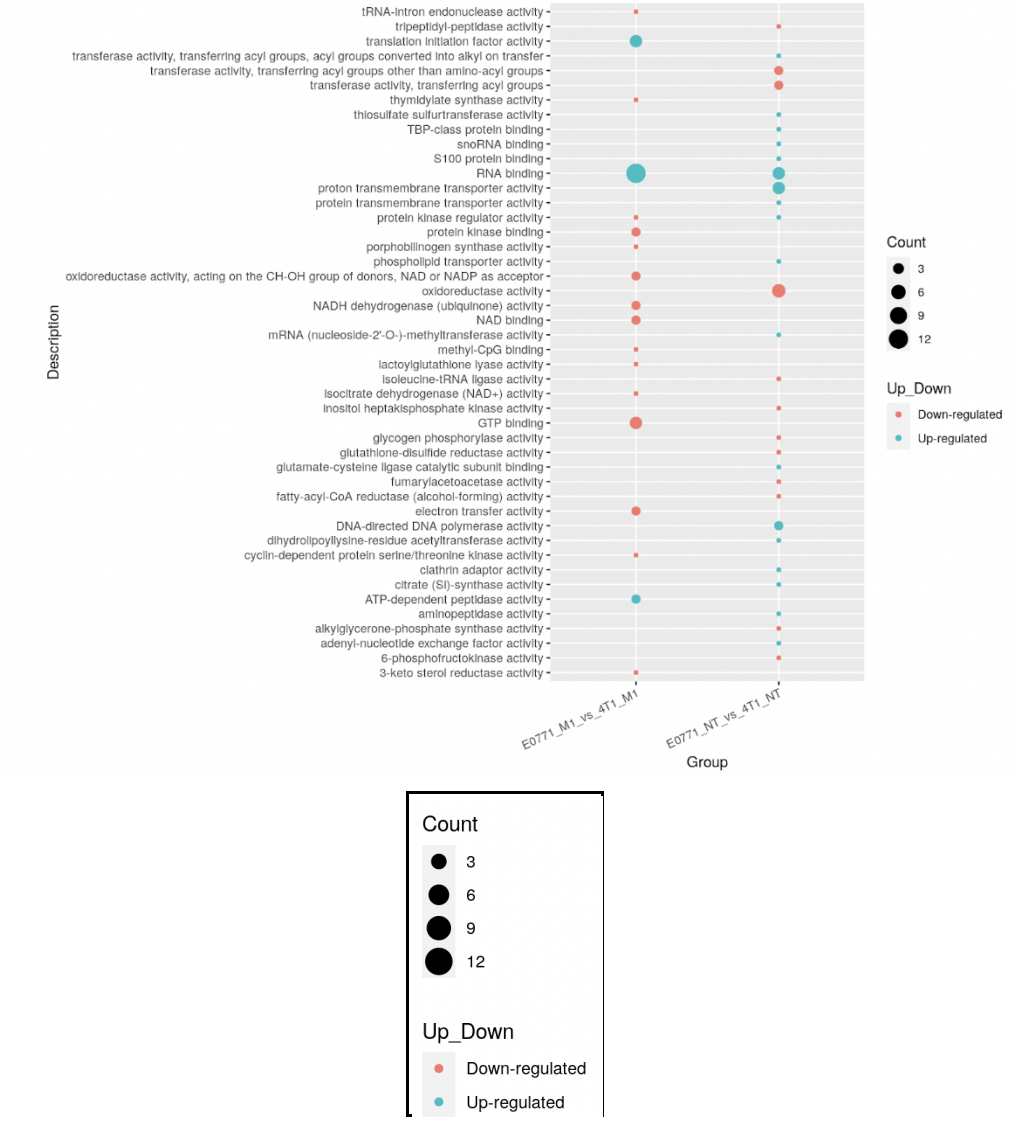

Figure 22. Proteins upregulated in EO771+M1 vs. 4T1+M1 by ORA analysis. Graph representing the functions identified in EO771 + M1 vs. 4T1 + M1 in GO.MF. The size of the point indicates the number

of genes in the experiment present in the determined function, while the color represents upregulation (blue) or downregulation (red).

Interestingly, upregulated proteins in Group B have been implicated in cancer progression (**Figure 23**). RNA binding proteins orchestrate the fate and function of mRNA by regulating RNA splicing, polyadenylation, stability, and localization [51] to maintain gene expression homeostasis and are often aberrantly expressed in cancer [52] [53]

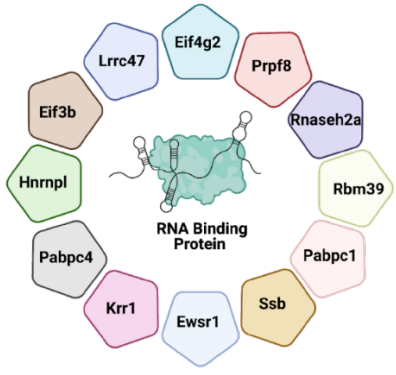

Figure 23. RNA Binding proteins upregulated in EO771+M1 vs. 4T1+M1.

Previous studies have demonstrated that suppression of Eukaryotic translation initiation factor 4 gamma 2 (EIF4G2) significantly reduced the development of acute myeloid leukemia [54], diffuse large B cell lymphoma [55], osteosarcoma [56], and lung cancer [57]. Li et al. [58] reported the upregulation of EIF4G2 in hepatocellular carcinoma (HCC) patient tissues and demonstrated that EIF4G2 silencing inhibited HCC cell growth and metastasis *in vitro* and suppressed tumorigenesis *in vivo*. EIF4G1, the most abundant member of the eIF4G family, exhibits robust upregulation in breast cancer [59].

Other studies have reported tumorigenic functions for the Pre-mRNA Processing Factor 8 (PRPF8) protein in TNBC [60] and myeloid neoplasms [61].

Ribonuclease H2 Subunit A (RNASEH2A) has a well-described role in cancer. For example, RNASEH2A promotes proliferation in sarcoma, breast cancer, glioma

cell lines, and prostate cancer, suggesting a key role in cancer progression [62]. A recent study demonstrated RNASEH2A upregulation in invasive breast cancer at an early stage, which remained high with the progression of the disease [63].

Recent studies reported a role for Poly(A) Binding Protein Cytoplasmic 1 (PABPC1) in breast, esophageal cancer, and gastric carcinomas [64]; [65]. PABPC1 promotes translation initiation in breast cancer through interaction with EIF4G1 as a protein essential for emboli formation in inflammatory breast cancer [66]. Zhu et al. reported that PABPC1 regulates the proliferation and transformation of gastric cancer cells *in vitro and in vivo*, and PABPC1 knock-down induces apoptosis by upregulating pro-apoptotic proteins and downregulating anti-apoptotic proteins in gastric carcinoma [67].

RNA-binding motif protein 39 (RBM39) is involved in transcriptional co-regulation and alternative RNA splicing. Recent studies have revealed that RBM39 loss leads to aberrant splicing events and differential gene expression, thereby inhibiting cell cycle progression and causing tumor regression in several pre-clinical models [68].

Studies have reported the overexpression of KRR1 in brain metastases in metastatic breast cancer patients compared to the primary tumor [69].

Overall, we identified patterns of positively regulated proteins in EO771 + M1 (responding models) compared to 4T1 + M1 (non-responding model) that may have essential functions in tumor progression in different types of cancer.

The following research aims would complement these findings:

1. Study the expression of upregulated proteins in different breast cancer lines with and without M1 macrophage secretome stimulation
2. Study the expression of upregulated proteins in M1 macrophage secretome stimulated breast cancer lines in response to MM01 treatment
3. Validate the function of these proteins as possible prognostic biomarkers
4. Study and correlate their function with inflammatory pathways

Conclusions

We demonstrated the efficacy of MM01 in preventing NLRP3 inflammasome activation in pro- inflammatory M1 macrophages. Treatment with MM01 reduced IL-1B release, pyroptotic cell death, and the expression of inflammatory proteins in M1 macrophages.

We identified models of breast cancer that recapitulate different migration responses to the inflammatory environment. We divided the models into responders, which increase migration in response to the M1 secretome, and non-responder models unaffected by the M1 secretome. In the responder models, the treatment of M1 with MM01 reduced the migration of the different breast cancer lines.

Notably, the murine models of breast cancer (EO771 and 4T1), exhibited the same responses during *in vitro* migration and *in vivo* experiments. Significantly, the EO771 cell line increased migration in response to M1 and decreased migration with MM01 treatment (Responder). In the same way, the EO771 orthotopic model presented a reduction in tumor size with the treatment of MM01. On the contrary, we observed a lack of response in 4T1 cells treated with the M1 secretome; however, 4T1 migration increased with MM01 treatment. Similarly, the 4T1 orthotopic model presented an increase in tumor size and lung metastasis with the MM01 treatment. These results reinforce the hypothesis of developing a functional migration experiment that could predict the *in vivo* response to treatment with an inflammasome inhibitor.

Finally, to search for biomarkers of response through proteomic studies, we have identified patterns of over-expressed proteins in the EO771 model treated with the secretome of M1 macrophages, compared to the model 4T1 treated with the secretome of M1. Many identified proteins have a role in tumor progression and metastasis in cancer. These preliminary results require validation to identify response biomarkers.

References

1. Shrihari, T.G., *Dual role of inflammatory mediators in cancer.* Ecancermedicalscience, 2017. **11**: p. 721.
2. Balkwill, F.R., M. Capasso, and T. Hagemann, *The tumor microenvironment at a glance.* J Cell Sci, 2012. **125**(Pt 23): p. 5591-6.
3. Hinshaw, D.C. and L.A. Shevde, *The Tumor Microenvironment Innately Modulates Cancer Progression.* Cancer Res, 2019. **79**(18): p. 4557-4566.
4. Jang, J.H., D.H. Kim, and Y.J. Surh, *Dynamic roles of inflammasomes in inflammatory tumor microenvironment.* NPJ Precis Oncol, 2021. **5**(1): p. 18.
5. Wei, R., et al., *Cellular and Extracellular Components in Tumor Microenvironment and Their Application in Early Diagnosis of Cancers.* Anal Cell Pathol (Amst), 2020. **2020**: p. 6283796.
6. Protti, M.P. and L. De Monte, *Dual Role of Inflammasome Adaptor ASC in Cancer.* Front Cell Dev Biol, 2020. **8**: p. 40.
7. Tulotta, C. and P. Ottewell, *The role of IL-1B in breast cancer bone metastasis.* Endocr Relat Cancer, 2018. **25**(7): p. R421-R434.
8. Jang, J.H., et al., *Breast Cancer Cell-Derived Soluble CD44 Promotes Tumor Progression by Triggering Macrophage IL1beta Production.* Cancer Res, 2020. **80**(6): p. 1342-1356.
9. Guo, B., et al., *Targeting inflammasome/IL-1 pathways for cancer immunotherapy.* Sci Rep, 2016. **6**: p. 36107.
10. Weichand, B., et al., *S1PR1 on tumor-associated macrophages promotes lymphangiogenesis and metastasis via NLRP3/IL-1beta.* J Exp Med, 2017. **214**(9): p. 2695-2713.
11. Zhang, L., et al., *NLRP3 inflammasome inactivation driven by miR2233p reduces tumor growth and increases anticancer immunity in breast cancer.* Mol Med Rep, 2019. **19**(3): p. 2180-2188.
12. Chen, I.F., et al., *AIM2 suppresses human breast cancer cell proliferation in vitro and mammary tumor growth in a mouse model.* Mol Cancer Ther, 2006. **5**(1): p. 1-7.
13. Voloshin, T., et al., *Blocking IL1beta Pathway Following Paclitaxel Chemotherapy Slightly Inhibits Primary Tumor Growth but Promotes Spontaneous Metastasis.* Mol Cancer Ther, 2015. **14**(6): p. 1385-94.
14. Kaplanov, I., et al., *Blocking IL-1beta reverses the immunosuppression in mouse breast cancer and synergizes with anti-PD-1 for tumor abrogation.* Proc Natl Acad Sci U S A, 2019. **116**(4): p. 1361-1369.
15. Mantovani, A., et al., *Cancer-related inflammation.* Nature, 2008. **454**(7203): p. 436-44.
16. Allen, M. and J. Louise Jones, *Jekyll and Hyde: the role of the microenvironment on the progression of cancer.* J Pathol, 2011. **223**(2): p. 162-76.
17. Qiu, S.Q., et al., *Tumor-associated macrophages in breast cancer: Innocent bystander or important player?* Cancer Treat Rev, 2018. **70**: p. 178-189.
18. Jeong, H., et al., *Tumor-Associated Macrophages as Potential Prognostic Biomarkers of Invasive Breast Cancer.* J Breast Cancer, 2019. **22**(1): p. 38-51.
19. Choi, J., et al., *The role of tumor-associated macrophage in breast cancer biology.* Histol Histopathol, 2018. **33**(2): p. 133-145.
20. Tariq, M., et al., *Macrophage Polarization: Anti-Cancer Strategies to Target Tumor-Associated Macrophage in Breast Cancer.* J Cell Biochem, 2017. **118**(9): p. 2484-2501.
21. Ma, R.Y., et al., *Monocyte-derived macrophages promote breast cancer bone metastasis outgrowth.* J Exp Med, 2020. **217**(11).
22. Chimal-Ramirez, G.K., et al., *Monocyte Differentiation towards Protumor Activity Does Not Correlate with M1 or M2 Phenotypes.* J Immunol Res, 2016. **2016**: p. 6031486.
23. Awad, F., et al., *Impact of human monocyte and macrophage polarization on NLR expression and NLRP3 inflammasome activation.* PLoS One, 2017. **12**(4): p. e0175336.
24. Chanput, W., et al., *Characterization of polarized THP-1 macrophages and polarizing ability of LPS and food compounds.* Food Funct, 2013. **4**(2): p. 266-76.
25. Orecchioni, M., et al., *Macrophage Polarization: Different Gene Signatures in M1(LPS+) vs. Classically and M2(LPS-) vs. Alternatively Activated Macrophages.* Front Immunol, 2019. **10**: p. 1084.
26. Genin, M., et al., *M1 and M2 macrophages derived from THP-1 cells differentially modulate the response of cancer cells to etoposide.* BMC Cancer, 2015. **15**: p. 577.
27. Daigneault, M., et al., *The identification of markers of macrophage differentiation in PMA-stimulated THP-1 cells and monocyte-derived macrophages.* PLoS One, 2010. **5**(1): p. e8668.

28. Sanchez-Sanchez, N., et al., *Chemokine receptor CCR7 induces intracellular signaling that inhibits apoptosis of mature dendritic cells.* Blood, 2004. **104**(3): p. 619-25.
29. Liu, M., S. Guo, and J.K. Stiles, *The emerging role of CXCL10 in cancer (Review).* Oncol Lett, 2011. **2**(4): p. 583-589.
30. Storr, S.J., et al., *Macrophage-derived interleukin-1beta promotes human breast cancer cell migration and lymphatic adhesion in vitro.* Cancer Immunol Immunother, 2017. **66**(10): p. 1287-1294.
31. Arroyo-Crespo, J.J., et al., *Characterization of triple-negative breast cancer preclinical models provides functional evidence of metastatic progression.* Int J Cancer, 2019. **145**(8): p. 2267-2281.
32. Zhao, R., et al., *Novel roles of apoptotic caspases in tumor repopulation, epigenetic reprogramming, carcinogenesis, and beyond.* Cancer Metastasis Rev, 2018. **37**(2-3): p. 227-236.
33. Yang, X., et al., *Caspase-3 over-expression is associated with poor overall survival and clinicopathological parameters in breast cancer: a meta-analysis of 3091 cases.* Oncotarget, 2018. **9**(9): p. 8629-8641.
34. Huang, Q., et al., *Caspase 3-mediated stimulation of tumor cell repopulation during cancer radiotherapy.* Nat Med, 2011. **17**(7): p. 860-6.
35. Zhou, M., et al., *Caspase-3 regulates the migration, invasion and metastasis of colon cancer cells.* Int J Cancer, 2018. **143**(4): p. 921-930.
36. Gdynia, G., et al., *Basal caspase activity promotes migration and invasiveness in glioblastoma cells.* Mol Cancer Res, 2007. **5**(12): p. 1232-40.
37. Artjoms Spaks, I.J., Simona Donina, Ainis Pirtnieks, Jelena Grusina-Ujumaza, Irina Spaka, Aurika Babjoniseva & Dainis Krievins *Dynamics of CXC group chemokine platelet factor 4 (PF4) plasma levels in non-small cell lung cancer (NSCLC).* Journal of Translational Medicine
38. Pucci, F., et al., *PF4 Promotes Platelet Production and Lung Cancer Growth.* Cell Rep, 2016. **17**(7): p. 1764-1772.
39. Jiang, L., et al., *Platelet releasate promotes breast cancer growth and angiogenesis via VEGF-integrin cooperative signalling.* Br J Cancer, 2017. **117**(5): p. 695-703.
40. Franci, C., et al., *Biomarkers of residual disease, disseminated tumor cells, and metastases in the MMTV-PyMT breast cancer model.* PLoS One, 2013. **8**(3): p. e58183.
41. Kunita, A., et al., *Inflammatory Cytokines Induce Podoplanin Expression at the Tumor Invasive Front.* Am J Pathol, 2018. **188**(5): p. 1276-1288.
42. Tian, L., et al., *IRGM1 enhances B16 melanoma cell metastasis through PI3K-Rac1 mediated epithelial mesenchymal transition.* Sci Rep, 2015. **5**: p. 12357.
43. Clark, A.M., et al., *IP-10 (CXCL10) Can Trigger Emergence of Dormant Breast Cancer Cells in a Metastatic Liver Microenvironment.* Front Oncol, 2021. **11**: p. 676135.
44. Li, S., et al., *Plasminogen activator inhibitor-1 in cancer research.* Biomed Pharmacother, 2018. **105**: p. 83-94.
45. Zhang, Q., L. Lei, and D. Jing, *Knockdown of SERPINE1 reverses resistance of triplenegative breast cancer to paclitaxel via suppression of VEGFA.* Oncol Rep, 2020. **44**(5): p. 1875-1884.
46. Xu, B., et al., *Global transcriptomic analysis identifies SERPINE1 as a prognostic biomarker associated with epithelial-to-mesenchymal transition in gastric cancer.* PeerJ, 2019. **7**: p. e7091.
47. Ju, J.A. and D.M. Gilkes, *RhoB: Team Oncogene or Team Tumor Suppressor?* Genes (Basel), 2018. **9**(2).
48. Figenschau, S.L., et al., *ICAM1 expression is induced by proinflammatory cytokines and associated with TLS formation in aggressive breast cancer subtypes.* Sci Rep, 2018. **8**(1): p. 11720.
49. Wang, W., S.A. Nag, and R. Zhang, *Targeting the NFkappaB signaling pathways for breast cancer prevention and therapy.* Curr Med Chem, 2015. **22**(2): p. 264-89.
50. Yu, G., et al., *clusterProfiler: an R package for comparing biological themes among gene clusters.* OMICS, 2012. **16**(5): p. 284-7.
51. Qin, H., et al., *RNA-binding proteins in tumor progression.* J Hematol Oncol, 2020. **13**(1): p. 90.
52. Wurth, L., *Versatility of RNA-Binding Proteins in Cancer.* Comp Funct Genomics, 2012. **2012**: p. 178525.
53. Pereira, B., M. Billaud, and R. Almeida, *RNA-Binding Proteins in Cancer: Old Players and New Actors.* Trends Cancer, 2017. **3**(7): p. 506-528.
54. Emmrich, S., et al., *miR-139-5p controls translation in myeloid leukemia through EIF4G2.* Oncogene, 2016. **35**(14): p. 1822-31.

55. Mazan-Mamczarz, K., et al., *Down-regulation of eIF4GII by miR-520c-3p represses diffuse large B cell lymphoma development.* PLoS Genet, 2014. **10**(1): p. e1004105.
56. Xie, X., et al., *MicroRNA-379 inhibits the proliferation, migration and invasion of human osteosarcoma cells by targetting EIF4G2.* Biosci Rep, 2017. **37**(3).
57. Hao, G.J., et al., *Suppression of EIF4G2 by miR-379 potentiates the cisplatin chemosensitivity in nonsmall cell lung cancer cells.* FEBS Lett, 2017. **591**(4): p. 636-645.
58. Li, S., et al., *MiR-144-3p-mediated dysregulation of EIF4G2 contributes to the development of hepatocellular carcinoma through the ERK pathway.* J Exp Clin Cancer Res, 2021. **40**(1): p. 53.
59. Badura, M., et al., *DNA damage and eIF4G1 in breast cancer cells reprogram translation for survival and DNA repair mRNAs.* Proc Natl Acad Sci U S A, 2012. **109**(46): p. 18767-72.
60. Chan, S., et al., *Basal-A Triple-Negative Breast Cancer Cells Selectively Rely on RNA Splicing for Survival.* Mol Cancer Ther, 2017. **16**(12): p. 2849-2861.
61. Kurtovic-Kozaric, A., et al., *PRPF8 defects cause missplicing in myeloid malignancies.* Leukemia, 2015. **29**(1): p. 126-36.
62. Yang, C.A., et al., *Prognostic Value of RNASEH2A-, CDK1-, and CD151-Related Pathway Gene Profiling for Kidney Cancers.* Int J Mol Sci, 2018. **19**(6).
63. Stefania Marsili, A.T., Francesca Storici, *Gene co-expression analysis of human RNASEH2A reveals functional networks associated with DNA replication, DNA damage response, and cell cycle regulation.* Biology.
64. Feng, C., et al., *Functional implications of PABPC1 in the development of ovarian cancer.* Open Med (Wars), 2021. **16**(1): p. 805-815.
65. An, T., et al., *The prognostic impacts of PABPC1 expression on gastric cancer patients.* Future Oncol, 2021. **17**(33): p. 4471-4479.
66. Silvera, D., et al., *Essential role for eIF4GI overexpression in the pathogenesis of inflammatory breast cancer.* Nat Cell Biol, 2009. **11**(7): p. 903-8.
67. Zhu, J., et al., *PABPC1 exerts carcinogenesis in gastric carcinoma by targeting miR-34c.* Int J Clin Exp Pathol, 2015. **8**(4): p. 3794-802.
68. Xu, Y., A. Nijhuis, and H.C. Keun, *RNA-binding motif protein 39 (RBM39): An emerging cancer target.* Br J Pharmacol, 2022. **179**(12): p. 2795-2812.
69. Shahan Mamoor, M., *KRR1 is a differentially expressed gene in brain metastatic human breast cancer.* .

Ch.VI

A Rationally Designed Polypeptide-based MM01 Nanomedicine Improves Antitumor Efficacy in Breast Cancer Models

Graphical Abstract

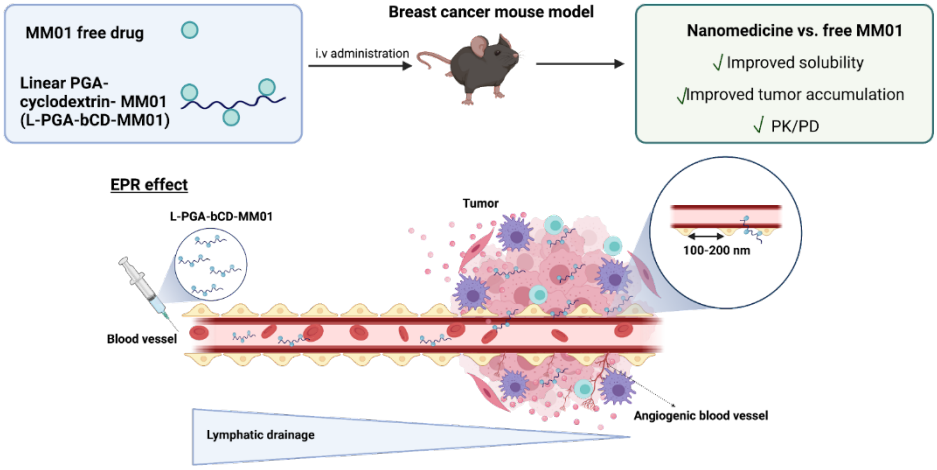

Antecedents and Background

As described in the **General Introduction**, conventional treatments for breast cancer induce unwanted side effects due to low efficacy and bioavailability, uncontrolled pharmacokinetics/pharmacodynamics (PK/PD), and the development of drug resistance [1]. The formulation of said treatments as nanomedicines may improve their specificity and efficacy and overcome any limitations to their use [2, 3].

In previous chapters, we demonstrated how MM01 inhibited the activity of ASC-dependent inflammasomes *in vitro* and *in vivo* (**Chapter IV**) and studied the potential of MM01 as a breast cancer treatment (**Chapter V**). In this chapter, we explore MM01 as the bioactive moiety in a polypeptide-based nanomedicine in order to improve the therapeutic effects of the parent free MM01 by enhancing MM01 PK/PD in the responder EO771 breast cancer model.

As mentioned above, polypeptides in particular polyglutamates have been selected as polymeric carrier due to its intrinsic properties [4]. The main advantages of polypeptides as drug carriers, include multivalency, biocompatibility and biodegradability [5]; [4]. Polypeptides also possess structural versatility, which supports the formation of multiple architectures with different physicochemical characteristics (e.g., charge, polarity, and hydrophilicity) [4]; [6]. Moreover, due to its

biodegradability into endogenous metabolites (aminoacids), there is the possibility of using these carriers with a higher molecular weight, which trigger longer circulation times and therefore an improvement of tumor accumulation through the enhanced permeability and retention (EPR) effect [7].

Features representing essential considerations when designing a polypeptide-based nanomedicine include (i) the structural elements of the nanomedicine (e.g., linker, drug nature, ligand pattern, and surface modification), (III) the physico-chemical properties of the nanomedicine (e.g., size, charge, conformation, geometry, and topology), and (IV) the biological barriers to be faced by the nanomedicine. Moreover, the administration route, cellular target, tumor microenvironment, and dosing schedule significantly influence the translation of a given nanomedicine and therapeutic outcomes [8].

In this thesis chapter, we implement a hybrid synthetic strategy comprising the conjugation of β-cyclodextrin to a linear poly-L-glutamic acid (PGA) (L-PGA-βCD) that possess the capability to entrap MM01 within the cyclodextrin rings in a concentration dependent manner yielding to L-PGA-βCD-MM01. We then explore the antitumor potential of this novel family of MM01 nanomedicines triggered by an increase in passive tumor accumulation as well as a sustained MM01 release at the TME.

Abstract

We developed a synthetic strategy to obtain a novel nanomedicine that improved the solubility and tumor-targeting of MM01 in a breast cancer model. We implemented a hybrid conjugation-complexation approach by comprising the conjugation of β-cyclodextrin to a linear poly-L-glutamic acid (PGA) (L-PGA-βCD) to provide with the capability of entrapping MM01 within the cyclodextrin rings in a concentration dependent manner yielding to L-PGA-βCD-MM01 with different physico-chemical characteristics (i.e. drug loading, size). The obtained nanosystem exhibited improved solubility in aqueous solutions compared to the free form of MM01. While we failed to observe a significant improvement in function in vitro compared to free MM01 as expected due to the different pharmacokinetics, our novel nanosystem demonstrated better efficacy in an orthotopic model of breast cancer by resulting in a more significant reduction in tumor size in those mice treated with L-PGA-βCD-MM01 nanomedicine.

Results and Discussion

VI.1 Synthesis of an MM01 Nanomedicine

Polypeptides offer significant advantages as nanocarriers for targeted drug delivery of small Mw drugs, such as MM01 [4]. In particular, Polyglutamates (PGA) has demonstrated safety and efficacy in the clinics. Therefore, herein we selected PGA as a biodegradable, multivalent polypeptide carrier and followed well-established synthetic methodologies to develop a family of novel nanomedicines modulators of the inflammasome by means of the incorporation of MM01 as the bioactive drug [4].

VI.1.1 Development of the L-PGA-βCD: Synthesis and Physico-Chemical Characterization

As mentioned in the introduction chapter, the design of polypeptide-based nanomedicines to treat a given disease or disorder must follow a rational stepwise design considering the different processes involved following administration [4]. The

physico-chemical characteristics of the nanomedicine will determine their capacity to cross the required biological barriers, its PK/PD and, therefore, their biological activity. The successful activity of a given nanomedicine depends primarily on its response to specific physiological environments where the selected molecular target is placed [2]. This could be achieved by the adequate selection of the different design features including the biodegradable polypeptide carrier, with adequate functionalities, the linking chemistry used, or the strategies for drug incorporation and the therapeutic agent involved (MM01).

PGA possesses a myriad of orthogonal reactive groups (carboxylic acid moieties) that can easily undergo chemical modification. Activating reagents condense carboxyl and amino groups to create amide bonds, including carbodimides, carbonyl dimidazole, 1-ethyl-3-(3-dimethyl aminopropyl)-1-carbodiimide hydrochloride (EDC), N-hydroxysuccinimide (NHS), and 4-(4,6-dimethoxy-1,3,5-triazin-2-yl)-4-methylmorpholinium chloride (DMTMM·Cl). The initial activation of the carboxyl group via adduct formation represents a common mechanism of action; this step is followed by the nucleophilic attack of the amine moiety to create the amide bond. This mechanism precludes the activating agent from being incorporated into the final product.

Chemical conjugation is always preferred for small Mw drugs by means of bioresponsive linking chemistries as this allows a better control of the kinetics of drug release in the site of action, avoiding a possible burst effect observed from different drug encapsulation approaches [4]; [9]. For this reason, through the presence of a carboxylic acid group within MM01 structure, a PGA liking strategy was implemented. The final goal was the conjugation to the PGA mainchain through a bioresponsive ester bond. Unexpectedly, MM01 was found to be extremely unstable molecule due to the presence of a double bond that degrades and triggers MM01 decomposition (**Figure 1**).

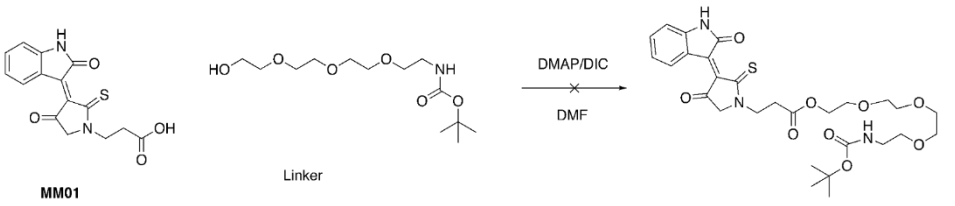

Figure 1. Example of an unsuccessful reaction conducted to try to achieve a direct conjugation to the polymer. The result obtained indicates the decomposition of the initial reagent.

Many conditions for MM01 conjugation were tested, including very mild flow conditions, with no luck due to problems either with solubility and/or MM01 stability-decomposition; therefore, an intermediate strategy between conjugation and encapsulation was finally devised by selecting a cyclodextrin ring for MM01 encapsulation.

Cyclodextrins are non-reducing cyclic oligosaccharides composed of glucopyranose units [10]. The α-, β-, and γ-cyclodextrins are widely known, which contain 6, 7, and 8 glucopyranose units respectively. The glucopyranose units form a conical cylinder, which has a hydrophobic inner cavity and a hydrophilic outer surface. This structure allows them to form inclusion complexes with hydrophobic molecules. Cyclodextrin rings can be chemically modified, bonded with substituents or other cyclodextrin rings and used to build larger nanostructures. The most common application of cyclodextrins is the solubility and bioavailability enhancement of poorly water-soluble drugs by complexation, moreover the application of these nanoconstructions are continuously increasing. For example, cyclodextrins can form complexes with biologically important natural molecules such as phospholipids, cholesterol or other lipophilic molecules. In turn, the cholesterol complexation properties of hydroxypropyl-cyclodextrin are applied in the treatment of Niemann Pick type C disease (NPC) and was approved as an orphan drug [10].

In this work, we focused on the development of an encapsulating carrier that protects MM01 from oxidative damage and decomposition. Our synthetic approach employed amide bond formation between carboxylic groups of linear PGA (L-PGA) and the amine of 6-monodeoxy-6-monoamino-β-cyclodextrin (βCD) using the amines of the cyclodextrin moiety and DMTMM·BF_4 as the activating coupling agent. The use

of DMTMM·BF for peptidic coupling of cyclodextrin and PGA through the amine moiety in organic solutions has been widely reported in the literature (**Figure 2**) [11].

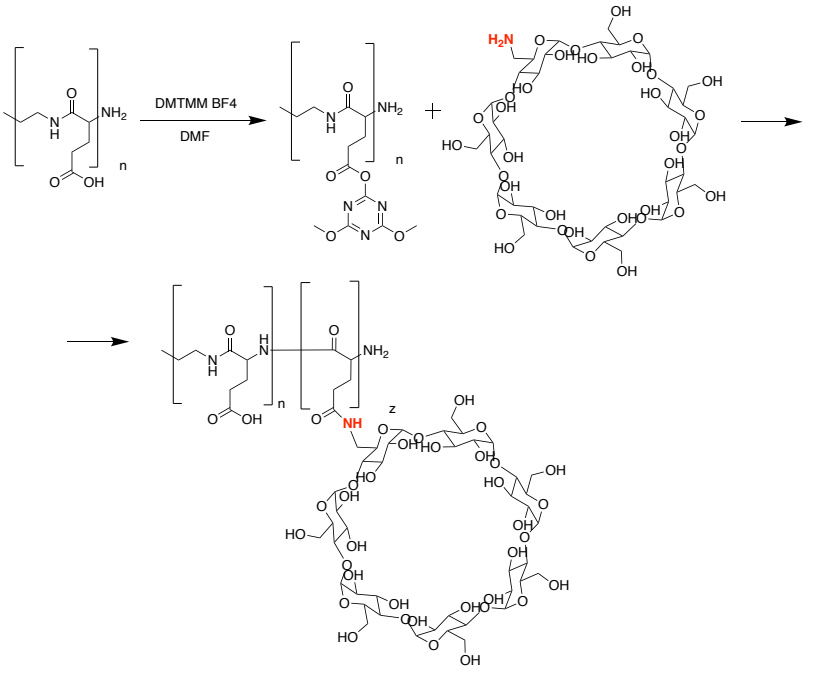

Figure 2: **synthetic scheme of PGA activation with DMTMM BF4 for subsequent in situ coupling of cyclodextrin.**

A family of L-PGA-βCD conjugates was achieved with total βCD loading ranging from 1% to 10% (in molar %) with high yields and good batch to batch reproducibility. We characterized the L-PGA-βCD conjugates through various physico-chemical techniques to ensure identity, purity, total βCD loading and size distribution. NMR spectroscopy demonstrated that our synthetic strategy yielded the desired conjugates with high purity (**Figure 3**). After βCD conjugation to PGA (**Figure 3**), we observed a broadening of the bands while still retaining the characteristic peaks of the parent cyclodextrin derivative at 5 ppm. As shown in **Figure 3**, the ^{1}H NMR spectra of L-PGA-βCD demonstrated the preservation of the characteristic maximum absorbance of the parent cyclodextrin (5 ppm). The six protons of the hydroxy groups of the cyclodextrin (green box in **Figure 3**) of around 5 ppm relate to a single proton of a PGA unit (red box in **Figure 3**).

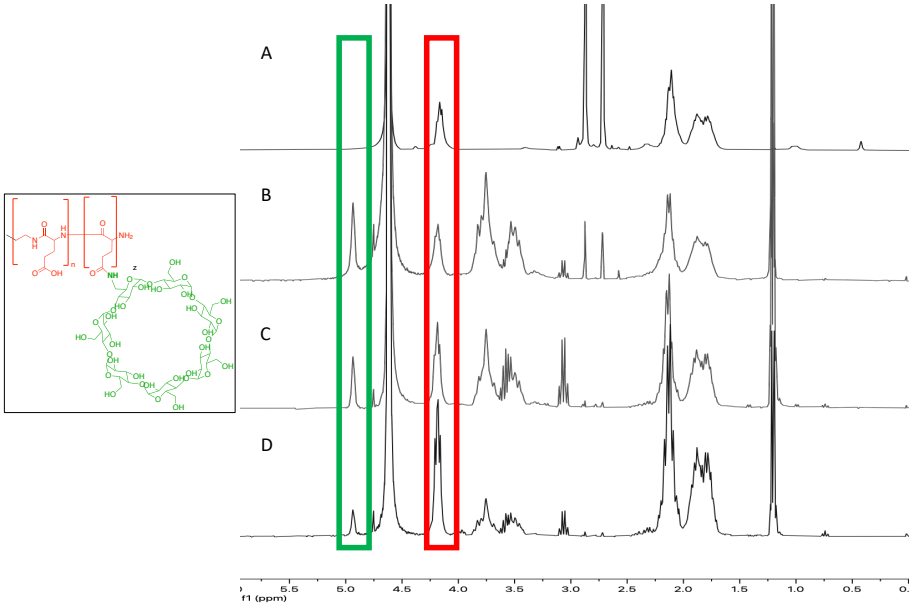

Figure 3. ^{1}H NMR spectrum of L-PGA-βCD with A) PGA B) 10% C) 5% and D) 1% of functionalization %mol of βCD in relation to PGA units (300 MHz, D_2O).

Different physicochemical properties of the polymer family were calculated, such as size by diffraction techniques (DLS) and cyclodextrin loading and molecular weight by resonance magnetics techniques. (See **Table 1**)

Table 1. Comparation of different batches of L-PGA with variable amount of βCD using different approaches.

	PGA1% βCD	***PGA5% βCD***	***PGA 10% βCD***
Mw by H-NMR	***23412,8***	***26610,1***	***36413,6***
Size by DLS	***35***	***55***	***62***
Loading of βCD by H-NMR (%mol)	***2,1***	***4,8***	***9,8***

VI.1.2 Development of L-PGA-βCD Encapsulated MM01: Synthesis and Physico-Chemical Characterization

We next studied the encapsulation of the inflammasome inhibitor MM01 with L-PGA-βCD to yield the desired family of L-PGA-βCD-MM01 nanomedicines. To obtain the optimal conditions and high-performance encapsulation, we employed a statistical program (Response Surface Methodology - RSM) to estimate optimal reaction conditions [12].

RSM represents a collection of mathematical and statistical techniques widely used to develop, improve, and optimize processes such as the chemical processes employed to generate a desired compound. RSM is also applicable in the design, development, and formulation of new chemical products and the improvement of already implemented product designs [13].

Modeling the analysis of problems in which several quantitative factors (variables) influence a response of interest represents the most broadly applied application of RSM [14]. The program attempts to optimize responses by determining optimal values for the factors involved [13]. For example, Baris et al. developed a graphical interface by utilizing RSM to determine the optimal weight of aggregates [15], while Mohammed et al. utilized RSM to attain a relationship between fly ash, nano-silica, and superplasticizer as variables and flow value, setting time and compressive strength as responses [16].

In this work, we employed RSM to optimize the encapsulation of MM01 (the "response") by encountering optimal values for reaction variables.

VI.1.2.1 Optimization and Statistical Analysis

The use of RSM include employing theories of mathematical and statistical analysis techniques between variables and responses [13]. There are two main types of analysis models available within RSM: = central composite design (CCD) and Box–Behnken design. Choosing a model type depends on the accessibility of the program, as well as the type of application. For example, a design plan that requires sequential experimentation often employs CCD. CCD can include information from an

experiment whose design consists of two or more factors, each with different values or levels. [17]; [18]. Furthermore, CCD represents a widely used statistical tool to determine the desired constraints and interactions between factors [18].

In this work, we employed Design Expert (CCD version 11.0) to model the best conditions for the encapsulation of MM01 by L-PGA-βCD. The experimental design included the creation of a set of procedures to optimize the encapsulation of MM01, taking into account different types of variables.

The steps followed for the experimental design included:

1) <u>Consider the variables and how they relate</u>

We evaluated the effects of three independent variables using CCD to optimize the encapsulation of MM01 with L-PGA-βCD:

A: Concentration of βCD in the polymer (%mol)

B: Exchange solvent mixture H_2O/DMF

C: Amount of MM01 (in mg)

2) <u>Write a specific and testable hypothesis</u>

Factors such as encapsulation, particle size, and functional activity of the nanomedicine must be related to the selected variables: Cyclodextrin polymer charge (the encapsulating agent) and the amount of drug available in the medium. In addition, the percentages of solvents in the reaction mixture can influence encapsulation, as they directly affect solubility.

3) <u>Design experimental treatments to predict optimal responses</u>

We developed a total of thirty-five mix combinations in RSM. We investigated the interaction effects of three independent variables – (A) the concentration of βCD in the polymer, (B) the mixture of H_2O/DMF exchange solvents, and (C) the amount of

MM01 using a CCD matrix. **Table 2** describes the predicted parameters for the selected variables for defined variable combinations. As shown in **Table 2,** the program assigns different parameters of the variables, represented as -1, 0, or 1 in **Table 2** (variable values). After performing fifteen experiments (each with three repetitions to formulate the encapsulation potential), the program determines a complete quadratic equation.

Table 2. Independent variable ranges

Variables	*Symbol*	*Unit*	*Variable value*		
			-1	***0***	***1***
Concentration of βCD in the polymer	***A***	*% mol*	*1*	*5*	*10*
Exchange solvent mixture H_2O/DMF	***B***	*% mL*	*90:10*	*75:25*	*50:50*
MM01	***C***	*mg*	*1*	*3*	*6*

4) <u>Locate optimal conditions using graphical and/or mathematical tools</u>

Design-Expert offers a wide selection of graphs to help identify prominent effects and visualize results. A three-dimensional (3D) response surface plot illustrates the relationship between the independent variables and demonstrates how the independent variables affects MM01 encapsulation. **Figure 4** depicts the 3D response surface plots illustrating the relationship between the βCD concentration in the polymer, H_2O/DMF exchange solvent mix, and amount of MM01 as variables.

In each graph depicted in **Figure 4**, we continuously varied two independent variables and fixed the remaining variable. We discovered significant correlations between independent parameters, with prominent peaks observed for response surface plots (**Figure 4**). All response plots exhibited visible peaks, thereby indicating all design space variables had values that best supported an optimal response.

The explanation of each graph in **Figure 4** as a function of the variables is as follows:

i. Milligrams of MM01 on MM01 Encapsulation: **Figure 4A** shows the effect of βCD percentage on solvents percentage regarding MM01encapsulation. The optimal value of 1 corresponds to 10% βCD loading and 50:50 H_2O/DMF.

ii. βCD Concentration on MM01 Encapsulation: **Figure 4B** shows the effect of MM01 amount and solvent percentage on MM01 encapsulation. The optimal value of 1 corresponds to 6 mg MM01 and 50:50 H_2O/DMF.

iii. Exchange solvent mixture H_2O/DMF on MM01 Encapsulation: **Figure 4C** depicts the effect of MM01 amount and βCD concentration on MM01 encapsulation. The optimal value of 1 corresponds to 6 mg MM01 and 10mol% βCD.

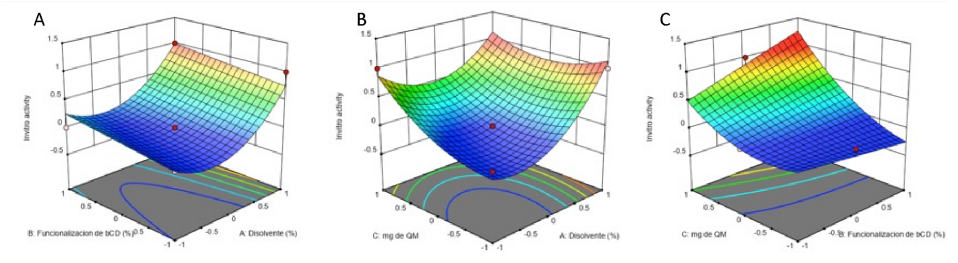

Figure 4. The combined effect of process variables A) MM01 amount, **B)** concentration of βCD in the polymer, and **C)** exchange solvent mixture % H_2O/DMF on MM01 encapsulation.

Overall, these 3D graphics predicted that optimal encapsulation of MM01 would occur with 10mol% of βCD in 50:50 H_2O/DMF with 6 mg MM01. The next step was the experimental validation of the best reaction estimated by the program.

5) Experimentally validated optimal conditions

Unfortunately, the predicted values (10mol% of βCD in 50:50 H_2O/DMF with 6 mg MM01) failed to provide for optimal encapsulation experimentally, as the low solubility of MM01 triggered a rapid precipitation and diminished encapsulation at the selected drug concentration (6 mg MM01). When the reaction mixture is carried out in

50:50 H_2O/DMF proportion, it does not allow enough time for encapsulation to occur due to the rapid MM01 precipitation.

Trying to overcome the issue of MM01 solubility, we validated the remaining fourteen reaction conditions selected by the DoE to identify the optimal encapsulation of MM01. **Table 3** describes the fourteen different reaction conditions established by the program Design Experts and experimentally tested. In all cases, MM01 loading and encapsulation efficiency by UV-Vis were quantified prior to the evaluation of the resulting nanosystems *in vitro*. We can use this technique, thanks to the aromaticity of MM01. The MM01 has an absorption maximum at a wavelength of 430 nm; when this maximum does not coincide with the absorption of the carrier (PGAs) that have it at 280nm, we can use it to calculate the percentage in mass of MM01. Experimentally, a calibration curve is carried out using different concentrations of MM01 in DMF and measuring its absorbance (**Figure 5**). This calibration curve (solvent DMF, maximum absorbance 450nm) was used to calculate the amount of drug encapsulated in all the reactions that have been carried out before the in vitro tests (**see table 2**)

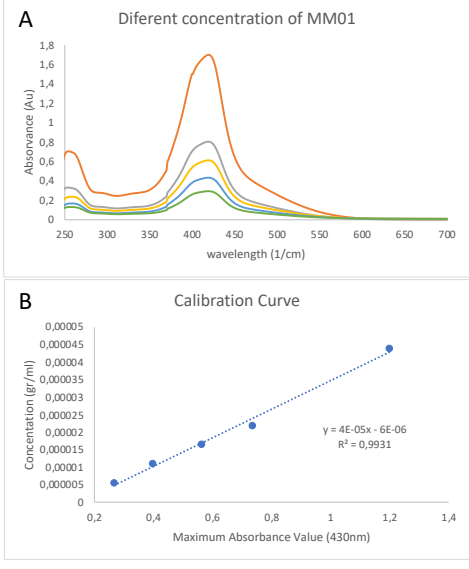

Figure 5: A) UV-Vis spectra of different solutions with different concentrations of MM01 in DMF, and B) the calibration curve to determine the MM01 loading (% W/W) and encapsulation efficiency using maximum of absorbance at 430nm.

Table 3. Experimental Conditions employed to yield L-PGA-βCD-MM01 nanomedicine family: Factors A, B, and C refer to the variables studied to yield MM01 entrapment. (A: Concentration of βCD in the polymer% mol, B: Exchange solvent mixture, and C: Amount (mg) of MM01) The numbers assigned as -1, 0, 1 refer to the values established in *Table 1* for each variable.

Name	%W/W By UV-Visible (in PBS 0,5 mg/ml	Size By DLS (in PBS 0,5 mg/ml)	Factor A	Factor B	Factor C
L-PGA-βCD-MM01-1	**4.05**	< 5	0	-1	-1
L-PGA-βCD-MM01-2	**18.70**	< 5	0	0	0
L-PGA-βCD-MM01-3	**19.76**	122	1	1	0
L-PGA-βCD-MM01-4	**4.99**	25	0	0	0
L-PGA-βCD-MM01-5	**3.89**	70	-1	0	-1
L-PGA-βCD-MM01-6	**7.45**	25	-1	-1	0
L-PGA-βCD-MM0-7	**9.10**	10	1	0	-1
L-PGA-βCD-MM01-8	**11.65**	65	1	-1	0
L-PGA-βCD-MM01-9	**3.89**	40	0	0	0
L-PGA-βCD-MM01-10	**23.19**	90	0	1	-1
L-PGA-βCD-MM01-11	**14.50**	30	1	1	0
L-PGA-βCD-MM01-12	**11.19**	< 5	1	0	1
L-PGA-βCD-MM01-13	**9.55**	20	-1	1	0
L-PGA-βCD-MM01-14	**12.30**	< 5	0	-1	1

VI.2 The *in vitro* Evaluation and Selection of an Optimal Nanomedicine Candidate

Studying the properties and advantages of nanomedicines requires subsequent biological evaluations in model systems ranging from *in vitro* cell line-based assays to *in vivo* testing in animal models [19]. In this section, we focus on studying the efficacy of our synthesized nanomedicines (**Table 3**) in cell models to highlight the best candidate based on their cellular uptake and induced responses [20]; [21].

VI.2.1 Selection of L-PGA-βCD-MM01-3 as the Optimal Candidate

In **Chapter IV** of this thesis, we evaluated the inhibitory capacity of free MM01 on different ASC-dependent inflammasomes in a THP-1-derived macrophage model. In this section, we evaluated the capacity of each of our nanomedicine family (**Table 3**) to inhibit NLRP3 inflammasome activation. The NLRP3 inflammasome activates inflammation by inducing the release of inflammatory cytokines such as IL-1β and increasing pyroptotic cell death. We pretreated THP-1-derived macrophages with a 20 μM equivalent MM01 dose of each nanomedicine for two hours and then stimulated THP-1-derived macrophages with LPS and nigericin to activate the NLRP3 inflammasome and then evaluated the levels of IL-1β release and pyroptosis.

Figure 6 demonstrates that LPS and nigericin stimuli (+ LPS/Nig) increase IL-1β secretion and pyroptosis compared to untreated cells. As expected, free MM01 pretreatment (+MM01) led to a significant reduction in IL-1β and pyroptosis (compare + LPS/Nig to + LPS/Nig + MM01). Treatment with specific nanomedicines significantly inhibited the LPS/Nig-induced increased in IL-1β secretion and pyroptosis; however, only two candidates presented statistically significant results (L-PGA-βCD-MM01-3 and 8). Of note, we failed to observe significant differences between L-PGA-βCD-MM01-3 and free MM01.

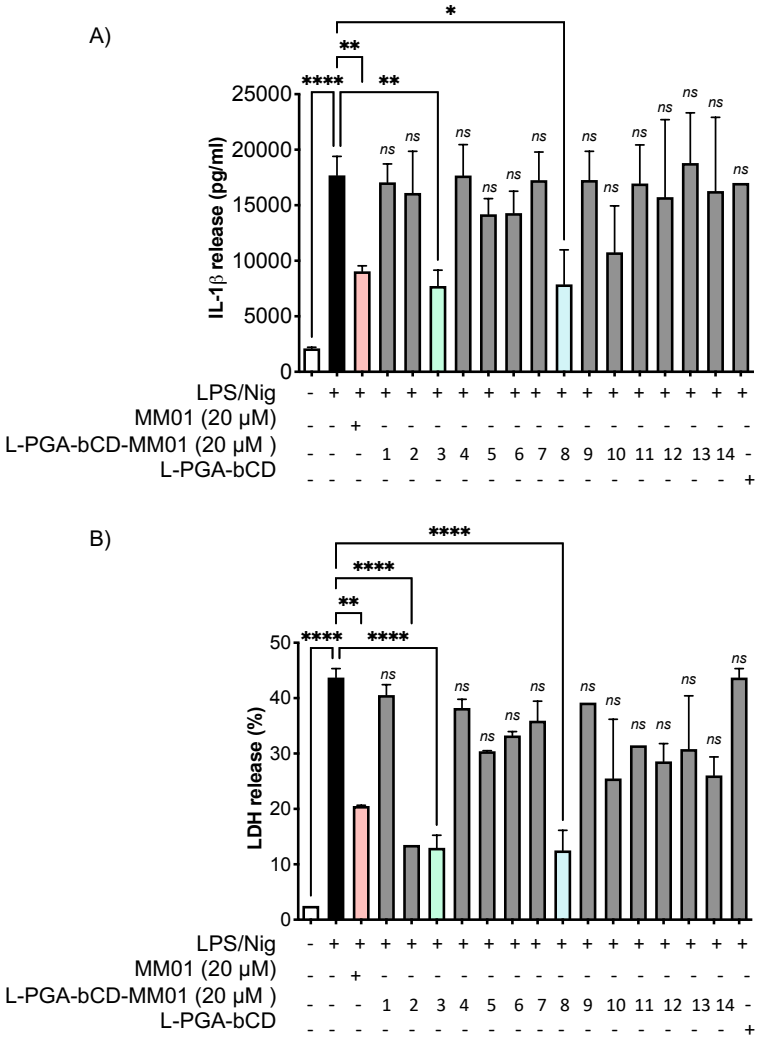

Figure 6. Inhibition of theNLRP3 inflammasome inhibition in THP-1 derived macrophages by free MM01 and L-PGA-βCD-MM01 family members. The numbers on the x-axis with relation to L-PGA-βCD-MM01 refer to the reactions noted in **Table 3. A**) IL-1β secretion evaluated by ELISA and **B**) measurement of LDH release into the extracellular medium following activation of the NLRP3 inflammasome with 100 ng/ml LPS and 10 μM nigericin. Data represent the mean ± SD of almost three independent experiments. Asterisks represent significant differences determined by one-way ANOVA test with Tukey's multiple post-test comparisons (ns = not-significant; **p<0.01; ****p<0.0001).

VI.2.2 Candidate validation: L-PGA-βCD-MM01-3

After selecting the best candidates, L-PGA-βCD-MM01-3 and L-PGA-βCD-MM01-8, the next step was to scale up the synthesis and perform a thorough

characterization of the nanosystems prior to future more specific *in vitro* and *in vivo* experiments. To determine drug loading, nuclear magnetic resonance (NMR) was employed as described above, as well as dynamic light scattering (DLS) to complete the physicochemical characterization of the nanosystem and explore batch-to-batch reproducibility (**Figure 7**).

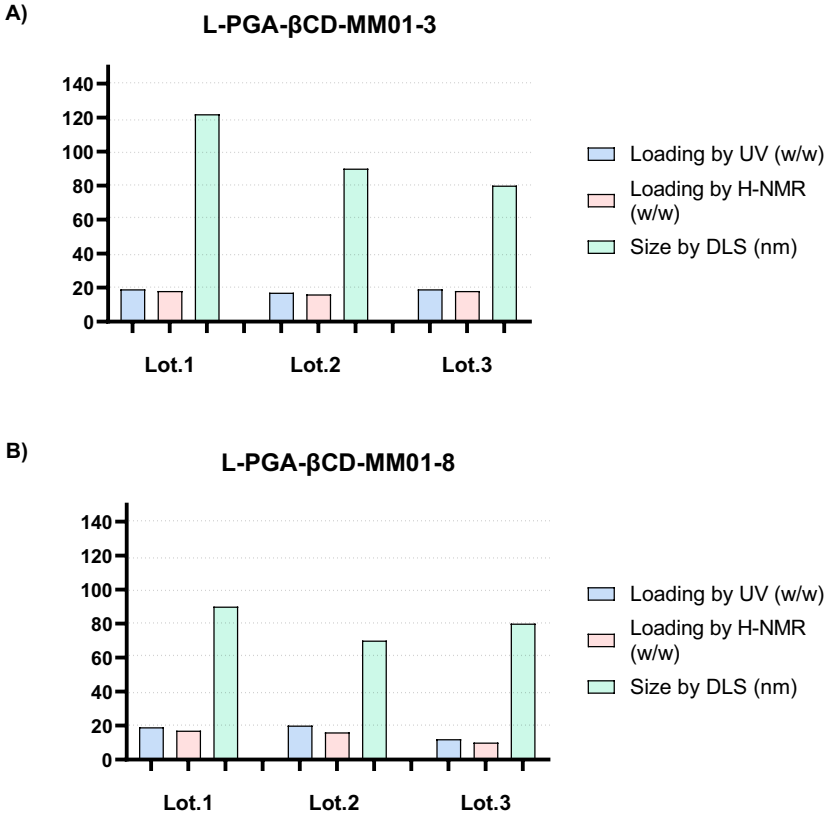

Figure 7. Physicochemical characterization of the nanosystem and exploration of batch-to-batch reproducibility.

UV-Vis spectra of PGA-βCD-MM01-3 and PGA-βCD-MM01-8 demonstrate the preservation of the maximum absorbance characteristic of the parent drug (430 nm). As already explained previously, with this measure, we can calculate the drug load that we have. We also demonstrated that even if a scale-up is performed, the percentage of

encapsulation w/w is maintained if we compare the result obtained in table 2 and this scale-up (**See figure 7**), around 19% in all cases.

Another qualitative and non-quantitative test to demonstrate encapsulation is a nuclear magnetic resonance using deuterated water as a solvent at a concentration of 10 mg/ml **(Figure 8).** With this analysis method, you can see the different signals corresponding to the various components of our material. The signals corresponding to the PGA can be seen in two regions: multiplet at 4,3ppm and two multiplets at 2,5-1,7ppm (blue color). Also, the signs are also shown of the β-CD directly bound to the polymer in the ranges: singlet at 5ppm and two multiplets at 3,4-4ppm (blue color) In the case of MM01, the most notable are the well-defined signals of the molecule in the aromatic region (8,5-6,5 ppm in red). This means that this molecule has been total solubilized in a hydrophilic medium. The importance of this is because this molecule in its natural form is insoluble in hydrophilic media. In other words, it means that we could not solubilize it in aqueous media or physiological environment. With this analytical test, we can demonstrate that encapsulation is valid and it takes place.

We can deduce the qualitative relationship between the PGA and the calculated drug with this technique. It has also been used previously to calculate the charge on the cyclodextrin polymer. In this case, the ratio between the signals gives a ratio of 10% molar, which is equivalent to 18% by weight. We corroborate the value obtained for the same batch with the other technique with this method.

Also, we can calculate a relationship between concentrations of the cyclodextrin, and the amount of drug is encapsulation, taking into account the relationship of existing signals in the H-NMR spectrum at 8-6,5 ppm (in red = MM01) and 5ppm (in green = βCD). According to this relationship, we would have 100% of the DC drug load. To be more specific, release studies would need to be performed, as it is reported that various cd molecules can often form complexes with a host.

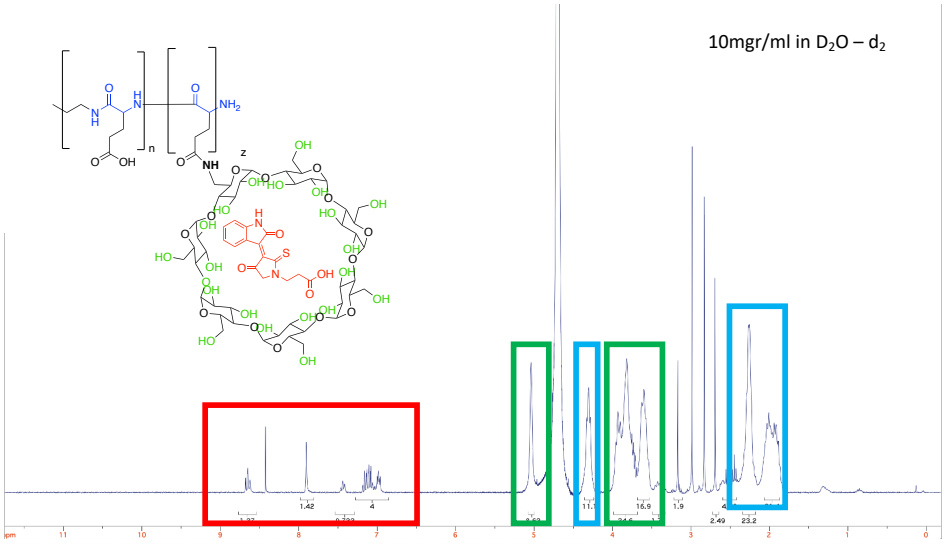

Figure 8. H-NMR. In D_2O (10mg/ml): In red the aromatic signals of MM01; in green the βCD and in blue the PGA

VI.2.3 L-PGA-βCD-MM01-3 and L-PGA-βCD-MM01-8 Prevent NLRP3 Activation in THP-1 derived Macrophages

We next fully explored the *in vitro* activity of L-PGA-βCD-MM01-3 and L-PGA-βCD-MM01-8 by analyzing IL-1β release and levels of pyroptosis in THP-1 derived macrophages after NLPR3 inflammasome activation (LPS/Nig stimuli). We studied the inhibitory capacity of both nanosystems at different equivalent concentrations of free MM01 (20, 40, and 100 μM) (**Figure 9**). The upper part of **Figure 9** shows the activity of L-PGA-βCD-MM01-3, while the lower part shows the activity of L-PGA-βCD-MM01-8 in cells after treatment with LPS and Nigericine (LPS/Nig) stimuli. As expected, **Figure 9** demonstrates an increase of IL-1β secretion (**Figure 9A and 9C**) and pyroptosis (**Figure 9B and 9D**) upon stimulation with LPS and nigericin (+ LPS/Nig) compared to untreated cells. Again, in both cases, free MM01 pretreatment (+MM01) led to a significant reduction in IL-1β and pyroptosis (compare + LPS/Nig to + LPS/Nig + MM01), while we failed to observe significant differences between PGA-βCD-MM01-3 or PGA-βCD-MM01-8 vs free MM01 at 20 μM equivalent dose. While we failed to observe an improved effect of both nanosystems with respect to free MM01 at an equivalent concentration, higher

concentrations of L-PGA-βCD-MM01-3 (40 and 100 μM) induced an improved effect in a dose-response manner (**Figure 9A and 9B**). However, we failed to observe a significant improvement with L-PGA-βCD-MM01-8 treatment with respect to MM01 at any of the concentrations studied. (**Figure 9C and 9D**).

Overall, we demonstrated the efficacy of L-PGA-βCD-MM01-3 to efficiently inhibit the NLRP3 inflammasome in THP-1-derived macrophages at a high equivalent concentration of MM01. Moreover, L-PGA-βCD-MM01-3 displayed better activity in inflammasome-activated cells than L-PGA-βCD-MM01-8, possibly due to the higher MM01 load present in L-PGA-βCD-MM01-3 vs L-PGA-βCD-MM01-8 (19,76% w/w in L-PGA-βCD-MM01-3 vs 11,65% w/w in L-PGA-βCD-MM01-8). Therefore, we selected L-PGA-βCD-MM01-3 (conditions of encapsulation 10% βCD, 50:50 H_2O/DMF and 3 mg of MM01; final loading of MM01 19,7% w/w by ultraviolet-visible. See **Table 3**) as candidate nanomedicine for subsequent *in vitro* and *in vivo* experiments

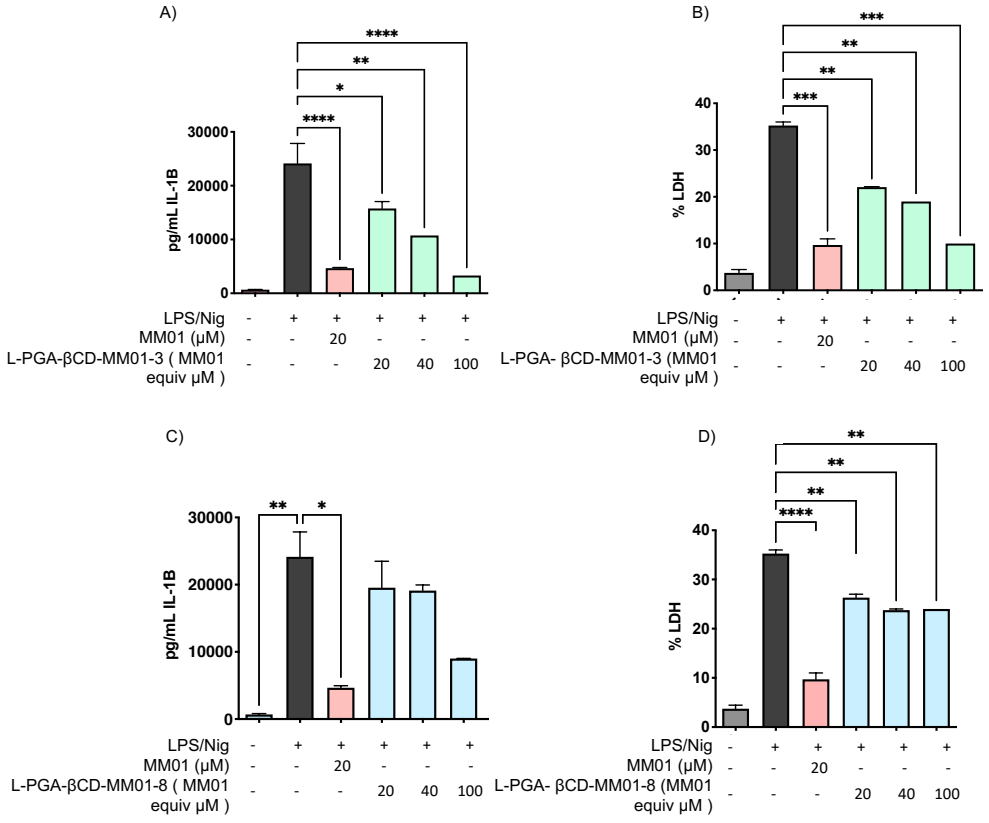

Figure 9. L-PGA-βCD-MM01-3 and L-PGA-βCD-MM01-8 inhibit NLRP3 inflammasome in THP-1 derived macrophages. A) IL-1β secretion evaluated by ELISA and **B**) measurement of LDH release into the extracellular medium following activation of the NLRP3 inflammasome with 100 ng/ml LPS and 10 μM nigericin. Cells were pre-treated with MM01 and L-PGA- βCD-MM01-3 at MM01 equivalent doses**. C**) IL-1β secretion evaluated by ELISA and **D**) measurement of LDH release into the extracellular medium following activation of the NLRP3 inflammasome with 100 ng/ml LPS and 10 μM nigericin. Cells were pre-treated with MM01 and L-PGA-CD-MM01-8 at MM01 equivalent doses. Data represent the mean ± SD of three independent experiments. Asterisks represent significant differences determined by one-way ANOVA test with Tukey's multiple post-test comparisons *p<0.05; **p<0.01; ***p<0.001; ****p<0.0001.

VI.3 Therapeutic Efficacy of L-PGA-βCD-MM01-3 in Breast Cancer Models

The exploration of the inflammasome's role in breast cancer development aims to foster the development of novel efficient therapeutics [22]. While studies have shown the efficacy of inflammasome inhibition in supporting cancer progression [23]; [24], other studies report an anti-tumorigenic role of the inflammasome [25]. Therefore, treatment with inflammasome inhibitors requires a more in-depth study to identify what types of tumors may benefit from these therapeutic approaches.

In **Chapter V**, we developed a functional cell-based assay that could predict the behavior of breast tumors after treatment with our inflammasome inhibitor *in vivo*. The functional assay consists of studying the migration of breast cancer cells in response to the secretome of pro-inflammatory macrophages (M1) after treatment with MM01. We demonstrated that MM01 treatment of M1 macrophages reduced the migration of EO771 breast cancer cells and reduced tumor growth *in vivo*. In contrast, MM01 treatment increased cell migration, tumor growth, and metastasis in the 4T1 model. These two models reflect the two contradictory responses that treatment with an inflammasome inhibitor may have in breast cancer progression.

VI.3.1 L-PGA-βCD-MM01-3 treatment affect migration dependent upon breast cancer subtype

To study the effect of the selected polymer *in vivo*, we first evaluated the effect of M1 macrophages treated with L-PGA-βCD-MM01-3 on the migration of the 4T1 and EO771 murine breast cancer lines. We treated J744A.1 murine macrophages with L-PGA-βCD-MM01-3 at 20 μM MM01 equivalent dose and subsequently induced their polarization into M1 macrophages with 25 ng/mL IFN-γ and 10 pg/mL LPS. At 24 hours, we collected the M1 cell supernatant as a migration stimulus for breast cancer lines. We seeded the murine 4T1 and EO771 breast cancer cells in the upper part of the transwell (25,000 cells/transwell), added the M1 macrophage secretome, with or without treatments, to the well below, and then analyzed the number of migrating cells at 6 h by confocal microscopy (**Figure 10**).

The results illustrated in **Figure 10A** demonstrate an increase in EO771 cell migration in response to the secretome of the M1 macrophages (compare NT to M1). Moreover, we demonstrated a significant inhibition of EO771 cell migration when we treated M1 macrophages with free MM01 and L-PGA-βCD-MM01-3 (compare M1+ L-PGA-βCD-MM01-3 to M1 and M1+MM01 to M1). Again, we failed to observe an improved effect of L-PGA-βCD-MM01-3 with respect to free MM01 in the inhibition of EO771 cell migration. Moreover, **Figure 10B**, which shows the migration of EO771 by confocal microscopy in response to the different stimuli, depicts an increase of migrated cells with the M1 secretome, as well as the reduction of migrated cells with the two treatments (compare M1+MM01 to M1 and M1+L-PGA-βCD-MM01-3 to M1 in **Figure 10B**).

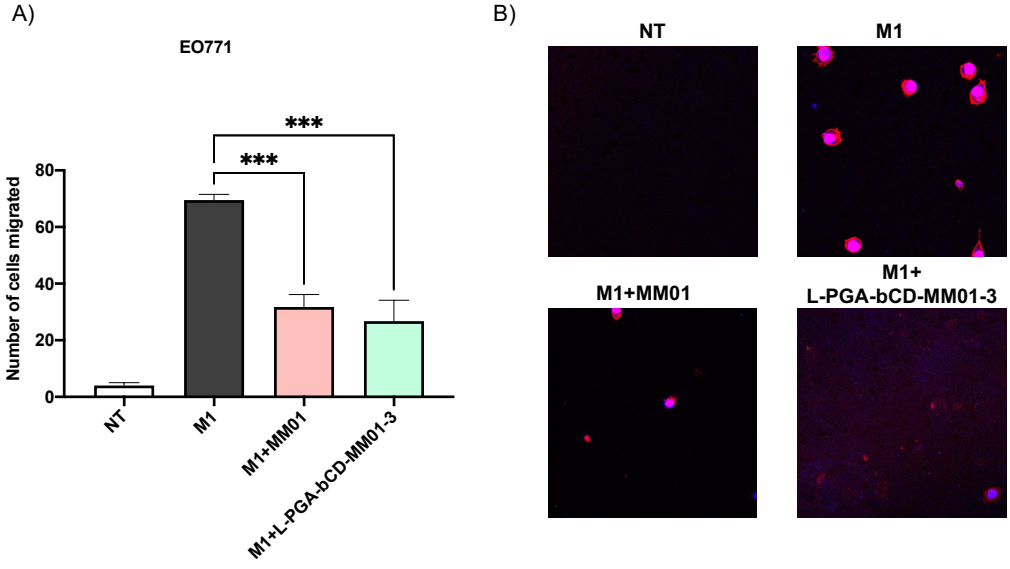

Figure 10. EO771 breast cancer cell migration A) Quantification of EO771 cell migration in response to the M1 macrophage secretome +/- MM01 or L-PGA-βCD-MM01-3. **B**) Confocal microscopy analysis of EO771 cell migration. DAPI (blue) staining marks cell nuclei, and wheat germ agglutinin (WGA – red) staining marks the cell membrane. Data represent the means ± SEM of at least three independent experiments. Statistical significance determined using a one-way ANOVA. (1-way ANOVA, Tukey test *** $p < 0.001$).

On the contrary, as shown in **Figure 11A**, the supernatant of M1 macrophages failed to alter the migration of the 4T1 cell line compared to untreated cells (compare M1 to NT). Moreover, we failed to observe an effect in 4T1 cell migration upon stimulation with macrophages treated with L-PGA-βCD-MM01-3 or free MM01 (compare M1+ L-PGA-βCD-MM01-3 to M1 and M1+MM01 to M1). In the same line of evidence, **Figure 11B**, which shows the migration of 4T1 by confocal microscopy in response to the different stimuli, failed to demonstrate a change in cell migration upon treatment with the different stimuli.

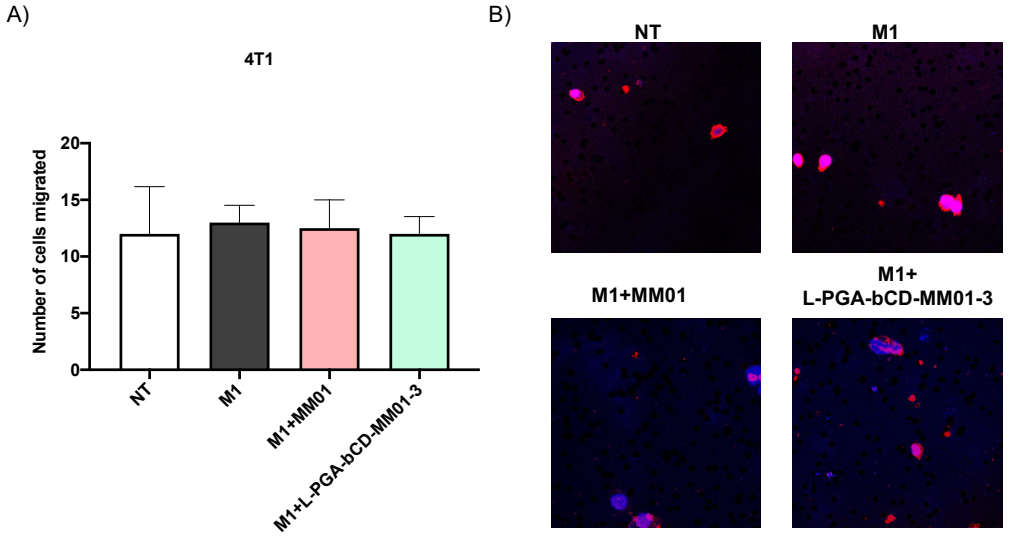

Figure 11. 4T1 breast cancer cell migration A) Quantification of 4T1 cell migration in response to the M1 macrophage secretome +/- MM01 or L-PGA-βCD-MM01-3. **B**) Confocal microscopy analysis of 4T1 cell migration. DAPI (blue) staining marks cell nuclei, and wheat germ agglutinin (WGA – red) staining marks the cell membrane. Data represent the means ± SEM of at least three independent experiments. Statistical significance determined using a one-way ANOVA.

These results confirm that both the nanosystem and the free drug have the same effect at the cellular level.

VI.4 *In vivo* Validation of L-PGA-βCD-MM01-3 in a Breast Cancer Model

We next investigated the antitumor potential and safety of L-PGA-βCD-MM01-3 treatment compared to free MM01. Overall, we expected to see a more significant antitumor effect of with L-PGA-βCD-MM01-3 treatment *in vivo* due to the EPR effect. The EPR effect describes the passive accumulation of macromolecules in tumor tissues due to pathological alterations of the vasculature within tumors or sites of inflammation. In addition, said areas also suffer from failures in lymphatic drainage, which also favor the retention of nanomedicines within the tumor [26].

We selected the orthotopic EO771 breast cancer model that previously responded to MM01 treatment for this approach (**chapter V**).

V.4.1 L-PGA-βCD-MM01-3 Antitumor Activity and Safety in the EO771 TNBC Murine Model

We injected $1x10^6$ EO771 cells into the fourth mammary fat pad of female C57BL/6 mice between 6-8 weeks of age. When tumors reached a size of approximately 0.02 cm^3 (day 13), we randomly divided mice into three groups (n=8) (**Figure 12A**):

1) Control group - intravenous treatment with PBS+5%DMSO

2) Intravenously treatment of 10 mg/kg MM01 three times per week

3) Intravenously treatment of 10 mg/kg L-PGA-βCD-MM01-3 three times per week

We made an evaluation every 3 days of animal weight and tumor growth (using calipers) during the whole experiment (31 days) (**Figure 12**). Relative body weight measurements made over time suggests the maintenance of mouse body weight throughout the whole experiment in the three treatment groups (**Figure 12B**). Moreover, from a safety point of view, daily monitoring of the general aspect of mice failed to reveal any deterioration in animal welfare. In **Figure 12C,** which shows the size of tumors at end point, we observe a reduction in tumor size in animals treated with

the MM01 inhibitor and the L-PGA-βCD-MM01-3 polymer compared to untreated animals. In the same line of evidence, **Figure 12D**, which depicts the tumor growth (cm^3) over time, demonstrates a significant and enhanced reduction of tumor growth in animals treated with the polymer compared to untreated animals, demonstrating that L-PGA-βCD-MM01-3 improves the effect of free drug at tumor growth level. We also represented the fold increase (final tumor volume/initial tumor volume) of tumor size (cm^3) at the end point, taking as reference the tumor volume in cm^3 measured by caliper on the first day of treatment (**Figure 12E**). As expected, both the mice treated with the free drug and L-PGA-βCD-MM01-3 polymer displayed a significant tumor growth inhibition as evidenced by the inhibition in the fold change measurement of both treatments compared with the control group. However, L-PGA-βCD-MM01-3 presented a more relevant effect compared to free MM01 to reduce tumor volume.

These results demonstrated the efficacy of L-PGA-βCD-MM01-3 to improve the efficacy of the free drug to reduce tumor growth in the orthotopic EO771 breast cancer model.

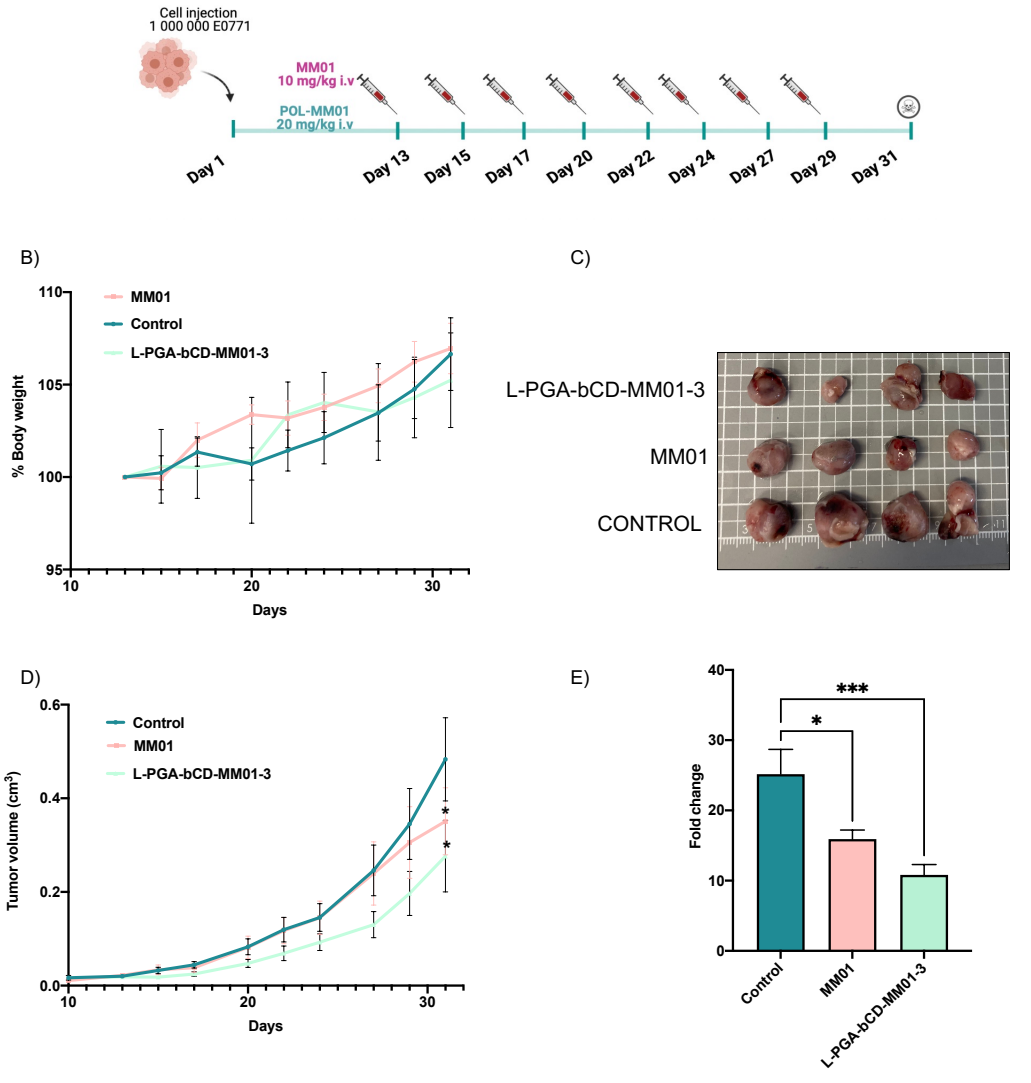

Figure 12. MM01 and L-PGA-βCD-MM01-3 Treatment in an Orthotopic breast cancer EO771 Mouse Model. Mice were treated with MM01 at 10 mg/kg, L-PGA-βCD-MM01-3 at 20 mg/kg, or PBS+5%DMSO as vehicle control. **A**) Schematic representation of in vivo animal experiment. **B**) Relative changes to body weight of mice (as a percentage) over time. **C**) Representative images of tumors at the experimental endpoint. **D**) Tumor volume measured in cm^3 with caliper over time. **E**) Fold change of tumor volume at the experimental endpoint. Data expressed as mean±SEM, n>3. Statistical analysis performed using ANOVA. (1-way ANOVA, Tukey test * $p < 0.05$; *** $p < 0.001$

Finally, at the end of the experiment, once the animals were sacrificed, we obtained the blood from the heart and carried out hematological studies to identify the development of systemic pathologies during tumor growth, such as marked inflammatory response derived from the tumor, anemia, thrombocytosis, reticulocytosis, leukocytosis, or lymphocytosis. **Figure 13** shows the count in g/L of leukocytes, erythrocytes, thrombocytes, neutrophils, monocytes, and lymphocytes present in the blood at the endpoint of the EO771 model compared to healthy animals. However, we failed to observe any significant changes in the EO771-Luc2 model animals, treated or untreated with MM01 and L-PGA-βCD-3, compared to healthy animals.

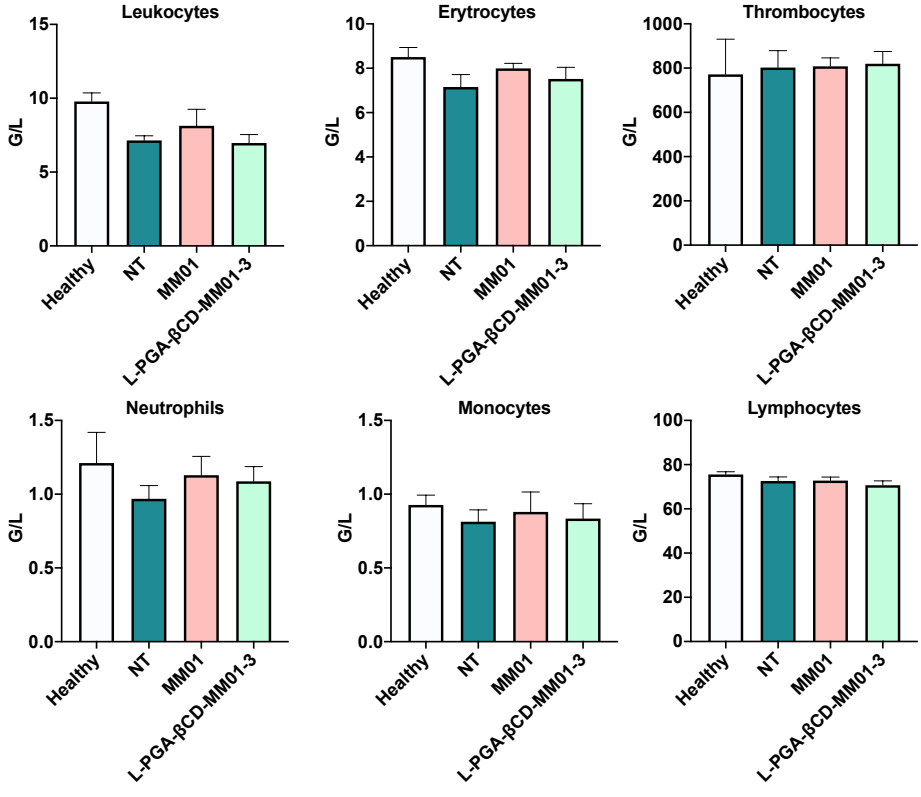

Figure 13. Complete Hemogram of EO771 model. Counts in g/L of leukocytes, erythrocytes, thrombocytes, neutrophils, monocytes, and lymphocytes present in the blood at the endpoint of the EO771-Luc2 animals. Data expressed as mean±SEM, n>3. Statistical significance determined using one-way ANOVA.

Conclusions

As conclusions of this chapter, to improve the effects of MM01, we have designed a new chemical entity based on a hybrid synthetic strategy that presents 1) the chemical conjugation of a linear poly-L-glutamate (PGA) with cyclodextrin moieties and 2) the encapsulation of MM01 into the cyclodextrin ring and 3) the resultant nanoparticulate hybrid nanomedicine with adequate polydispersity and fine-tuned size upon drug loading and cyclodextrin derivatization.

We have evaluated the effects of this new nanomedicine both in cellular models of inflammation and in tumor models of triple negative breast cancer. Cellular inflammation assays have shown that nanomedicine and free drug have the same effects at an equivalent concentration of MM01. Secondly, although the results in cells do not show an improvement in the effect of the free drug expected due to the different pharmacokinetics observed by the nanosystems (diffusion into the cell vs. endocytosis, for the free MM01 vs L-PGA-βCD-MM01, respectively), we have demonstrated an enhanced effect in reducing tumor size in the *in vivo* EO771 model. A greater accumulation of the nanosystem is expected at the tumor site due to the EPR effect and once there, a sustained release of MM01 at the TME that trigger the greater antitumor response. The validation of our approach is ongoing in a metastasic EO771-Luc2 model.

References

1. Senapati, S., et al., *Controlled drug delivery vehicles for cancer treatment and their performance.* Signal Transduct Target Ther, 2018. **3**: p. 7.
2. Patra, J.K., et al., *Nano based drug delivery systems: recent developments and future prospects.* J Nanobiotechnology, 2018. **16**(1): p. 71.
3. Bor, G., I.D. Mat Azmi, and A. Yaghmur, *Nanomedicines for cancer therapy: current status, challenges and future prospects.* Ther Deliv, 2019. **10**(2): p. 113-132.
4. Melnyk, T., et al., *Therapeutic potential of polypeptide-based conjugates: Rational design and analytical tools that can boost clinical translation.* Adv Drug Deliv Rev, 2020. **160**: p. 136-169.
5. Chow, D., et al., *Peptide-based Biopolymers in Biomedicine and Biotechnology.* Mater Sci Eng R Rep, 2008. **62**(4): p. 125-155.
6. Ekladious, I., Y.L. Colson, and M.W. Grinstaff, *Polymer-drug conjugate therapeutics: advances, insights and prospects.* Nat Rev Drug Discov, 2019. **18**(4): p. 273-294.
7. Zagorodko, O., et al., *Polypeptide-Based Conjugates as Therapeutics: Opportunities and Challenges.* Macromol Biosci, 2017. **17**(1).
8. Patel, S., et al., *Brief update on endocytosis of nanomedicines.* Adv Drug Deliv Rev, 2019. **144**: p. 90-111.
9. Liechty, W.B., et al., *Polymers for drug delivery systems.* Annu Rev Chem Biomol Eng, 2010. **1**: p. 149-73.
10. Haimhoffer, Á.R., Ágnes; Réti-Nagy, Katalin; Vasvári, Gábor; Váradi, Judit; et al.. , *Cyclodextrins in Drug Delivery Systems and Their Effects on Biological Barriers*
11. Duncan, R., *Development of HPMA copolymer-anticancer conjugates: clinical experience and lessons learnt.* Adv Drug Deliv Rev, 2009. **61**(13): p. 1131-48.
12. Vaezic, R.G.M.R.J.H.A.F.S.M.R., *Central composite design (CCD)-Response surface methodology (RSM) of effective electrospinning parameters on PVP-B-Hf hybrid nanofibrous composites for synthesis of HfB2-based composite nanofibers.*
13. Bezerra, M.A., et al., *Response surface methodology (RSM) as a tool for optimization in analytical chemistry.* Talanta, 2008. **76**(5): p. 965-77.
14. Adamuab, B.S.M.M.S.L.W.S.A.V.C.K.a.Y.H.a., *Properties of nano-silica modified pervious concrete.*
15. Güvenç, B.Ş.Y.T.E.H.Ş.A.B., *Development of a graphical user interface for determining the optimal mixture parameters of normal weight concretes: A response surface methodology based quadratic programming approach.*
16. Bashar S. Mohammed, B.E.A., Mohd Shahir Liew, W.S. Alaloul, Veerendrakumar C. Khed, *Effects of elevated temperature on the tensile properties of NS-modified self-consolidating engineered cementitious composites and property optimization using response surface methodology (RSM).* Construction and Building Materials.
17. Aydar, A.Y., *Utilization of Response Surface Methodology in Optimization of Extraction of Plant Materials.*
18. Bayuo, J., Abukari, M.A. & Pelig-Ba, K.B., *Optimization using central composite design (CCD) of response surface methodology (RSM) for biosorption of hexavalent chromium from aqueous media.* Appl Water Sci.
19. Boix-Montesinos, P., et al., *The past, present, and future of breast cancer models for nanomedicine development.* Adv Drug Deliv Rev, 2021. **173**: p. 306-330.
20. Behzadi, S., et al., *Cellular uptake of nanoparticles: journey inside the cell.* Chem Soc Rev, 2017. **46**(14): p. 4218-4244.
21. Villanueva-Flores, F., et al., *Understanding cellular interactions with nanomaterials: towards a rational design of medical nanodevices.* Nanotechnology, 2020. **31**(13): p. 132002.
22. Missiroli, S., et al., *Targeting the NLRP3 Inflammasome as a New Therapeutic Option for Overcoming Cancer.* Cancers (Basel), 2021. **13**(10).
23. Guo, B., et al., *Targeting inflammasome/IL-1 pathways for cancer immunotherapy.* Sci Rep, 2016. **6**: p. 36107.
24. Tezcan, G., et al., *Therapeutic Potential of Pharmacological Targeting NLRP3 Inflammasome Complex in Cancer.* Front Immunol, 2020. **11**: p. 607881.
25. Chen, I.F., et al., *AIM2 suppresses human breast cancer cell proliferation in vitro and mammary tumor growth in a mouse model.* Mol Cancer Ther, 2006. **5**(1): p. 1-7.

26. Greish, K., *Enhanced permeability and retention (EPR) effect for anticancer nanomedicine drug targeting.* Methods Mol Biol, 2010. **624**: p. 25-37.

Ch.VII

General Discussion

General Discussion

Cytosolic complexes known as inflammasomes are essential components of the innate immune system that coordinate the maturation and release of pro-inflammatory cytokines such as IL-1β and IL-18 in response to either microbe-derived pathogen-associated molecular patterns (PAMPs) and damaged-associated molecular patterns (DAMPs) [1]. At the structural level, this family of complexes comprises specific cytosolic pattern recognition receptors (PRRs), the apoptosis-associated speck-like protein containing CARD (ASC) adaptor protein (present in the vast majority of inflammasomes), and the pro-caspase-1 protease [2]. The inflammasome components self-organize to activate the inflammatory response in response to host damage or infection. The ASC protein oligomerizes to form "ASC specks" that recruit pro-caspase-1, thereby prompting the formation of active caspase-1. Finally, caspase-1 initiates the maturation and release of pro-inflammatory cytokines to mediate the inflammatory response [3].

This inflammasome-mediated inflammatory process represents a rapid response that removes harmful stimuli and prevents the spread of infections or tumorigenic growth [4]; [5]. However, inflammasome dysregulation has been linked to the development of several pathologies; for example, studies have indicated roles for the NLRP3, AIM2, NLRP6, and NLRC4 inflammasomes in tumor formation [6]; [7], neuroinflammation [8], and viral infections [9] among others conditions [10]; [11]. Interestingly, recent research into severe acute respiratory syndrome coronavirus-2 (SARS-CoV-2) indicates that disease severity correlates with inflammatory responses, in which ASC may play a role [12].

Several drugs have been used to effectively treat human inflammasome-related diseases, such as antibodies against IL-1β (canakinumab) or recombinant IL-1β receptor antagonists (anakinra). These drugs target the downstream products of the inflammatory process and, therefore, may fail to alleviate all the consequences of inflammasome activation (such as pro-inflammatory cytokine release, the extracellular accumulation of ASC specks, and pyroptotic cell death) that contribute to the propagation of pro-inflammatory signaling [13]. Specific inflammasome inhibitors,

such as the NLRP3 inhibitors MCC950 [14] or CY-09 [15], have specific and highly effective anti-inflammatory effects; however, they do not apply to multifactorial diseases that require a more general inhibitory strategy. Treatment with drugs that act upon components shared by many inflammasomes, such as ASC, may represent a more effective means of inhibiting inflammasome activation and its subsequent spread and treating multifactorial inflammasome-related diseases.

A recent study described the development of an antibody fragment that specifically recognizes the CARD domain of the human ASC protein [16]. This antibody disrupts ASC (CARD) interactions, inhibits inflammasome activation, and protects cells from inflammatory cell death. Furthermore, Desu et al. recently reported that ASC inhibition by treatment with an anti-ASC monoclonal antibody prompted clear improvements in a mouse model of multiple sclerosis [17].

Importantly, recent studies have also described inflammasome-independent ASC functions. For example, ASC speck can recruit caspase-8 and induce apoptosis [18], while Schneider et al. established that ASC specks activated Caspase-8 and induced secondary pyroptosis in the absence of Caspase-1 [19]. Another recent study discovered that the presence of ASC-deficient CD8+ T cells reduced the rejection of cell/tissue transplants in model mice [20]; therefore, ASC inhibition could represent a new approach to improving transplant therapies.

Given the need to identify new treatments capable of inhibiting several common points of the inflammatory response, Dr. Orzáez's laboratory proposed the search for new *pan*-inflammasome modulators.

Before this study, screening assays described how the compound MM01 inhibited ASC-dependent pro-caspase-1 activation, a common step in activating multiple inflammasomes. One of the main objectives of this Ph.D. thesis was the characterization of the molecular mechanism of action and pharmacological activity of MM01 (**See Chapter IV**).

We investigated how MM01 interacts with the protein ASC as a first step. Following the activation of ASC-dependent inflammasomes, the ASC protein

oligomerizes into large filaments. We demonstrated that MM01 treatment severely impacts ASC oligomerization by significantly reducing filament formation *in vitro* and in cellular models. Importantly, we discovered that MM01 interferes with ASC oligomer formation and facilitates ASC protein degradation in HEK293 via the autophagy-lysosome pathway.

We next evaluated the ability of MM01 to inhibit the activation of several ASC-dependent inflammasomes in vitro and in vivo (**Chapter IV.3**). One of the significant advantages of our inflammasome inhibitor compared to other inflammasome inhibitors described is targeting a component (ASC) common to the vast majority of inflammasomes. MM01 is the first small molecule capable of inhibiting ASC oligomerization, which confers numerous advantages in the cases of multifactorial disease that require the inhibition of multiple inflammasomes. We demonstrated that MM01 treatment prevents the activation of different ASC-dependent inflammasomes by significantly reducing IL-1β release, pyroptotic cell death, and ASC speck formation in THP-1-derived macrophages. To reinforce the ASC-specific mechanism of action, we studied how MM01 impacted the non-canonical inflammasome activation pathway, which does not depend on ASC. The non-canonical pathway requires the direct activation of human caspases 4/5 in response to intracellular LPS. Caspases 4/5 directly recognize intracellular LPS to prompt the cleavage of the pore-forming protein Gasdermin D (GSDMD) and trigger the secondary activation of the canonical NLRP3 inflammasome for cytokine release [21]; [22]. We demonstrated that MM01 failed to inhibit induced IL-1β release and pyroptosis by the non-canonical inflammasome pathway, reinforcing the ASC-specific mechanism of action of MM01.

Finally, we aimed to evaluate the efficacy of MM01 in vivo. We selected a murine model of monosodium urate (MSU)-induced peritonitis [23]. In this model, MSU crystals potently activate NLRP3, which is accompanied by increased levels of IL-1β and neutrophil infiltration in the intraperitoneal fluid [24] (**See Chapter IV.4**). We demonstrated that MM01 efficiently suppressed MSU-induced IL-1β release and peritoneal neutrophil recruitment, thereby providing evidence for the in vivo anti-inflammatory activity of the ASC inhibitor MM01.

Overall, in **Chapter IV** of this thesis, we identified the inhibition of ASC oligomerization as the mechanism of action of MM01. Therefore, we report MM01 as

a novel pan-inflammasome inhibitor for treating multifactorial diseases involving the pathological activation of several inflammasomes, such as cancer. As the first exploration of this disease-treating potential, we explored our novel ASC oligomerization inhibitor as a therapy for breast cancer (**Chapter V**).

In general, the role of inflammasomes in tumor progression is closely linked to the inflammatory tumor microenvironment (TME). Tumor cells cooperate closely with TME-resident cells, such as immune cells, to promote chronic inflammation and immunosuppression [25]. This state of chronic inflammation is mainly mediated by inflammasome activation in TME-resident immune cells and can dictate tumor growth and invasiveness [26]. However, the role of the inflammasome in cancer remains a controversial topic due to its double-edged role in tumor progression. While inflammasome activation can control and reduce tumor cell growth in early disease stages [27], uncontrolled inflammasome activation in the TME can promote the development of metastasis in many types of cancer [28].

In breast cancer, several studies have reported the pro-tumorigenic role of uncontrolled inflammasome activation [29];[30]; [31]. For example, Guo et al. [32] demonstrated that the knock-out (KO) of several inflammasome components fostered a reduction in tumor size and metastasis in the EO771 triple negative breast cancer (TNBC) mouse model. On the contrary, other studies have reported the anti-cancer potential of the inflammasome in breast cancer. Kaplanov et al. demonstrated that Il-1β-deficient mice exhibited a profound regression of primary tumor growth in a 4T1 orthotopic breast cancer mouse model [33].

Therefore, the inflammasome may represent a new therapeutic target in breast cancer; however, few studies have evaluated the impact of inflammasome inhibitors in breast tumor models. For example, Holen et al. demonstrated that Anakinra decreased tumor growth and bone metastasis in pre-clinical models of breast cancer [34]. In a similar study, Te-Chia et al. investigated the administration of Anakinra before standard chemotherapy in female HER2-negative metastatic breast cancer patients in a clinical pilot study [35]. They revealed a link between tumor-infiltrating CD11c+ myeloid cell-derived IL1β production in primary breast cancer tumors and advanced disease and

demonstrated that anakinra treatment prevented breast cancer progression in a humanized mouse model. In addition, patients with metastatic HER2− breast cancer treated with anakinra displayed an attenuated inflammatory transcriptional signature in blood leukocytes [35].

In another example, Zhai et al. examined the efficacy of the natural compound andrographolide, an inhibitor of NFκB and NLRP3 inflammasome [36, 37], in reducing breast cancer-induced osteolysis [38]. The study reported that andrographolide prevented human breast cancer-induced bone loss by suppressing receptor activator of NF-κB ligand (RANKL)-mediated human breast cancer cell-induced osteoclast differentiation. Molecular analysis revealed that andrographolide prevented osteoclast function by inhibiting the RANKL-induced NF-κB and ERK signaling pathway at lower doses (20 μM) and inducing apoptosis at higher doses (40 μM). In a related study, Zhai et al. demonstrated that andrographolide treatment inhibited the *in vitro* migration and invasion of an aggressive breast cancer cell line (MBA-MD-231) at non-lethal concentrations, suppressed proliferation, and induced apoptosis at high concentrations [39]. Andrographolide treatment also significantly inhibited the growth of bone-implanted tumors in vivo and attenuated cancer-induced osteolysis [39].

Therefore, we aimed to employ our pan-inflammasome inhibitor MM01 as a chemical tool to study the role of the inflammasome in breast cancer progression (**Chapter V**).

Notably, macrophages comprise the most abundant immune cell population in the breast cancer TME [40]; [41]. Moreover, excessive/prolonged pro-inflammatory signaling by activated M1 macrophages promotes angiogenesis and tumor spread [42]; [43]. Given the influence that macrophages have on the establishment of chronic inflammation in the TME, we established activated M1 macrophage cell lines (human; derived from THP-1 cells, and murine; derived from J774A.1 cells) to study the effect that inflammasome-mediated inflammation has on tumor progression (**see Chapter V.I**).

By migration experiments using the secretome of M1 macrophages, treated or untreated with our inhibitor, we demonstrated that intrinsic differences in breast cancer

cells condition their migration towards pro-inflammatory stimuli. We discovered some responder breast cancer cell lines, such as the human MDA-MB-231, MDA-MB-468, MCF7, and ZR-75 or the murine EO771, that increase cell migration in response to M1 secretome, and decrease cell migration in response to M1 secretome treated with MM01. On the contrary, we reported non-responder models such as the murine 4T1 cell line, that don't respond to the inflammatory stimuli, but increase their migration in response to MM01 treatment. Importantly, these cell migration experiments were reinforced *in vivo (***see Chapter V.2***),* in which MM01 treatment can exert positive or negative effects depending on the breast cancer model employed. Having these two murine models that recapitulate the contradictory responses to the treatment with an inflammasome inhibitor, we decided to study the differences between these two models in order to search for biomarkers capable of predicting the response to treatment with an inflammasome inhibitor.

Through proteomic studies, we identified patterns of over-expressed proteins in the EO771 model treated with the secretome of M1 (EO771+M1) macrophages compared to the 4T1 model (4T1+M1). Importantly, many proteins upregulated in EO771+M1 correspond to RNA binding proteins characterized as having a role in tumor progression and metastasis. For example, previous studies have demonstrated that suppression of Eukaryotic translation initiation factor 4 gamma 2 (EIF4G2) significantly reduced the development of acute myeloid leukemia [44], diffuse large B cell lymphoma [45], osteosarcoma [46], and lung cancer [47]. RNASEH2A promotes proliferation in sarcoma, breast cancer, glioma cell lines, and prostate cancer, suggesting a pivotal role in cancer progression [48]. Moreover, studies have reported the overexpression of KRR1 in brain metastases in metastatic breast cancer patients compared to the primary tumor [49]. Overall, we identified patterns of positively regulated proteins in EO771 + M1 (responding models) compared to 4T1 + M1 (non-responding model) that may have essential functions in tumor progression in different types of cancer. However, these preliminary results require validation to identify response biomarkers for future experiments.

Finally, we looked to create an improved treatment strategy in the EO771 responder model by derivatising MM01 as a nanomedicine (**Chapter VI**). The use of

nanomedicines in the field of cancer therapeutics provides numerous advantages compared to small drugs, such as increased solubility and chemical stability, controlled pharmacokinetics and pharmacodynamics, increased specificity and efficacy by improving tumor accumulation, reduced non-specific accumulation, enhanced biodegradation, improved distribution and controlled release, reduced toxicity and adverse effects in healthy cells, and inhibited drug resistance due to altered cellular internalization mechanisms [50].

Many nanomedicine strategies exist to improve the effects of conventional therapies such as small drugs – these include the implementation of polymers/polypeptides [51]. In this study, we designed a new therapeutic tool that combines a linear polymer of polyglutamic acid (PGA) conjugated to a cyclodextrin moiety conjugated orthogonally to PGA side chains that provides the polypeptidic carrier with the capability to encapsulate MM01 in a %mol derivatization manner.

Biodegradable, multivalent polypeptides such as PGA have benefits due to their similarities to native proteins, including safety, low immunogenicity, and biocompatibility as they degrade in endogenous safe metabolites (i.e. Glutamic acid) [52]. In addition, polypeptides also have advantages due to their structural versatility, which allows the formation of multiple architectures with different physicochemical characteristics (charge, polarity, and hydrophilicity) [53]. Moreover, using polypeptidic carriers with a higher Mw allows optimization of pharmacokinetics and improves passive tumor targeting by the EPR effect.

We first attempted to chemically conjugate MM01 directly to linear PGA; however, the chemical structure of MM01 represented a significant impediment to this process. Unexpectedly, we discovered the extreme instability of MM01 due to the presence of a double bond that degrades and triggers MM01 decomposition. Therefore, we decided to implement a hybrid strategy that combines the chemical conjugation of PGA with a bioresponsive linker (cyclodextrin) and the encapsulation of the drug within cyclodextrin rings.

The reformulation of conventional therapeutics as nanomedicine can change drug distribution or provide more targeted drug delivery to specific tissues or cells within those tissues through the versatility of synthetic chemistry and chemical conjugations. This spatiotemporal control of the administered drug leads to improved therapeutic

effects and/or reduced side toxicities [51]. One of the most significant benefits of nanomedicines for oncology is the active or passive targeting of the tumor area [54]. Active or ligand-mediated targeting allows nanomedicines to specific target cells using specific ligands. On the contrary, passive targeting through the EPR effect allows a more significant accumulation of nanomedicines in the tumor environment than the free form of the drug involved. The passive accumulation of nanomedicines relies on the pathological alterations inherent to the vasculature within tumors or sites of inflammation [54]; [55]. In this work, we explored how our MM01 nanomedicine benefited from passive tumor accumulation to enhance anti-cancer effects.

We first studied the effect of our MM01 nanomedicine compared to the free drug in cell models of inflammation. We employed THP-1-derived macrophages to study the ability of our MM01 nanomedicine to prevent the activation of the NLRP3 inflammasome. At equivalent concentrations of free drug, we discovered that our nanomedicine and free MM01 had the same effect in reducing IL-1β secretion and pyroptotic cell death.

To continue the functional characterization, we next studied the effect of our MM01 nanomedicine on tumor cell migration employing the 4T1and EO771 breast cancer cell lines. We studied the migration of tumor cells in response to the pro-inflammatory macrophage M1 secretome with and without pretreatment. As hoped for, we observed a similar effect for the free form of MM01 and the MM01 nanomedicine. We observed inhibited migration in the EO771 model and increased migration in the 4T1 model after pro-inflammatory stimulation. These results demonstrated that both free MM01 and MM01 nanomedicine had the same effect at the cellular level. It has been already reported that up to 100-fold greater activity could be seen when compare free vs conjugated drugs, so having similar activity predicts a greater activity in in vivo models due to the differential whole body biodistribution and greater tumor accumulation for PGA-βCD-MM01 by the EPR effect.

Importantly, we did demonstrate a more relevant reduction in tumor size in the EO771 model *in vivo*. The more significant effect at the tumor site level of the MM01 nanomedicine may derive from the enhanced tumor accumulation (and retention) effect.

Based on the results obtained in the migration assays, we expected to observe a more important effect of free MM01 drug and nanomedicine in reducing tumor progression and metastasis; however, the orthotopic model EO771 failed to display spontaneous metastasis. One of our main objectives was to study the inhibition of metastasis; therefore, future experiments will aim to study the activity of free and nanomedicine MM01 in a metastatic model of EO771 by intravenously injecting tumor cells in mice.

These results confirm the advantages of nanomedicine-based therapies in cancer with respect to the use of hydrophobic small drugs mainly due to changes in PK/PD due to tumor targeting and drug sustained release profiles.

References

1. Broz, P. and V.M. Dixit, *Inflammasomes: mechanism of assembly, regulation and signalling.* Nat Rev Immunol, 2016. **16**(7): p. 407-20.
2. Zheng, D., T. Liwinski, and E. Elinav, *Inflammasome activation and regulation: toward a better understanding of complex mechanisms.* Cell Discov, 2020. **6**: p. 36.
3. Boucher, D., et al., *Caspase-1 self-cleavage is an intrinsic mechanism to terminate inflammasome activity.* J Exp Med, 2018. **215**(3): p. 827-840.
4. Cronkite, D.A. and T.M. Strutt, *The Regulation of Inflammation by Innate and Adaptive Lymphocytes.* J Immunol Res, 2018. **2018**: p. 1467538.
5. Tartey, S. and T.D. Kanneganti, *Differential role of the NLRP3 inflammasome in infection and tumorigenesis.* Immunology, 2019. **156**(4): p. 329-338.
6. Masters, S.L., *Specific inflammasomes in complex diseases.* Clin Immunol, 2013. **147**(3): p. 223-8.
7. Qi, M., et al., *AIM2 promotes the development of non-small cell lung cancer by modulating mitochondrial dynamics.* Oncogene, 2020. **39**(13): p. 2707-2723.
8. Freeman, L., et al., *NLR members NLRC4 and NLRP3 mediate sterile inflammasome activation in microglia and astrocytes.* J Exp Med, 2017. **214**(5): p. 1351-1370.
9. Gram, A.M., J. Frenkel, and M.E. Ressing, *Inflammasomes and viruses: cellular defence versus viral offence.* J Gen Virol, 2012. **93**(Pt 10): p. 2063-2075.
10. Lamkanfi, M. and V.M. Dixit, *Inflammasomes and their roles in health and disease.* Annu Rev Cell Dev Biol, 2012. **28**: p. 137-61.
11. Karki, R., S.M. Man, and T.D. Kanneganti, *Inflammasomes and Cancer.* Cancer Immunol Res, 2017. **5**(2): p. 94-99.
12. Rodrigues, T.S., et al., *Inflammasomes are activated in response to SARS-CoV-2 infection and are associated with COVID-19 severity in patients.* J Exp Med, 2021. **218**(3).
13. Nowarski, R., et al., *Epithelial IL-18 Equilibrium Controls Barrier Function in Colitis.* Cell, 2015. **163**(6): p. 1444-56.
14. Coll, R.C., et al., *A small-molecule inhibitor of the NLRP3 inflammasome for the treatment of inflammatory diseases.* Nat Med, 2015. **21**(3): p. 248-55.
15. Jiang, H., et al., *Identification of a selective and direct NLRP3 inhibitor to treat inflammatory disorders.* J Exp Med, 2017. **214**(11): p. 3219-3238.
16. Schmidt, F.I., et al., *A single domain antibody fragment that recognizes the adaptor ASC defines the role of ASC domains in inflammasome assembly.* J Exp Med, 2016. **213**(5): p. 771-90.
17. Desu, H.L., et al., *IC100: a novel anti-ASC monoclonal antibody improves functional outcomes in an animal model of multiple sclerosis.* J Neuroinflammation, 2020. **17**(1): p. 143.
18. Van Opdenbosch, N., et al., *Caspase-1 Engagement and TLR-Induced c-FLIP Expression Suppress ASC/Caspase-8-Dependent Apoptosis by Inflammasome Sensors NLRP1b and NLRC4.* Cell Rep, 2017. **21**(12): p. 3427-3444.
19. Schneider, K.S., et al., *The Inflammasome Drives GSDMD-Independent Secondary Pyroptosis and IL-1 Release in the Absence of Caspase-1 Protease Activity.* Cell Rep, 2017. **21**(13): p. 3846-3859.
20. Cheong, M., et al., *ASC Modulates CTL Cytotoxicity and Transplant Outcome Independent of the Inflammasome.* Cancer Immunol Res, 2020. **8**(8): p. 1085-1098.
21. Elizagaray, M.L., et al., *Canonical and Non-canonical Inflammasome Activation by Outer Membrane Vesicles Derived From Bordetella pertussis.* Front Immunol, 2020. **11**: p. 1879.
22. Casson, C.N., et al., *Human caspase-4 mediates noncanonical inflammasome activation against gram-negative bacterial pathogens.* Proc Natl Acad Sci U S A, 2015. **112**(21): p. 6688-93.
23. Spalinger, M.R. and M. Scharl, *Mono Sodium Urate Crystal-induced Peritonitis for in vivoAssessment of Inflammasome Activation.* Bio Protoc, 2018. **8**(5): p. e2754.
24. Martinon, F., et al., *Gout-associated uric acid crystals activate the NALP3 inflammasome.* Nature, 2006. **440**(7081): p. 237-41.
25. Wang, J., et al., *Crosstalk between cancer and immune cells: Role of tumor-associated macrophages in the tumor microenvironment.* Cancer Med, 2019. **8**(10): p. 4709-4721.
26. Zhao, H., et al., *Inflammation and tumor progression: signaling pathways and targeted intervention.* Signal Transduct Target Ther, 2021. **6**(1): p. 263.

27. Hamarsheh, S. and R. Zeiser, *NLRP3 Inflammasome Activation in Cancer: A Double-Edged Sword.* Front Immunol, 2020. **11**: p. 1444.
28. Hibino, S., et al., *Inflammation-Induced Tumorigenesis and Metastasis.* Int J Mol Sci, 2021. **22**(11).
29. Kantono, M. and B. Guo, *Inflammasomes and Cancer: The Dynamic Role of the Inflammasome in Tumor Development.* Front Immunol, 2017. **8**: p. 1132.
30. Soria, G., et al., *Inflammatory mediators in breast cancer: coordinated expression of TNFalpha & IL-1beta with CCL2 & CCL5 and effects on epithelial-to-mesenchymal transition.* BMC Cancer, 2011. **11**: p. 130.
31. Reed, J.R., et al., *Interleukin-1beta and fibroblast growth factor receptor 1 cooperate to induce cyclooxygenase-2 during early mammary tumourigenesis.* Breast Cancer Res, 2009. **11**(2): p. R21.
32. Guo, B., et al., *Targeting inflammasome/IL-1 pathways for cancer immunotherapy.* Sci Rep, 2016. **6**: p. 36107.
33. Kaplanov, I., et al., *Blocking IL-1beta reverses the immunosuppression in mouse breast cancer and synergizes with anti-PD-1 for tumor abrogation.* Proc Natl Acad Sci U S A, 2019. **116**(4): p. 1361-1369.
34. Holen, I., et al., *IL-1 drives breast cancer growth and bone metastasis in vivo.* Oncotarget, 2016. **7**(46): p. 75571-75584.
35. Wu, T.C., et al., *IL1 Receptor Antagonist Controls Transcriptional Signature of Inflammation in Patients with Metastatic Breast Cancer.* Cancer Res, 2018. **78**(18): p. 5243-5258.
36. Ahmed, S., et al., *Andrographolide suppresses NLRP3 inflammasome activation in microglia through induction of parkin-mediated mitophagy in in-vitro and in-vivo models of Parkinson disease.* Brain Behav Immun, 2021. **91**: p. 142-158.
37. Cabrera, D., et al., *Andrographolide Ameliorates Inflammation and Fibrogenesis and Attenuates Inflammasome Activation in Experimental Non-Alcoholic Steatohepatitis.* Sci Rep, 2017. **7**(1): p. 3491.
38. Zhai, Z., et al., *Andrographolide prevents human breast cancer-induced osteoclastic bone loss via attenuated RANKL signaling.* Breast Cancer Res Treat, 2014. **144**(1): p. 33-45.
39. Zhai, Z., et al., *Inhibition of MDA-MB-231 breast cancer cell migration and invasion activity by andrographolide via suppression of nuclear factor-kappaB-dependent matrix metalloproteinase-9 expression.* Mol Med Rep, 2015. **11**(2): p. 1139-45.
40. Mantovani, A., et al., *Cancer-related inflammation.* Nature, 2008. **454**(7203): p. 436-44.
41. Allen, M. and J. Louise Jones, *Jekyll and Hyde: the role of the microenvironment on the progression of cancer.* J Pathol, 2011. **223**(2): p. 162-76.
42. Choi, J., et al., *The role of tumor-associated macrophage in breast cancer biology.* Histol Histopathol, 2018. **33**(2): p. 133-145.
43. Tariq, M., et al., *Macrophage Polarization: Anti-Cancer Strategies to Target Tumor-Associated Macrophage in Breast Cancer.* J Cell Biochem, 2017. **118**(9): p. 2484-2501.
44. Emmrich, S., et al., *miR-139-5p controls translation in myeloid leukemia through EIF4G2.* Oncogene, 2016. **35**(14): p. 1822-31.
45. Mazan-Mamczarz, K., et al., *Down-regulation of eIF4GII by miR-520c-3p represses diffuse large B cell lymphoma development.* PLoS Genet, 2014. **10**(1): p. e1004105.
46. Xie, X., et al., *MicroRNA-379 inhibits the proliferation, migration and invasion of human osteosarcoma cells by targetting EIF4G2.* Biosci Rep, 2017. **37**(3).
47. Hao, G.J., et al., *Suppression of EIF4G2 by miR-379 potentiates the cisplatin chemosensitivity in nonsmall cell lung cancer cells.* FEBS Lett, 2017. **591**(4): p. 636-645.
48. Yang, C.A., et al., *Prognostic Value of RNASEH2A-, CDK1-, and CD151-Related Pathway Gene Profiling for Kidney Cancers.* Int J Mol Sci, 2018. **19**(6).
49. Shahan Mamoor, M., *KRR1 is a differentially expressed gene in brain metastatic human breast cancer.* .
50. Gonzalez-Valdivieso, J., et al., *Advanced nanomedicine and cancer: Challenges and opportunities in clinical translation.* Int J Pharm, 2021. **599**: p. 120438.
51. Duncan, R., *The dawning era of polymer therapeutics.* Nat Rev Drug Discov, 2003. **2**(5): p. 347-60.
52. Chow, D., et al., *Peptide-based Biopolymers in Biomedicine and Biotechnology.* Mater Sci Eng R Rep, 2008. **62**(4): p. 125-155.
53. Dobrovolskaia, M.A., *Pre-clinical immunotoxicity studies of nanotechnology-formulated drugs: Challenges, considerations and strategy.* J Control Release, 2015. **220**(Pt B): p. 571-83.

54. Golombek, S.K., et al., *Tumor targeting via EPR: Strategies to enhance patient responses.* Adv Drug Deliv Rev, 2018. **130**: p. 17-38.
55. Rosenblum, D., et al., *Progress and challenges towards targeted delivery of cancer therapeutics.* Nat Commun, 2018. **9**(1): p. 1410.

Ch.VIII

Final Conclusions

1. MM01 interacts with the CARD domain of ASC, preventing the formation of oligomers.
2. The mechanism of action of MM01 on ASC provides a new drug with the ability to inhibit multiple inflammasomes.
3. MM01 is able to inhibit in vivo inflammation in a NLRP3-dependent model of MSU crystal-induced peritonitis.
4. We have shown that inflammasome inhibition plays a role in tumor progression in breast cancer.
5. We have characterized an in vitro functional assay that allows us to subdivide breast cancer lines into responders and non-responders to MM01 treatment. Functional characterization of drug response in vitro correlates well with in vivo results.
6. Preliminary proteomic analyses have identified putative biomarkers of MM01 sensitivity.
7. We have developed a new nanomedicine, L-PGA-βCD-MM01, to trap MM01 using a conjugation-complexation approach comprising conjugation of -cyclodextrin to a linear poly-L-glutamic acid (PGA) (L-PGA-βCD).
8. The obtained nanosystem demonstrated enhanced efficacy in an orthotopic model of breast cancer by resulting in a more relevant reduction of tumor size in those mice treated with the L-PGA-βCD-MM01 nanomedicine